To Ceren…

SYNTHETIC BIOLOGY APPROACH FOR POINT-OF-CARE DEVICE APPLICATIONS OF BIOSENSORS

A THESIS SUBMITTED TO

THE GRADUATE SCHOOL OF ENGINEERING AND SCIENCE

OF BILKENT UNIVERSITY

IN PARTIAL FULFILLMENT OF THE REQUIREMENTS FOR

THE DEGREE OF

MASTER OF SCIENCE

IN

MATERIALS SCIENCE AND NANOTECHNOLOGY

By

İLKAY ÇİSİL KÖKSALDI

SEPTEMBER 2021

SYNTHETIC BIOLOGY APPROACH FOR POINT-OF-CARE DEVICE APPLICATIONS OF BIOSENSORS

By İlkay Çisil Köksaldi

September 2021

We certify that we have read this dissertation and that in our opinion it is fully adequate, in scope and in quality, as a thesis for the degree of Master of Science.

Urartu Özgür Şafak Şeker (Advisor)

İbrahim Halil Kavaklı

Işık Yuluğ

Approved for the Graduate School of Engineering and Science:

Ezhan Karaşan

Director of the Graduate School

ABSTRACT

SYNTHETIC BIOLOGY APPROACH FOR POINT-OF-CARE DEVICE APPLICATIONS OF BIOSENSORS

İlkay Çisil KÖKSALDI

MSc in Materials Science and Nanotechnology

Advisor: Urartu Özgür Şafak Şeker

September, 2021

Synthetic biology has broadened the scope of detection tool alternatives, among which whole-cell biosensors and cell-free programmable riboregulators are straightforward, inexpensive to develop and easily implementable to fast-screening point-of-care devices. While considered as more convenient, reliable and low-cost alternatives to traditional detection and monitoring methods, the transfer rate of cellular bio-sensing devices to real life applications has been relatively slow. With the aim of precisely identifying and integrating multiple signals from environmental and serum samples, a series of whole-cell biosensors that respond to heavy metals including copper, lead, cadmium and arsenic were developed in *Escherichia coli* host. After characterization of single analyte biosensors, synthetic biology strategies such as promoter engineering and coupling with a genetic amplifier are used to enhance detection time and dynamic range for the signal output. Heavy metal bio-recognition modules were designed to produce different output molecules to employ multiplexed sensing where simultaneous detection of multiple molecules is needed for fast-screening. In addition, a novel attempt for

transforming these bio-sensing systems to a point-of-care device has been investigated. Thorough functional biofilm amyloid protein and cellulose interactions, immobilization of whole-cell biosensors on a low-cost, easy-storage and portable paper-based platform has been aspired to attain more widespread application globally. Secondly, SARS-CoV-2 is a human pathogen and the main cause of COVID-19 disease, announced as a global pandemic by the World Health Organization. COVID-19 is characterized by severe conditions and early diagnosis can make dramatic changes for both personal and public health. Low cost, easy-to-use diagnostic capabilities can have a very critical role to control the transmission of the disease. Here, a state-of-the-art diagnostic tool was developed with *in vitro* synthetic biology approach by employing engineered *de novo* riboregulators. Our design coupled with a home-made point-of-care device can detect and report the presence of SARS-CoV-2 specific genes. The presence of SARS-CoV-2 related genes triggers translation of sfGFP mRNAs, resulting in green fluorescence output. The approach proposed here has the potential of being a game changer in SARS-COV-2 diagnostics by providing an easy-to-run, low-cost-demanding diagnostic capability. Overall, point-of-care device applications of both whole-cell and cell-free biosensor systems have been developed for distinct applications of sensing analytes and nucleic acids.

Keywords: biosensors, heavy metals, surface immobilization, SARS-CoV-2, riboregulators, point-of-care device

ÖZET

BİYOSENSÖRLERİN BAKIM NOKTASI CİHAZ UYGULAMALARI İÇİN SENTETİK BİYOLOJİ YAKLAŞIMI

İlkay Çisil KÖKSALDI

Malzeme Bilimi ve Nanoteknoloji, Yüksek Lisans

Tez Danışmanı: Urartu Özgür Şafak Şeker

Eylül, 2021

Sentetik biyoloji, aralarında tam hücreli biyosensörlerin ve hücresiz programlanabilir riboregülatörlerin de bulunduğu basit, geliştirmesi ucuz ve hızlı taramalı bakım noktası cihazlarına kolayca uygulanabilir olduğu tespit aracı alternatiflerinin kapsamını genişletmiştir. Geleneksel algılama ve izleme yöntemlerine göre daha uygun, güvenilir ve düşük maliyetli alternatifler olarak düşünülmelerine rağmen, hücresel biyoalgılama cihazlarının gerçek yaşam uygulamalarına aktarım hızı nispeten yavaş olmuştur. Bu çalışma kapsamında, çevresel ve serum örneklerinden gelen çoklu sinyalleri tam olarak tanımlamak ve entegre etmek amacıyla, *Escherichia coli* konağında bakır, kurşun, kadmiyum ve arsenik ağır metallerine yanıt veren bir dizi tam hücreli biyosensör geliştirilmiştir. Promotör mühendisliği ve genetik bir amplifikatör ile birleştirme gibi sentetik biyoloji stratejileri kullanılarak tek analit biyosensörlerinin sinyal cevabı arttırılmış, algılama süresi kısaltılmış ve dinamik aralığı geliştirilmiştir. Ağır metal biyoalgılama modülleri, eşzamanlı birden fazla molekülün hızlı taramanabilmesi için çok katlı algılamayı kullanmak üzere farklı analitlerin farklı çıktı molekülleri üretmesi üzere

tasarlanmıştır. Ek olarak, bu biyoalgılama sistemlerini bir bakım noktası cihazına dönüştürmek için yeni bir girişim araştırılmıştır. Kapsamlı fonksiyonel biyofilm amiloid proteini ve selüloz etkileşimleri, tüm hücre biyosensörlerinin düşük maliyetli, kolay saklanan ve taşınabilir kağıt tabanlı bir platformda immobilizasyonu, küresel olarak daha yaygın bir uygulama elde etmek için hedeflenmiştir. İkinci olarak, SARS-CoV-2 bir insan patojenidir ve Dünya Sağlık Örgütü tarafından küresel bir salgın olarak ilan edilen COVID-19 hastalığının ana nedenidir. COVID-19, ağır koşullarla karakterizedir ve erken teşhis, hem kişisel hem de halk sağlığı için dramatik değişiklikler yapabilir. Düşük maliyetli, kullanımı kolay teşhis yöntemleri, hastalığın bulaşmasını kontrol etmede çok kritik bir role sahip olabilir. Bu çalışma kapsamında, de novo tasarlanmış riboregülatörler kullanılarak *in vitro* sentetik biyoloji yaklaşımıyla son teknoloji bir teşhis aracı geliştirilmiştir. Ev yapımı bir bakım noktası cihazıyla birleştirilmiş tasarımımız, SARS-CoV-2'ye özgü genlerin varlığını algılayabilir ve bildirebilir. SARS-CoV-2 ile ilgili genlerin varlığı, sfGFP mRNA'larının translasyonunu tetikleyerek yeşil floresan çıktısına neden olur. Burada önerilen yaklaşım, çalıştırması kolay, düşük maliyetli bir teşhis yöntemi sağlayarak SARS-COV-2 teşhisinde bir oyun değiştirici olma potansiyeline sahiptir. Genel olarak, hem tam hücreli hem de hücresiz biyosensör sistemlerinin bakım noktası cihaz uygulamaları, analitlerinin ve nükleik asitlerin farklı algılama uygulamaları için geliştirilmiştir.

Anahtar kelimeler: biyosensörler, ağır metaller, yüzey immobilizasyonu, SARS-CoV-2, riboregülatörler, bakım noktası cihazı

ACKNOWLEDGEMENTS

First and foremost, I would like to express my deepest gratitude to my advisor, Dr. Urartu ŞEKER. Joining his research team as a graduate researcher followed by being a MS student have been an extraordinary experience for me. He was a very encouraging and kind mentor; more importantly, the life lessons and supporting attitude made me endure hard times. Next, I would like to thank the members of my thesis committee Dr. Işık Yuluğ from Bilkent University and Dr. İbrahim Halil Kavaklı from Koç University for their insightful comments and feedback.

I am grateful to be a team member of Synthetic Biosystems Laboratory and collaborate with such hardworking and nice people. In particular, I would like to thank Sıla Köse and Recep Erdem Ahan for their support for biosensor project. Ebru Şahin Kehribar and Gökçe Özkul for their scientific advices on biofilm project. I also thank to our lab manager, Yeldem Gizem Makas; she is a life saver and mood booster. I thank all present and former SBL members; Ahmet Hınçer, Anooshay Khan, Aslıhan Gökaltun, Behide Saltepe, Burcu Gündüz, Büşra Merve Kırpat, Ebuzer Kalyoncu, Gozeel Binte Shahid, Julian Ostaku, Merve Erden Tüçer, Merve Yavuz, Murat Alp Güngen, Nedim Hacıosmanoğlu, Onur Apaydın, Orhan Nedim Kurt, Özge Beğli, Side Selin Su Yirmibeşoğlu, Suat Tüçer and Tolga Tarkan Ölmez. Moreover, I am grateful to be students of Dr. Seymur Jahangirov and Dr. Özgür Oktel. Their teaching not only contributed to my academic life but also they are role models for me.

During my research at UNAM, one of the most precious things that I gained is the lifelong friendships. I thank for all the delightful and memorable moments to Çiki Çiki members: Gökçe Özkul, Melis Özkan, Kerem Kurban, Abtin Saateh, Doğu Kaan Buğra Özyiğit, Can Çamiçi, Bouthaina Aoudi and Joudi Maskoun. Gökçe and Melis are very supportive and fun that our laughs made us cry all the time, I cannot image my life without you. I enjoy cooking and movie nights with Keremimo, he always makes me laugh even at my saddest moments. Abtin’s humor, support and expertise

in seeing things clearly made me see things from a different perspective, thanks for opening these doors for me. Doğu has a great talent for photo shooting, and introduced me with nice cafes. Can has a very entertaining side only very close ones gets to see; I am happy to be the lucky ones. Bouthaina and Joudi are inseparable sisters, I miss our chat, dancing and cooking time. Ebru Şahin Kehribar is one of the kindest persons I have met, her friendship and support made me endure very stressful moments. I thank to Nurdan Ersöz for our enjoyable movie nights, sleepovers, all the rewarding conversations and for her support. I also thank to Zafer Koşar for his support, amusing comments and misspelling of my name as Çişil. Cemile Elif Özçelik, Celif, is a very good cook and feeds me with creative delicious recipes. Recep and Eray helped me to shape my ideas on my research and we had many fruitful scientific conversations. Ebru Aras, Gizem Makas and Elif Duman are very kind and strong role models, I am grateful to be around them to learn from their experiences. I also thank to my friends from DOST, Kısakaya and DKSK for their support. We have many travel and activity plans that are yet to be completed and that I am looking forward to.

I owe my accomplishments to my kind and loving family, Serkan Kazak, Serap Kazak and Ufuk Kazak, Köksaldı and Özveri family members and Fındık. Ceren Özveri, my sister, had been a great support for not only personal but academic life as well. She was always there for me, and she knew that I was there for her as well. She has passed away during my thesis work without having the opportunity of saying the last goodbye. Not a day goes by without thinking of you, I will miss you forever. My family and my friends always support me in pursuing my dreams.

Finally, I would like to acknowledge the MS scholarship from UNAM (Bilkent University UNAM Graduate Fellowship for MS). Heavy metal whole-cell biosensors and paper immobilization projects are supported by TÜBİTAK (Project number: 115Z217 and 118S398). SARS-CoV-2 point-of-care device project is supported by TÜBİTAK COVID Platform and Bilkent University UNAM.

Table of Contents

List of Figures

List of Tables

Appendix Tables

Chapter 1 – Whole-Cell Heavy Metal Biosensors

1.1 Introduction

Synthetic biology is a new branch of engineering that intends to program cells with nucleic acids, proteins, and other biomolecules to develop unnatural biological capabilities and cellular networks. Biological parts are characterized as molecular building blocks to construct sophisticated synthetic genetic networks such as genetic recorders [1–3], genetic logic gates [1], synthetic oscillator [4], analog computation [5], synthetic riboregulators [6], programmable self-organizing multicellular systems [7], biofuel production [8], industrial enzymes [9,10], production of chemicals [11,12]. These characterized systems have been used for the development of more complex novel tools for environmental and biomedical monitoring. Conventional methods such as mass spectrometry, gas chromatography for detection of analytes from environmental or patient samples are expert and infrastructure dependent, expensive and time-consuming.

The scope of surveillance tool alternatives has been broadened with synthetic biology. Biosensors are widely used programmable biological devices that uses multiple biological components to respond changes in the environment. Until now, a variety of whole-cell and cell-free biosensors have been designed and implemented for environmental monitoring, theranostic and biomedical applications. Whole-cell biosensors were developed to monitor nanotoxicity [13–15], heavy metals [16], pesticides [17], infection [18] and food safety [19].

Cell-free biosensor systems have been developed for the detection of multiple water contaminants [20,21], nucleic acids [22], pathogens [23], profiling of human gut microbiome [24]. Unlike whole-cell biosensors, cell-free systems require purified proteins, nucleic acids, energy sources and other chemicals for proper functioning while increasing the cost of the end product. Whole-cell biosensors are comprised of three interconnected modules; selective biological recognition elements, transducing biocatalytic processes and specific bioreporter actuators as depicted in Figure 1. Complex systems for multi-input multi-output detection systems, multi-layered synthetic circuitry systems are required which are easily implemented in whole-cell biosensors. Sensing, processing and actuator elements can be programmed for specific functionalities; hence, developing whole-cell biosensors are quick, robust, easy-to-implement and low-cost.

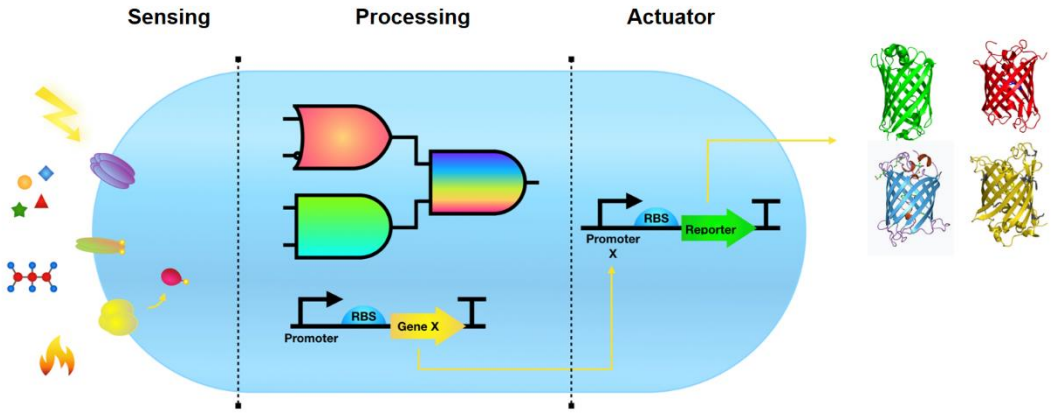

Figure 1. Shematic diagram of whole cell biosensor elements. Like other sensor types, cellular biosensors are composed of three interconnected units; selective biological recognition element as a receiver, biocatalytic processes as a transducer and reporter as an actuator. Sensing unit can respond to light, chemicals, metabolites or temperature through conformational change, kinase activity or intracellular receptors. Processing unit is composed of genetic circuits to respond to a single or multiple input signals. Actuators can be protein based reporters, chemical or electrical signal, or mobility. Illustration is drawn on Keynote.

Organisms evolved to respond to changes in their environment during the course of evolution. Appropriate sensing and processing elements can be selected through extensive genome-wide screening. A suitable actuator can be integrated to the sensory mechanism according to the application area. For increased specificity and sensitivity, biological components such as promoter, ribosome binding site (RBS), post-transcriptional modifiers or transcription factor of the sensory mechanism can be engineered. In addition, cross reactivity with similar analytes should be assessed to eliminate false positive results from complex samples.

Water is vital to all organisms; however, water-quality is not monitored routinely nor clean-water is accessible to everyone. In recent years, heavy metal contamination of water rises the global health concern [25]. The main sources of heavy metal toxicity are agricultural, atmospheric, industrial and pharmaceutical [26]. Even though, some metals such as copper (Cu), iron (Fe), nickel (Ni) and zinc (Zn) are essential in trace amounts for bio-functioning of the cells. The others such as aluminum (Al), arsenic (As), cadmium (Cd), gold (Au), lead (Pb), mercury (Hg) excess amounts trigger poisoning [27,28]. As UNICEF reported in 2020, around 800 million children was poisoned with lead. Although there is no reported data for heavy metal poisoning world-wide, countries reported millions of affected people with single or multiple heavy metals.

Detection of heavy metals is of great importance as they pose a threat to ecosystems and human health. Heavy metal contaminants cannot be detected easily with conventional methods; reliable testing techniques require the use of expertise-dependent advanced instruments. In addition, heavy metal pollution is evident in low-source areas such as mines and smelters with no access to centralized laboratories for water-quality or poisoning testing. Propitiously, whole-cell biosensors allow for rapid, sensitive and specific platform for heavy metal detection in decentralized areas. As whole-cell biosensor analyte detection system is going to be implemented into a point-of-care device, various optimizations for environmental conditions (pH, temperature and salt concentration) and inducer solutions (water and serum) must be conducted. Therefore, whole-cell biosensors are promising candidates for the development of a sensory platform for analytes in environmental and biological samples.

Heavy metals replace their bivalent or monovalent cation counterparts in the cells, this results in the malfunctioning metabolism of the cells. Copper, even though is a heavy metal, is used as a cofactor for enzymes such as catalase, cytochrome c oxidases, ferroxidases, peroxidase, etc. in cells [29,30]. Excess storage of copper ions resulted by a genetic disorder causes Wilson's Disease [31]. Lead exerts its toxicity by elevated reactive oxygen species (ROS) production in the plant cells [32]. Lead ions can replace calcium, magnesium and iron cations, cellular mechanisms such as intercellular signaling, ion transportation, neurotransmitter release and protein folding are impaired [33].

Symptoms of copper and lead heavy metal poisonings across human body have been demonstrated in Figure 2.

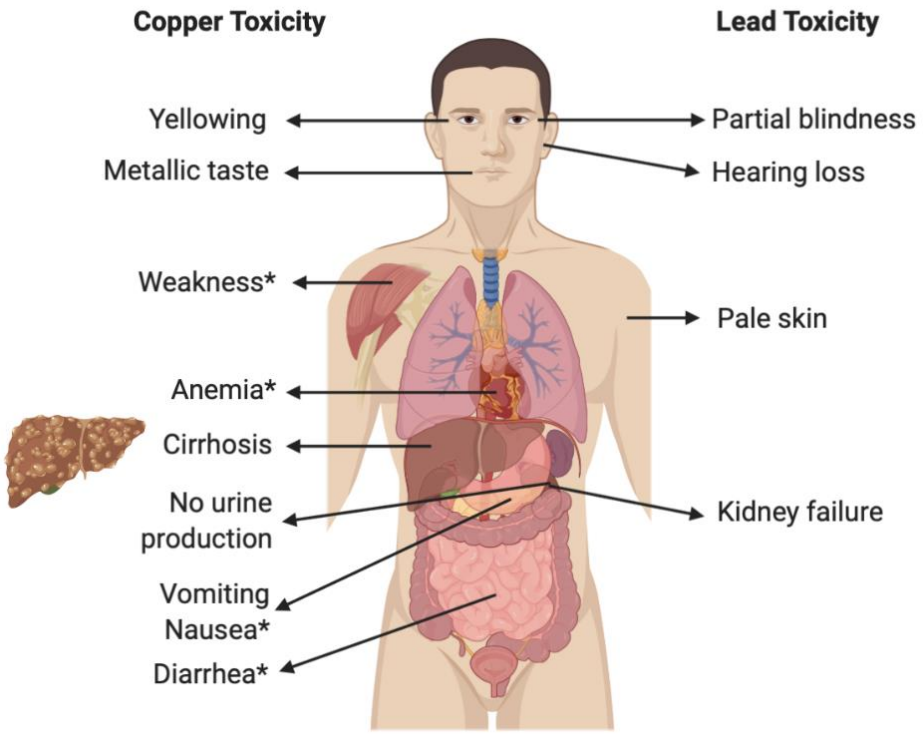

Figure 2. Symptoms of copper and lead heavy metal poisonings across human body. Illustration is drawn on Biorender.

Cadmium poisoning cause anemia, also kidneys lose their function to remove acids from the blood hence imbalanced hemostasis [34]. Excess cadmium triggers apoptosis and instability of genome via impairing DNA repair mechanism at cellular level [35–37]. Arsenic toxicity results in malfunctioning more than 200 enzymes which are involved in several cellular mechanisms including DNA synthesis, DNA repair and energy production pathway [38]. Electron transport chain element are inhibited by arsenic ions, hence ROS production increases and mitochondria are disturbed, these results in

apoptosis of microglial cells [39]. Symptoms of cadmium and arsenic heavy metal poisonings across human body have been demonstrated in Figure 3.

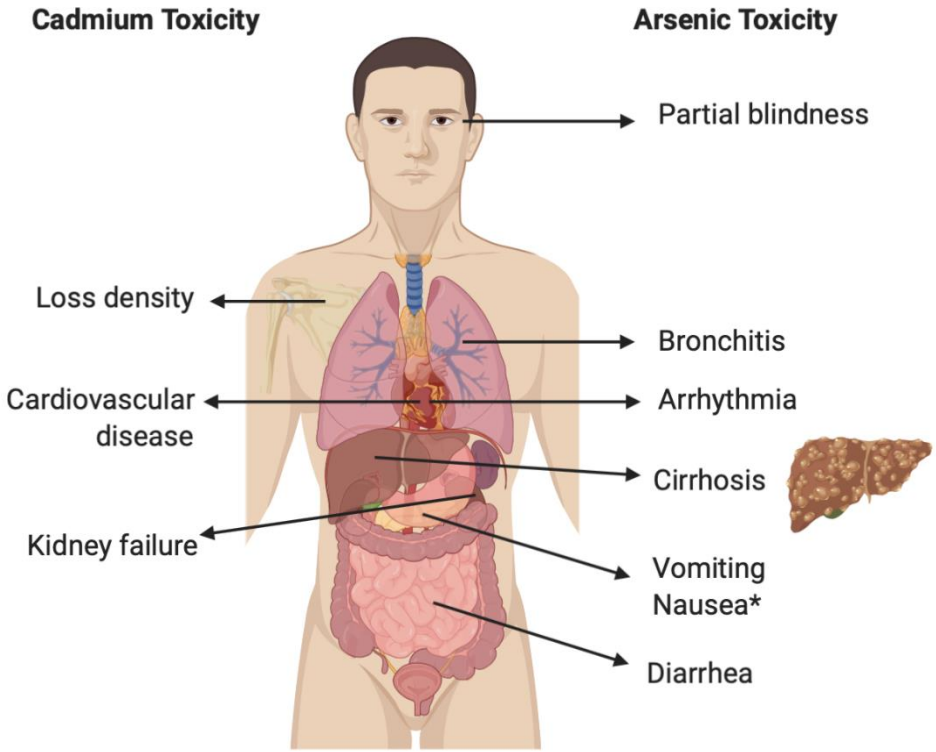

Figure 3. Symptoms of cadmium and arsenic heavy metal poisonings across human body. Illustration is drawn on Biorender.

To address the need of a point-of-care device for multiple analyte detection for heavy metals for water quality control at low-cost, we aim to design and optimize whole-cell biosensors for copper (Cu), lead (Pb), cadmium (Cd) and arsenic (As) heavy metals. *Escherichia coli* has been used as the host organism. In order to construct the circuits for corresponding heavy metals, transcription factor and their cognate promoters have been cloned upstream of a reporter protein (super fold green fluorescent protein (sfGFP), mScarlet or mTagBFP). Constructed circuits have been analyzed for time dependency, then dynamic range measurements were done at maximum response time

obtained from time dependent experiments. For signal amplification and to increase output range, various synthetic biology approaches for optimizations of biosensors have been used: promoter engineering, stronger ribosome binding site (RBS) and hrp synthetic amplification [40]. Through implementation of synthetic amplifier unit, the behavior of repressor based whole-cell biosensors was changed from analog to digital. Then, copper and lead biosensors are implemented in a multiplexed system for multi-input multi-output sensory system for simultaneous detection. These modular whole-cell biosensors aim to precisely identify and integrate multiple analyte condition signals Figure 4.

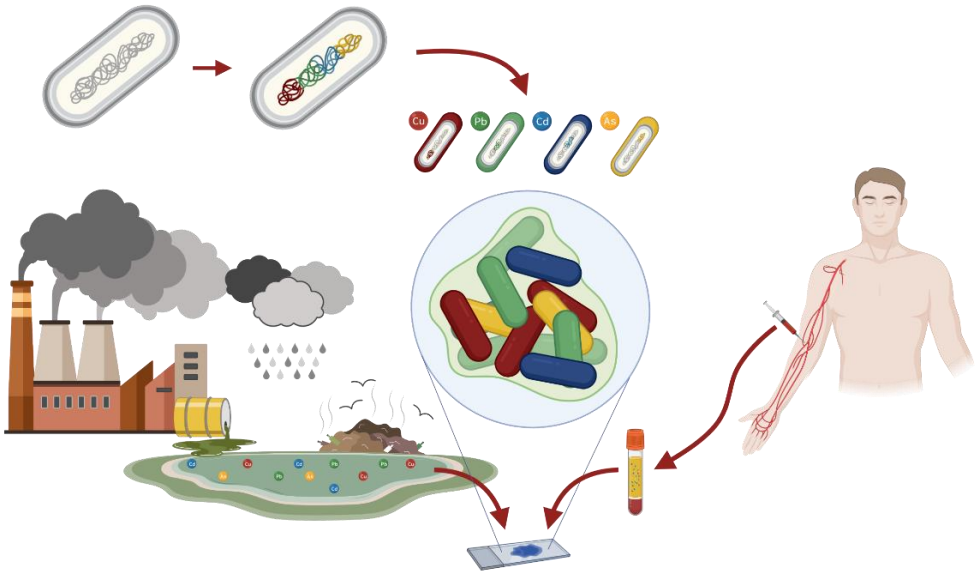

Figure 4. Point-of-care device implementation of multi-input multi-output detection system for heavy metals from environmental or biological samples. Illustration is drawn on Biorender.

1.2 Materials and Methods

1.2.1 Cell Strains, Growth, Maintenance and Storage

In this study, *Escherichia coli (E. coli)* DH5α PRO (New England Biolabs, Inc.) strain was used for cloning and characterization assays. *hsdR17* and *recAI* mutations in genome of *E. coli* DH5α strain enable high efficiency transformation while recA mutation reduces plasmid's recombination, endA mutation enhances plasmid quality via preventing plasmid cleavage (R.Bloom, 1991) (Aaron E. Carnes, 2010). *E. coli* DH5α PRO strain constitutively express *tetR, lacI*, and *araC* genes its genome and spectinomycin is its resistance marker. Cells were grown in Lysogeny Broth (LB) growth media (recipe can be found in Appendix Table 7) with proper antibiotics (1:1000) at 37˚C with shaking at 200 rpm unless otherwise stated. To store cells for further analysis, overnight grown cells in LB media with proper antibiotics were mixed with 50%(v/v) glycerol in equal volumes, and cell stocks were stored at -80˚C storage. Overnight cultures were prepared from glycerol cell stocks, and incubated for 12-16 hours as described previously. Sensor experiments were started with inoculating (1:100) overnight grown cells into fresh growth media (either LB or MOPS buffered growth media) with proper antibiotics. To monitor optical density at 600 nm (OD_{600}) a spectrophotometer (GENESYS 10 Bio, Thermo Scientific) was used.

1.2.2 Chemical Competent Cell Preparation and Transformation

Cells were grown overnight from glycerol stocks as described previously. Next day, overnight grown cells were inoculated (1:100) into fresh LB media with proper antibiotics, and grown at 37˚C with shaking at 200 rpm until OD_{600}

reached 0.2-0.3. Cells were cooled on ice for 10 minutes, then cell suspension were centrifuged at 4˚C for 10 minutes at 3000 rpm. Supernatant was discarded and cell pellet was dissolved in 10% (v/v) TSS Buffer (recipe can be found in Appendix Table 8). Competent cell aliquots were prepared with 100 µl of cell suspension, and competent cell stocks were stored in micro-centrifuge tubes at -80°C.

Transformation procedure was performed as follows: competent cell aliquot was taken out from -80°C storage, and thawed on ice for 30 minutes. Plasmid DNA (50-100 ng) or total reaction volume of completed Gibson assembly reaction was added to thawed competent cell aliquot. DNA-competent cell mixture was incubated on ice for 20-30 minutes. Then, cells are treated with heat-shock at 42˚C for 45 seconds followed by immediate cold-shock on ice for 2 minutes. Next, 250 µl of LB was added onto cell-plasmid suspension, and samples were incubated at 37°C with shaking at 200 rpm for 45-60 minutes. Upon completion of the incubation, cells were collected with centrifugation at 3000 g for 10 minutes, supernatant was discarded until the remaining volume of supernatant was 50-100 µl. Cell pellet was re-suspended in remaining supernatant, cell suspension was spread onto LB-agar plate which is prepared with proper antibiotics, plates were incubated at 37°C without shaking overnight.

1.2.3 Construction of Plasmids and Cloning Procedure

All the plasmid constructs were designed using Benchling (http://benchling.com). Copper and arsenic sensory unit's promoters were amplified with polymerase chain reaction (PCR) from *E. coli* DH5α PRO

genome. Promoters of lead and cadmium sensors were inserted into plasmid backbone with PCR. Engineered promoters with modified -10 mer region for lead promoter and ribosome binding site 30 (RBS30) constructs for copper, lead and cadmium sensors were inserted into plasmid backbone with PCR. Synthetic amplification circuit consisting of *hrpR* and *hrpS* genes together with PhrpL promoter was amplified from plasmid which was ordered from Addgene (Catalog # 78638). Transcription factors of lead and cadmium sensors were synthesized by GENEWIZ Company. Cadmium sensing transcription factor was synthesized with riboregulator part consists of trans activating RNA (taRNA) and cis repressing RNA (crRNA) under control of PltetO promoter. Different reporter units, mScarlet-I gene was amplified from Addgene pEB2-mScarlet-I plasmid (Catalog # 104007) and mTagBFP gene (BBa_K592100) was amplified from iGEM repository part. Forward and reverse primers of aforementioned parts in this study can be seen in Appendix Table 5. For all PCR amplified parts, Q5 Hot Start High-Fidelity DNA Polymerase (New England Biolabs, Inc.) was used, constituents and conditions of PCRs can be found in Appendix Table 9 and Table 10, respectively.

All the PCR amplified products and restriction digestion reactions' products were run in 1% agarose gel stained with 1:1000 SYBR Safe DNA Gel Stain (Thermo Fisher Scientific) for 20-40 minutes at 130 V unless otherwise stated. PCR and digestion products with appropriate size were isolated from agarose gel with Macherey-Nagel's PCR Clean-up kit according to the manufacturer's instructions. 50 ng backbone (either restriction digestion or PCR amplification product) and equal molar insert(s) were assembled with in-house prepared Gibson assembly mixture. The solution was incubated at 50°C for 1 hour. Upon

completion of Gibson assembly protocol, the products were transformed directly into chemical competent *E. coli* DH5α PRO cells.

1.2.4 Verification of Constructs and Sequence Alignments

Single colonies were selected from LB-agar plates and grown overnight in 3-10 mL of LB media with proper antibiotics. For each colony, cells were collected with centrifugation at 8000 rpm for 10 minutes, supernatant was discarded and plasmid isolation was performed with GeneJET Plasmid Miniprep Kit (Thermo Fisher Scientific) according to the manufacturer's instructions. Sequence verification of constructs were done by Sanger Sequencing (GENEWIZ). Sequence alignment verification was done on either Benchling or Geneious software. To do sequence alignment, .gb files were exported from Benchling. Sanger sequencing results (.ab files) and .gb files of plasmid maps were imported to Geneious. Sanger sequencing result was aligned to plasmid map with pairwise alignment tool. When Benchling was used as the alignment tool, Sanger sequencing results (.ab files) were imported to Benchling alignment tool. Then using Multiple Alignment using Fast Fourier Transform (MAFFT) algorithm with standard parameters, Sanger sequencing results were aligned to their corresponding plasmid maps. Sequences of promoters, transcription factors and regulatory subunits used in this study can be found in Appendix Table 1. Maps of all the vectors constructed in this study and their respective verification results of Sanger sequencing can be found in Appendix C and Appendix D, respectively.

1.2.5 Characterization of Whole-Cell Biosensors

E. coli DH5α PRO cells were used as the host organism. Cells carrying sensory plasmids were grown overnight in LB with proper antibiotics, then 1% inoculated into fresh 10 mL of MOPS buffered minimal growth media (recipe can be found in Appendix Table 12) with 0.2% glucose and proper antibiotics, and cells were incubated at 37°C with shaking at 200 rpm. For copper, lead and arsenic biosensors, samples were grown until OD_{600} reached 0.4-0.5. Then, copper biosensor was induced with freshly prepared 10mM $CuSO_4$. Lead and arsenic biosensors were induced with 10 mM PbCl2 and 2 mM As stock solutions, respectively. Unlike others, cells carrying cadmium biosensor parts were grown until OD_{600} reached 0.3, and induced with anhydrotetracycline (aTc) with final concentration of 100ng/µL. Cadmium biosensors grown another 2 hours at 37°C with shaking at 200 rpm, then induced with 10 mM $Cd(CH_3CO_2)_2$ stock solution. Time dependent measurements were done at 0, 2, 4, 6, 8, 16 and 24 hours after induction with specified heavy metals. Dynamic range measurements were made at the earliest time points where the maximum signal from the time dependent measurements was observed.

1.2.6 Heavy Metal Detection in Serum Samples

Overnight grown whole-cell biosensors for copper, lead, cadmium or arsenic cells were 1% inoculated into M63 minimal growth media (recipe can be found in Appendix Table 13) with their respective antibiotics. Copper, lead and arsenic biosensor cells were grown at 37°C with 200 rpm shaking until their OD_{600} reached to 0.4-0.6. Cadmium biosensor cells were grown at 37°C with

200 rpm shaking until their OD_{600} reached to 0.3, and induced with aTc with final concentration of 100ng/µL, cells were incubated for another 2 hours at the same growth conditions. 300 µL of cells were added into 1.5 mL micro-centrifuge tubes, and induced with their respective heavy metals at different concentrations. Cells were incubated for 4 hours before fluorescence and OD_{600} measurements.

1.2.7 Sample Preparation and Fluorescence Measurement

All the fluorescence measurements in this study was conducted with a microplate reader (SpectraMax M5, Molecular Devices), SoftMax Pro (Molecular Devices) software was used for measurements. Samples were prepared for fluorescence measurements as follows: 300 µL of samples were taken into 1.5 mL micro-centrifuge tubes at specified time points mentioned earlier. Samples were centrifuged for 3 minutes at 14000 rpm, supernatant was discarded, and pellets were resuspended in 300 µL 1x PBS (recipe can be found in Appendix Table 14). Then 200 µL of resuspended samples were transferred to Corning 96-well plates (clear flat bottom, polystyrene). Excitation and emisson wavelengths for fluorescence reporters were set as follows: sfGFP (ex: 485 nm, em: 538 nm), mScarlet (ex: 544 nm, em: 612 nm) and mTagBFP (ex: 485 nm, em: 538 nm). OD_{600} measurement was done by setting wavelength to 600 nm at absorbance measurement tool in SoftMax Pro software.

1.2.8 Restriction Digestion, Clean Up, DNA Isolation

All restriction reactions were performed with NEB Restriction enzymes according to the digestion reaction protocol given in Appendix Table 11. All enzymes were purchased from NEB. Clean up and DNA isolation steps were performed with NucleoSpin Gel and PCR Clean-up kit (Macherey-Nagel) according to manufacturer's guidelines.

1.2.9 Statistical Data Analysis

For all the whole-cell biosensor assays' data analysis in this study signal normalization was done as follows: blank fluorescence measurement was subtracted from each samples' fluorescence measurement, and blank OD_{600} measurement was subtracted from each samples' OD_{600} measurement. Then calculated fluorescence value was divided by calculated OD_{600} value for each sample. All measurements were done as triplicates, unless otherwise stated. Data was displayed as mean ± standard deviation. Plotting of graphs and statistical analysis were done on GraphPad Prism version 9.0.0 for Windows, GraphPad Software (www.graphpad.com). Depending on the experimental data sets, one-way or two-way analysis of variance (ANOVA) followed by Dunnett's multiple comparisons tests were performed. Dynamic range graphs of whole-cell biosensors were fitted using "specific binding with Hill slope" equation of GraphPad.

1.3. Results and Discussion

1.3.1 Construction of Whole-Cell Copper Biosensor

To build copper heavy metal biosensor, a suitable promoter region from *E. coli*'s genome PcopA was selected for the synthetic gene circuit. CueR transcription factor binds to PcopA promoter and activates downstream expression in the presence of copper ions in the environment. CueR-PcopA binding plays an active role in copper resistance in *E.coli*. Copper biosensor was constructed by cloning PcopA promoter upstream of sfGFP gene in pET22b vector (Figure 5). Copper biosensor plasmid backbone was constructed from two PCR amplified parts: pET22b-sfGFP backbone and PcopA promoter region, which were amplified from pET22b PhucO sfGFP ProD HucR (gift from Recep Erdem Ahan) and genome of *E. coli* DH5α PRO, respectively (Figure 6). PcopA promoter region was amplified with primers suitable for the Gibson Assembly method. Primers can be found at Appendix B. After PCR products were run on 1% agarose gel, they were isolated from the gel with Macherey-Nagel's PCR Clean-up kit according to the manufacturer's instructions and assembled with the Gibson Assembly method. CueR transcription factor was already expressed in *E.coli*, hence it was not cloned for extra expression as it might be problematic in terms of toxicity and burden on the cell.

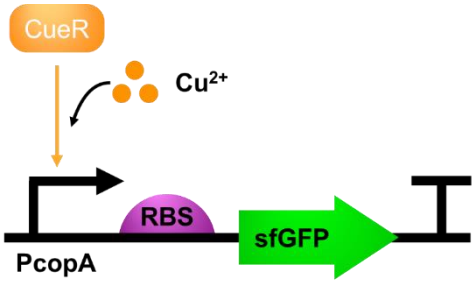

Figure 5. Copper biosensor biological parts and working mechanism. CueR transcription factor binds to PcopA promoter in the presence of copper ions within the cell, and activates downstream expression of sfGFP.

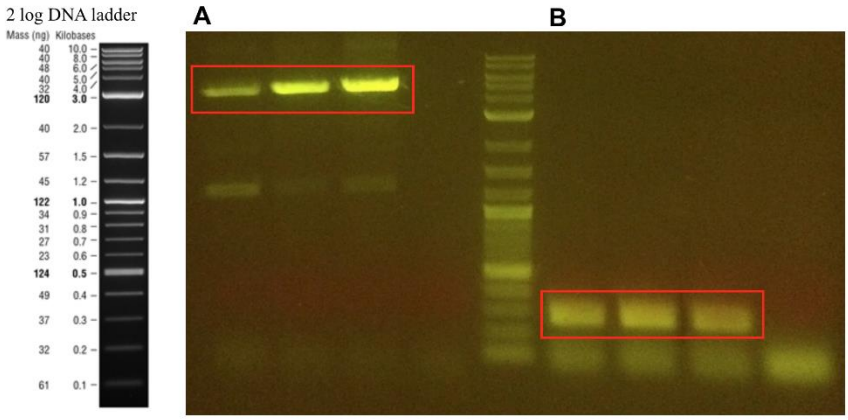

Figure 6. Agarose gel image of the biological parts required for the cloning of the pET22b-PcopA-sfGFP vector. A. PCR product of the linear pET22b-sfGFP backbone, 5300 bp. B. PCR product of PcopA promoter region, 300 bp.

Samples selected from the colonies were first verified by restriction enzyme digestion (Figure 7), and then the samples selected from the restriction enzyme digestion reaction were sent for Sanger sequencing analysis. Plasmid map for copper biosensor and Sanger sequencing result can be found at Appendix C and D, respectively.

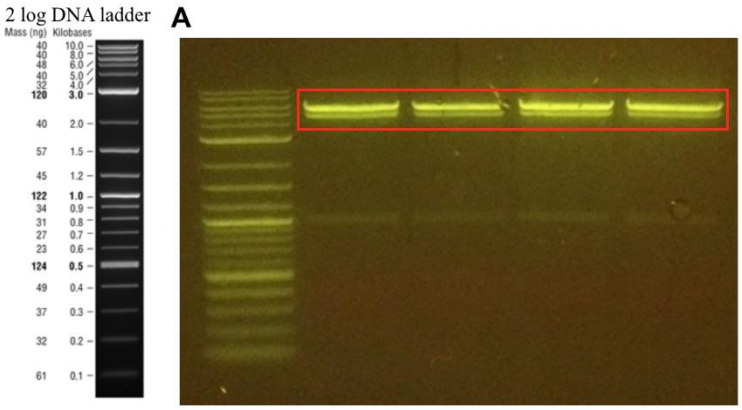

Figure 7. Confirmation of the pET22b-PcopA-sfGFP vector by restriction enzyme digestion. A. The bands expected for the pET22b-PcopA-sfGFP vector as a result of cleavage of XhoI and MluI enzymes were observed at 5000 bp, 650 bp and 400 bp lines, but it is thought that cuts did not appear as a result of mutation in the cut region.

1.3.2 Characterization of Whole-Cell Copper Biosensor

Time dependent and dynamic range analysis of the pET22b-PcopA-sfGFP sensor was made with copper (II) sulfate ($CuSO_4$) salt. Uninduced *E. coli* PRO cells carrying the same vector was used as control. Time dependent measurements were taken at 1^{st}, 2^{nd}, 4^{th}, 6^{th}, 8^{th}, 16^{th} and 24^{th} hours after induction with $CuSO_4$ (Figure 8). In order to understand the response of the pET22b-PcopA-sfGFP sensor to different $CuSO_4$ concentrations, dynamic range with varying $CuSO_4$ concentrations was performed at 2^{nd} hour after induction. Copper biosensor responded even to a concentration as low as 10 µM (Figure 9).

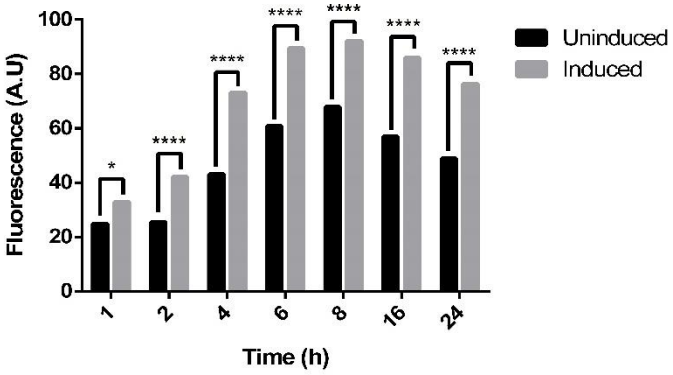

Figure 8. Time dependent characterization of the pET22b-PcopA-sfGFP sensor with 50 µM Copper (II) Sulfate ($CuSO_4$). Experiments were performed in triplicates and measurements were taken at the 1st, 2nd, 4th, 6th, 16th and 24th hours after induction. The results were analyzed with two-way analysis of variance (ANOVA) (GraphPad Prism version 9.0.0), the differences between the groups were marked with "*" ($p \leq 0.05$, $p \leq 0.01$, $p \leq 0.001$ and $p \leq 0.0001$ is represented by "*", "**", "***" and "****" respectively). No marking was made in the groups that did not show significant differences. E. coli cells were grown in LB medium.

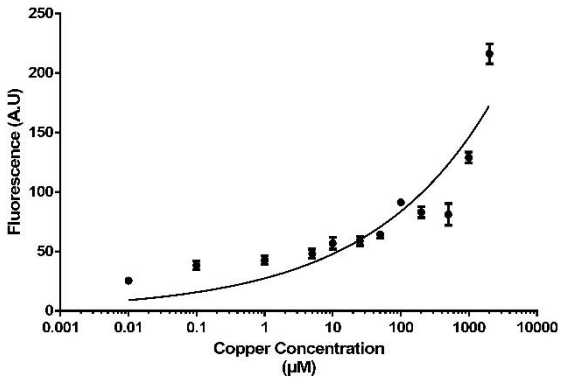

Figure 9. Concentration-dependent characterization of the pET22b-PcopA-sfGFP sensor with $CuSO_4$. Experiments were repeated in triplicates, and measurements were taken at the 2nd hour of induction. E. coli cells were grown in LB medium.

1.3.3 Construction of Whole-Cell Copper RBS30 Biosensor

In order to increase the signal strength of the copper sensor (pET22b-PcopA-sfGFP) but not changing the copper specificity of the PcopA promoter, the ribosome binding site (RBS) between the PcopA promoter and the sfGFP gene was replaced with another stronger ribosome binding site, iGEM BBa_B0030 (referred as RBS30 in this study) (Figure 10). The same vector backbone was

used to see its effect. For this, firstly, pET22b-PcopA-sfGFP vector was linearly amplified by PCR reaction by adding RBS30 parts while removing the old RBS region (Figure 11). Then PCR product was extracted from agarose gel and subjected to Gibson Assembly for self-assembly. Plasmid map for copper RBS30 biosensor and Sanger sequencing result can be found at Appendix C and D, respectively.

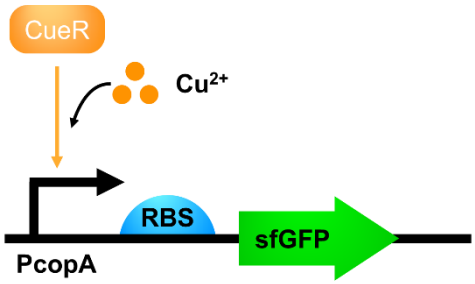

Figure 10. Copper RBS30 sfGFP biosensor biological parts and working mechanism. CueR transcription factor binds to PcopA promoter in the presence of copper ions within the cell, and activates downstream expression of sfGFP with stronger RBS30.

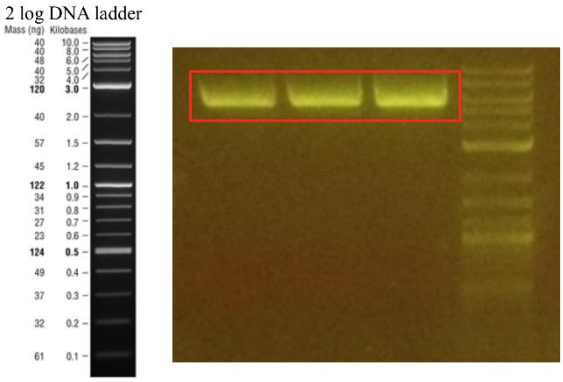

Figure 11. Agarose gel image of the biological parts required for the cloning of the pET22b-PcopA-RBS30-sfGFP vector. PCR product of the linear pET22b-PcopA-RBS30-sfGFP backbone, 5500 bp.

1.3.4 Characterization of Whole-Cell Copper RBS30 Biosensor

Time dependent and dynamic range analysis of the pET22b-PcopA-RBS30-sfGFP sensor was made with Copper (II) sulfate ($CuSO_4$) salt. Uninduced *E. coli* PRO cells carrying the same vector was used as a control. Time dependent measurements were taken at 1st, 2nd, 4th, 6th, 8th, 16th and 24th hours after induction with CuSO4 (Figure 12). In order to understand the response of the pET22b-PcopA-RBS30-sfGFP sensor to different $CuSO_4$ concentrations, dynamic range with varying $CuSO_4$ concentrations was performed at 2nd hour after induction. Copper RBS30 biosensor responded even to a concentration as low as 1 µM (Figure 13).

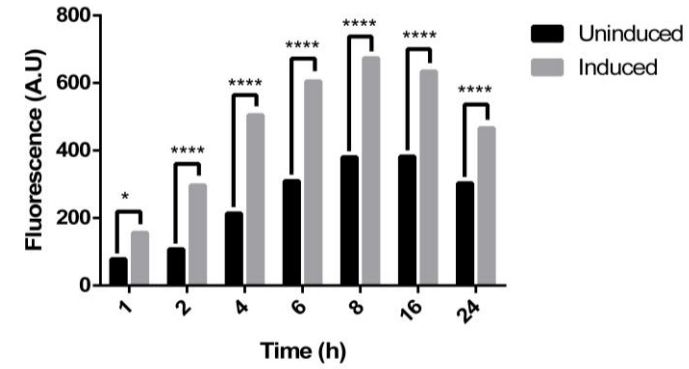

Figure 12. Time dependent characterization of the pET22b-PcopA-RBS30-sfGFP sensor with 50 µM Copper (II) Sulfate ($CuSO_4$). Experiments were performed in triplicates and measurements were taken at the 1st, 2nd, 4th, 6th, 16th and 24th hours after induction. The results were analyzed with two-way analysis of variance (ANOVA) (GraphPad Prism version 9.0.0), the differences between the groups were marked with "*" ($p \leq 0.05$, $p \leq 0.01$, $p \leq 0.001$ and $p \leq 0.0001$ is represented by "*", "**", "***" and "****" respectively). No marking was made in the groups that did not show significant differences. E. coli cells were grown in LB medium.

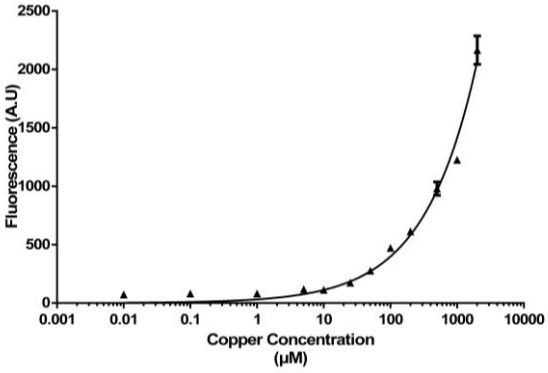

Figure 13. Concentration-dependent characterization of the pET22b-PcopA-RBS30-sfGFP sensor with $CuSO_4$. Experiments were repeated in triplicates, and measurements were taken at the 2nd hour of induction. E. coli cells were grown in LB medium.

1.3.5 Construction of Whole-Cell Copper hrp Biosensor

To increase the signal strength of the copper sensor (pET22b-PcopA-sfGFP) while not changing the copper specificity of the PcopA promoter, a synthetic amplifier system was used. The hrp synthetic signal amplifier system was used to increase the signal of other sensors including arsenic. Syhthetic amplifier biological part, hrp, was added to the region between the PcopA promoter and the sfGFP gene (Figure 14). The same vector backbone was used to see its effect. For this, firstly, the pET22b-PcopA-sfGFP vector was amplified linearly (Figure 15A.) and the hrp signal amplifier system was linearly amplified from the pBW103ParsR-Amp30C vector (from Addgene, Plasmid #78638) (Figure 15B.). After PCR products were run on 1% agarose gel, they were isolated from the gel with Macherey-Nagel's PCR Clean-up kit according to the manufacturer's instructions, and assembled with the Gibson Assembly method.

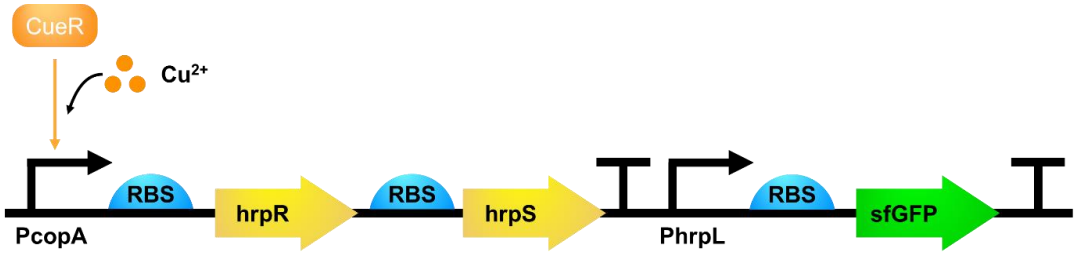

Figure 14.Copper hrp biosensor biological parts and working mechanism. CueR transcription factor binds to PcopA promoter in the presence of copper ions within the cell, and activates downstream expression of hrpR and hrpS proteins. Then these two proteins form a complex, and bind to PhrpL promoter and activates sfGFP expression.

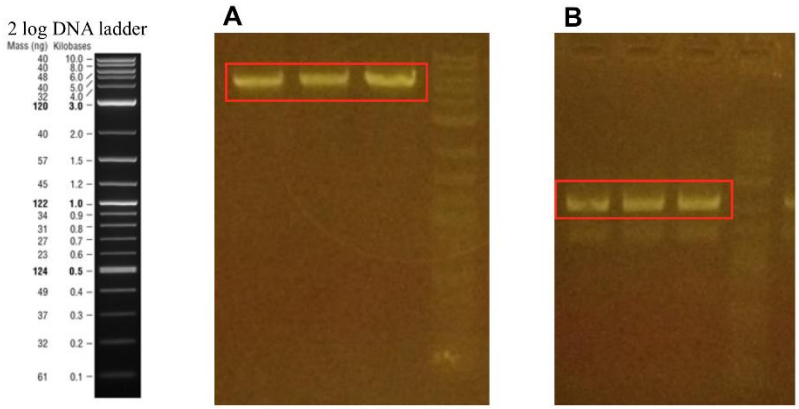

Figure 15. Agarose gel image of the biological parts required for the cloning of the pET22b-PcopA-hrp-sfGFP vector. A. PCR product of the linear pET22b-PcopA-sfGFP backbone, 5300 bp. B. PCR product of hrp signal enhancer region, 2300 bp.

Samples selected from the colonies were first verified with colony PCR (Figure 16), and then colony PCR verified samples were sent for Sanger sequencing analysis. Plasmid map for copper hrp biosensor and Sanger sequencing result can be found at Appendix C and D, respectively.

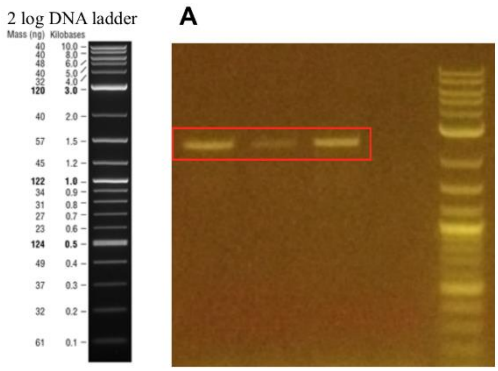

Figure 16. Confirmation of the pET22b-PcopA-hrp-sfGFP vector with colony PCR. A. The bands expected for the PCR amplified hrp biological parts were observed at 2300 bp.

1.3.6 Characterization of Whole-Cell Copper hrp Biosensor

Time dependent and dynamic range analysis of the pET22b-PcopA-hrp-sfGFP sensor was made with $CuSO_4$ salt. Uninduced *E. coli* PRO cells carrying the same vector was used as control in the time dependent measurements taken at 1^{st}, 2^{nd}, 4^{th}, 6^{th}, 8^{th}, 16^{th} and 24^{th} hours of induction (Figure 17). To understand the response of the pET22b-PcopA-hrp-sfGFP sensor to different $CuSO_4$ concentrations, dynamic range with varying $CuSO_4$ concentrations was performed at 6^{th} hour after induction. Copper hrp biosensor response was observed to be very high even to concentrations as low as 10 nM, but signal level was decreased at high concentrations (Figure 18).

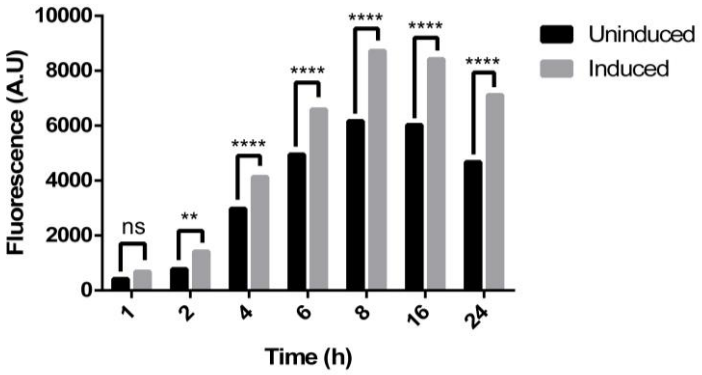

Figure 17. Time dependent characterization of the pET22b-PcopA-hrp-sfGFP sensor with 50 µM Copper (II) Sulfate ($CuSO_4$). Experiments were repeated in triplicates and measurements were taken at the 1st, 2nd, 4th, 6th, 16th and 24th hours after induction. The results were analyzed with two-way analysis of variance (ANOVA) (GraphPad Prism version 9.0.0), the differences between the groups were marked with "*" ($p \leq 0.05$, $p \leq 0.01$, $p \leq 0.001$ and $p \leq 0.0001$ is represented by "*", "**", "***" and "****" respectively). "ns" was used in the groups that did not show significant differences. E. coli cells were grown in LB medium.

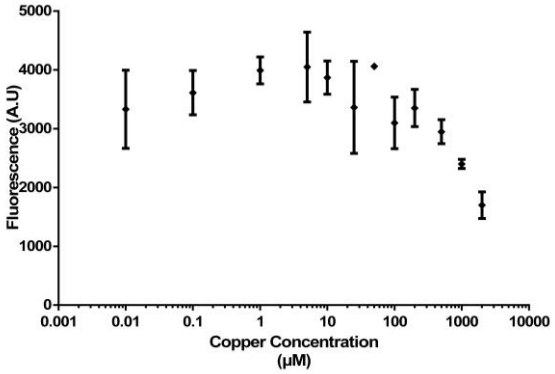

Figure 18. Concentration-dependent characterization of the pET22b-PcopA-hrp-sfGFP sensor with $CuSO_4$. Experiments were repeated in triplicates, and measurements were taken at the 6th hour of induction. E. coli cells were grown in LB medium.

Comparative characterization of the concentration dependent dynamics of pET22b-PcopA-sfGFP (denoted as *E.coli*), pET22b-PcopA-RBS30-sfGFP (denoted as RBS30) and pET22b-PcopA-hrp-sfGFP (denoted as hrp) biosensors with $CuSO_4$ was given below (Figure 19).

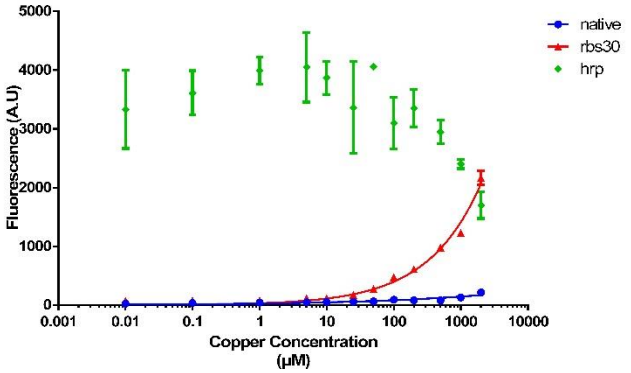

Figure 19. Comparative characterization of the concentration-dependent dynamics of pET22b-PcopA-sfGFP (denoted as *E.coli*), pET22b-PcopA-RBS30-sfGFP (denoted as RBS30) and pET22b-PcopA-hrp-sfGFP (denoted as hrp) biosensors with $CuSO_4$. Experiments were repeated in triplicates, and measurements were taken at the 2nd hour of induction for pET22b-PcopA-sfGFP and pET22b-PcopA-RBS30-sfGFP biosensors and 6th hour of induction for and pET22b-PcopA-hrp-sfGFP biosensor E. coli cells were grown in LB medium.

1.3.7 Construction of Whole-Cell Copper RBS30 mScarlet Biosensor

To combine the copper RBS30 biosensor (pET22b-PcopA-RBS30-mScarlet) with other heavy metal biosensors for multi-input multi-output system, sfGFP reporter gene was replaced with mScarlet gene (which can be distinguished from sfGFP) (Figure 20). For this purpose, pET22b-PcopA-RBS30 vector and mScarlet gene were amplified with PCR. After PCR products were run on 1% agarose gel, they were isolated from the gel with Macherey-Nagel's PCR Clean-up kit according to the manufacturer's instructions and assembled with the Gibson Assembly method (Figure 21). Samples were sent for Sanger sequencing analysis. Plasmid map for copper RBS30 mScarlet biosensor and Sanger sequencing result can be found at Appendix C and D, respectively.

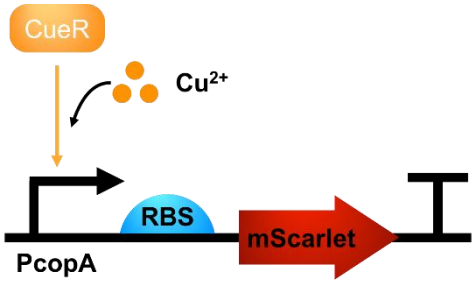

Figure 20. Copper RBS30 mScarlet biosensor biological parts and working mechanism. CueR transcription factor binds to PcopA promoter in the presence of copper ions within the cell, and activates downstream expression of mScarlet with stronger RBS30.

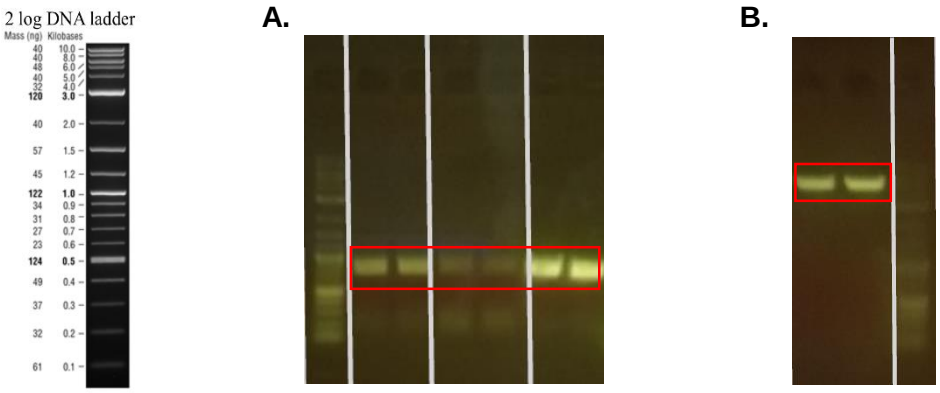

Figure 21. Agarose gel image of the fragment required for the cloning of the pET22b-PcopA-RBS30-mScarlet vector. A. mScarlet linear DNA fragment, 700bp. B The backbone vector pET22b-PcopA-RBS30, 5000 bp.

1.3.8 Characterization of Whole-Cell Copper RBS30 mScarlet Biosensor

Time dependent and dynamic range analysis of the pET22b-PcopA-RBS30-mScarlet biosensor was made with Copper (II) sulfate ($CuSO_4$) salt. Uninduced *E. coli* PRO cells carrying the same vector was used as a control. Time dependent measurements were taken at 0^{th}, 2^{nd}, 4^{th}, 6^{th}, 8^{th}, 16^{th} and 24^{th} hours after induction with $CuSO_4$ (Figure 22). To understand the response of the pET22b-PcopA-RBS30-mScarlet biosensor to different $CuSO_4$ concentrations, dynamic range with varying $CuSO_4$ concentrations was performed at 2^{nd} hour

after induction. Copper RBS30 mScarlet biosensor responded even to a concentration as low as 5 µM (Figure 23).

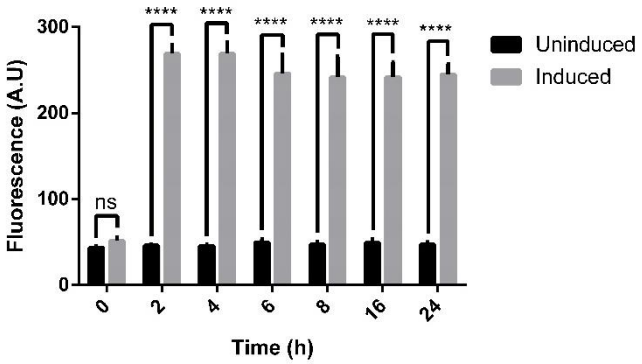

Figure 22. Time-dependent characterization of the pET22b-PcopA-RBS30-mScarlet biosensor with 50 µM Copper (II) Sulfate (CuSO4). Experiments were repeated in triplicates, and measurements were taken at 0th, 2nd, 4th, 6th, 16th and 24th hours after induction. The results were analyzed with two-way analysis of variance (ANOVA) (GraphPad Prism version 9.0.0), the differences between the groups were marked with "*" ($p \leq 0.05$, $p \leq 0.01$, $p \leq 0.001$ and $p \leq 0.0001$ is represented by "*", "**", "***" and "****" respectively). "ns" was used in the groups that did not show significant differences. *E. coli* cells were grown in chemically defined MOPS buffered minimal growth media.

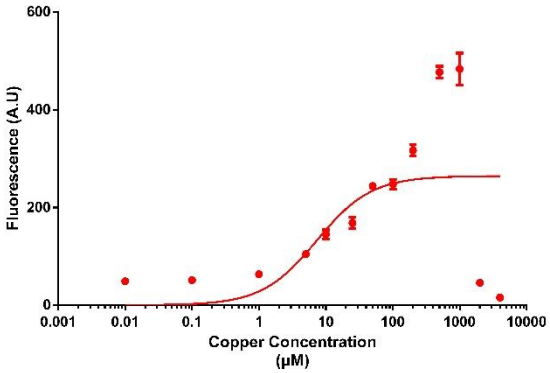

Figure 23. Concentration-dependent characterization of the pET22b-PcopA-RBS30-mScarlet biosensor with Copper (II) Sulfate ($CuSO_4$) Experiments were repeated in triplicates and measurements taken at the 2nd hour of induction. *E. coli* cells were grown in chemically defined MOPS buffered minimal growth media.

1.3.9 Characterization of Whole-Cell Copper Biosensors with Serum Samples

To test the applicability of biosensors for diagnosis of heavy metal poisoning, biosensors were tested with M63 growth media mixed with fetal bovine serum (FBS). Dynamic range analysis of the pET22b-PcopA-RBS30-sfGFP and

pET22b-PcopA-RBS30-mScarlet biosensors were made with Copper (II) sulfate ($CuSO_4$) salt. *E.coli* PRO cells carrying their corresponding biosensor circuits were grown overnight in LB, then 1% inoculated into fresh LB media with proper antibiotics. When OD_{600} reached 0.4-0.5, samples were centrifuged at 3000 rpm for 10 minutes. Supernatant was discarded from each sample, and pellets were resuspended in equal volume of a mixture of heat-treated FBS and M63 minimal media (3:1), and induced with different concentrations of $CuSO_4$. Fluorescence and OD_{600} measurements were taken at 16th hour of induction. Copper RBS30 sfGFP biosensor was observed to be responsive to concentrations as low as 10 µM $CuSO_4$ (Figure 24). However, copper RBS30 mScarlet different reporter biosensor was observed to be responsive to concentrations as low as 100 µM (Figure 25). Comparative serum response characterization of the concentration dependent dynamics of pET22b-PcopA-RBS30-sfGFP (denoted as rbs30 sfGFP) and pET22b-PcopA-RBS30-mScarlet (denoted as rbs30 mScarlet) biosensors with $CuSO_4$ was given below (Figure 26).

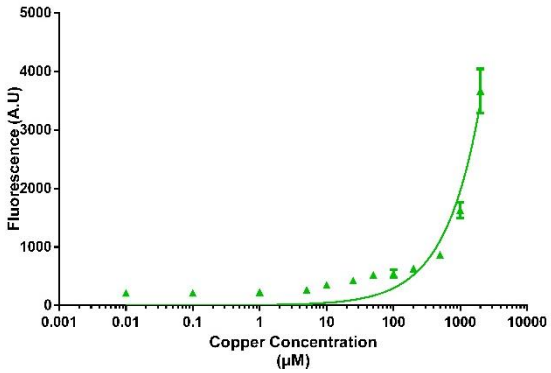

Figure 24. Concentration-dependent characterization of the pET22b-PcopA-RBS30-sfGFP biosensor with Copper (II) Sulfate ($CuSO_4$). Experiments were repeated in triplicates, and measurements were taken at the 16th hour of induction. E. coli cells were grown in LB media until OD_{600} reached 0.4-0.5, then transferred to a mixture of heat-treated FBS and M63 minimal media (3:1) and induced with different concentrations of $CuSO_4$.

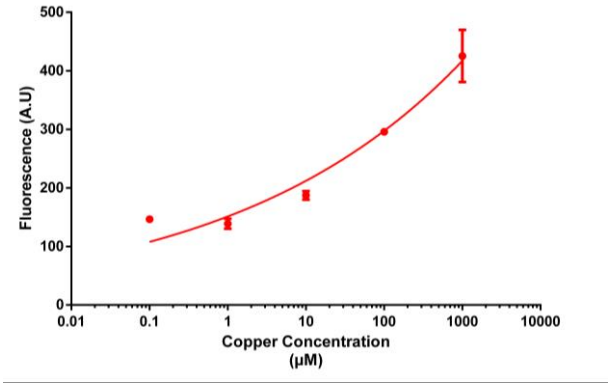

Figure 25. Concentration-dependent characterization of the pET22b-PcopA-RBS30-mScarlet biosensor with Copper (II) Sulfate ($CuSO_4$). A. Concentration-dependent graph of relative fluorescence value. B. Image of cells growing in the falcon under blue light. C. Visualization of the remaining pellet after centrifugation of the samples under blue light. D. Image of cell pellet dissolved in 1xPBS under blue light. Experiments were repeated in triplicates, and measurements were taken at the 16th hour of induction. E. coli cells were grown in LB media until OD_{600} reached 0.4-0.5, then transferred to a mixture of heat-treated FBS and M63 minimal media (3:1) and induced with different concentrations of $CuSO_4$.

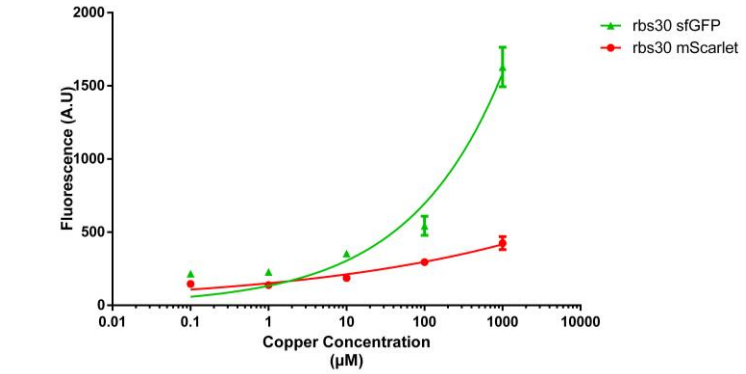

Figure 26. Comparative characterization of the concentration-dependent dynamics of pET22b-PcopA-RBS30-sfGFP (denoted as *rbs30 sfGFP*) and pET22b-PcopA-RBS30-mScarlet (denoted as *rbs30 mScarlet*) biosensors with Copper (II) Sulfate ($CuSO_4$). Experiments were repeated in triplicates, and measurements were taken at the 16th hour of induction for both biosensors. E. coli cells were grown in LB media until OD_{600} reached 0.4-0.5, then transferred to a mixture of heat-treated FBS and M63 minimal media (3:1) and induced with different concentrations of $CuSO_4$.

1.3.10 Characterization of Whole-Cell Copper Biosensors with Different Inoculation Conditions

Copper biosensors: pET22b-PcopA-sfGFP, pET22b-PcopA-RBS30-sfGFP and pET22b-PcopA-hrp-sfGFP circuits were tested under different growth conditions. Copper is already present within the cell as it is used as cofactor.

Previously all the characterization experiments were performed in LB containing yeast extract. For example, copper-dependent cytochrome c oxidase [41] and other copper dependent enzymes require trace amounts of copper within the cell. Therefore, background signal in LB grown E.coli cells is higher. Hence, *E.coli* PRO cells containing copper biosensor circuits were grown and inoculated in either LB or MOPS buffered minimal media to determine best option for characterization of biosensors. Time dependent analysis of the pET22b-PcopA-sfGFP, pET22b-PcopA-RBS30-sfGFP and pET22b-PcopA-hrp-sfGFP biosensors was made with Copper (II) sulfate ($CuSO_4$) salt. Uninduced *E. coli* PRO cells carrying their corresponding vectors were used as control, measurements were taken at 1^{st}, 2^{nd}, 4^{th}, 6^{th}, 8^{th}, 16^{th} and 24^{th} hours of induction (Figure 27). *E.coli* PRO cells containing each of the copper biosensor circuits were grown on agar plate, were grown in LB media overnight, then inoculated into MOPS buffered chemically defined minimal media the next day (Figure 27 A, B, C). E.coli PRO cells containing each of the copper biosensor circuits were grown on agar plate, were grown in chemically defined MOPS buffered minimal media, then inoculated into chemically defined MOPS buffered minimal media the next day (Figure 27 D, E, F). Then, when the cells reached the desired OD_{600} value 0.4-0.5, samples were induced with 50 μM $CuSO_4$. There was significant decrease in the background signal of pET22b-PcopA-sfGFP, pET22b-PcopA-RBS30-sfGFP biosensor circuits compared to the growth condition performed before (overnight cells were grown in LB media, and inoculation was done in LB media). Moreover, for both biosensors significant signal response increase was observed at 1^{st} hour after induction, as earliest detection was one of the

purposes. These inoculation optimizations were necessary to get the best performing and quickest biosensors. However, neither inoculation conditions can decrease the background signal of pET22b-PcopA-hrp-sfGFP biosensor, so this biosensor was excluded from further characterizations.

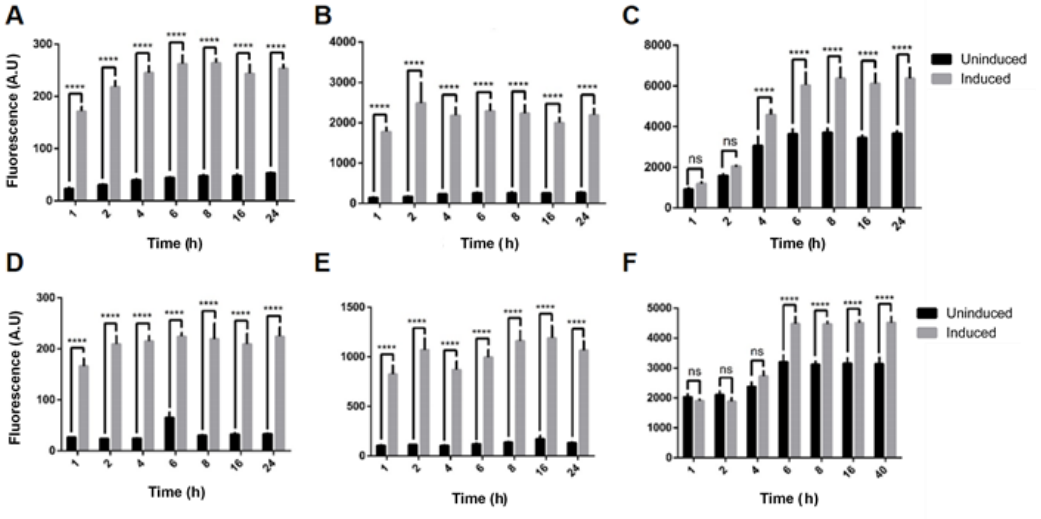

Figure 27. Time-dependent characterization of copper biosensors pET22b-PcopA-sfGFP (A, D), pET22b-PcopA-RBS30-sfGFP (B, E) and pET22b-PcopA-hrp-sfGFP (C, F) with 50 µM Copper (II) Sulfate (CuSO4). Time-dependent graphs of relative fluorescence values. Uninduced *E. coli* PRO cells carrying their corresponding vectors were used as control, measurements were taken at 1st, 2nd, 4th, 6th, 8th, 16th and 24th hours of induction. *E.coli* PRO cells containing each of the copper biosensor circuits were grown on agar plate, were grown in LB media overnight, then inoculated into MOPS buffered chemically defined minimal media the next day (A, B, C). E.coli PRO cells containing each of the copper biosensor circuits were grown on agar plate, were grown in chemically defined MOPS buffered minimal media, then inoculated into chemically defined MOPS buffered minimal media the next day (D, E, F). Experiments were repeated in triplicates, and measurements were taken at 1st, 2nd, 4th, 6th, 16th and 24th hours after induction. The results were analyzed with two-way analysis of variance (ANOVA) (GraphPad Prism version 9.0.0), the differences between the groups were marked with "*" ($p \leq 0.05$, $p \leq 0.01$, $p \leq 0.001$ and $p \leq 0.0001$ is represented by "*", "**", "***" and "****" respectively). "ns" was used in the groups that did not show significant differences. *E. coli* cells were grown in chemically defined MOPS buffered minimal growth media.

1.3.11 Characterization of Whole-Cell Copper Biosensors at Different pH Values

To design a point-of-care sensor system, testing platform (in this case whole-cell biosensors) should be adaptable to environmental changes and sensing behavior must be characterized. In this part of the study, whole-cell biosensors were tested at different pH, temperature and salt concentrations. Here, copper whole-cell biosensor was characterized under pH values 5, 7 and 9. MOPS buffered chemically defined media was adjusted with HCl and NaOH to have the desired pH value. Time-dependent analysis of the pET22b-PcopA-RBS30-sfGFP biosensor was made with Copper (II) sulfate ($CuSO_4$) salt. Uninduced *E. coli* PRO cells carrying the pET22b-PcopA-RBS30-sfGFP vector was used as a control. *E.coli* PRO cells carrying pET22b-PcopA-RBS30-sfGFP copper sensing circuit were grown overnight in LB, then 1% inoculated into fresh MOPS buffered minimal media with proper antibiotics. When OD_{600} reached 0.4-0.5, samples were induced with 200 μM $CuSO_4$. Fluorescence and OD_{600} measurements were taken at 0^{th}, 2^{nd}, 4^{th}, 6^{th}, 8^{th}, 16^{th} and 24^{th} hours after induction with $CuSO_4$. Copper RBS30 sfGFP biosensor was observed to have higher background signal when pH value of the growth media was 5 (Figure 28) compared to cases when pH value was either 7 (Figure 29) or 9 (Figure 30).

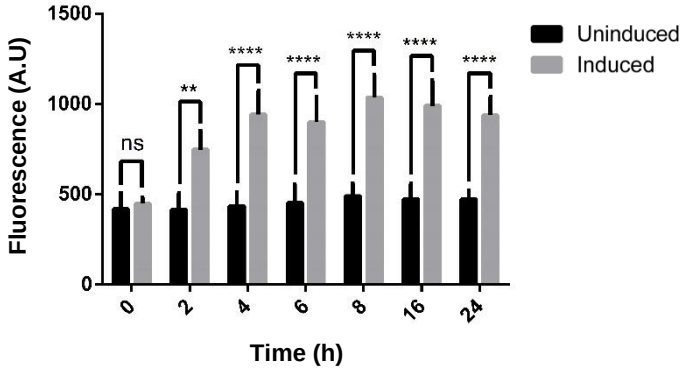

Figure 28. Time-dependent characterization of the pET22b-PcopA-RBS30-sfGFP sensor with 200 µM Copper (II) Sulfate (CuSO4).. *E. coli PRO* cells were grown in chemically defined MOPS buffered minimal growth media with pH value equal to 5. A. Time-dependent graph of relative fluorescence value. B. Image of cells growing in the falcon under blue light. C. Visualization of the remaining pellet after centrifugation of the samples under blue light. D. Image of cell pellet dissolved in 1xPBS under blue light. Experiments were repeated in triplicates, and measurements were taken at 0^{th}, 2^{nd}, 4^{th}, 6^{th}, 16^{th} and 24^{th} hours after induction. The results were analyzed with two-way analysis of variance (ANOVA) (GraphPad Prism version 9.0.0), the differences between the groups were marked with "*" ($p \leq 0.05$, $p \leq 0.01$, $p \leq 0.001$ and $p \leq 0.0001$ is represented by "*", "**", "***" and "****" respectively). "ns" was used in the groups that did not show significant differences.

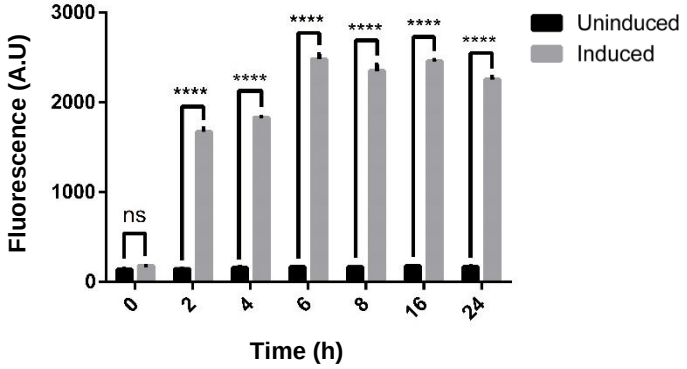

Figure 29. Time-dependent characterization of the pET22b-PcopA-RBS30-sfGFP sensor with 200 µM Copper (II) Sulfate (CuSO4).. *E. coli PRO* cells were grown in chemically defined MOPS buffered minimal growth media with pH value equal to 7. A. Time-dependent graph of relative fluorescence value. B. Image of cells growing in the falcon under blue light. C. Visualization of the remaining pellet after centrifugation of the samples under blue light. D. Image of cell pellet dissolved in 1xPBS under blue light. Experiments were repeated in triplicates, and measurements were taken at 0^{th}, 2^{nd}, 4^{th}, 6^{th}, 16^{th} and 24^{th} hours after induction. The results were analyzed with two-way analysis of variance (ANOVA) (GraphPad Prism version 9.0.0), the differences between the groups were marked with "*" ($p \leq 0.05$, $p \leq 0.01$, $p \leq 0.001$ and $p \leq 0.0001$ is represented by "*", "**", "***" and "****" respectively). "ns" was used in the groups that did not show significant differences.

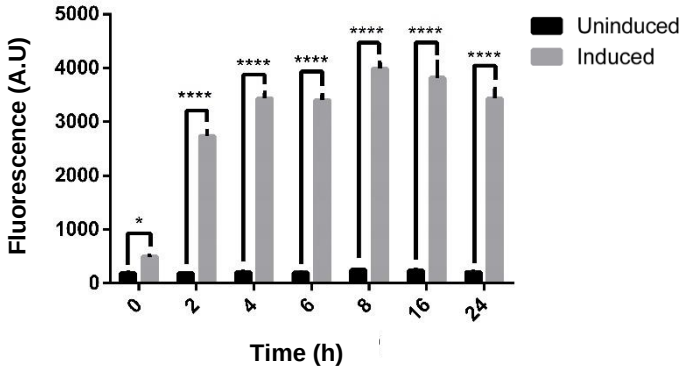

Figure 30. Time-dependent characterization of the pET22b-PcopA-RBS30-sfGFP sensor with 200 µM Copper (II) Sulfate (CuSO4).. *E. coli PRO* cells were grown in chemically defined MOPS buffered minimal growth media with pH value equal to 9. A. Time-dependent graph of relative fluorescence value. B. Image of cells growing in the falcon under blue light. C. Visualization of the remaining pellet after centrifugation of the samples under blue light. D. Image of cell pellet dissolved in 1xPBS under blue light. Experiments were repeated in triplicates, and measurements were taken at 0^{th}, 2^{nd}, 4^{th}, 6^{th}, 16^{th} and 24^{th} hours after induction. The results were analyzed with two-way analysis of variance (ANOVA) (GraphPad Prism version 9.0.0), the differences between the groups were marked with "*" ($p \leq 0.05$, $p \leq 0.01$, $p \leq 0.001$ and $p \leq 0.0001$ is represented by "*", "**", "***" and "****" respectively). "ns" was used in the groups that did not show significant differences.

1.3.12 Characterization of Whole-Cell Copper Biosensors at Different Temperature Values

Copper whole-cell biosensor was characterized under different temperature values of 25°C, 37°C and 42°C. Time-dependent analysis of the pET22b-PcopA-RBS30-sfGFP biosensor was made with Copper (II) sulfate ($CuSO_4$) salt. Uninduced *E. coli* PRO cells carrying the pET22b-PcopA-RBS30-sfGFP vector was used as a control. *E.coli* PRO cells carrying pET22b-PcopA-RBS30-sfGFP copper sensing circuit were grown overnight in LB, then 1% inoculated into fresh MOPS buffered minimal media with proper antibiotics. When OD_{600} reached 0.4-0.5, samples were induced with 200 µM $CuSO_4$. After dilution, samples were grown at either 25°C, 37°C and 42°C. Fluorescence and OD_{600} measurements were taken at 0^{th}, 2^{nd}, 4^{th}, 6^{th}, 8^{th}, 16^{th} and 24^{th} hours after induction with $CuSO_4$. Copper RBS30 sfGFP biosensor was observed to have higher background signal when temperature was 42°C (Figure 33)

compared to cases when temperature was either 25°C (Figure 31) or 37°C (Figure 32). Relative fluorescence signal level was observed to be lower at 25°C temperature (Figure 31).

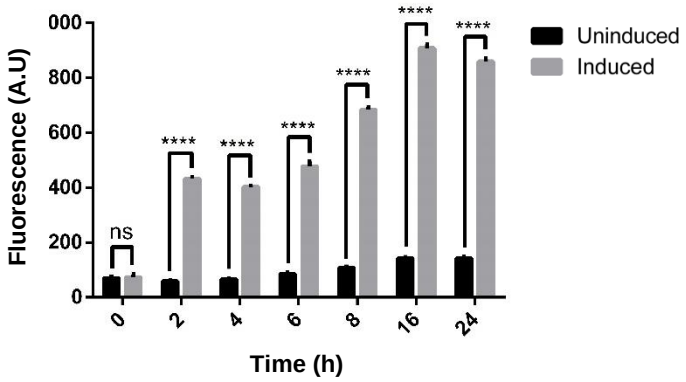

Figure 31. Time-dependent characterization of the pET22b-PcopA-RBS30-sfGFP sensor with 200 µM Copper (II) Sulfate (CuSO4).. *E. coli PRO* cells were grown in chemically defined MOPS buffered minimal growth media at 25°C. A. Time-dependent graph of relative fluorescence value. B. Image of cells growing in the falcon under blue light. C. Visualization of the remaining pellet after centrifugation of the samples under blue light. D. Image of cell pellet dissolved in 1xPBS under blue light. Experiments were repeated in triplicates, and measurements were taken at 0th, 2nd, 4th, 6th, 16th and 24th hours after induction. The results were analyzed with two-way analysis of variance (ANOVA) (GraphPad Prism version 9.0.0), the differences between the groups were marked with "*" ($p \leq 0.05$, $p \leq 0.01$, $p \leq 0.001$ and $p \leq 0.0001$ is represented by "*", "**", "***" and "****" respectively). "ns" was used in the groups that did not show significant differences.

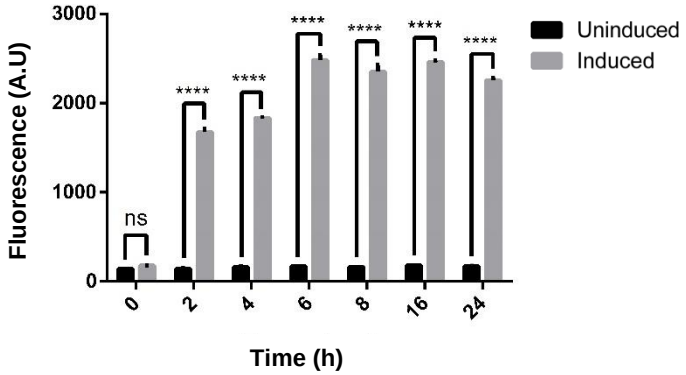

Figure 32. Time-dependent characterization of the pET22b-PcopA-RBS30-sfGFP sensor with 200 µM Copper (II) Sulfate (CuSO4).. *E. coli PRO* cells were grown in chemically defined MOPS buffered minimal growth media at 37°C. A. Time-dependent graph of relative fluorescence value. B. Image of cells growing in the falcon under blue light. C. Visualization of the remaining pellet after centrifugation of the samples under blue light. D. Image of cell pellet dissolved in 1xPBS under blue light. Experiments were repeated in triplicates, and measurements were taken at 0th, 2nd, 4th, 6th, 16th and 24th hours after induction. The results were analyzed with two-way analysis of variance (ANOVA) (GraphPad Prism version 9.0.0), the differences between the groups were marked with "*" ($p \leq 0.05$, $p \leq 0.01$, $p \leq 0.001$ and $p \leq 0.0001$ is represented by "*", "**", "***" and "****" respectively). "ns" was used in the groups that did not show significant differences.

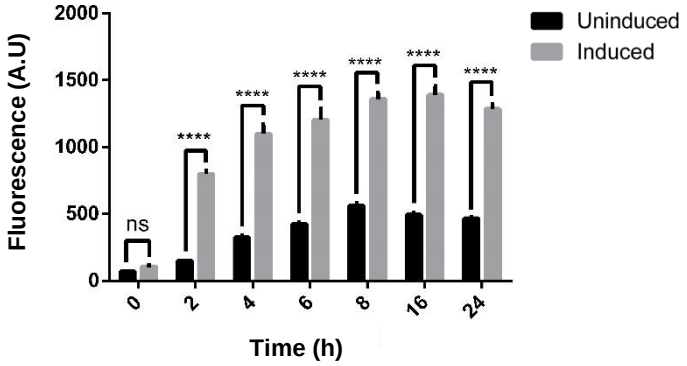

Figure 33. Time-dependent characterization of the pET22b-PcopA-RBS30-sfGFP sensor with 200 µM Copper (II) Sulfate (CuSO4).. *E. coli PRO* cells were grown in chemically defined MOPS buffered minimal growth media at 42°C. A. Time-dependent graph of relative fluorescence value. B. Image of cells growing in the falcon under blue light. C. Visualization of the remaining pellet after centrifugation of the samples under blue light. D. Image of cell pellet dissolved in 1xPBS under blue light. Experiments were repeated in triplicates, and measurements were taken at 0^{th}, 2^{nd}, 4^{th}, 6^{th}, 16^{th} and 24^{th} hours after induction. The results were analyzed with two-way analysis of variance (ANOVA) (GraphPad Prism version 9.0.0), the differences between the groups were marked with "*" ($p \leq 0.05$, $p \leq 0.01$, $p \leq 0.001$ and $p \leq 0.0001$ is represented by "*", "**", "***" and "****" respectively). "ns" was used in the groups that did not show significant differences.

1.3.13 Characterization of Whole-Cell Copper Biosensors at Different Salt Concentrations

Copper whole-cell biosensor was characterized under different sodium chloride (NaCl) concentration values: 10mM, 50mM and 100mM. MOPS buffered chemically defined media was prepared so that the final concentration of NaCl in the media was either 10mM, 50mM or 100mM. Time-dependent analysis of the pET22b-PcopA-RBS30-sfGFP biosensor was made with Copper (II) sulfate ($CuSO_4$) salt. Uninduced *E. coli* PRO cells carrying the pET22b-PcopA-RBS30-sfGFP vector was used as a control. *E.coli* PRO cells carrying pET22b-PcopA-RBS30-sfGFP copper sensing circuit were grown overnight in LB, then 1% inoculated into fresh MOPS buffered minimal media with proper antibiotics. When OD_{600} reached 0.4-0.5, samples were induced with 200 µM $CuSO_4$. Fluorescence and OD_{600} measurements were taken at

0^{th}, 2^{nd}, 4^{th}, 6^{th}, 8^{th}, 16^{th} and 24^{th} hours after induction with $CuSO_4$. Copper RBS30 sfGFP biosensor was observed to have lower relative fluorescence signal when cells were grown in MOPS buffered growth media with 10mM NaCl (Figure 34) compared to cases when NaCl concentration was either 50mM (Figure 35) or 100mM (Figure 36).

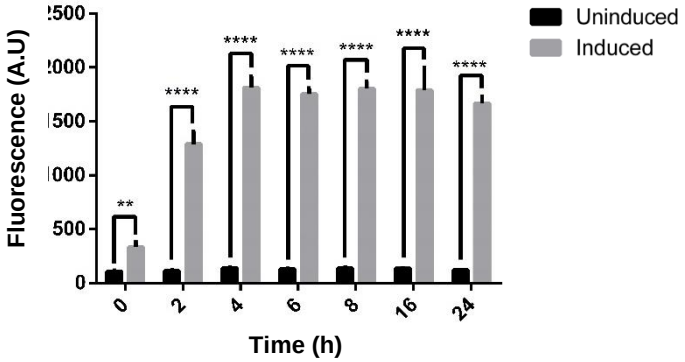

Figure 34. Time-dependent characterization of the pET22b-PcopA-RBS30-sfGFP sensor with 200 µM Copper (II) Sulfate (CuSO4).. *E. coli PRO* cells were grown in chemically defined MOPS buffered minimal growth media with 10 mM NaCl. A. Time-dependent graph of relative fluorescence value. B. Image of cells growing in the falcon under blue light. C. Visualization of the remaining pellet after centrifugation of the samples under blue light. D. Image of cell pellet dissolved in 1xPBS under blue light. Experiments were repeated in triplicates, and measurements were taken at 0^{th}, 2^{nd}, 4^{th}, 6^{th}, 16^{th} and 24^{th} hours after induction. The results were analyzed with two-way analysis of variance (ANOVA) (GraphPad Prism version 9.0.0), the differences between the groups were marked with "*" ($p \leq 0.05$, $p \leq 0.01$, $p \leq 0.001$ and $p \leq 0.0001$ is represented by "*", "**", "***" and "****" respectively). "ns" was used in the groups that did not show significant differences.

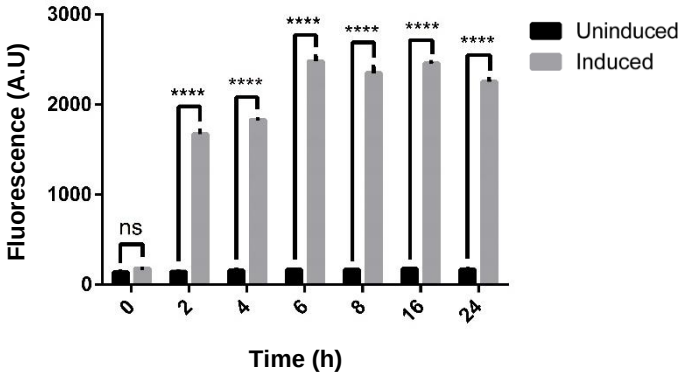

Figure 35. Time-dependent characterization of the pET22b-PcopA-RBS30-sfGFP sensor with 200 µM Copper (II) Sulfate (CuSO4).. *E. coli PRO* cells were grown in chemically defined MOPS buffered minimal growth media with 50 mM NaCl. A. Time-dependent graph of relative fluorescence value. B. Image of cells growing in the falcon under blue light. C. Visualization of the remaining pellet after centrifugation of the samples under blue light. D. Image of cell pellet dissolved in 1xPBS under blue light. Experiments were repeated in triplicates, and measurements were taken at 0^{th}, 2^{nd}, 4^{th}, 6^{th}, 16^{th} and 24^{th} hours after induction. The results were analyzed with two-way analysis of variance (ANOVA) (GraphPad Prism version 9.0.0), the differences between the groups were marked with "*" ($p \leq 0.05$, $p \leq 0.01$, $p \leq 0.001$ and $p \leq 0.0001$ is represented by "*", "**", "***" and "****" respectively). "ns" was used in the groups that did not show significant differences.

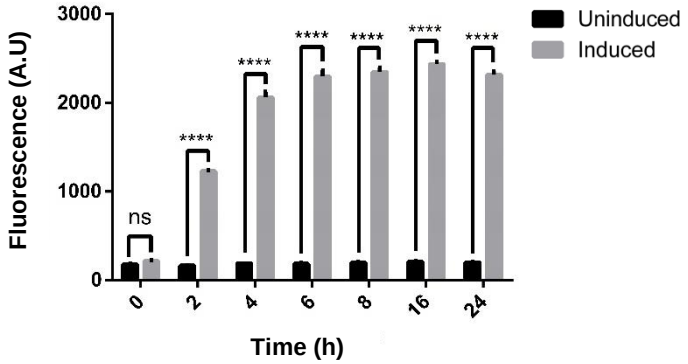

Figure 36. Time-dependent characterization of the pET22b-PcopA-RBS30-sfGFP sensor with 200 µM Copper (II) Sulfate (CuSO4).. *E. coli PRO* cells were grown in chemically defined MOPS buffered minimal growth media with 100 mM NaCl. A. Time-dependent graph of relative fluorescence value. B. Image of cells growing in the falcon under blue light. C. Visualization of the remaining pellet after centrifugation of the samples under blue light. D. Image of cell pellet dissolved in 1xPBS under blue light. Experiments were repeated in triplicates, and measurements were taken at 0^{th}, 2^{nd}, 4^{th}, 6^{th}, 16^{th} and 24^{th} hours after induction. The results were analyzed with two-way analysis of variance (ANOVA) (GraphPad Prism version 9.0.0), the differences between the groups were marked with "*" ($p \leq 0.05$, $p \leq 0.01$, $p \leq 0.001$ and $p \leq 0.0001$ is represented by "*", "**", "***" and "****" respectively). "ns" was used in the groups that did not show significant differences.

1.3.14 Cross Reactivity Analysis of Whole-Cell Copper RBS30 Biosensor

Copper RBS30 whole-cell biosensor was characterized with copper (II) sulfate ($CuSO_4$), lead(II) chloride ($PbCl_2$), cadmium acetate $Cd(CH_3CO_2)_2$ and sodium arsenate (Na_3AsO_4) salts for cross reactivity. Uninduced *E. coli* PRO cells carrying the same vector was used as a control. *E.coli* PRO cells carrying pET22b-PcopA-RBS30-sfGFP copper sensing circuit were grown overnight in LB, then 1% inoculated into fresh MOPS buffered minimal media with proper antibiotics. When OD_{600} reached 0.4-0.5, samples were induced with 200 µM $CuSO_4$, 200 µM $PbCl_2$, 10 µM $Cd(CH_3CO_2)_2$, 10 µM Na_3AsO_4 separately. Fluorescence and OD_{600} measurements were taken at 0^{th}, 2^{nd}, 4^{th}, 6^{th}, 8^{th}, 16^{th} and 24^{th} hours after induction with aforementioned heavy metals (Figure 37).

Copper RBS30 sfGFP biosensor was observed to have no significant signal when cells were induced with heavy metals except for copper.

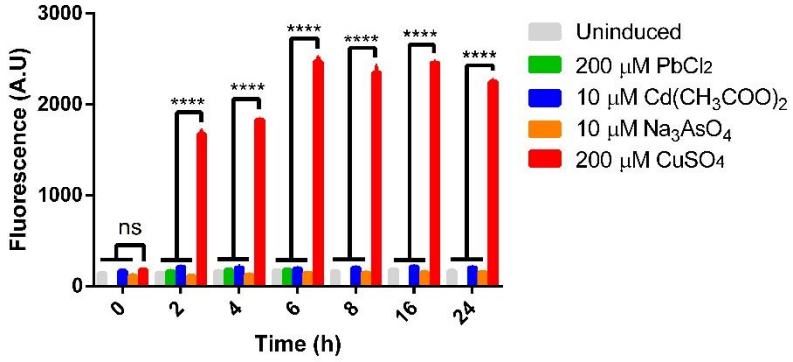

Figure 37. Time-dependent cross-reactivity characterization of the pET22b-PcopA-RBS30-sfGFP sensor with 200 µM $CuSO_4$, 200 µM $PbCl_2$, 10 µM $Cd(CH_3CO_2)_2$, 10 µM Na_3AsO_4 separately. *E. coli PRO* cells were grown in chemically defined MOPS buffered minimal growth media. Experiments were repeated in triplicates, and measurements were taken at 0^{th}, 2^{nd}, 4^{th}, 6^{th}, 8^{th}, 16^{th} and 24^{th} hours after induction. The results were analyzed with two-way analysis of variance (ANOVA) (GraphPad Prism version 9.0.0), the differences between the groups were marked with "*" ($p \leq 0.05$, $p \leq 0.01$, $p \leq 0.001$ and $p \leq 0.0001$ is represented by "*", "**", "***" and "****" respectively). "ns" was used in the groups that did not show significant differences.

1.3.15 Construction of Whole-Cell Lead Biosensor

To build lead heavy metal whole-cell biosensor, the sequences of a promoter (PpbrR) and its cognate transcription factor (PbrR) from *Cupriavidus metallidurans CH34* genome were selected to sense the presence of lead ions in the environment. PbrR transcriptional repressor binds to PpbrR promoter to repress its downstream gene expression. When there are lead ions within the cell, upon binding of lead ions to PbrR protein conformational change happens. PbrR protein lead ion complex is released from PpbrR promoter, then downstream expression of gene(s) starts (Figure 38).

Lead biosensor was constructed by inserting PpbrR promoter region upstream of sfGFP gene region by replacing PhucO promoter in pET22b-PhucO-sfGFP-

prod-HucR vector (gift from Sıla Köse) with PCR (Figure 39). PpbrR promoter region was amplified with primers suitable for the Gibson Assembly method. Primers can be found at Appendix B. After PCR products were run on 1% agarose gel, they were isolated from the gel with Macherey-Nagel's PCR Clean-up kit according to the manufacturer's instructions and assembled with the Gibson Assembly method. Samples selected from the single colonies were sent for Sanger sequencing analysis. Plasmid map for lead biosensor and Sanger sequencing result can be found at Appendix C and D, respectively.

Then, PbrR transcription factor's gene sequence (synthesized from Genewiz) was cloned downstream of constitutively active ProD promoter. First, PbrR gene was amplified with PCR from the gene fragment with overhangs to backbone. Second, pET22b-PpbrR-sfGFP-ProD vector was amplified with PCR (Figure 40). Finally, pET22b-PpbrR-sfGFP-ProD-PbrR vector was constructed with Gibson assembly.

Samples selected from single colonies were first verified by restriction enzyme digestion (Figure 41), and then the samples selected from the restriction enzyme digestion reaction were sent for Sanger sequencing analysis. Plasmid map for lead biosensor and Sanger sequencing result can be found at Appendix C and D, respectively.

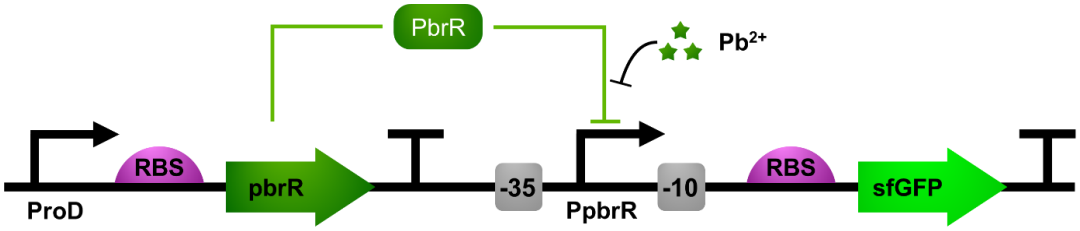

Figure 38. Lead biosensor biological parts and working mechanism. PbrR transcription factor binds to PpbrR promoter in the absence of lead ions within the cell. When lead ions present, upon release of PbrR from PpbrR promoter, downstream expression of sfGFP is activated.

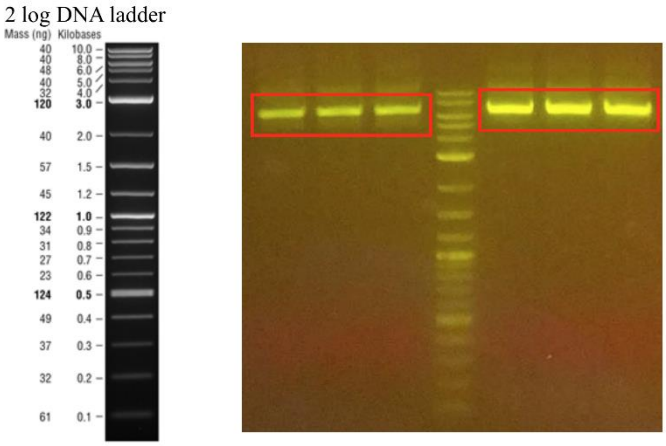

Figure 39. Agarose gel image of the biological parts required for the cloning of the pET22b-PpbrR-sfGFP-ProD-HucR vector. PCR product of the linear pET22b-PbrR-sfGFP-ProD-HucR backbone, 6500 bp.

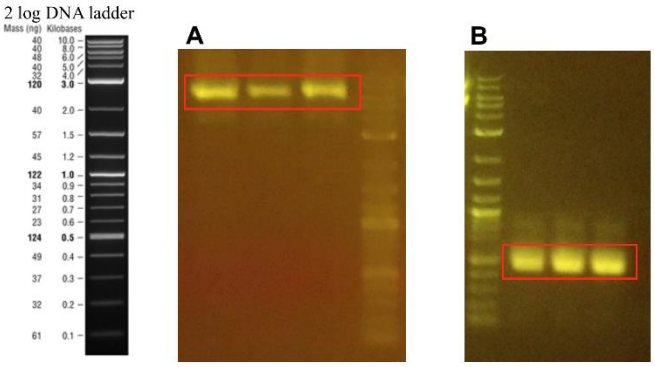

Figure 40. Agarose gel image of the biological parts required for the cloning of the pET22b-PpbrR-sfGFP-ProD-PbrR vector. A. PCR product of the linear pET22b-PpbrR-sfGFP-ProD backbone, 6000 bp. B. PCR product of PbrR transcription factor gene region, 500 bp.

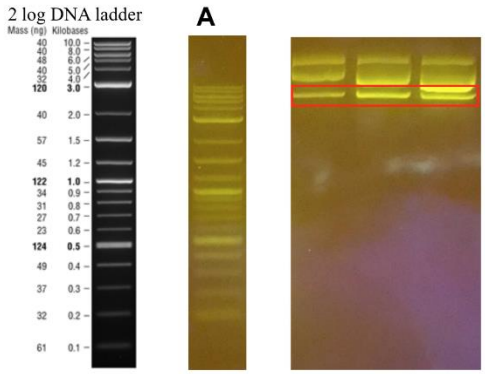

Figure 41. Confirmation of the pET22b-PpbrR-sfGFP-ProD-PbrR vector by restriction enzyme digestion. A. The bands expected for the pET22b-PpbrR-sfGFP-ProD-PbrR vector as a result of cleavage of AvrII and SpeI enzymes were observed at 6000 bp, 650 bp and 100 bp lines, but it is thought that digested parts did not appear as a result of mutation in the cleavage region.

1.3.16 Characterization of Whole-Cell Lead Biosensor

Time dependent and dynamic range analysis of the pET22b-PpbrR-sfGFP-ProD-PbrR sensor was made with lead(II) chloride ($PbCl_2$) salt. Uninduced *E. coli* PRO cells carrying the same vector was used as a control. Time dependent measurements were taken at 1^{st}, 2^{nd}, 4^{th}, 6^{th}, 8^{th}, 16^{th} and 24^{th} hours after induction with $PbCl_2$ (Figure 42). In order to understand the response of the pET22b-PpbrR-sfGFP-ProD-PbrR sensor to different $PbCl_2$ concentrations, dynamic range with varying $PbCl_2$ concentrations was performed at 16^{th} hour after induction. Lead biosensor responded even to a concentration as low as 50 µM (Figure 43).

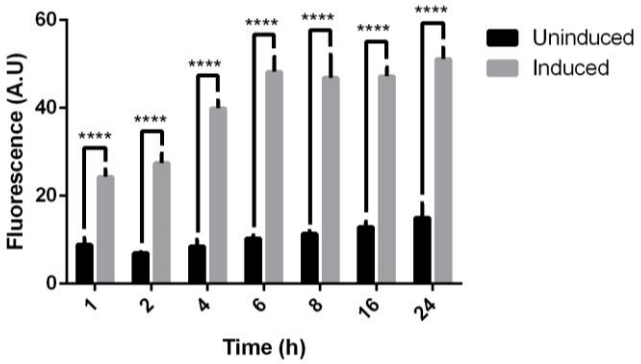

Figure 42. Time dependent characterization of the pET22b-PpbrR-sfGFP-ProD-PbrR sensor with 25 µM Lead(II) chloride ($PbCl_2$). Experiments were performed in triplicates and measurements were taken at the 1st, 2nd, 4th, 6th, 16th and 24th hours after induction. The results were analyzed with two-way analysis of variance (ANOVA) (GraphPad Prism version 9.0.0), the differences between the groups were marked with "*" ($p \leq 0.05$, $p \leq 0.01$, $p \leq 0.001$ and $p \leq 0.0001$ is represented by "*", "**", "***" and "****" respectively). No marking was made in the groups that did not show significant differences. E. coli cells were grown in chemically defined MOPS buffered minimal growth media.

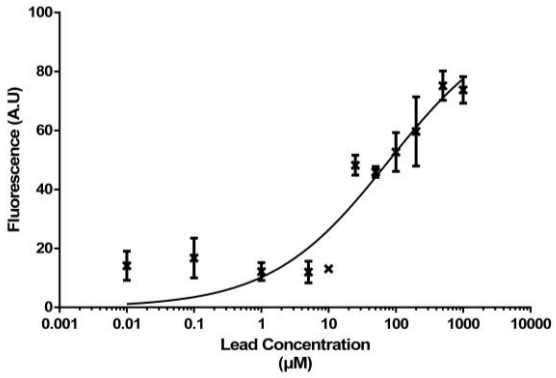

Figure 43. Concentration-dependent characterization of the pET22b-PpbrR-sfGFP-ProD-PbrR sensor with $PbCl_2$. Experiments were repeated in triplicates, and measurements were taken at the 16th hour of induction. E. coli cells were grown in chemically defined MOPS buffered minimal growth media.

1.3.17 Construction of Whole-Cell Lead -10mer Biosensor

Since the pET22b-PpbrR-sfGFP-ProD-PbrR whole-cell biosensor created with the PpbrR promoter from the *Cupriavidus metallidurans CH34* species was not at the desired level. Hence, -10 region of the PpbrR promoter was replaced with the common -10 sequence from Mer promoter family with PCR reaction (Figure 44). The pET22b-PpbrR-sfGFP-ProD-PbrR construct was used as template DNA, and the -10 mer region was linearly inserted while amplification with PCR (Figure 45). The new vector was named as pET22b-10mer-PpbrR-sfGFP-ProD-PbrR. Samples selected from the single colonies that emerged

as a result of the Gibson Assembly method were sent to DNA sequencing analysis and confirmed. Plasmid map for lead -10 mer biosensor and Sanger sequencing result can be found at Appendix C and D, respectively.

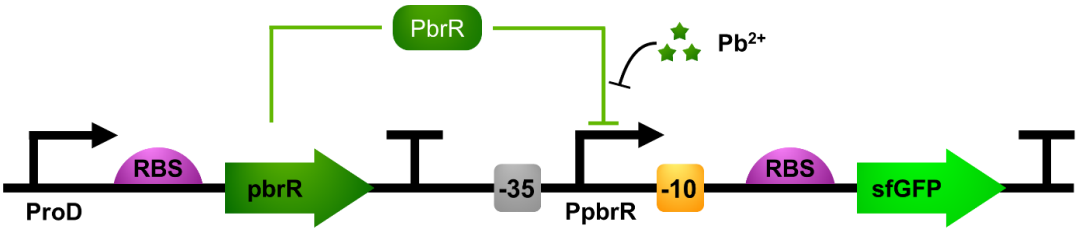

Figure 44. Lead -10mer biosensor biological parts and working mechanism. PbrR transcription factor binds to PpbrR promoter in the absence of lead ions within the cell. When lead ions present, upon release of PbrR from PpbrR promoter, downstream expression of sfGFP is activated.

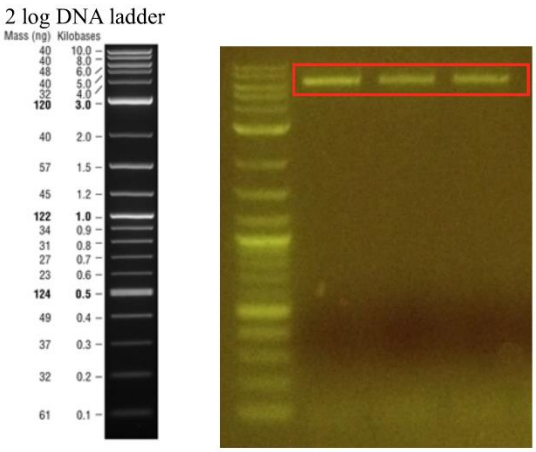

Figure 45. Agarose gel image of the biological part required for the cloning of the pET22b-10mer-PpbrR-sfGFP-ProD-PbrR vector. PCR product of the linear pET22b-10mer-PpbrR-sfGFP-ProD-PbrR backbone, 6400 bp.

1.3.18 Characterization of Whole-Cell Lead -10mer Biosensor

Time dependent and dynamic range analysis of the pET22b-10mer-PpbrR-sfGFP-ProD-PbrR sensor was made with lead(II) chloride ($PbCl_2$) salt. Uninduced *E. coli* PRO cells carrying the same vector was used as a control. Time dependent measurements were taken at 1^{st}, 2^{nd}, 4^{th}, 6^{th}, 8^{th}, 16^{th} and 24^{th} hours after induction with $PbCl_2$ (Figure 46). In order to understand the response of the pET22b-10mer-PpbrR-sfGFP-ProD-PbrR sensor to different

$PbCl_2$ concentrations, dynamic range with varying $PbCl_2$ concentrations was performed at 6th hour after induction. Lead biosensor responded even to a concentration as low as 10 µM (Figure 47).

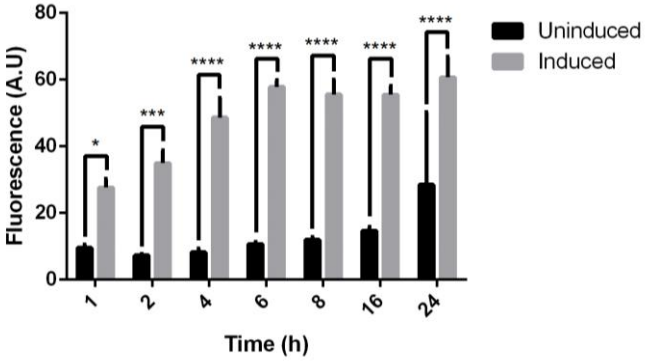

Figure 46. Time dependent characterization of the pET22b-10mer-PpbrR-sfGFP-ProD-PbrR sensor with 25 µM Lead(II) chloride ($PbCl_2$). Experiments were performed in triplicates and measurements were taken at the 1st, 2nd, 4th, 6th, 16th and 24th hours after induction. The results were analyzed with two-way analysis of variance (ANOVA) (GraphPad Prism version 9.0.0), the differences between the groups were marked with "*" ($p \leq 0.05$, $p \leq 0.01$, $p \leq 0.001$ and $p \leq 0.0001$ is represented by "*", "**", "***" and "****" respectively). No marking was made in the groups that did not show significant differences. E. coli cells were grown in chemically defined MOPS buffered minimal growth media.

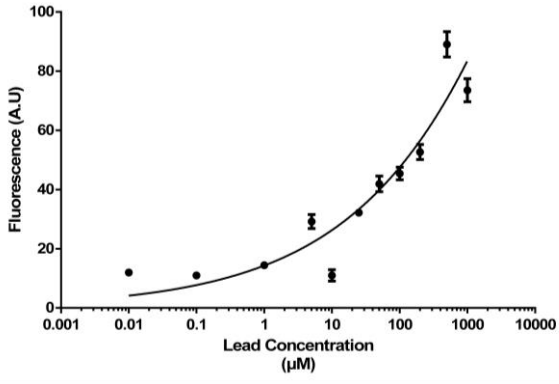

Figure 47. Concentration-dependent characterization of the pET22b-10mer-PpbrR-sfGFP-ProD-PbrR sensor with $PbCl_2$. Experiments were repeated in triplicates, and measurements were taken at the 6th hour of induction. E. coli cells were grown in chemically defined MOPS buffered minimal growth media.

1.3.19 Construction of Whole-Cell Lead -10mer RBS30 Biosensor

The output signal level of lead -10 mer biosensor was not at desired level. To prevent the possibility of changing biosensor's sensitivity, RBS site between the PpbrR -10 mer promoter and the sfGFP gene was replaced with another stronger RBS, BBa_B0030 from iGEM repository's RBS library (referred as RBS30 in this study) (Figure 48). To do so, pET22b-10mer-PpbrR-sfGFP-ProD-PbrR was linearly amplified with PCR reaction by adding RBS30 parts while removing the old RBS region (Figure 49). Then PCR product was extracted from agarose gel and subjected to Gibson assembly. The new vector was named as pET22b-10mer-RBS30-PpbrR-sfGFP-ProD-PbrR. Plasmid map for lead -10 mer RBS30 biosensor and Sanger sequencing result can be found at Appendix C and D, respectively.

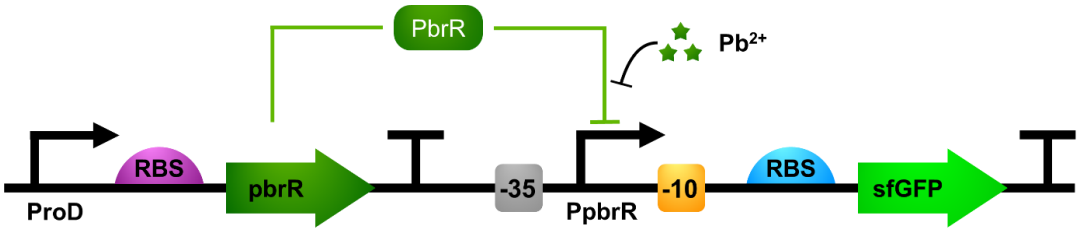

Figure 48. Lead -10mer RBS30 biosensor biological parts and working mechanism. PbrR transcription factor binds to PpbrR promoter in the absence of lead ions within the cell. When lead ions present, upon release of PbrR from PpbrR promoter, downstream expression of sfGFP is activated with stronger RBS30.

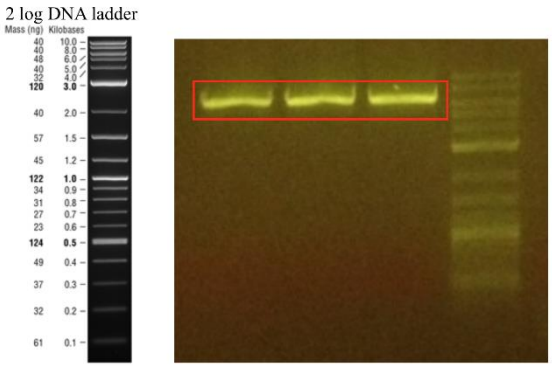

Figure 49. Agarose gel image of the biological part required for the cloning of the pET22b-10mer-RBS30-PpbrR-sfGFP-ProD-PbrR vector. PCR product of the linear pET22b-10mer-RBS30-PpbrR-sfGFP-ProD-PbrR backbone, 6400 bp.

1.3.20 Characterization of Whole-Cell Lead -10mer RBS30 Biosensor

Time dependent and dynamic range analysis of the pET22b-10mer-RBS30-PpbrR-sfGFP-ProD-PbrR sensor was made with lead(II) chloride ($PbCl_2$) salt. Uninduced *E. coli* PRO cells carrying the same vector was used as a control. Time dependent measurements were taken at 1st, 2nd, 4th, 6th, 8th, 16th and 24th hours after induction with $PbCl_2$ (Figure 50). In order to understand the response of the pET22b-10mer-RBS30-PpbrR-sfGFP-ProD-PbrR sensor to different $PbCl_2$ concentrations, dynamic range with varying $PbCl_2$ concentrations was performed at 6th hour after induction. Lead biosensor responded even to a concentration as low as 5 µM (Figure 51).

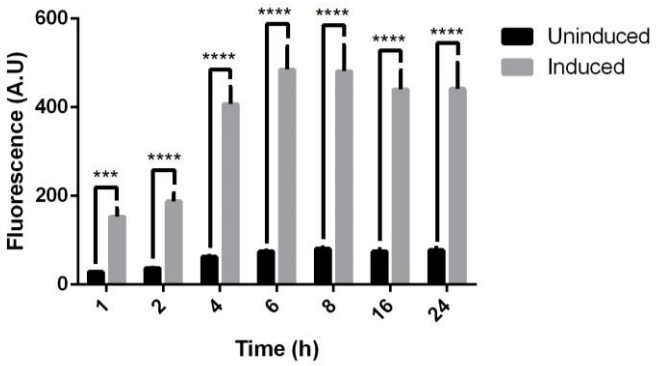

.

Figure 50. Time dependent characterization of the pET22b-10mer-RBS30-PpbrR-sfGFP-ProD-PbrR sensor with 25 µM Lead(II) chloride ($PbCl_2$). Experiments were performed in triplicates and measurements were taken at the 1st, 2nd, 4th, 6th, 16th and 24th hours after induction. The results were analyzed with two-way analysis of variance (ANOVA) (GraphPad Prism version 9.0.0), the differences between the groups were marked with "*" ($p \leq 0.05$, $p \leq 0.01$, $p \leq 0.001$ and $p \leq 0.0001$ is represented by "*", "**", "***" and "****" respectively). No marking was made in the groups that did not show significant differences. E. coli cells were grown in chemically defined MOPS buffered minimal growth media.

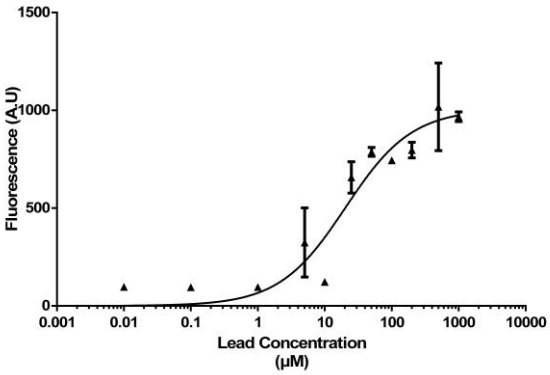

Figure 51. Concentration-dependent characterization of the pET22b-10mer-RBS30-PpbrR-sfGFP-ProD-PbrR sensor with $PbCl_2$. Experiments were repeated in triplicates, and measurements were taken at the 6^{th} hour of induction. E. coli cells were grown in chemically defined MOPS buffered minimal growth media.

1.3.21 Construction of Whole-Cell Lead -10mer hrp Biosensor

To further increase the strength of output signal level, a synthetic amplification circuit unit was integrated between PpbrR -10 mer promoter and sfGFP gene. The synthetic amplification circuit consists of PhrpL promoter controlled by hrpR and hrpS genes, referred as hrp circuit in this study (Figure 52).

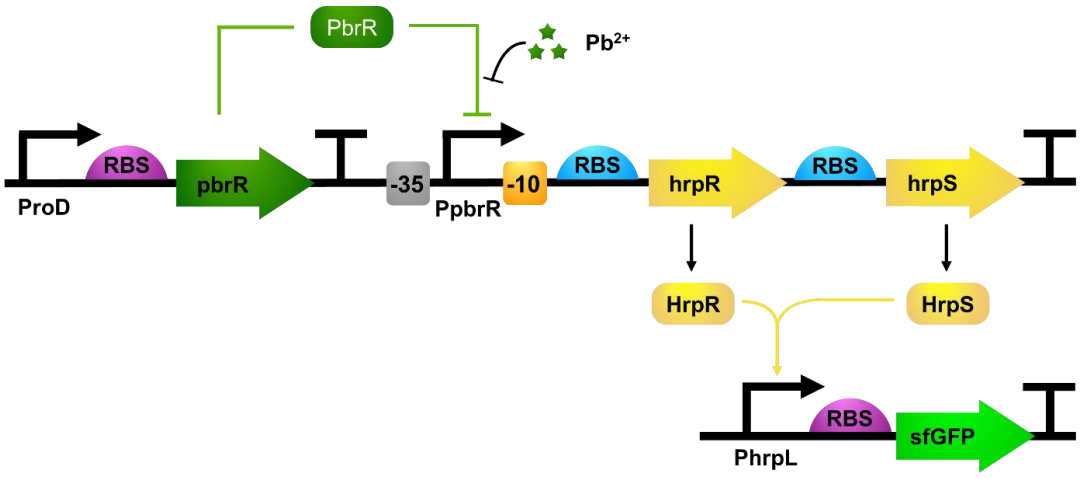

Figure 52. Lead -10mer hrp biosensor biological parts and working mechanism. PbrR transcription factor binds to PpbrR promoter in the absence of lead ions within the cell. When lead ions present, upon release of PbrR from PpbrR promoter, downstream expression of HrpR and HrpS protein expression is activated. Upon binding of HrpR and HrpS complex to PhrpL promoter, sfGFP protein expression is activated.

To construct lead -10 mer hrp biosensor circuit, pET22b-10mer-PpbrR-sfGFP-ProD-PbrR backbone was linearly amplified with PCR reaction by adding necessary overhangs (Figure 53). Synthetic amplification circuit (hrp region) was amplified with PCR from pBW103ParsR-Amp30C vector (purchased from Addgene, ID: 78638) (Figure 53). Then PCR products were extracted from agarose gel and subjected to Gibson assembly. The new vector was named as pET22b-10mer-PpbrR-hrp-sfGFP-ProD-PbrR.

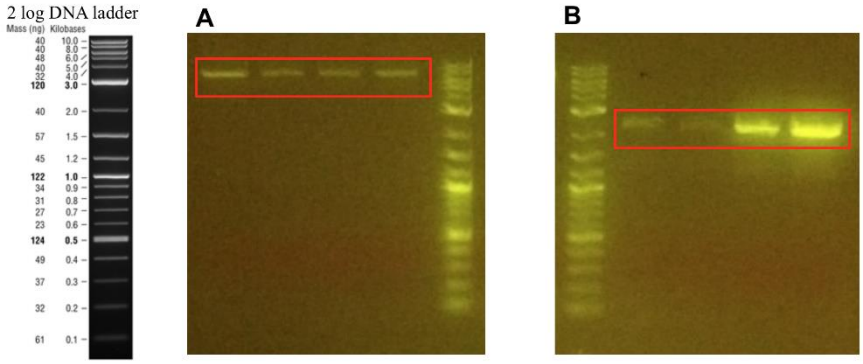

Figure 53. Agarose gel image of the biological parts required for the cloning of the pET22b-10mer-PpbrR-hrp-sfGFP-ProD-PbrR vector. A. PCR product of the linear pET22b-10mer-PpbrR-sfGFP-ProD-PbrR vector backbone, 6400 bp. B. hrp amplification circuit linear DNA fragment, 2300 bp.

Samples selected from the colonies were first verified with colony PCR (Figure 54), and then colony PCR verified samples were sent for Sanger sequencing analysis. Plasmid map for lead -10 mer hrp biosensor and Sanger sequencing result can be found at Appendix C and D, respectively.

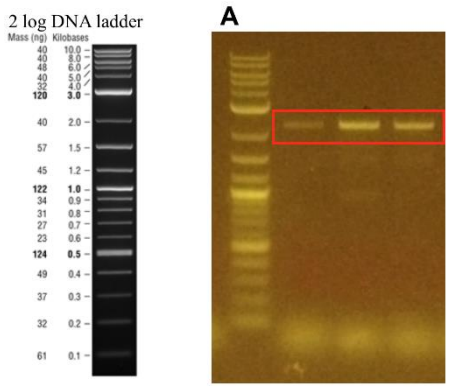

Figure 54. Confirmation of the pET22b-10mer-PpbrR-hrp-sfGFP-ProD-PbrR vector with colony PCR. A. The bands expected for the PCR amplified hrp biological parts were observed at 2300 bp.

1.3.22 Characterization of Whole-Cell Lead -10mer hrp Biosensor

Time dependent and dynamic range analysis of the pET22b-10mer-PpbrR-hrp-sfGFP-ProD-PbrR sensor was made with lead(II) chloride ($PbCl_2$) salt. Uninduced *E. coli* PRO cells carrying the same vector was used as a control. Time dependent measurements were taken at 1^{st}, 2^{nd}, 4^{th}, 6^{th}, 8^{th}, 16^{th} and 24^{th} hours after induction with $PbCl_2$ (Figure 55). In order to understand the response of the pET22b-10mer-PpbrR-hrp-sfGFP-ProD-PbrR sensor to different $PbCl_2$ concentrations, dynamic range with varying $PbCl_2$ concentrations was performed at 6^{th} hour after induction. Lead biosensor responded even to a concentration as low as 5 µM (Figure 56).

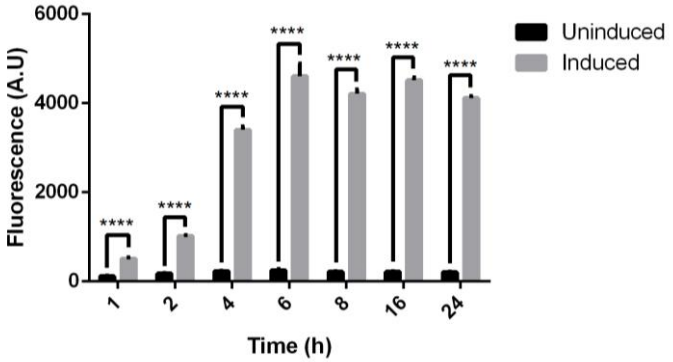

Figure 55. Time dependent characterization of the pET22b-10mer-PpbrR-hrp-sfGFP-ProD-PbrR sensor with 25 µM Lead(II) chloride ($PbCl_2$). Experiments were performed in triplicates and measurements were taken at the 1st, 2nd, 4th, 6th, 16th and 24th hours after induction. The results were analyzed with two-way analysis of variance (ANOVA) (GraphPad Prism version 9.0.0), the differences between the groups were marked with "*" ($p \leq 0.05$, $p \leq 0.01$, $p \leq 0.001$ and $p \leq 0.0001$ is represented by "*", "**", "***" and "****" respectively). No marking was made in the groups that did not show significant differences. E. coli cells were grown in chemically defined MOPS buffered minimal growth media.

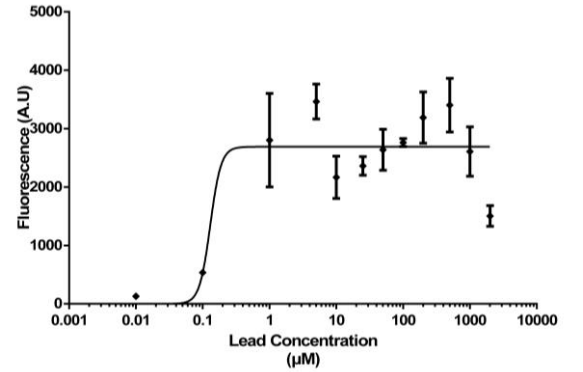

Figure 56. Concentration-dependent characterization of the pET22b-10mer-PpbrR-hrp-sfGFP-ProD-PbrR sensor with $PbCl_2$. Experiments were repeated in triplicates, and measurements were taken at the 6th hour of induction. E. coli cells were grown in chemically defined MOPS buffered minimal growth media.

Comparative characterization of the concentration dependent dynamics of pET22b-PpbrR-sfGFP-ProD-PbrR (denoted as *native*), pET22b-10mer-PpbrR-sfGFP-ProD-PbrR (denoted as -10 mer), pET22b-10mer-RBS30-PpbrR-sfGFP-ProD-PbrR (denoted as -10 mer RBS30) and pET22b-10mer-PpbrR-hrp-sfGFP-ProD-PbrR (denoted as -10 mer hrp) biosensors with $PbCl_2$was given below (Figure 57).

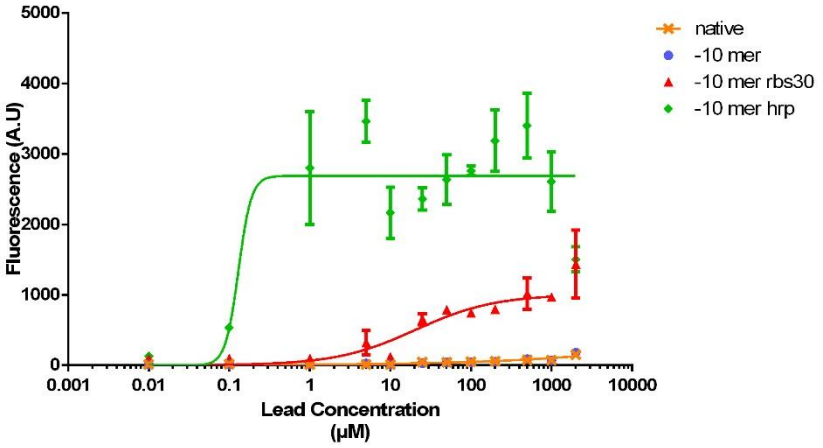

Figure 57. Comparative characterization of the concentration-dependent dynamics of pET22b-PpbrR-sfGFP-ProD-PbrR (denoted as *native*), pET22b-10mer-PpbrR-sfGFP-ProD-PbrR (denoted as -10 mer), pET22b-10mer-RBS30-PpbrR-sfGFP-ProD-PbrR (denoted as -10 mer RBS30) and pET22b-10mer-PpbrR-hrp-sfGFP-ProD-PbrR (denoted as -10 mer hrp) biosensors with $PbCl_2$. Experiments were repeated in triplicates, and measurements were taken after 16th hour for *native* and 6th hour for -10 mer, -10 mer RBS30 and -10 mer hrp biosensors after induction. E. coli cells were grown in chemically defined MOPS buffered minimal growth media.

1.3.23 Characterization of Whole-Cell Lead Biosensors with Serum Samples

To test the applicability of biosensors for diagnosis of heavy metal poisoning, biosensors were tested with M63 growth media mixed with fetal bovine serum (FBS). Dynamic range analysis of the pET22b-10mer-RBS30-PpbrR-sfGFP-ProD-PbrR and pET22b-10mer-PpbrR-hrp-sfGFP-ProD-PbrR biosensors were made with lead(II) chloride ($PbCl_2$) salt. *E.coli PRO* cells carrying their corresponding biosensor circuits were grown overnight in LB, then 1% inoculated into fresh LB media with proper antibiotics. When OD_{600} reached 0.4-0.5, samples were centrifuged at 3000 rpm for 10 minutes. Supernatant was discarded from each sample, and pellets were resuspended in equal volume of a mixture of heat-treated FBS and M63 minimal media (3:1), and induced with different concentrations of $PbCl_2$. Fluorescence and OD_{600} measurements were taken at 16th hour of induction. Lead -10 mer RBS30 sfGFP biosensor was observed to be responsive to concentrations as low as

10 µM $PbCl_2$ (Figure 58). Similarly, lead -10 mer hrp sfGFP biosensor was observed to be responsive to concentrations as low as 100 µM but with a higher relative fluorescence value (Figure 59). Comparative serum response characterization of the concentration dependent dynamics of pET22b-10mer-RBS30-PpbrR-sfGFP-ProD-PbrR (denoted as lead rbs30) and pET22b-10mer-PpbrR-hrp-sfGFP-ProD-PbrR (denoted as lead hrp) biosensors with $PbCl_2$ was given below (Figure 60).

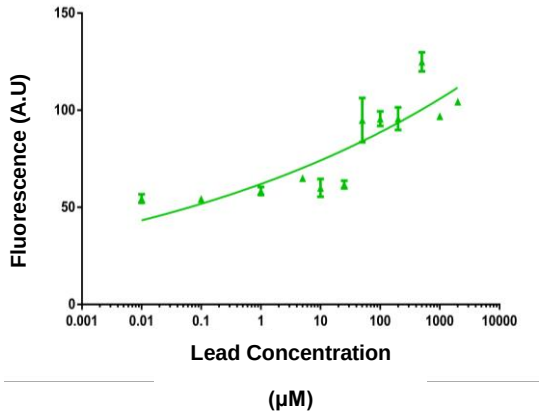

Figure 58. Concentration-dependent characterization of the pET22b-10mer-RBS30-PpbrR-sfGFP-ProD-PbrR biosensor with lead(II) chloride ($PbCl_2$). Experiments were repeated in triplicates, and measurements were taken at the 16th hour of induction. E. coli cells were grown in LB media until OD_{600} reached 0.4-0.5, then transferred to a mixture of heat-treated FBS and M63 minimal media (3:1) and induced with different concentrations of $PbCl_2$.

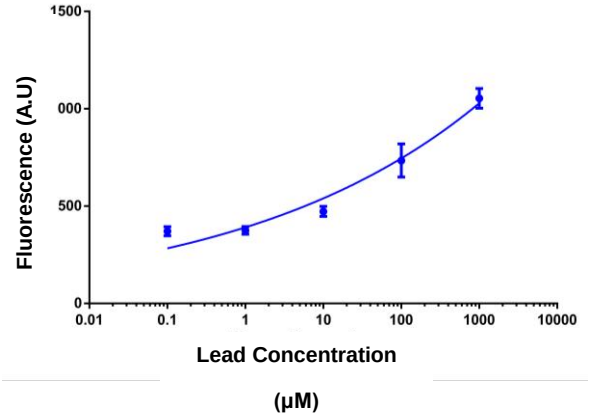

Figure 59. Concentration-dependent characterization of the pET22b-10mer-PpbrR-hrp-sfGFP-ProD-PbrR biosensor with lead(II) chloride ($PbCl_2$). Experiments were repeated in triplicates, and measurements were taken at the 16th hour of induction. E. coli cells were grown in LB media until OD_{600} reached 0.4-0.5, then transferred to a mixture of heat-treated FBS and M63 minimal media (3:1) and induced with different concentrations of $PbCl_2$.

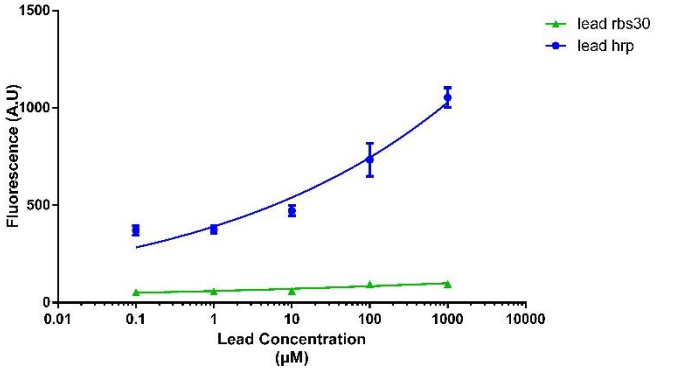

Figure 60. Comparative characterization of the concentration-dependent dynamics of pET22b-10mer-RBS30-PpbrR-sfGFP-ProD-PbrR (denoted as lead rbs30) and pET22b-10mer-PpbrR-hrp-sfGFP-ProD-PbrR (denoted as lead hrp) biosensors with lead(II) chloride ($PbCl_2$). Experiments were repeated in triplicates, and measurements were taken at the 16^{th} hour of induction for both biosensors. E. coli cells were grown in LB media until OD_{600} reached 0.4-0.5, then transferred to a mixture of heat-treated FBS and M63 minimal media (3:1) and induced with different concentrations of $PbCl_2$.

1.3.24 Characterization of Whole-Cell Lead -10mer RBS30 and Lead -10mer hrp Biosensors at Different pH Values

Lead -10 mer RBS30 whole-cell biosensor was characterized under pH values 5, 7 and 9. MOPS buffered chemically defined media was adjusted with HCl and NaOH to have the desired pH value. Time-dependent analysis of the pET22b-10mer-RBS30-PpbrR-sfGFP-ProD-PbrR biosensor was made with lead(II) chloride ($PbCl_2$) salt. Uninduced *E. coli* PRO cells carrying the same vector was used as a control. *E.coli* PRO cells carrying pET22b-10mer-RBS30-PpbrR-sfGFP-ProD-PbrR lead sensing circuit were grown overnight in LB, then 1% inoculated into fresh MOPS buffered minimal media with proper antibiotics. When OD_{600} reached 0.4-0.5, samples were induced with 200 µM $PbCl_2$. Fluorescence and OD_{600} measurements were taken at 0^{th}, 2^{nd}, 4^{th}, 6^{th}, 8^{th}, 16^{th} and 24^{th} hours after induction with $PbCl_2$. Lead -10 mer RBS30 sfGFP biosensor was observed to have lower signal when pH value of the growth

media was 5 (Figure 61) compared to cases when pH value was either 7 (Figure 62) or 9 (Figure 63).

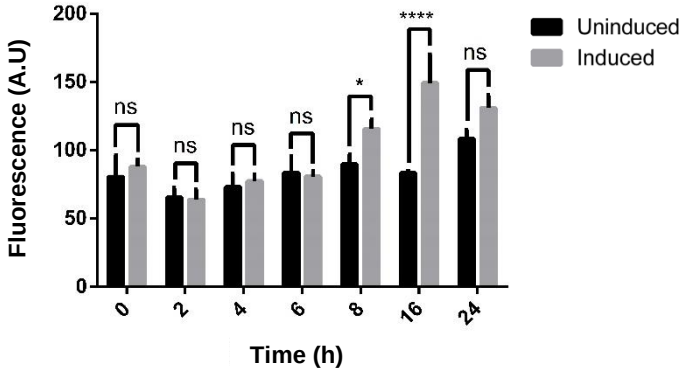

Figure 61. Time-dependent characterization of the pET22b-10mer-RBS30-PpbrR-sfGFP-ProD-PbrR sensor with 200 µM lead(II) chloride ($PbCl_2$). *E. coli PRO* cells were grown in chemically defined MOPS buffered minimal growth media with pH value equal to 5. Experiments were repeated in triplicates, and measurements were taken at 0^{th}, 2^{nd}, 4^{th}, 6^{th}, 16^{th} and 24^{th} hours after induction. The results were analyzed with two-way analysis of variance (ANOVA) (GraphPad Prism version 9.0.0), the differences between the groups were marked with "*" ($p \leq 0.05$, $p \leq 0.01$, $p \leq 0.001$ and $p \leq 0.0001$ is represented by "*", "**", "***" and "****" respectively). "ns" was used in the groups that did not show significant differences.

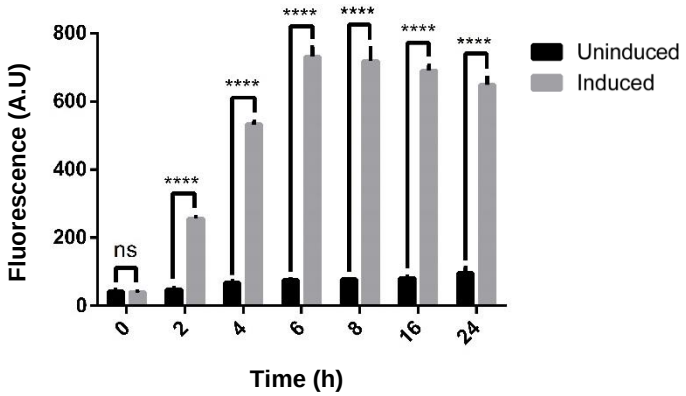

Figure 62. Time-dependent characterization of the pET22b-10mer-RBS30-PpbrR-sfGFP-ProD-PbrR sensor with 200 lead(II) chloride ($PbCl_2$). *E. coli PRO* cells were grown in chemically defined MOPS buffered minimal growth media with pH value equal to 7. Experiments were repeated in triplicates, and measurements were taken at 0^{th}, 2^{nd}, 4^{th}, 6^{th}, 16^{th} and 24^{th} hours after induction. The results were analyzed with two-way analysis of variance (ANOVA) (GraphPad Prism version 9.0.0), the differences between the groups were marked with "*" ($p \leq 0.05$, $p \leq 0.01$, $p \leq 0.001$ and $p \leq 0.0001$ is represented by "*", "**", "***" and "****" respectively). "ns" was used in the groups that did not show significant differences.

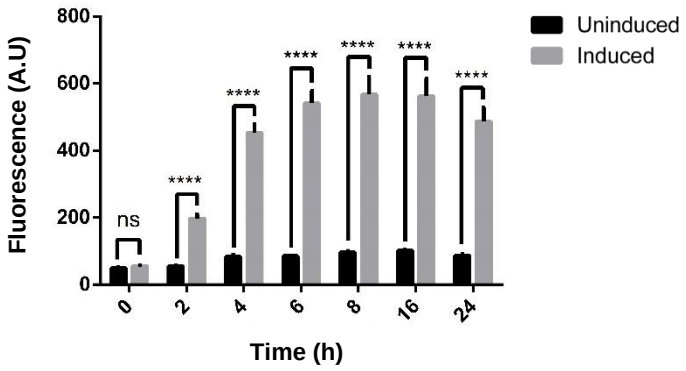

Figure 63. Time-dependent characterization of the pET22b-10mer-RBS30-PpbrR-sfGFP-ProD-PbrR sensor with 200 µM lead(II) chloride ($PbCl_2$). *E. coli PRO* cells were grown in chemically defined MOPS buffered minimal growth media with pH value equal to 9. Experiments were repeated in triplicates, and measurements were taken at 0^{th}, 2^{nd}, 4^{th}, 6^{th}, 16^{th} and 24^{th} hours after induction. The results were analyzed with two-way analysis of variance (ANOVA) (GraphPad Prism version 9.0.0), the differences between the groups were marked with "*" ($p \leq 0.05$, $p \leq 0.01$, $p \leq 0.001$ and $p \leq 0.0001$ is represented by "*", "**", "***" and "****" respectively). "ns" was used in the groups that did not show significant differences.

Lead -10 mer hrp whole-cell biosensor was characterized under pH values 5, 7 and 9. MOPS buffered chemically defined media was adjusted with HCl and NaOH to have the desired pH value. Time-dependent analysis of the pET22b-10mer-PpbrR-hrp-sfGFP-ProD-PbrR biosensor was made with lead(II) chloride ($PbCl_2$) salt. Uninduced *E. coli* PRO cells carrying the same vector was used as a control. *E.coli* PRO cells carrying pET22b-10mer-PpbrR-hrp-sfGFP-ProD-PbrR lead sensing circuit were grown overnight in LB, then 1% inoculated into fresh MOPS buffered minimal media with proper antibiotics. When OD_{600} reached 0.4-0.5, samples were induced with 200 µM $PbCl_2$. Fluorescence and OD_{600} measurements were taken at 0^{th}, 2^{nd}, 4^{th}, 6^{th}, 8^{th}, 16^{th} and 24^{th} hours after induction with $PbCl_2$. Lead -10 mer hrp sfGFP biosensor was observed to have lower signal when pH value of the growth media was 5 (Figure 64) compared to cases when pH value was either 7 (Figure 65) or 9 (Figure 66).

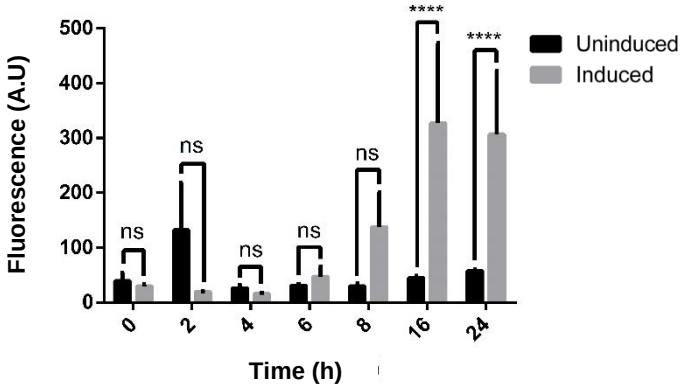

Figure 64. Time-dependent characterization of the pET22b-10mer-PpbrR-hrp-sfGFP-ProD-PbrR sensor with 200 µM lead(II) chloride ($PbCl_2$). *E. coli PRO* cells were grown in chemically defined MOPS buffered minimal growth media with pH value equal to 5. Experiments were repeated in triplicates, and measurements were taken at 0^{th}, 2^{nd}, 4^{th}, 6^{th}, 16^{th} and 24^{th} hours after induction. The results were analyzed with two-way analysis of variance (ANOVA) (GraphPad Prism version 9.0.0), the differences between the groups were marked with "*" ($p \leq 0.05$, $p \leq 0.01$, $p \leq 0.001$ and $p \leq 0.0001$ is represented by "*", "**", "***" and "****" respectively). "ns" was used in the groups that did not show significant differences.

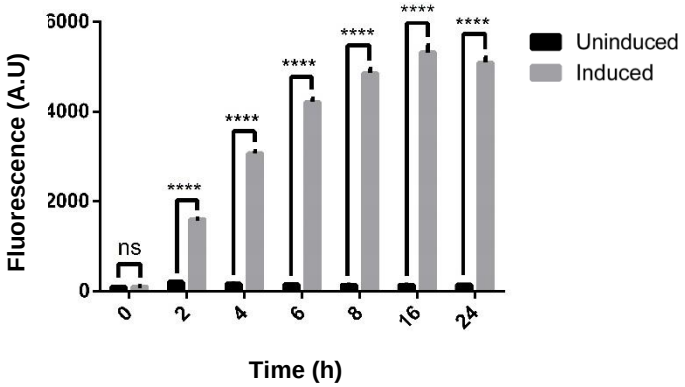

Figure 65. Time-dependent characterization of the pET22b-10mer-PpbrR-hrp-sfGFP-ProD-PbrR sensor with 200 lead(II) chloride ($PbCl_2$). *E. coli PRO* cells were grown in chemically defined MOPS buffered minimal growth media with pH value equal to 7. Experiments were repeated in triplicates, and measurements were taken at 0^{th}, 2^{nd}, 4^{th}, 6^{th}, 16^{th} and 24^{th} hours after induction. The results were analyzed with two-way analysis of variance (ANOVA) (GraphPad Prism version 9.0.0), the differences between the groups were marked with "*" ($p \leq 0.05$, $p \leq 0.01$, $p \leq 0.001$ and $p \leq 0.0001$ is represented by "*", "**", "***" and "****" respectively). "ns" was used in the groups that did not show significant differences.

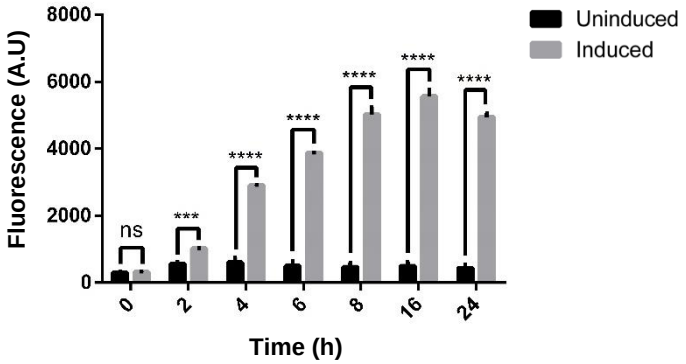

Figure 66. Time-dependent characterization of the pET22b-10mer-PpbrR-hrp-sfGFP-ProD-PbrR sensor with 200 µM lead(II) chloride ($PbCl_2$). *E. coli PRO* cells were grown in chemically defined MOPS buffered minimal growth media with pH value equal to 9. Experiments were repeated in triplicates, and measurements were taken at 0^{th}, 2^{nd}, 4^{th}, 6^{th}, 16^{th} and 24^{th} hours after induction. The results were analyzed with two-way analysis of variance (ANOVA) (GraphPad Prism version 9.0.0), the differences between the groups were marked with "*" ($p \leq 0.05$, $p \leq 0.01$, $p \leq 0.001$ and $p \leq 0.0001$ is represented by "*", "**", "***" and "****" respectively). "ns" was used in the groups that did not show significant differences.

1.3.25 Characterization of Whole-Cell Lead -10mer RBS30 and Lead -10mer hrp Biosensors at Different Temperature Values

Lead -10 mer RBS30 whole-cell biosensor was characterized under different temperature values of 25°C, 37°C and 42°C. Time-dependent analysis of the pET22b-10mer-RBS30-PpbrR-sfGFP-ProD-PbrR biosensor was made with lead(II) chloride ($PbCl_2$) salt. Uninduced *E. coli* PRO cells carrying the same vector was used as a control. *E.coli* PRO cells carrying pET22b-10mer-RBS30-PpbrR-sfGFP-ProD-PbrR lead sensing circuit were grown overnight in LB, then 1% inoculated into fresh MOPS buffered minimal media with proper antibiotics. When OD_{600} reached 0.4-0.5, samples were induced with 200 µM $PbCl_2$. Fluorescence and OD_{600} measurements were taken at 0^{th}, 2^{nd}, 4^{th}, 6^{th}, 8^{th}, 16^{th} and 24^{th} hours after induction with $PbCl_2$. Lead -10 mer RBS30 sfGFP biosensor was observed to have lower signal when temperature was 25°C (Figure 67) compared to cases when temperature was either 37°C (Figure 68)

or 42°C (Figure 69). Relative fluorescence signal level was observed to be higher at 42°C temperature (Figure 69).

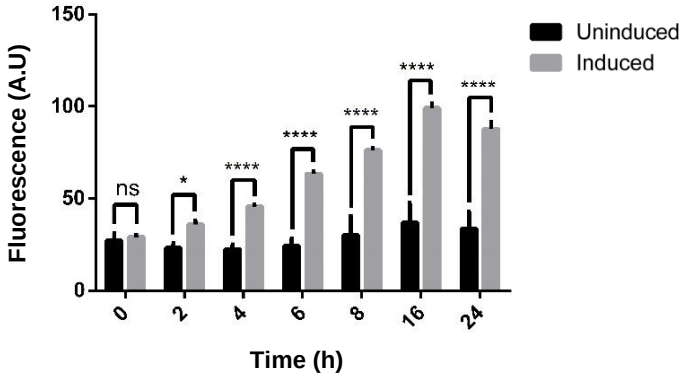

Figure 67. Time-dependent characterization of the pET22b-10mer-RBS30-PpbrR-sfGFP-ProD-PbrR sensor with 200 µM lead(II) chloride ($PbCl_2$). *E. coli PRO* cells were grown in chemically defined MOPS buffered minimal growth media at 25°C. Experiments were repeated in triplicates, and measurements were taken at 0^{th}, 2^{nd}, 4^{th}, 6^{th}, 16^{th} and 24^{th} hours after induction. The results were analyzed with two-way analysis of variance (ANOVA) (GraphPad Prism version 9.0.0), the differences between the groups were marked with "*" ($p \leq 0.05$, $p \leq 0.01$, $p \leq 0.001$ and $p \leq 0.0001$ is represented by "*", "**", "***" and "****" respectively). "ns" was used in the groups that did not show significant differences.

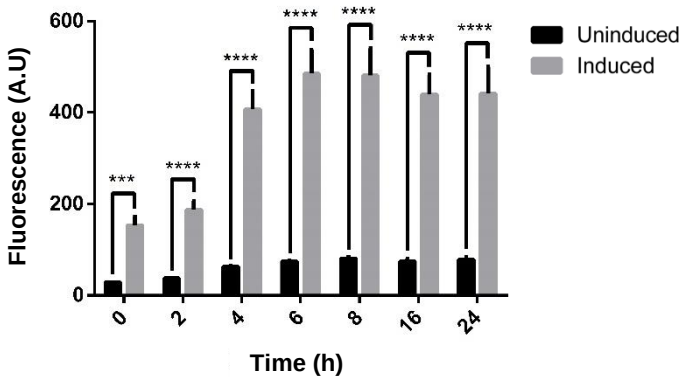

Figure 68. Time-dependent characterization of the pET22b-10mer-RBS30-PpbrR-sfGFP-ProD-PbrR sensor with 200 µM lead(II) chloride ($PbCl_2$). *E. coli PRO* cells were grown in chemically defined MOPS buffered minimal growth media at 37°C. Experiments were repeated in triplicates, and measurements were taken at 0^{th}, 2^{nd}, 4^{th}, 6^{th}, 16^{th} and 24^{th} hours after induction. The results were analyzed with two-way analysis of variance (ANOVA) (GraphPad Prism version 9.0.0), the differences between the groups were marked with "*" ($p \leq 0.05$, $p \leq 0.01$, $p \leq 0.001$ and $p \leq 0.0001$ is represented by "*", "**", "***" and "****" respectively). "ns" was used in the groups that did not show significant differences.

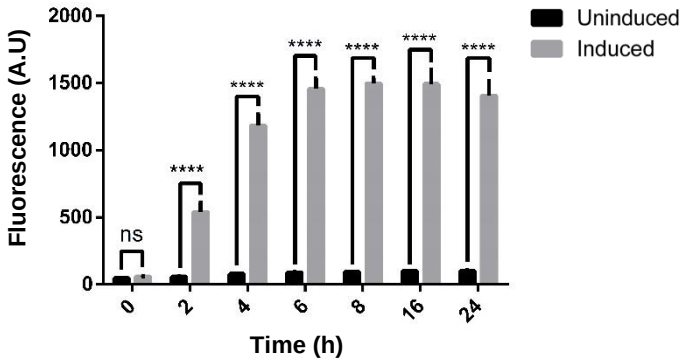

Figure 69. Time-dependent characterization of the pET22b-10mer-RBS30-PpbrR-sfGFP-ProD-PbrR sensor with 200 µM lead(II) chloride ($PbCl_2$). *E. coli PRO* cells were grown in chemically defined MOPS buffered minimal growth media at 42°C. Experiments were repeated in triplicates, and measurements were taken at 0^{th}, 2^{nd}, 4^{th}, 6^{th}, 16^{th} and 24^{th} hours after induction. The results were analyzed with two-way analysis of variance (ANOVA) (GraphPad Prism version 9.0.0), the differences between the groups were marked with "*" ($p \leq 0.05$, $p \leq 0.01$, $p \leq 0.001$ and $p \leq 0.0001$ is represented by "*", "**", "***" and "****" respectively). "ns" was used in the groups that did not show significant differences.

Lead -10 mer hrp whole-cell biosensor was characterized under different temperature values of 25°C, 37°C and 42°C. Time-dependent analysis of the pET22b-10mer-PpbrR-hrp-sfGFP-ProD-PbrR biosensor was made with lead(II) chloride ($PbCl_2$) salt. Uninduced *E. coli* PRO cells carrying the same vector was used as a control. *E.coli* PRO cells carrying pET22b-10mer-PpbrR-hrp-sfGFP-ProD-PbrR lead sensing circuit were grown overnight in LB, then 1% inoculated into fresh MOPS buffered minimal media with proper antibiotics. When OD_{600} reached 0.4-0.5, samples were induced with 200 µM $PbCl_2$. Fluorescence and OD_{600} measurements were taken at 0^{th}, 2^{nd}, 4^{th}, 6^{th}, 8^{th}, 16^{th} and 24^{th} hours after induction with $PbCl_2$. Lead -10 mer RBS30 sfGFP biosensor was observed to have increasing higher background signal when temperature was 25°C (Figure 70) compared to cases when temperature was either 37°C (Figure 71) or 42°C (Figure 72). Relative fluorescence signal level was observed to be lower at 42°C temperature (Figure 72) compared to 37°C (Figure 71).

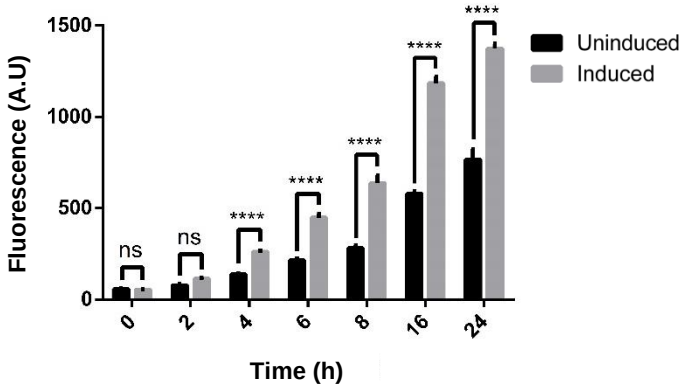

Figure 70. Time-dependent characterization of the pET22b-10mer-PpbrR-hrp-sfGFP-ProD-PbrR sensor with 200 µM lead(II) chloride ($PbCl_2$). *E. coli PRO* cells were grown in chemically defined MOPS buffered minimal growth media at 25°C. Experiments were repeated in triplicates, and measurements were taken at 0^{th}, 2^{nd}, 4^{th}, 6^{th}, 16^{th} and 24^{th} hours after induction. The results were analyzed with two-way analysis of variance (ANOVA) (GraphPad Prism version 9.0.0), the differences between the groups were marked with "*" ($p \leq 0.05$, $p \leq 0.01$, $p \leq 0.001$ and $p \leq 0.0001$ is represented by "*", "**", "***" and "****" respectively). "ns" was used in the groups that did not show significant differences.

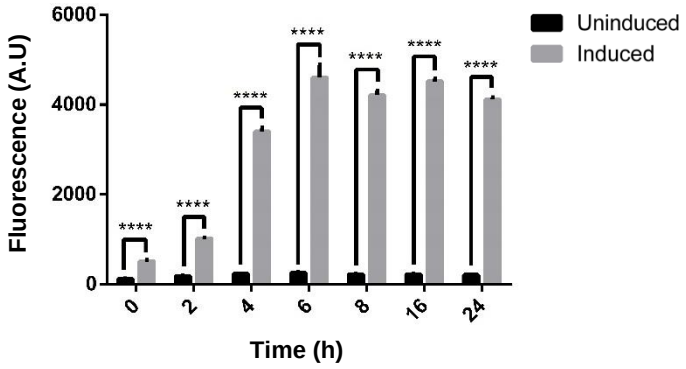

Figure 71. Time-dependent characterization of the pET22b-10mer-PpbrR-hrp-sfGFP-ProD-PbrR sensor with 200 µM lead(II) chloride ($PbCl_2$). *E. coli PRO* cells were grown in chemically defined MOPS buffered minimal growth media at 37°C. Experiments were repeated in triplicates, and measurements were taken at 0^{th}, 2^{nd}, 4^{th}, 6^{th}, 16^{th} and 24^{th} hours after induction. The results were analyzed with two-way analysis of variance (ANOVA) (GraphPad Prism version 9.0.0), the differences between the groups were marked with "*" ($p \leq 0.05$, $p \leq 0.01$, $p \leq 0.001$ and $p \leq 0.0001$ is represented by "*", "**", "***" and "****" respectively). "ns" was used in the groups that did not show significant differences.

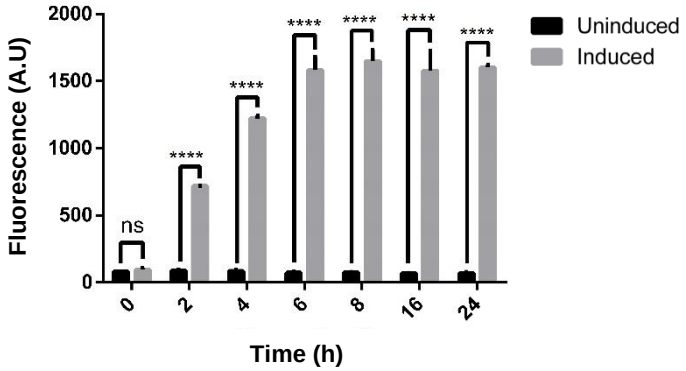

Figure 72. Time-dependent characterization of the pET22b-10mer-PpbrR-hrp-sfGFP-ProD-PbrR sensor with 200 µM lead(II) chloride ($PbCl_2$). *E. coli PRO* cells were grown in chemically defined MOPS buffered minimal growth media at 42°C. Experiments were repeated in triplicates, and measurements were taken at 0^{th}, 2^{nd}, 4^{th}, 6^{th}, 16^{th} and 24^{th} hours after induction. The results were analyzed with two-way analysis of variance (ANOVA) (GraphPad Prism version 9.0.0), the differences between the groups were marked with "*" ($p \leq 0.05$, $p \leq 0.01$, $p \leq 0.001$ and $p \leq 0.0001$ is represented by "*", "**", "***" and "****" respectively). "ns" was used in the groups that did not show significant differences.

1.3.26 Characterization of Whole-Cell Lead -10mer RBS30 and Lead -10mer hrp Biosensors at Different Salt Concentrations

Lead -10 mer RBS30 whole-cell biosensor was characterized under different sodium chloride (NaCl) concentration values: 10mM, 50mM and 100mM. MOPS buffered chemically defined media was prepared so that the final concentration of NaCl in the media was either 10mM, 50mM or 100mM. Time-dependent analysis of the pET22b-10mer-RBS30-PpbrR-sfGFP-ProD-PbrR biosensor was made with lead(II) chloride ($PbCl_2$) salt. Uninduced *E. coli* PRO cells carrying the same vector was used as a control. *E.coli* PRO cells carrying pET22b-10mer-RBS30-PpbrR-sfGFP-ProD-PbrR lead sensing circuit were grown overnight in LB, then 1% inoculated into fresh MOPS buffered minimal media with proper antibiotics. When OD_{600} reached 0.4-0.5, samples were induced with 200 µM $PbCl_2$. Fluorescence and OD_{600} measurements were taken at 0^{th}, 2^{nd}, 4^{th}, 6^{th}, 8^{th}, 16^{th} and 24^{th} hours after induction with $PbCl_2$. Lead -10 mer RBS30 sfGFP biosensor was observed to have lower signal when cells were grown in MOPS buffered growth media with 50mM NaCl (Figure 74)

compared to cases when NaCl concentration was either 10mM (Figure 73) or 100mM (Figure 75).

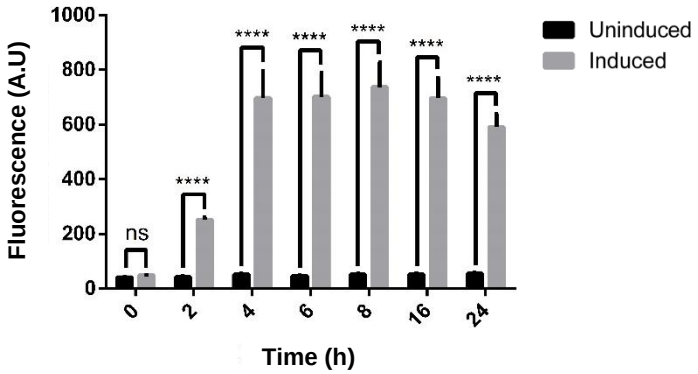

Figure 73. Time-dependent characterization of the pET22b-10mer-RBS30-PpbrR-sfGFP-ProD-PbrR sensor with 200 µM lead(II) chloride ($PbCl_2$). *E. coli PRO* cells were grown in chemically defined MOPS buffered minimal growth media with 10 mM NaCl. Experiments were repeated in triplicates, and measurements were taken at 0th, 2nd, 4th, 6th, 16th and 24th hours after induction. The results were analyzed with two-way analysis of variance (ANOVA) (GraphPad Prism version 9.0.0), the differences between the groups were marked with "*" ($p \leq 0.05$, $p \leq 0.01$, $p \leq 0.001$ and $p \leq 0.0001$ is represented by "*", "**", "***" and "****" respectively). "ns" was used in the groups that did not show significant differences.

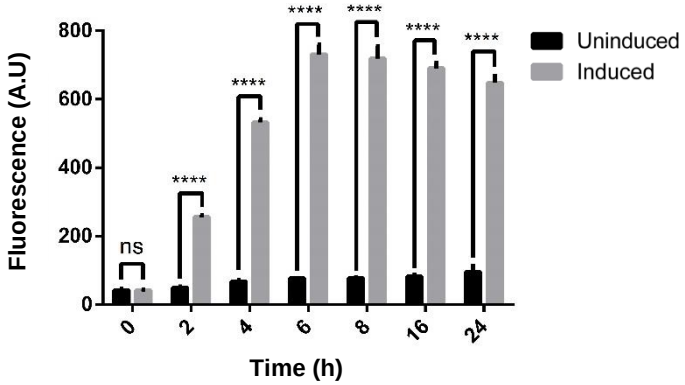

Figure 74. Time-dependent characterization of the pET22b-10mer-RBS30-PpbrR-sfGFP-ProD-PbrR sensor with 200 lead(II) chloride ($PbCl_2$). *E. coli PRO* cells were grown in chemically defined MOPS buffered minimal growth media with 50 mM NaCl. Experiments were repeated in triplicates, and measurements were taken at 0th, 2nd, 4th, 6th, 16th and 24th hours after induction. The results were analyzed with two-way analysis of variance (ANOVA) (GraphPad Prism version 9.0.0), the differences between the groups were marked with "*" ($p \leq 0.05$, $p \leq 0.01$, $p \leq 0.001$ and $p \leq 0.0001$ is represented by "*", "**", "***" and "****" respectively). "ns" was used in the groups that did not show significant differences.

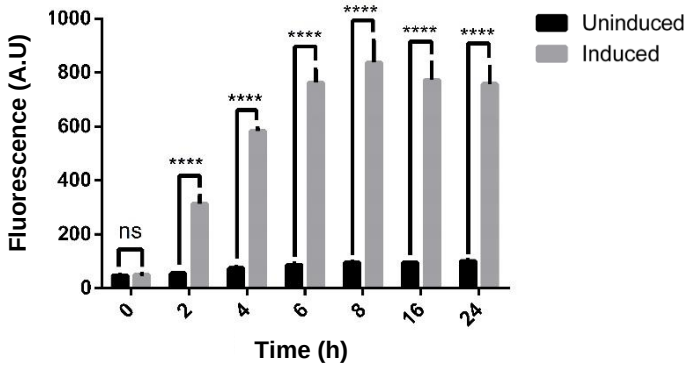

Figure 75. Time-dependent characterization of the pET22b-10mer-RBS30-PpbrR-sfGFP-ProD-PbrR sensor with 200 µM lead(II) chloride ($PbCl_2$). *E. coli PRO* cells were grown in chemically defined MOPS buffered minimal growth media with 100 mM NaCl. Experiments were repeated in triplicates, and measurements were taken at 0^{th}, 2^{nd}, 4^{th}, 6^{th}, 16^{th} and 24^{th} hours after induction. The results were analyzed with two-way analysis of variance (ANOVA) (GraphPad Prism version 9.0.0), the differences between the groups were marked with "*" ($p \leq 0.05$, $p \leq 0.01$, $p \leq 0.001$ and $p \leq 0.0001$ is represented by "*", "**", "***" and "****" respectively). "ns" was used in the groups that did not show significant differences.

Lead -10 mer hrp whole-cell biosensor was characterized under different sodium chloride (NaCl) concentration values: 10mM, 50mM and 100mM. MOPS buffered chemically defined media was prepared so that the final concentration of NaCl in the media was either 10mM, 50mM or 100mM. Time-dependent analysis of the pET22b-10mer-PpbrR-hrp-sfGFP-ProD-PbrR biosensor was made with lead(II) chloride ($PbCl_2$) salt. Uninduced *E. coli* PRO cells carrying the same vector was used as a control. *E.coli* PRO cells carrying pET22b-10mer-PpbrR-hrp-sfGFP-ProD-PbrR lead sensing circuit were grown overnight in LB, then 1% inoculated into fresh MOPS buffered minimal media with proper antibiotics. When OD_{600} reached 0.4-0.5, samples were induced with 200 µM $PbCl_2$. Fluorescence and OD_{600} measurements were taken at 0^{th}, 2^{nd}, 4^{th}, 6^{th}, 8^{th}, 16^{th} and 24^{th} hours after induction with $PbCl_2$. Lead -10 mer hrp sfGFP biosensor was observed to have lower signal when cells were grown in MOPS buffered growth media with 10mM NaCl (Figure 76) compared to cases

when NaCl concentration was either 50mM (Figure 77) or 100mM (Figure 78). Compared to cases when NaCl concentration was 50mM (Figure 77), background signal level is higher when NaCl concentration is 100mM (Figure 78).

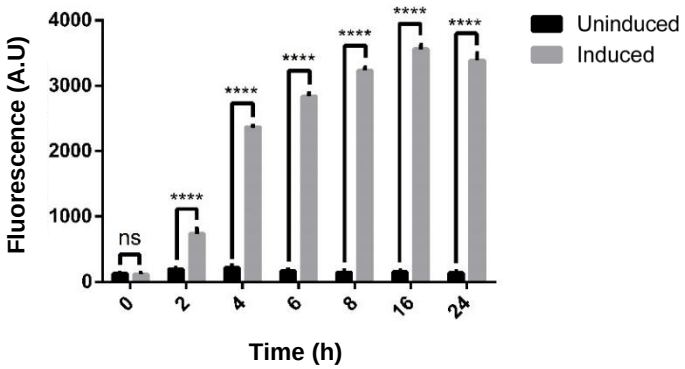

Figure 76. Time-dependent characterization of the pET22b-10mer-PpbrR-hrp-sfGFP-ProD-PbrR sensor with 200 µM lead(II) chloride ($PbCl_2$). *E. coli PRO* cells were grown in chemically defined MOPS buffered minimal growth media with 10 mM NaCl. Experiments were repeated in triplicates, and measurements were taken at 0^{th}, 2^{nd}, 4^{th}, 6^{th}, 16^{th} and 24^{th} hours after induction. The results were analyzed with two-way analysis of variance (ANOVA) (GraphPad Prism version 9.0.0), the differences between the groups were marked with "*" ($p \leq 0.05$, $p \leq 0.01$, $p \leq 0.001$ and $p \leq 0.0001$ is represented by "*", "**", "***" and "****" respectively). "ns" was used in the groups that did not show significant differences.

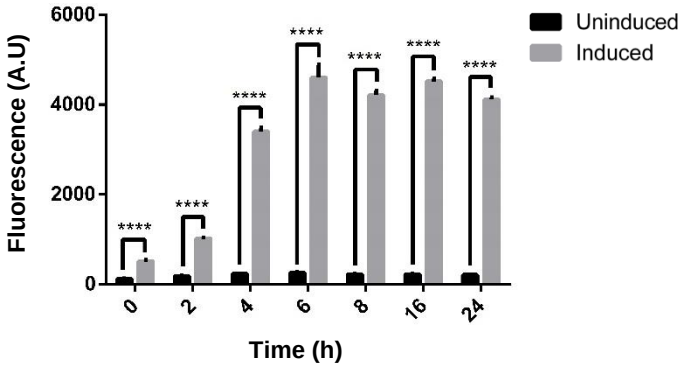

Figure 77. Time-dependent characterization of the pET22b-10mer-PpbrR-hrp-sfGFP-ProD-PbrR sensor with 200 lead(II) chloride ($PbCl_2$). *E. coli PRO* cells were grown in chemically defined MOPS buffered minimal growth media with 50 mM NaCl. A. Time-dependent graph of relative fluorescence value. B. Image of cells growing in the falcon under blue light. C. Visualization of the remaining pellet after centrifugation of the samples under blue light. D. Image of cell pellet dissolved in 1xPBS under blue light. Experiments were repeated in triplicates, and measurements were taken at 0^{th}, 2^{nd}, 4^{th}, 6^{th}, 16^{th} and 24^{th} hours after induction. The results were analyzed with two-way analysis of variance (ANOVA) (GraphPad Prism version 9.0.0), the differences between the groups were marked with "*" ($p \leq 0.05$, $p \leq 0.01$, $p \leq 0.001$ and $p \leq 0.0001$ is represented by "*", "**", "***" and "****" respectively). "ns" was used in the groups that did not show significant differences.

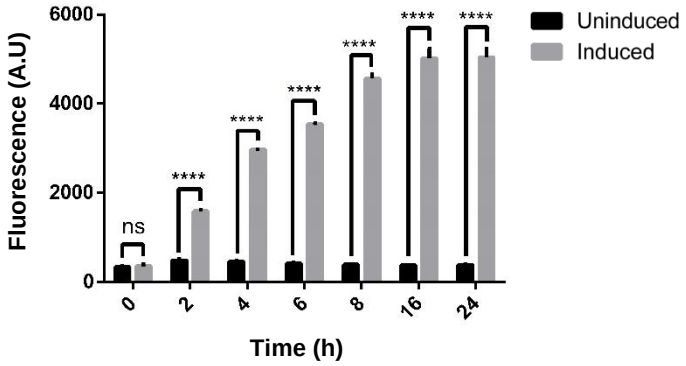

Figure 78. Time-dependent characterization of the pET22b-10mer-PpbrR-hrp-sfGFP-ProD-PbrR sensor with 200 µM lead(II) chloride ($PbCl_2$). *E. coli PRO* cells were grown in chemically defined MOPS buffered minimal growth media with 100 mM NaCl. A. Time-dependent graph of relative fluorescence value. B. Image of cells growing in the falcon under blue light. C. Visualization of the remaining pellet after centrifugation of the samples under blue light. D. Image of cell pellet dissolved in 1xPBS under blue light. Experiments were repeated in triplicates, and measurements were taken at 0^{th}, 2^{nd}, 4^{th}, 6^{th}, 16^{th} and 24^{th} hours after induction. The results were analyzed with two-way analysis of variance (ANOVA) (GraphPad Prism version 9.0.0), the differences between the groups were marked with "*" ($p \leq 0.05$, $p \leq 0.01$, $p \leq 0.001$ and $p \leq 0.0001$ is represented by "*", "**", "***" and "****" respectively). "ns" was used in the groups that did not show significant differences.

1.3.27 Cross Reactivity Analysis of Whole-Cell Lead -10 mer RBS30 Biosensor

Lead -10 mer RBS30 whole-cell biosensor was characterized with copper (II) sulfate ($CuSO_4$), lead(II) chloride ($PbCl_2$), cadmium acetate $Cd(CH_3CO_2)_2$ and sodium arsenate (Na_3AsO_4) salts for cross reactivity. Uninduced *E. coli* PRO cells carrying the same vector was used as a control. *E.coli* PRO cells carrying pET22b-10mer-RBS30-PpbrR-sfGFP-ProD-PbrR lead sensing circuit were grown overnight in LB, then 1% inoculated into fresh MOPS buffered minimal media with proper antibiotics. When OD_{600} reached 0.4-0.5, samples were induced with 200 µM $CuSO_4$, 200 µM $PbCl_2$, 10 µM $Cd(CH_3CO_2)_2$, 10 µM Na_3AsO_4 separately. Fluorescence and OD_{600} measurements were taken at 0^{th}, 2^{nd}, 4^{th}, 6^{th}, 8^{th}, 16^{th} and 24^{th} hours after induction with aforementioned heavy metals (Figure 79). Lead RBS30 sfGFP biosensor was observed to have

no significant signal when cells were induced with copper or arsenic heavy metals except for cadmium.

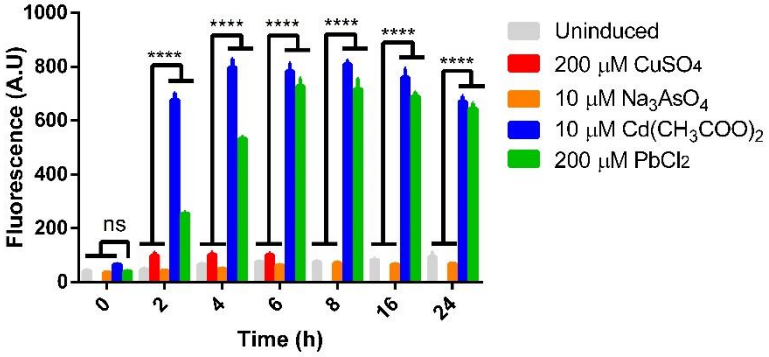

Figure 79. Time-dependent cross-reactivity characterization of the pET22b-10mer-RBS30-PpbrR-sfGFP-ProD-PbrR sensor with 200 μM $CuSO_4$, 200 μM $PbCl_2$, 10 μM $Cd(CH_3CO_2)_2$, 10 μM Na_3AsO_4 separately. *E. coli PRO* cells were grown in chemically defined MOPS buffered minimal growth media. Experiments were repeated in triplicates, and measurements were taken at 0th, 2nd, 4th, 6th, 8th, 16th and 24th hours after induction. The results were analyzed with two-way analysis of variance (ANOVA) (GraphPad Prism version 9.0.0), the differences between the groups were marked with "*" ($p \leq 0.05$, $p \leq 0.01$, $p \leq 0.001$ and $p \leq 0.0001$ is represented by "*", "**", "***" and "****" respectively). "ns" was used in the groups that did not show significant differences.

Lead -10 mer RBS30 sensor responds to cadmium ions, hence the concentration-dependent behavior of the sensor for cadmium was investigated. As seen in dynamic range graph (Figure 80) lead -10 mer RBS30 responds to cadmium as well.

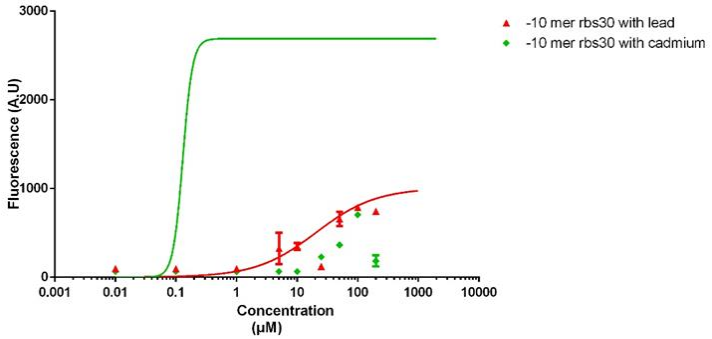

Figure 80. Concentration-dependent characterization of the pET22b-10mer-RBS30-PpbrR-sfGFP-ProD-PbrR sensor with $PbCl_2$ and $Cd(CH_3CO_2)_2$. Experiments were repeated in triplicates, and measurements were taken at the 6th hour of induction. E. coli cells were grown in chemically defined MOPS buffered minimal growth media.

1.3.28 Construction of Whole-Cell Cadmium Biosensor

Cadmium heavy metal whole-cell biosensor was built with promoter sequence (PcadA) and its corresponding transcription factor (CadR) from *Pseudomonas putida.* In the absence of cadmium ions, CadR protein represses the downstream expression through binding to PcadA promoter. When cadmium ions are present in the environment, binding of cadmium ions to CadR leads to conformational change of CadR protein. Then, CadR protein is released from the PcadR promoter, and PcadA promoter becomes accessible by RNA polymerase to activate downstream expression of gene(s) (Figure 81).

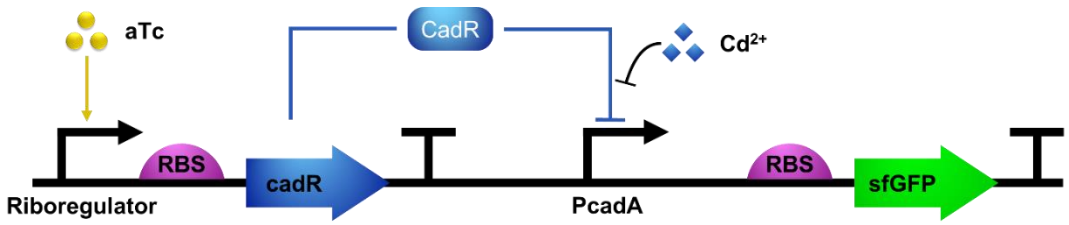

Figure 81. Figure of cadmium biosensor working mechanism. Cadmium biosensor biological parts and working mechanism. CadR transcription factor binds to PcadA promoter in the absence of cadmium ions within the cell. When cadmium ions present, upon release of CadR from PcadA promoter, downstream expression of sfGFP is activated.

Cadmium biosensor was constructed by replacing PpbrR promoter site within the lead biosensor circuit vector, pET22b-PpbrR-sfGFP-ProD-PbrR, with PcadA promoter sequence with PCR amplification (Figure 82). PpbrR promoter region was amplified with primers suitable for the Gibson Assembly method. Primers can be found at Appendix B. After PCR products were run on 1% agarose gel, they were isolated from the gel with Macherey-Nagel's PCR Clean-up kit according to the manufacturer's instructions and assembled with the Gibson Assembly method. Samples selected from the single colonies were

sent for Sanger sequencing analysis. Plasmid map for cadmium biosensor and Sanger sequencing result can be found at Appendix C and D, respectively.

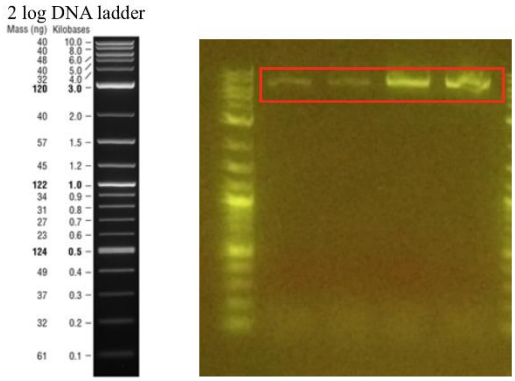

Figure 82. Agarose gel image of the biological parts required for the cloning of the pET22b-PcadA-sfGFP-ProD-PbrR vector. PCR product of the linear pET22b-PcadA-sfGFP-ProD-PbrR backbone, 6400 bp.

Then, CadR transcription factor's gene sequence (synthesized from Genewiz) was cloned downstream of constitutively active ProD promoter while replacing PbrR gene. First, CadR gene was amplified with PCR from the gene fragment with overhangs to backbone (Figure 83 B). Second, pET22b-PcadA-sfGFP-ProD vector was amplified with PCR (Figure 83 A). After PCR products were run on 1% agarose gel, they were isolated from the gel with Macherey-Nagel's PCR Clean-up kit according to the manufacturer's instructions. Finally, pET22b-PcadA-sfGFP-ProD-CadR vector was constructed with Gibson Assembly method. Samples selected from single colonies were sent for Sanger sequencing analysis. Plasmid map for cadmium biosensor and Sanger sequencing result can be found at Appendix C and D, respectively.

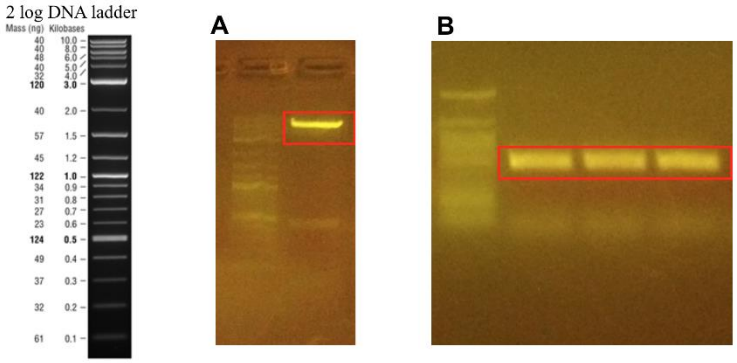

Figure 83. Agarose gel image of the biological parts required for the cloning of the pET22b-PcadA-sfGFP-ProD-CadR vector. A. PCR product of the linear pET22b-PcadA-sfGFP-ProD backbone, 6000 bp. B. PCR product of CadR transcription factor gene region, 500 bp.

Several mutations occurred in CadR genomic region when it was cloned downstream of ProD promoter. Although cloning step was repeated, different mutations in CadR gene site were detected. Hence, constitutive expression of CadR was considered to be toxic to the cells. To obtain mutation-free and controlled CadR protein expression within the cell, ProD constitutive promoter was removed from pET22b-PcadA-sfGFP-ProD-CadR vector by digestion with XhoI (Figure 84). Then, cleavage product was self-ligated with Gibson Assembly method. Samples selected from single colonies were sent for Sanger sequencing analysis. Plasmid map for cadmium biosensor and Sanger sequencing result can be found at Appendix C and D, respectively.

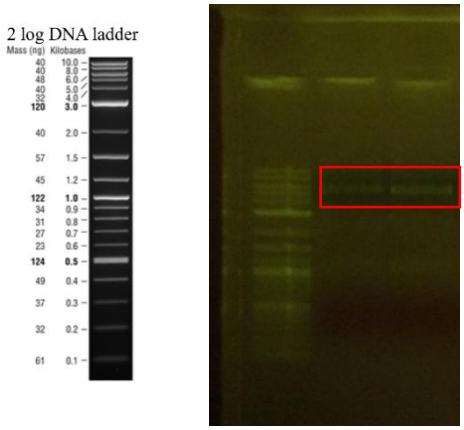

Figure 84. Agarose gel image of the restriction of pET22b-PcadA-sfGFP-ProD-CadR vector with XhoI, biological part required for the cloning of the pET22b-PcadA-sfGFP vector, 5340 bp.

CadR gene region was cloned into pZs vector downstream of PlTetO promoter controlled riboregulator region. Trans activator and cis repressing – CadR DNA regions are controlled by anhydrotetracycline (aTc) induction as both of them are located downstream of PlTetO promoter (Figure 85). pZs vector backbone was obtained from pZs-mProD-merR-KanR vector (gift from Behide Saltepe) by restriction with HindIII and AatII enzymes, 3506 bp. Samples selected from the colonies were first verified with colony PCR (Figure 86), and then colony PCR verified samples were sent for Sanger sequencing analysis. Plasmid map for cadmium biosensor and Sanger sequencing result can be found at Appendix C and D, respectively.

Figure 85. Agarose gel image of the biological part required for the cloning of the pZs-PlTetO-riboregulator-CadR-KanR vector. PCR product of the PlTetO-riboregulator-CadR gene region, 878 bp.

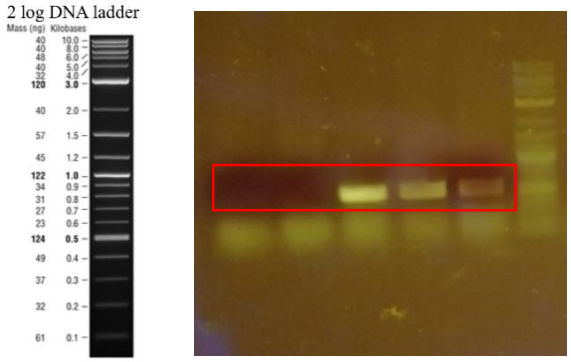

Figure 86. Confirmation of the pZs-PlTetO-riboregulator-CadR-KanR vector with colony PCR. A. The bands expected for the PCR amplified PlTetO-riboregulator-CadR biological parts were observed at 878 bp.

1.3.29 Construction of Whole-Cell Cadmium RBS30 Biosensor

The output signal level of cadmium biosensor was not at desired level. To prevent the possibility of changing biosensor's sensitivity, RBS site between the PcadA promoter and the sfGFP gene was replaced with a stronger RBS30 (Figure 87). To do so, pET22b-PcadA-sfGFP-ProD-CadR was linearly amplified with PCR reaction by adding RBS30 parts while removing the old RBS region (Figure 88). Then PCR product was extracted from agarose gel and subjected to Gibson Assembly. The new vector was named as pET22b-PcadA- RBS30-sfGFP-ProD-CadR. Plasmid map for cadmium RBS30

biosensor and Sanger sequencing result can be found at Appendix C and D, respectively.

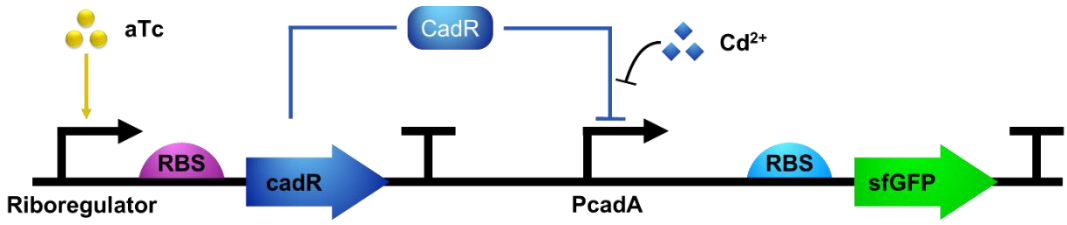

Figure 87. Figure of cadmium RBS30 biosensor working mechanism. Cadmium biosensor biological parts and working mechanism. CadR transcription factor binds to PcadA promoter in the absence of cadmium ions within the cell. When cadmium ions present, upon release of CadR from PcadA promoter, downstream expression of sfGFP is activated with stronger RBS30.

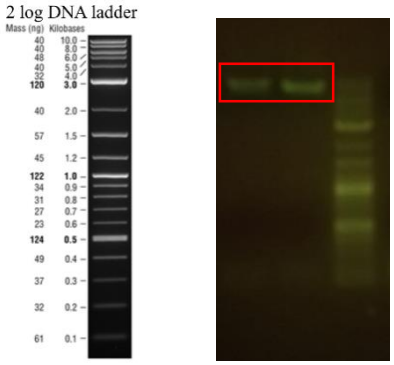

Figure 88. Agarose gel image of the biological part required for the cloning of the pET22b-PcadA-RBS30-sfGFP-ProD-CadR vector. PCR product of the linear pET22b-PcadA-RBS30-sfGFP-ProD-CadR backbone, 6428 bp.

As there were several mutations in CadR gene when it was cloned downstream of ProD promoter, ProD CadR region was removed from pET22b-PcadA-RBS30-sfGFP-ProD-CadR vector by digestion with XhoI (Figure 89). Then, cleavage product was self-ligated with Gibson Assembly method. Samples selected from single colonies were sent for Sanger sequencing

analysis. Plasmid map for cadmium biosensor and Sanger sequencing result can be found at Appendix C and D, respectively.

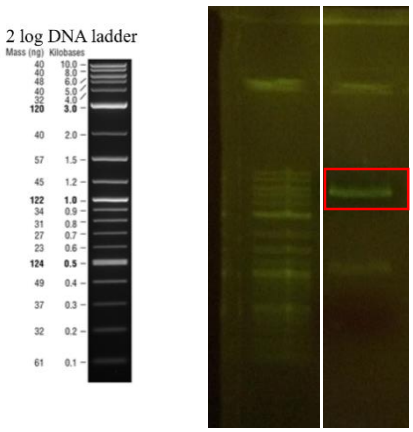

Figure 89. Agarose gel image of the restriction of pET22b-PcadA-RBS30-sfGFP-ProD-CadR vector with XhoI, biological part required for the cloning of the pET22b-PcadA-RBS30-sfGFP vector, 5340 bp.

1.3.30 Characterization of Whole-Cell Cadmium RBS30 Biosensor

Time dependent and dynamic range analysis of the pET22b-PcadA-RBS30-sfGFP cotransformed with pZs-PlTetO-riboregulator-CadR-KanR sensor was made with cadmium acetate $Cd(CH_3CO_2)_2$ salt. Uninduced *E. coli* PRO cells carrying the same vectors was used as a control. Unlike others, cells carrying cadmium biosensor parts were grown until OD_{600} reached 0.3, and induced with anhydrotetracycline (aTc) with final concentration of 100ng/µL. Cadmium biosensors grown another 2 hours at 37°C with shaking at 200 rpm, then cells are induced with heavy metals. Time dependent measurements were taken at 0^{th}, 2^{nd}, 4^{th}, 6^{th}, 8^{th}, 16^{th} and 24^{th} hours after induction with $Cd(CH_3CO_2)_2$ (Figure 90). In order to understand the response of the pET22b-PcadA-RBS30-sfGFP cotransformed with pZs-PlTetO-riboregulator-CadR-KanR sensor to different $Cd(CH_3CO_2)_2$ concentrations, dynamic range with varying $Cd(CH_3CO_2)_2$ concentrations was performed at 8^{th} hour after induction.

Cadmium RBS30 biosensor responded even to a concentration as low as 10 µM (Figure 91).

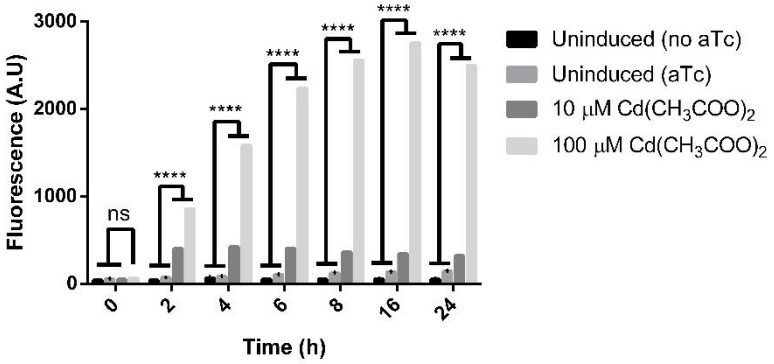

Figure 90. Time dependent characterization of the pET22b-PcadA-RBS30-sfGFP cotransformed with pZs-PlTetO-riboregulator-CadR-KanR sensor was made with 10 µM cadmium acetate $Cd(CH_3CO_2)_2$. Experiments were performed in triplicates and measurements were taken at the 0th, 2nd, 4th, 6th, 8th, 16th and 24th hours after induction. The results were analyzed with two-way analysis of variance (ANOVA) (GraphPad Prism version 9.0.0), the differences between the groups were marked with "*" ($p \leq 0.05$, $p \leq 0.01$, $p \leq 0.001$ and $p \leq 0.0001$ is represented by "*", "**", "***" and "****" respectively). No marking was made in the groups that did not show significant differences. E. coli cells were grown in chemically defined MOPS buffered minimal growth media.

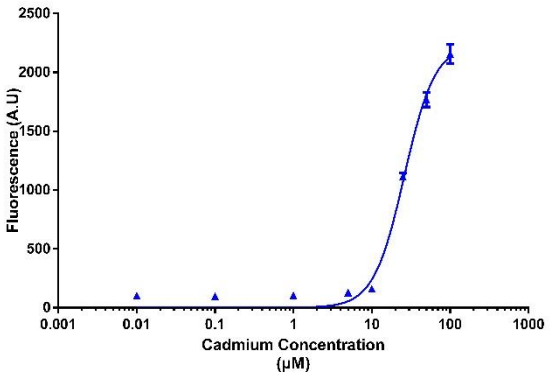

Figure 91. Concentration-dependent characterization of the pET22b-PcadA-RBS30-sfGFP cotransformed with pZs-PlTetO-riboregulator-CadR-KanR sensor with $Cd(CH_3CO_2)_2$. Experiments were repeated in triplicates, and measurements were taken at the 8th hour of induction. E. coli cells were grown in chemically defined MOPS buffered minimal growth media.

1.3.31 Construction of Whole-Cell Cadmium RBS30 mTagBFP Biosensor

To combine the cadmium RBS30 biosensor (pET22b-PcadA-RBS30-mTagBFP) with other heavy metal biosensors for multi-input multi-output system, sfGFP reporter gene was replaced with mTagBFP gene (which can

be distinguished from sfGFP and mScarlet) (Figure 92). For this purpose, pET22b-PcadA-RBS30 vector backbone and mTagBFP gene (iGEM repository: BBa_K592100) were amplified with PCR. After PCR products were run on 1% agarose gel, they were isolated from the gel with Macherey-Nagel's PCR Clean-up kit according to the manufacturer's instructions and assembled with the Gibson Assembly method (Figure 93). Samples were sent for Sanger sequencing analysis. Plasmid map for cadmium RBS30 mTagBFP biosensor and Sanger sequencing result can be found at Appendix C and D, respectively.

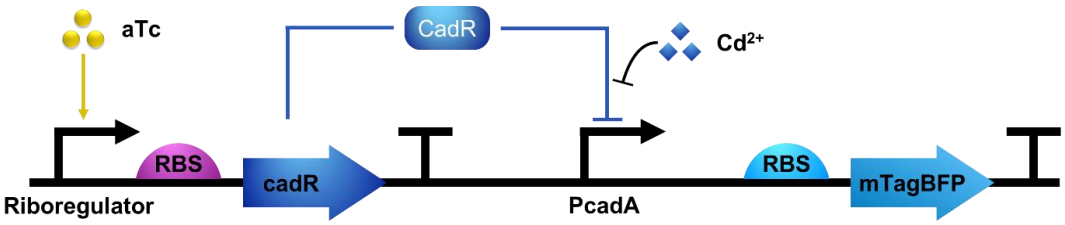

Figure 92. Figure of cadmium RBS30 biosensor working mechanism. Cadmium biosensor biological parts and working mechanism. CadR transcription factor binds to PcadA promoter in the absence of cadmium ions within the cell. When cadmium ions present, upon release of CadR from PcadA promoter, downstream expression of sfGFP is activated with stronger RBS30.

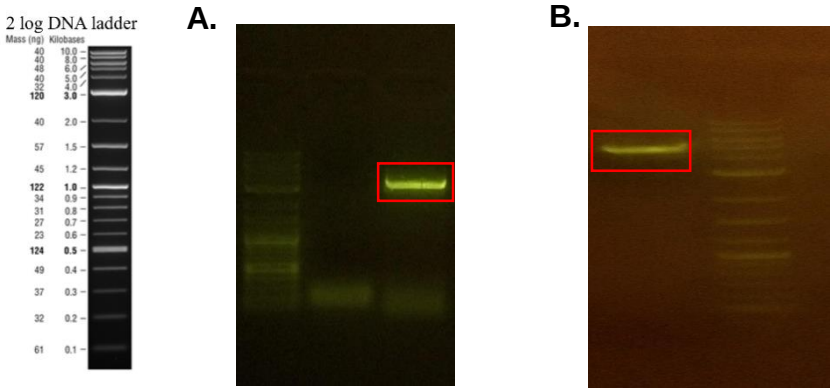

Figure 93. Agarose gel image of the fragment required for the cloning of the pET22b-PcadA-RBS30-mTagBFP vector. A. mTagBFP linear DNA fragment, 700bp. B The backbone vector the pET22b-PcadA, 5000 bp.

1.3.32 Characterization of Whole-Cell Cadmium RBS30 mTagBFP Biosensor

Time dependent and dynamic range analysis of the pET22b-PcadA-RBS30-mTagBFP cotransformed with pZs-PlTetO-riboregulator-CadR-KanR sensor was made with cadmium acetate $Cd(CH_3CO_2)_2$ salt. Uninduced *E. coli* PRO cells carrying the same vectors was used as a control. Unlike others, cells carrying cadmium biosensor parts were grown until OD_{600} reached 0.3, and induced with anhydrotetracycline (aTc) with final concentration of 100ng/µL. Cadmium biosensors grown another 2 hours at 37°C with shaking at 200 rpm, then cells are induced with heavy metals. Time dependent measurements were taken at 0^{th}, 2^{nd}, 4^{th}, 6^{th}, 8^{th}, 16^{th} and 24^{th} hours after induction with $Cd(CH_3CO_2)_2$ (Figure 94). In order to understand the response of the pET22b-PcadA-RBS30-mTagBFP cotransformed with pZs-PlTetO-riboregulator-CadR-KanR sensor to different $Cd(CH_3CO_2)_2$ concentrations, dynamic range with varying $Cd(CH_3CO_2)_2$ concentrations was performed at 8^{th} hour after induction. Cadmium RBS30 mTagBFP biosensor responded even to a concentration as low as 10 µM (Figure 95).

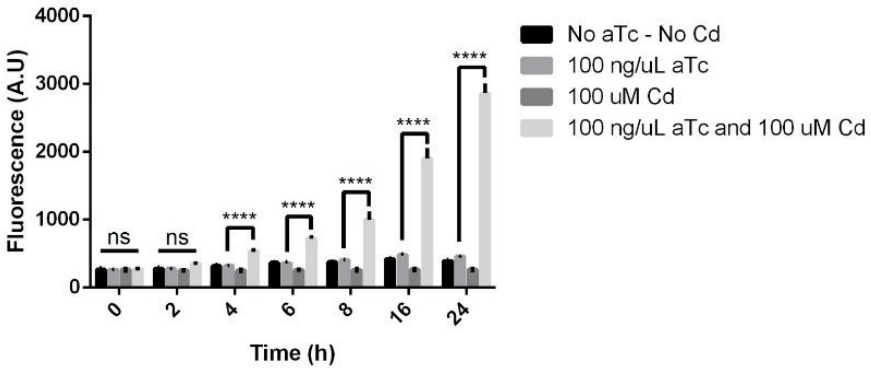

Figure 94. Time dependent characterization of the pET22b-PcadA-RBS30-mTagBFP cotransformed with pZs-PlTetO-riboregulator-CadR-KanR sensor was made with 100 µM cadmium acetate $Cd(CH_3CO_2)_2$. Experiments were performed in triplicates and measurements were taken at the 0^{th}, 2^{nd}, 4^{th}, 6^{th}, 8^{th}, 16^{th} and 24^{th} hours after induction. The results were analyzed with two-way analysis of variance (ANOVA) (GraphPad Prism version 9.0.0), the differences between the groups were marked with "*" ($p \leq 0.05$, $p \leq 0.01$, $p \leq 0.001$ and $p \leq 0.0001$ is represented by "*", "**", "***" and "****" respectively). No marking was made in the groups that did not show significant differences. E. coli cells were grown in chemically defined MOPS buffered minimal growth media.

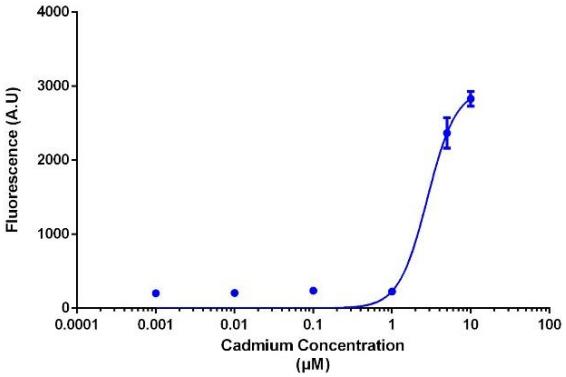

Figure 95. Concentration-dependent characterization of the pET22b-PcadA-RBS30-mTagBFP cotransformed with pZs-PlTetO-riboregulator-CadR-KanR sensor with $Cd(CH_3CO_2)_2$. Experiments were repeated in triplicates, and measurements were taken at the 8th hour of induction. E. coli cells were grown in chemically defined MOPS buffered minimal growth media.

1.3.33 Construction of Whole-Cell Cadmium hrp Biosensor

To further increase the strength of output signal level, a synthetic amplification circuit unit was integrated between PcadA promoter and sfGFP gene. The synthetic amplification circuit consists of PhrpL promoter controlled by hrpR and hrpS genes, referred as hrp circuit as mentioned earlier in Lead hrp biosensor part (Figure 96). To construct cadmium hrp biosensor circuit, pET22b-PcadA-sfGFP backbone was linearly amplified with PCR reaction by adding necessary overhangs (not shown), 5370 bp. Synthetic amplification circuit (hrp region) was amplified with PCR from pBW103ParsR-Amp30C vector (purchased from Addgene, ID: 78638) (Figure 53 B), 2300 bp. Then PCR products were extracted from agarose gel and subjected to Gibson Assembly. The new vector was named as pET22b-PcadA-hrp-sfGFP. Samples selected from the colonies were first verified with colony PCR (Figure 97), and then colony PCR verified samples were sent for Sanger sequencing analysis. Plasmid map for cadmium hrp biosensor and Sanger sequencing result can be found at Appendix C and D, respectively.

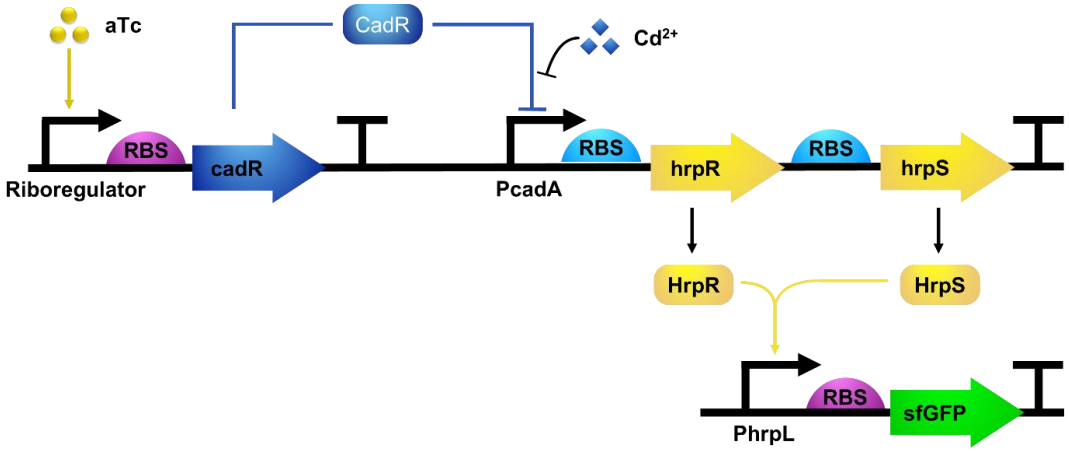

Figure 96. Figure of cadmium hrp sfGFP biosensor working mechanism. Cadmium biosensor biological parts and working mechanism. CadR transcription factor binds to PcadA promoter in the absence of cadmium ions within the cell. When cadmium ions present, upon release of CadR from PcadA promoter, downstream expression of sfGFP is activated.

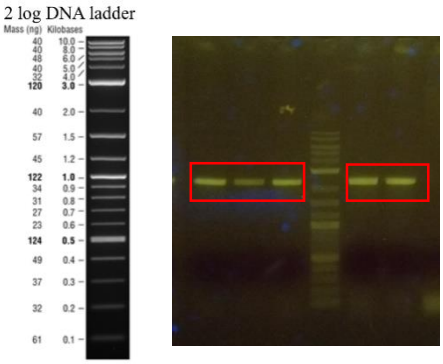

Figure 97. Confirmation of the pET22b-PcadA-hrp-sfGFP vector with colony PCR. A. The bands expected for the PCR amplified hrp biological parts were observed at 2300 bp.

1.3.34 Characterization of Whole-Cell Cadmium hrp Biosensor

Time dependent and dynamic range analysis of the pET22b-PcadA-hrp-sfGFP cotransformed with pZs-PlTetO-riboregulator-CadR-KanR sensor was made with cadmium acetate $Cd(CH_3CO_2)_2$ salt. Uninduced *E. coli* PRO cells carrying the same vectors was used as a control. Unlike others, cells carrying cadmium biosensor parts were grown until OD_{600} reached 0.3, and induced with anhydrotetracycline (aTc) with final concentration of 100ng/µL. Cadmium

biosensors grown another 2 hours at 37°C with shaking at 200 rpm, then cells are induced with heavy metals. Time dependent measurements were taken at 0^{th}, 2^{nd}, 4^{th}, 6^{th}, 8^{th}, 16^{th} and 24^{th} hours after induction with $Cd(CH_3CO_2)_2$ (Figure 98). In order to understand the response of the pET22b-PcadA-hrp-sfGFP cotransformed with pZs-PlTetO-riboregulator-CadR-KanR sensor to different $Cd(CH_3CO_2)_2$ concentrations, dynamic range with varying $Cd(CH_3CO_2)_2$ concentrations was performed at 8^{th} hour after induction. Cadmium hrp biosensor responded even to a concentration as low as 10 nM (Figure 99).

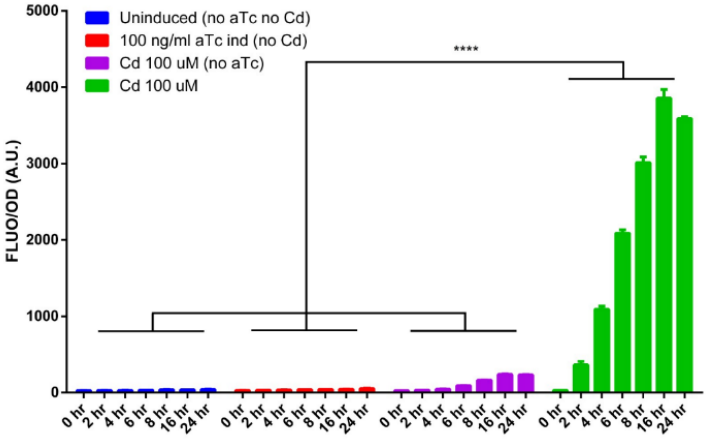

Figure 98. Time dependent characterization of the pET22b-PcadA-hrp-sfGFP cotransformed with pZs-PlTetO-riboregulator-CadR-KanR sensor was made with 100 µM cadmium acetate $Cd(CH_3CO_2)_2$. Experiments were performed in triplicates and measurements were taken at the 0^{th}, 2^{nd}, 4^{th}, 6^{th}, 8^{th}, 16^{th} and 24^{th} hours after induction. The results were analyzed with two-way analysis of variance (ANOVA) (GraphPad Prism version 9.0.0), the differences between the groups were marked with "*" ($p \leq 0.05$, $p \leq 0.01$, $p \leq 0.001$ and $p \leq 0.0001$ is represented by "*", "**", "***" and "****" respectively). No marking was made in the groups that did not show significant differences. E. coli cells were grown in chemically defined MOPS buffered minimal growth media.

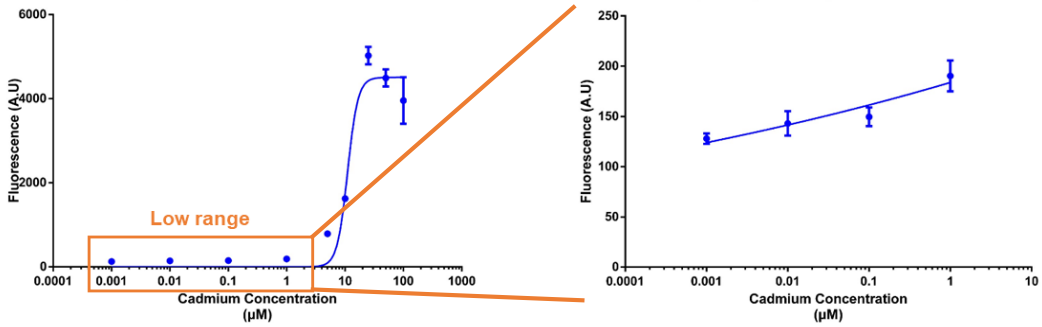

Figure 99. Concentration-dependent characterization of the pET22b-PcadA-hrp-sfGFP cotransformed with pZs-PlTetO-riboregulator-CadR-KanR sensor with $Cd(CH_3CO_2)_2$. Experiments were repeated in triplicates, and measurements were taken at the 8th hour of induction. E. coli cells were grown in chemically defined MOPS buffered minimal growth media.

1.3.35 Construction of Whole-Cell Cadmium hrp mTagBFP Biosensor

To combine the cadmium hrp biosensor (pET22b-PcadA-hrp-mTagBFP) with other heavy metal biosensors for multi-input multi-output system, hrp amplification circuit was integrated into pET22b-PcadA-RBS30-mTagBFP vector (which can be distinguished from sfGFP and mScarlet) (Figure 100). For this purpose, pET22b-PcadA-RBS30- mTagBFP vector backbone and hrp amplification circuit were amplified with PCR. After PCR products were run on 1% agarose gel, they were isolated from the gel with Macherey-Nagel's PCR Clean-up kit according to the manufacturer's instructions and assembled with the Gibson Assembly method (Figure 101). Samples were sent for Sanger sequencing analysis. Plasmid map for cadmium RBS30 mTagBFP biosensor and Sanger sequencing result can be found at Appendix C and D, respectively.

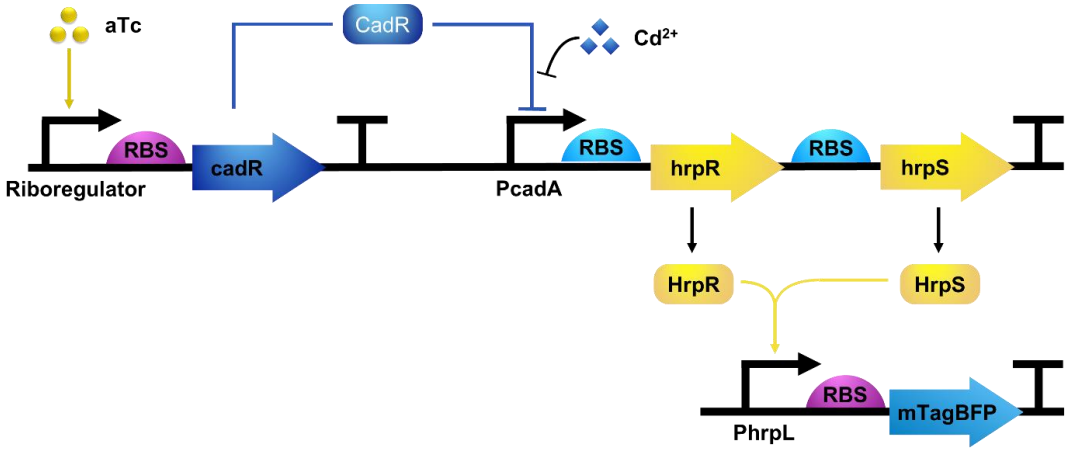

Figure 100.Figure of cadmium hrp mTagBFP biosensor working mechanism. Cadmium biosensor biological parts and working mechanism. CadR transcription factor binds to PcadA promoter in the absence of cadmium ions within the cell. When cadmium ions present, upon release of CadR from PcadA promoter, downstream expression of sfGFP is activated.

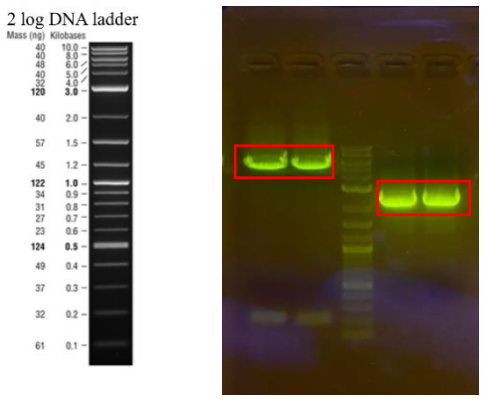

Figure 101. Agarose gel image of the fragment required for the cloning of the pET22b-PcadA-hrp-mTagBFP vector. A. The backbone vector the pET22b-PcadA-mTagBFP, 5325 bp. B. hrp amplification circuit linear DNA fragment, 2300 bp.

1.3.36 Characterization of Whole-Cell Cadmium Biosensors with Serum Samples

To test the applicability of biosensors for diagnosis of heavy metal poisoning, biosensors were tested with M63 growth media mixed with fetal bovine serum (FBS). Dynamic range analysis of the pET22b-PcadA-RBS30-sfGFP cotransformed with pZs-PlTetO-riboregulator-CadR-KanR sensor was made

with cadmium acetate $Cd(CH_3CO_2)_2$ salt. *E.coli* PRO cells carrying their corresponding biosensor circuits were grown overnight in LB, then 1% inoculated into fresh LB media with proper antibiotics. Unlike others, cells carrying cadmium biosensor parts were grown until OD_{600} reached 0.3, and induced with anhydrotetracycline (aTc) with final concentration of 100ng/µL. Cadmium biosensors grown another 2 hours at 37°C with shaking at 200 rpm, then cells are induced with heavy metals. When OD_{600} reached 0.4-0.5, samples were centrifuged at 3000 rpm for 10 minutes. Supernatant was discarded from each sample, and pellets were resuspended in equal volume of a mixture of heat-treated FBS and M63 minimal media (3:1), and induced with different concentrations of $Cd(CH_3CO_2)_2$. Fluorescence and OD_{600} measurements were taken at 16th hour of induction. Cadmium RBS30 sfGFP biosensor was observed to be responsive to concentrations 100 µM $Cd(CH_3CO_2)_2$ (Figure 102).

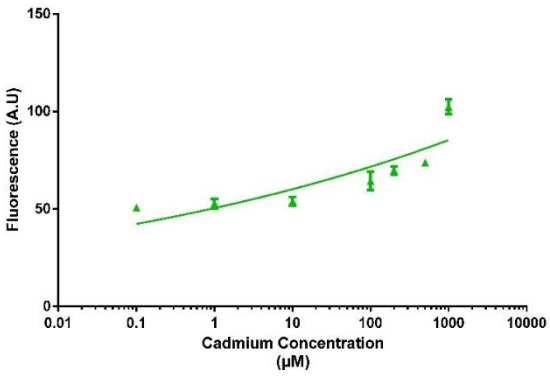

Figure 102. Concentration-dependent characterization of the pET22b-PcadA-RBS30-sfGFP cotransformed with pZs-PlTetO-riboregulator-CadR-KanR biosensor with cadmium acetate $Cd(CH_3CO_2)_2$. Experiments were repeated in triplicates, and measurements were taken at the 16th hour of induction. E. coli cells were grown in LB media until OD_{600} reached 0.4-0.5, then transferred to a mixture ofheat-treated FBS and M63 minimal media (3:1) and induced with different concentrations of $Cd(CH_3CO_2)_2$.

1.3.37 Cross Reactivity Analysis of Whole-Cell Cadmium Biosensor

Cadmium RBS30 whole-cell biosensor was characterized with copper (II) sulfate ($CuSO_4$), lead(II) chloride ($PbCl_2$), cadmium acetate $Cd(CH_3CO_2)_2$ and sodium arsenate (Na_3AsO_4) salts for cross reactivity. Uninduced *E. coli* PRO cells carrying the same vector was used as a control. *E.coli* PRO cells carrying pET22b-PcadA-RBS30-sfGFP cotransformed with pZs-PlTetO-riboregulator-CadR-KanR cadmium sensing circuit were grown overnight in LB, then 1% inoculated into fresh MOPS buffered minimal media with proper antibiotics. Cells were grown until OD_{600} reached 0.3, and induced with anhydrotetracycline (aTc) with final concentration of 100ng/µL. Cadmium RBS30 biosensor grown another 2 hours at 37°C with shaking at 200 rpm, then cells are induced with 200 µM $CuSO_4$, 200 µM $PbCl_2$, 10 µM and 100 µM $Cd(CH_3CO_2)_2$, 10 µM Na_3AsO_4 separately. Fluorescence and OD_{600} measurements were taken at 0^{th}, 2^{nd}, 4^{th}, 6^{th}, 8^{th}, 16^{th} and 24^{th} hours after induction with aforementioned heavy metals (Figure 103). Cadmium RBS30 sfGFP biosensor was observed to have no significant signal when cells were induced with copper or arsenic heavy metals except for lead.

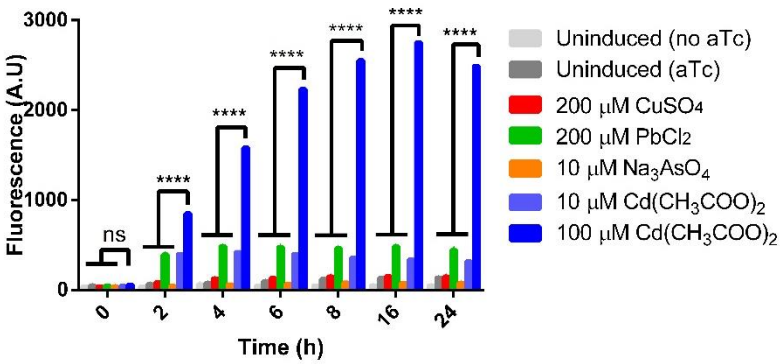

Figure 103. Time-dependent cross-reactivity characterization of the pET22b-PcadA-RBS30-sfGFP cotransformed with pZs-PlTetO-riboregulator-CadR-KanR sensor with 200 µM $CuSO_4$, 200 µM $PbCl_2$, 10 µM and 100 µM $Cd(CH_3CO_2)_2$, 10 µM Na_3AsO_4 separately. *E. coli PRO* cells were grown in chemically defined MOPS buffered minimal growth media. Experiments were repeated in triplicates, and measurements were taken at 0^{th}, 2^{nd}, 4^{th}, 6^{th}, 8^{th}, 16^{th} and 24^{th} hours after induction. The results were

analyzed with two-way analysis of variance (ANOVA) (GraphPad Prism version 9.0.0), the differences between the groups were marked with "*" ($p \leq 0.05$, $p \leq 0.01$, $p \leq 0.001$ and $p \leq 0.0001$ is represented by "*", "**", "***" and "****" respectively). "ns" was used in the groups that did not show significant differences.

Cadmium hrp whole-cell biosensor was characterized with copper (II) sulfate ($CuSO_4$), lead(II) chloride ($PbCl_2$), cadmium acetate $Cd(CH_3CO_2)_2$ and sodium arsenate (Na_3AsO_4) salts for cross reactivity. Uninduced *E. coli* PRO cells carrying the same vector was used as a control. *E.coli* PRO cells carrying pET22b-PcadA-hrp-sfGFP cotransformed with pZs-PlTetO-riboregulator-CadR-KanR cadmium sensing circuit were grown overnight in LB, then 1% inoculated into fresh MOPS buffered minimal media with proper antibiotics. Cells were grown until OD_{600} reached 0.3, and induced with anhydrotetracycline (aTc) with final concentration of 100ng/µL. Cadmium hrp biosensor grown another 2 hours at 37°C with shaking at 200 rpm, then cells are induced with 200 µM $CuSO_4$, 200 µM $PbCl_2$, 10 µM and 100 µM $Cd(CH_3CO_2)_2$, 10 µM Na_3AsO_4 separately. Fluorescence and OD_{600} measurements were taken at 0^{th}, 2^{nd}, 4^{th}, 6^{th}, 8^{th}, 16^{th} and 24^{th} hours after induction with aforementioned heavy metals (Figure 104). Cadmium hrp sfGFP biosensor was observed to have no significant signal when cells were induced with copper or arsenic heavy metals except for lead.

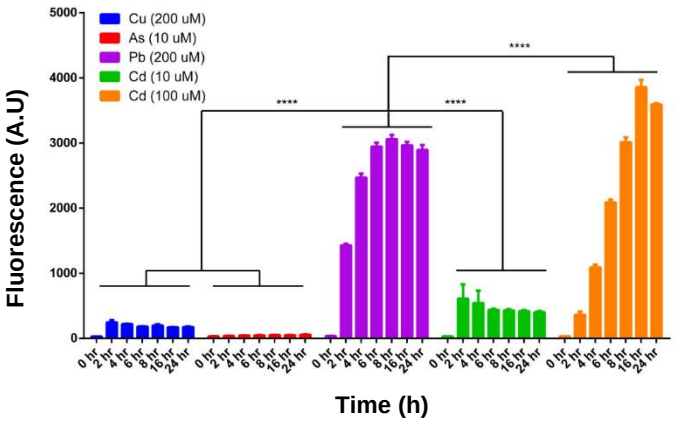

Figure 104. Time-dependent cross-reactivity characterization of the pET22b-PcadA-hrp-sfGFP cotransformed with pZs-PlTetO-riboregulator-CadR-KanR sensor with 200 µM $CuSO_4$, 200 µM $PbCl_2$, 10 µM and 100 µM $Cd(CH_3CO_2)_2$, 10 µM Na_3AsO_4 separately. *E. coli PRO* cells were grown in chemically defined MOPS buffered minimal growth media. Experiments were repeated in triplicates, and measurements were taken at 0th, 2nd, 4th, 6th, 8th, 16th and 24th hours after induction. The results were analyzed with two-way analysis of variance (ANOVA) (GraphPad Prism version 9.0.0), the differences between the groups were marked with "*" ($p \leq 0.05$, $p \leq 0.01$, $p \leq 0.001$ and $p \leq 0.0001$ is represented by "*", "**", "***" and "****" respectively). "ns" was used in the groups that did not show significant differences.

Cadmium hrp sensor responds to lead ions, so the concentration-dependent behavior of the sensor for lead was investigated. As seen in dynamic range graph (Figure 105) cadmium hrp responds to lead as well even though signal level is lower compared to cadmium induction with the same concentration.

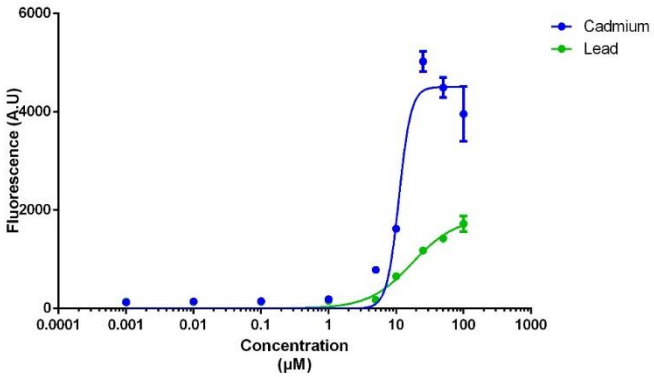

Figure 105. Concentration-dependent characterization of the the pET22b-PcadA-RBS30-sfGFP cotransformed with pZs-PlTetO-riboregulator-CadR-KanR sensor with $PbCl_2$ and $Cd(CH_3CO_2)_2$. Experiments were repeated in triplicates, and measurements were taken at the 6th hour of induction. E. coli cells were grown in chemically defined MOPS buffered minimal growth media.

1.3.43 Construction of Whole-Cell Arsenic Biosensors

To build arsenic heavy metal whole-cell biosensor, the sequences of a promoter (ParsR) and its cognate transcription factor (ArsR) from *E. coli* DH5α genome were selected to sense the presence of arsenic ions in the environment. ArsR-ParsR binding plays an active role in arsenic resistance in *E.coli*. ArsR transcriptional repressor binds to ParsR promoter to repress its downstream gene expression. When arsenic ions present within the cell, upon binding of arsenic ions to ArsR protein conformational change happens. ArsR protein arsenic ion complex is released from ParsR promoter, then downstream expression of gene(s) starts (Figure 106).

Arsenic biosensor plasmid backbone was constructed from two PCR amplified parts: pET22b-sfGFP backbone and ParsR promoter region, which were amplified from pET22b-sfGFP backbone PCR amplified from pET22b (+) synpHucO sfGFP proD HucR (gift from Sıla Köse) and genome of *E. coli* DH5α PRO, respectively (Figure 107). ParsR promoter region was amplified with primers suitable for the Gibson Assembly method. Arsenic biosensor plasmid construct was named as of pET22b-ParsR-sfGFP-ProD-HucR. Primers can be found at Appendix B. After PCR products were run on 1% agarose gel, they were isolated from the gel with Macherey-Nagel's PCR Clean-up kit according to the manufacturer's instructions and assembled with the Gibson Assembly method. In the first step, ArsR transcription factor was already expressed in *E.coli* DH5α, hence it was not cloned for extra expression as it might be toxic and cause burden to the cell. Samples selected from the colonies were verified

with Sanger sequencing analysis. Plasmid map for arsenic biosensor and Sanger sequencing result can be found at Appendix C and D, respectively.

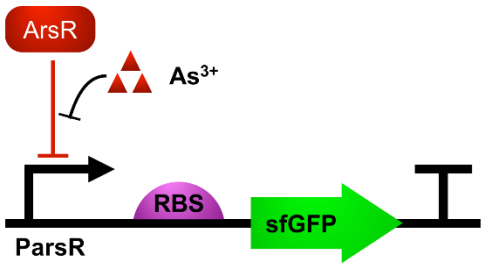

Figure 106. Arsenic biosensor biological parts and working mechanism. ArsR transcription factor bound to ParsR promoter is released from the promoter in the presence of arsenic ions within the cell, then downstream expression of sfGFP is activated. ArsR protein is expressed by the E.coli cells.

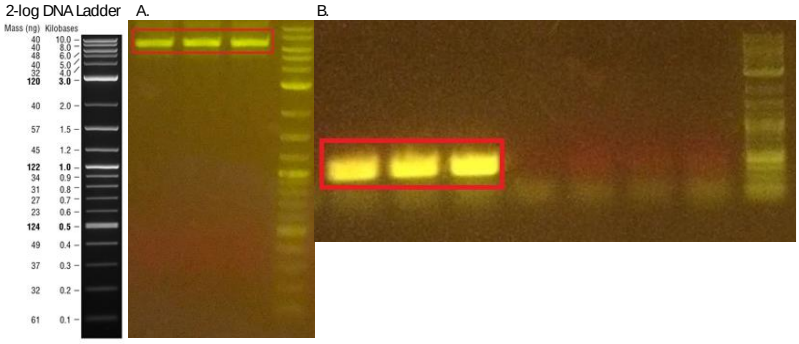

Figure 107. Agarose gel image of the biological parts required for the cloning of the pET22b -ParsR-sfGFP-ProD-HucR vector. A. PCR product of the linear pET22b-sfGFP-ProD-HucR backbone, 6469 bp. B. PCR product of ParsR promoter region, 371 bp.

Then, ArsR transcription factor's gene sequence from *E. coli* DH5α was cloned downstream of constitutively active ProD promoter (Figure 108). First, ArsR gene was amplified with PCR from *E. coli* DH5α genome with overhangs to backbone. Second, pET22b-ParsR-sfGFP-ProD-HucR vector was amplified with PCR (Figure 109). Finally, pET22b-ABS-ParsR-sfGFP-ProD-ArsR vector was constructed with Gibson assembly.

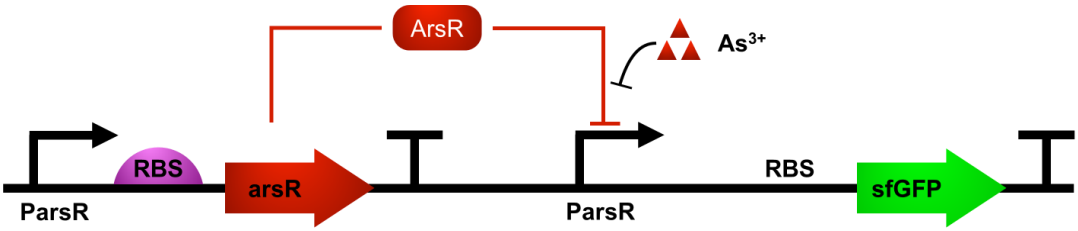

Figure 108. Arsenic biosensor biological parts and working mechanism. ArsR transcription factor bound to ParsR promoter is released from the promoter in the presence of arsenic ions within the cell, then downstream expression of sfGFP is activated. ArsR protein is expressed by the E.coli cells and by the constitutive promoter ProD.

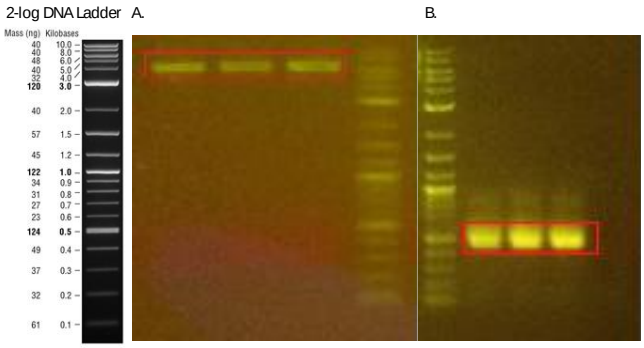

Figure 109.Agarose gel image of the biological parts required for the cloning of the pET22b-ABS-ParsR-sfGFP-ProD-ArsR vector. A. PCR product of the linear pET22b-ABS-ParsR-sfGFP-ProD backbone, 6252 bp. B. PCR product of ArsR transcription factor gene region, 426 bp.

Samples selected from single colonies were first verified by restriction enzyme digestion (Figure 110), and then the samples selected from the restriction enzyme digestion reaction were sent for Sanger sequencing analysis. Plasmid map for arsenic biosensor and Sanger sequencing result can be found at Appendix C and D, respectively.

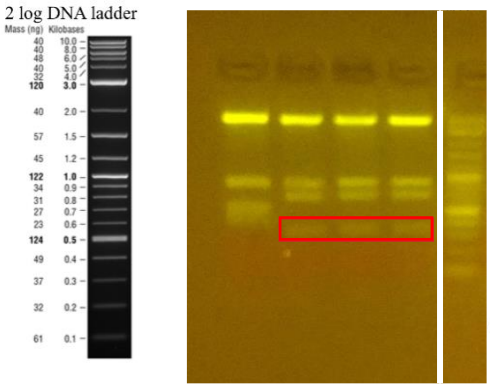

Figure 110. Confirmation of the pET22b-ABS-ParsR-sfGFP-ProD-ArsR vector by restriction enzyme digestion. A. The bands expected for the pET22b-ABS-ParsR-sfGFP-ProD-ArsR vector as a result of cleavage of BamHI and MluI enzymes were observed at 363 bp lines.

To increase the efficiency of arsenic whole-cell biosensor, ArsR transcription repressor factor was cloned downstream of ParsR promoter (Figure 111). Inducible arsenic biosensor plasmid backbone was constructed from two PCR amplified parts: pET22b-ParsR-sfGFP-ProD-HucR backbone and ArsR transcription factor region, which were amplified from pET22b-ParsR-sfGFP-ProD-HucR and genome of *E. coli* DH5α PRO, respectively (Figure 112). ArsR gene region was amplified with primers suitable for the Gibson Assembly method. Inducible arsenic biosensor plasmid construct was named as pET22b-ABS-ParsR-ArsR-sfGFP-ProD-HucR. Primers can be found at Appendix B. After PCR products were run on 1% agarose gel, they were isolated from the gel with Macherey-Nagel's PCR Clean-up kit according to the manufacturer's instructions and assembled with the Gibson Assembly method. Samples selected from the colonies were verified with Sanger sequencing analysis. Plasmid map for inducible arsenic biosensor and Sanger sequencing result can be found at Appendix C and D, respectively.

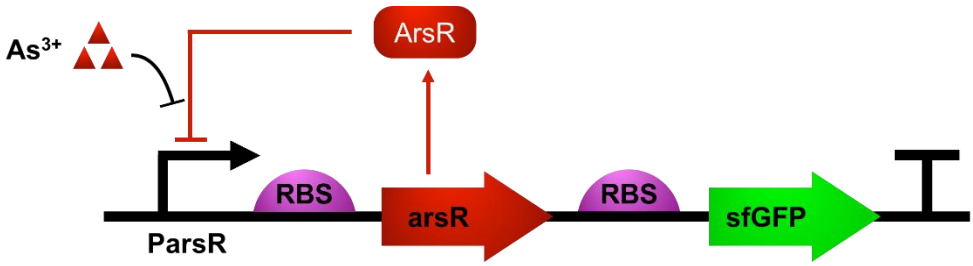

Figure 111. Arsenic biosensor biological parts and working mechanism. ArsR transcription factor bound to ParsR promoter is released from the promoter in the presence of arsenic ions within the cell, then downstream expression of ArsR and sfGFP is activated. ArsR protein is expressed by the E.coli cells and by the inducible promoter ParsR.

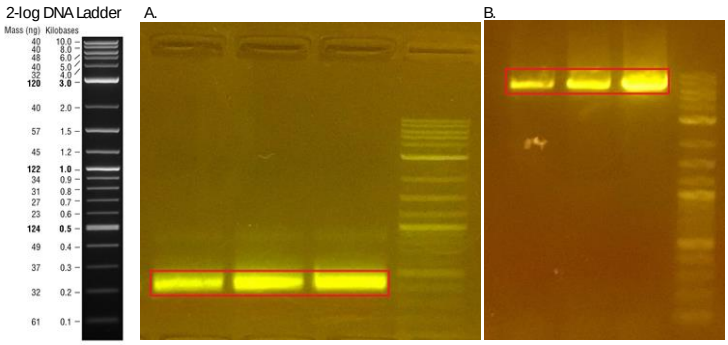

Figure 112.Agarose gel image of the biological parts required for the cloning of the pET22b-ABS-ParsR-ArsR-sfGFP-ProD-HucR vector. A. PCR product of ArsR transcription factor gene region, 434 bp. B. PCR product of the linear pET22b-ABS-ParsR-sfGFP-ProD backbone, 6810 bp

1.3.44 Characterization of Whole-Cell Arsenic Biosensors

Time dependent and dynamic range analysis of the pET22b -ParsR-sfGFP-ProD-HucR sensor was made with sodium Arsenate (Na_3AsO_4) salt. Uninduced *E. coli* PRO cells carrying the same vector was used as a control. Time dependent measurements were taken at 1st, 2nd, 4th and 24th hours after induction with Na_3AsO_4 (Figure 113). Arsenic biosensor responded even to a concentration as low as 1 µM (Figure 113).

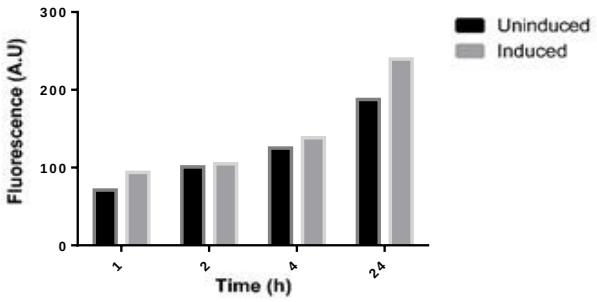

Figure 113. Time dependent characterization of the pET22b -ParsR-sfGFP-ProD-HucR sensor with 1 µM Sodium arsenate (Na_3AsO_4). Experiments were performed in triplicates and measurements were taken at the 1st, 2nd, 4th and 24th hours after induction. The results were analyzed with two-way analysis of variance (ANOVA) (GraphPad Prism version 9.0.0), the differences between the groups were marked with "*" ($p \leq 0.05$, $p \leq 0.01$, $p \leq 0.001$ and $p \leq 0.0001$ is represented by "*", "**", "***" and "****" respectively). No marking was made in the groups that did not show significant differences. E. coli cells were grown in LB medium at 30°C with 200 rpm shaking.

Time dependent and dynamic range analysis of the pET22b-ABS-ParsR-sfGFP-ProD-ArsR sensor was made with Sodium Arsenate (Na_3AsO_4) salt. Uninduced *E. coli* PRO cells carrying the same vector was used as a control. Time dependent measurements were taken at 1st, 2nd, 4th and 24th hours after induction with Na_3AsO_4 (Figure 114). Arsenic biosensor responded even to a concentration as low as 1 µM (Figure 114).

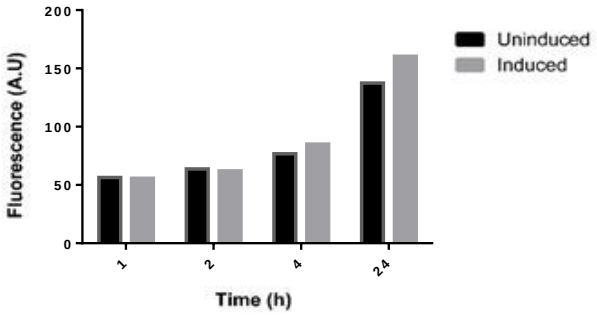

Figure 114. Time dependent characterization of the pET22b-ABS-ParsR-sfGFP-ProD-ArsR sensor with 1 µM Sodium arsenate (Na_3AsO_4). Experiments were performed in triplicates and measurements were taken at the 1st, 2nd, 4th and 24th hours after induction. The results were analyzed with two-way analysis of variance (ANOVA) (GraphPad Prism version 9.0.0), the differences between the groups were marked with "*" ($p \leq 0.05$, $p \leq 0.01$, $p \leq 0.001$ and $p \leq 0.0001$ is represented by "*", "**", "***" and "****" respectively). No marking was made in the groups that did not show significant differences. E. coli cells were grown in LB medium at 30°C with 200 rpm shaking.

Time dependent and dynamic range analysis of the pET22b-ABS-ParsR-ArsR-sfGFP-ProD-HucR sensor was made with Sodium Arsenate (Na_3AsO_4) salt. Uninduced *E. coli* PRO cells carrying the same vector was used as a control. Time dependent measurements were taken at 4th, 6th 8th and 16th hours after induction with Na_3AsO_4 (Figure 115). In order to understand the response of the pET22b-ABS-ParsR-ArsR-sfGFP-ProD-HucR sensor to different Na_3AsO_4 concentrations, dynamic range with varying Na_3AsO_4 concentrations was performed at 2nd hour after induction. Arsenic biosensor responded even to a concentration as low as 10 µM (Figure 116).

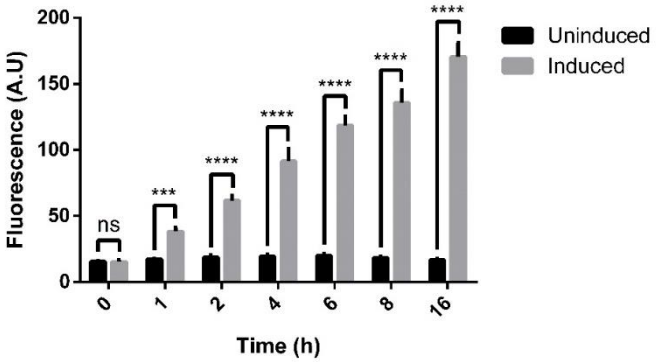

Figure 115. Time dependent characterization of the pET22b-ABS-ParsR-ArsR-sfGFP-ProD-HucR sensor with 10 µM Sodium arsenate (Na_3AsO_4). Experiments were performed in triplicates and measurements were taken at the 4th, 6th 8th and 16th hours after induction. The results were analyzed with two-way analysis of variance (ANOVA) (GraphPad Prism version 9.0.0), the differences between the groups were marked with "*" ($p \leq 0.05$, $p \leq 0.01$, $p \leq 0.001$ and $p \leq 0.0001$ is represented by "*", "**", "***" and "****" respectively). No marking was made in the groups that did not show significant differences. E. coli cells were grown in LB medium at 37°C with 200 rpm shaking.

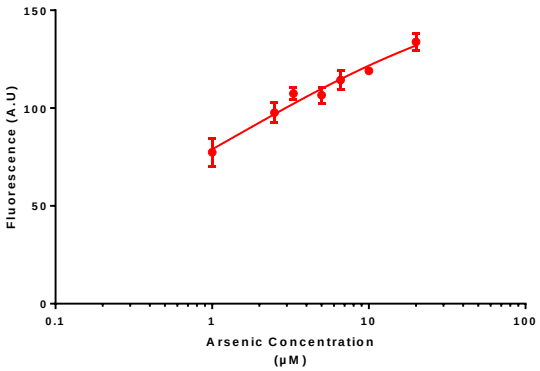

Figure 116. Concentration-dependent characterization of the pET22b-ABS-ParsR-ArsR-sfGFP-ProD-HucR sensor with Na_3AsO_4. Experiments were repeated in triplicates, and measurements were taken at the 2nd hour of induction. E. coli cells were grown in LB medium at 37°C with 200 rpm shaking.

To see the effect of growth media on sensor's behavior, pET22b-ABS-ParsR-ArsR-sfGFP-ProD-HucR sensor was grown and induced in MOPS buffered minimal growth media. Time dependent analysis of the pET22b-ABS-ParsR-ArsR-sfGFP-ProD-HucR sensor was made with Sodium Arsenate (Na_3AsO_4) salt. Uninduced *E. coli* PRO cells carrying the same vector was used as a control. Time dependent measurements were taken at 0^{th}, 2^{nd}, 4^{th}, 6^{th} 8^{th}, 16^{th} and 24^{th} hours after induction with Na_3AsO_4 (Figure 117).

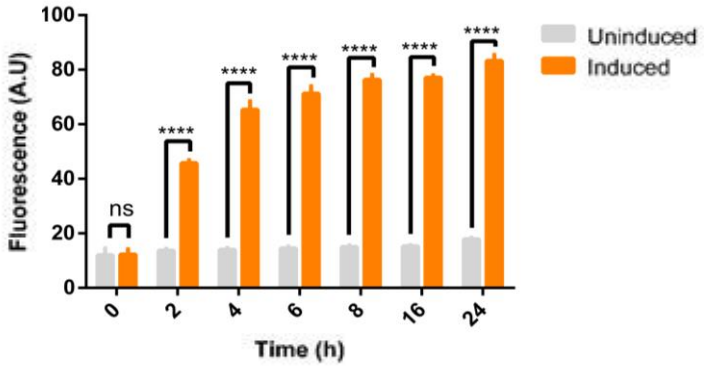

Figure 117. Time dependent characterization of the pET22b-ABS-ParsR-ArsR-sfGFP-ProD-HucR sensor with 10 µM Sodium arsenate (Na_3AsO_4). Experiments were performed in triplicates and measurements were taken at the 0^{th}, 2^{nd}, 4^{th}, 6^{th} 8^{th}, 16^{th} and 24^{th} hours after induction. The results were analyzed with two-way analysis of variance (ANOVA) (GraphPad Prism version 9.0.0), the differences between the groups were marked with "*" ($p \leq 0.05$, $p \leq 0.01$, $p \leq 0.001$ and $p \leq 0.0001$ is represented by "*", "**", "***" and "****" respectively). No marking was made in the groups that did not show significant differences. E. coli cells were grown in MOPS buffered chemically defined minimal growth medium at 37°C with 200 rpm shaking.

1.3.45 Characterization of Whole-Cell Arsenic Biosensor with Serum Samples

To test the applicability of biosensors for diagnosis of heavy metal poisoning, biosensors were tested with M63 growth media mixed with fetal bovine serum (FBS). Dynamic range analysis of the pET22b-ABS-ParsR-ArsR-sfGFP-ProD-HucR biosensor was made with Sodium Arsenate (Na_3AsO_4) salt. *E.coli* PRO cells carrying the same biosensor circuit was grown overnight in LB, then 1% inoculated into fresh LB media with proper antibiotics. When OD_{600} reached

0.4-0.5, samples were centrifuged at 3000 rpm for 10 minutes. Supernatant was discarded from each sample, and pellets were resuspended in equal volume of a mixture of heat-treated FBS and M63 minimal media (3:1), and induced with different concentrations of Na_3AsO_4. Fluorescence and OD_{600} measurements were taken at 16th hour of induction. Inducible Arsenic sfGFP biosensor was observed to be responsive to concentrations as low as 5 µM Na_3AsO_4 (Figure 118).

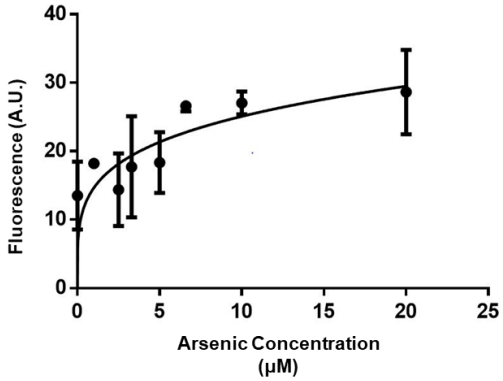

Figure 118. Concentration-dependent characterization of the pET22b-ABS-ParsR-ArsR-sfGFP-ProD-HucR biosensor with Sodium Arsenate (Na_3AsO_4). Concentration-dependent graph of relative fluorescence value. Experiments were repeated in triplicates, and measurements were taken at the 16th hour of induction. E. coli cells were grown in LB media until OD_{600} reached 0.4-0.5, then transferred to a mixture of heat-treated FBS and M63 minimal media (3:1) and induced with different concentrations of Na_3AsO_4.

1.3.46 Characterization of Whole-Cell Arsenic Biosensor at Different pH Values

Inducible arsenic whole-cell biosensor (pET22b-ABS-ParsR-ArsR-sfGFP-ProD-HucR) was characterized under pH values 5, 7 and 9. LB growth media was adjusted with potassium phosphate (KH_2PO_4) solution to have the desired pH value. Time-dependent analysis of the pET22b-ABS-ParsR-ArsR-sfGFP-ProD-HucR biosensor was made with Sodium Arsenate (Na_3AsO_4) salt. Uninduced *E. coli* PRO cells carrying the same vector was used as a control. *E.coli* PRO cells carrying pET22b-ABS-ParsR-ArsR-sfGFP-ProD-HucR

arsenic sensing circuit were grown overnight in LB, then 1% inoculated into fresh LB media with proper antibiotics. When OD_{600} reached 0.4-0.5, samples were induced with 10 µM Na_3AsO_4. Fluorescence and OD_{600} measurements were taken at 4^{th}, 6^{th}, 8^{th} and 16^{th} hours after induction with Na_3AsO_4. Inducible arsenic sfGFP biosensor was observed to have higher background signal when pH value of the growth media was 5 (Figure 119) compared to cases when pH value was either 7(Figure 120) or 9 (Figure 121).

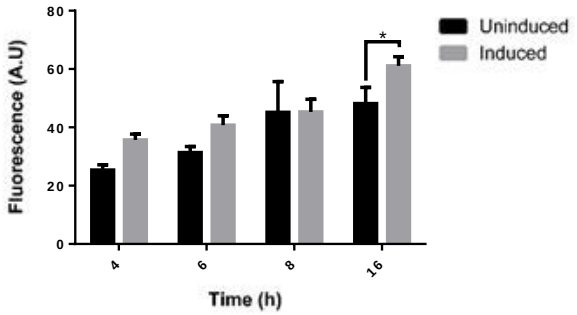

Figure 119. Time-dependent characterization of the pET22b-ABS-ParsR-ArsR-sfGFP-ProD-HucR sensor with 10 µM Sodium Arsenate (Na_3AsO_4). *E. coli PRO* cells were grown in LB growth media with pH value equal to 5. Experiments were repeated in triplicates, and measurements were taken at 4^{th}, 6^{th}, 8^{th} and 16^{th} hours after induction. The results were analyzed with two-way analysis of variance (ANOVA) (GraphPad Prism version 9.0.0), the differences between the groups were marked with "*" ($p \leq 0.05$, $p \leq 0.01$, $p \leq 0.001$ and $p \leq 0.0001$ is represented by "*", "**", "***" and "****" respectively). "ns" was used in the groups that did not show significant differences.

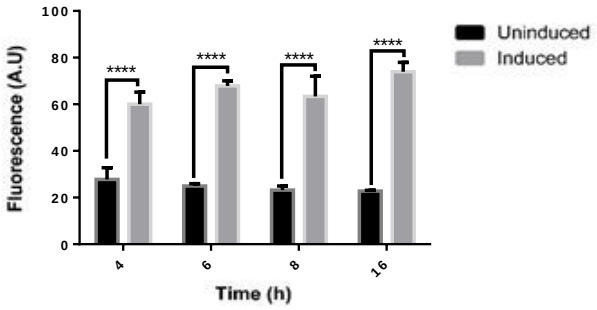

Figure 120. Time-dependent characterization of the pET22b-ABS-ParsR-ArsR-sfGFP-ProD-HucR sensor with 10 µM Sodium Arsenate (Na_3AsO_4). *E. coli PRO* cells were grown in LB growth media with pH value equal to 7. Experiments were repeated in triplicates, and measurements were taken at 4^{th}, 6^{th}, 8^{th} and 16^{th} hours after induction. The results were analyzed with two-way analysis of variance (ANOVA) (GraphPad Prism version 9.0.0), the differences between the groups were marked with "*" ($p \leq 0.05$, $p \leq 0.01$, $p \leq 0.001$ and $p \leq 0.0001$ is represented by "*", "**", "***" and "****" respectively). "ns" was used in the groups that did not show significant differences.

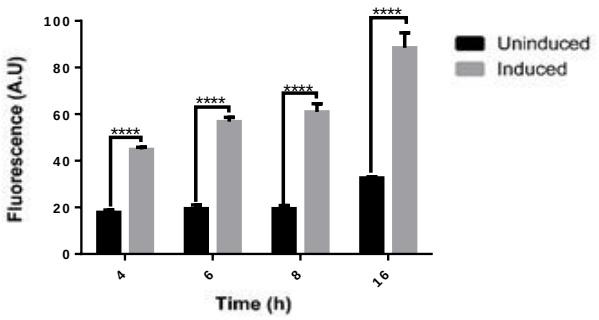

Figure 121. Time-dependent characterization of the pET22b-ABS-ParsR-ArsR-sfGFP-ProD-HucR sensor with 10 µM Sodium Arsenate (Na_3AsO_4). *E. coli PRO* cells were grown in LB growth media with pH value equal to 9. Experiments were repeated in triplicates, and measurements were taken at 4th, 6th, 8th and 16th hours after induction. The results were analyzed with two-way analysis of variance (ANOVA) (GraphPad Prism version 9.0.0), the differences between the groups were marked with "*" ($p \leq 0.05$, $p \leq 0.01$, $p \leq 0.001$ and $p \leq 0.0001$ is represented by "*", "**", "***" and "****" respectively). "ns" was used in the groups that did not show significant differences.

1.3.47 Characterization of Whole-Cell Arsenic Biosensor at Different Temperature Values

Inducible arsenic whole-cell biosensor (pET22b-ABS-ParsR-ArsR-sfGFP-ProD-HucR) was characterized under different temperature values of 25°C and 42°C. Time-dependent analysis of the pET22b-ABS-ParsR-ArsR-sfGFP-ProD-HucR biosensor was made with Sodium Arsenate (Na_3AsO_4) salt. Uninduced *E. coli* PRO cells carrying the same vector was used as a control. *E.coli* PRO cells carrying pET22b-ABS-ParsR-ArsR-sfGFP-ProD-HucR arsenic sensing circuit were grown overnight in LB, then 1% inoculated into fresh LB media with proper antibiotics. When OD_{600} reached 0.4-0.5, samples were induced with 10 µM Na_3AsO_4. After dilution, samples were grown at either 25°C (Figure 122) or 42°C (Figure 123). Fluorescence and OD_{600} measurements were taken at 4th, 6th, 8th and 16th hours after induction with Na_3AsO_4.

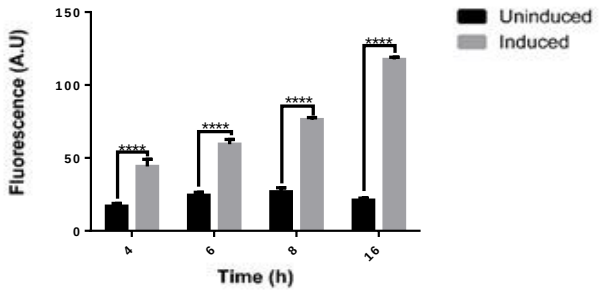

Figure 122. Time-dependent characterization of the pET22b-ABS-ParsR-ArsR-sfGFP-ProD-HucR sensor with 10 µM Sodium Arsenate (Na_3AsO_4). *E. coli PRO* cells were grown in LB growth media at 25°C. Experiments were repeated in triplicates, and measurements were taken at at 4th, 6th, 8th and 16th hours after induction. The results were analyzed with two-way analysis of variance (ANOVA) (GraphPad Prism version 9.0.0), the differences between the groups were marked with "*" ($p \leq 0.05$, $p \leq 0.01$, $p \leq 0.001$ and $p \leq 0.0001$ is represented by "*", "**", "***" and "****" respectively). "ns" was used in the groups that did not show significant differences.

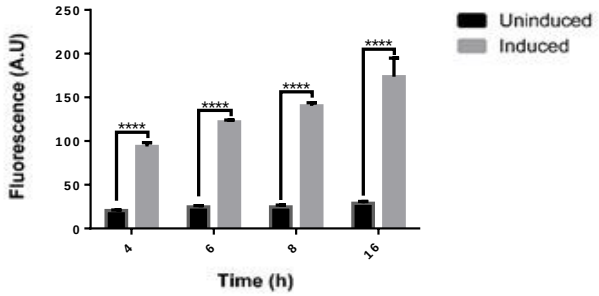

Figure 123. Time-dependent characterization of the pET22b-ABS-ParsR-ArsR-sfGFP-ProD-HucR sensor with 10 µM Sodium Arsenate (Na_3AsO_4). *E. coli PRO* cells were grown in LB growth media at 42°C. Experiments were repeated in triplicates, and measurements were taken at at 4th, 6th, 8th and 16th hours after induction. The results were analyzed with two-way analysis of variance (ANOVA) (GraphPad Prism version 9.0.0), the differences between the groups were marked with "*" ($p \leq 0.05$, $p \leq 0.01$, $p \leq 0.001$ and $p \leq 0.0001$ is represented by "*", "**", "***" and "****" respectively). "ns" was used in the groups that did not show significant differences.

1.3.48 Characterization of Whole-Cell Arsenic Biosensor at Different Salt Concentrations

Inducible arsenic whole-cell biosensor was characterized under different sodium chloride (NaCl) concentration values: 0%, 1% and 3%. 1% NaCl containing LB media is the unmodified LB media used throughout this study. LB growth media was prepared so that the final concentration of NaCl in the media was either 0%, 1% and 3%. Time-dependent analysis of the pET22b-ABS-ParsR-ArsR-sfGFP-ProD-HucR biosensor was made with Sodium Arsenate (Na_3AsO_4) salt. Uninduced *E. coli* PRO cells carrying the same vector was used as a control. *E.coli* PRO cells carrying pET22b-ABS-ParsR-

ArsR-sfGFP-ProD-HucR arsenic sensing circuit were grown overnight in LB, then 1% inoculated into fresh LB media with proper antibiotics. When OD_{600} reached 0.4-0.5, samples were induced with 10 µM Na_3AsO_4. Fluorescence and OD_{600} measurements were taken at 4^{th}, 6^{th}, 8^{th} and 16^{th} hours after induction with Na_3AsO_4. Inducible arsenic sfGFP biosensor was observed to have higher relative fluorescence signal when cells were grown in LB growth media with 0% NaCl (Figure 124) compared to cases when NaCl amount was either 1% or 3% (Figure 125).

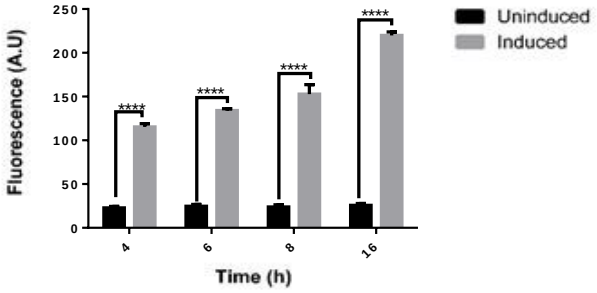

Figure 124. Time-dependent characterization of the pET22b-ABS-ParsR-ArsR-sfGFP-ProD-HucR sensor with 10 µM Sodium Arsenate (Na_3AsO_4). *E. coli PRO* cells were grown in LB growth media without NaCl. Experiments were repeated in triplicates, and measurements were taken at 4^{th}, 6^{th}, 8^{th} and 16^{th} hours after induction. The results were analyzed with two-way analysis of variance (ANOVA) (GraphPad Prism version 9.0.0), the differences between the groups were marked with "*" ($p \leq 0.05$, $p \leq 0.01$, $p \leq 0.001$ and $p \leq 0.0001$ is represented by "*", "**", "***" and "****" respectively). "ns" was used in the groups that did not show significant differences.

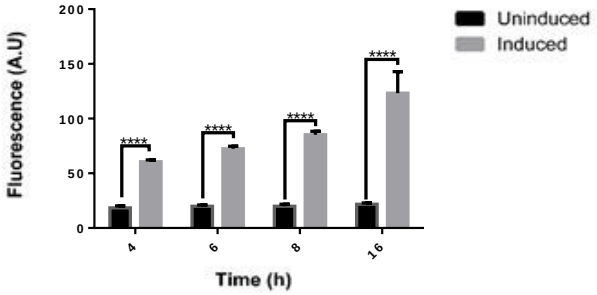

Figure 125. Time-dependent characterization of the pET22b-ABS-ParsR-ArsR-sfGFP-ProD-HucR sensor with 10 µM Sodium Arsenate (Na_3AsO_4). *E. coli PRO* cells were grown in LB growth media with 3% NaCl. Experiments were repeated in triplicates, and measurements were taken at 4^{th}, 6^{th}, 8^{th} and 16^{th} hours after induction. The results were analyzed with two-way analysis of variance (ANOVA) (GraphPad Prism version 9.0.0), the differences between the groups were marked with "*" ($p \leq 0.05$, $p \leq 0.01$, $p \leq 0.001$ and $p \leq 0.0001$ is represented by "*", "**", "***" and "****" respectively). "ns" was used in the groups that did not show significant differences.

1.3.49 Cross Reactivity Analysis of Whole-Cell Arsenic Biosensor

Inducible arsenic whole-cell biosensor was characterized with copper (II) sulfate ($CuSO_4$), lead(II) chloride ($PbCl_2$), cadmium acetate $Cd(CH_3CO_2)_2$ and sodium arsenate (Na_3AsO_4) salts for cross reactivity. Uninduced *E. coli* PRO cells carrying the same vector was used as a control. *E.coli* PRO cells carrying pET22b-ABS-ParsR-ArsR-sfGFP-ProD-HucR arsenic sensing circuit were grown overnight in LB, then 1% inoculated into fresh MOPS buffered minimal media with proper antibiotics. When OD_{600} reached 0.4-0.5, samples were induced with 200 µM $CuSO_4$, 200 µM $PbCl_2$, 10 µM $Cd(CH_3CO_2)_2$, 10 µM Na_3AsO_4 separately. Fluorescence and OD_{600} measurements were taken at 0^{th}, 2^{nd}, 4^{th}, 6^{th}, 8^{th}, 16^{th} and 24^{th} hours after induction with aforementioned heavy metals (Figure 126). Inducible arsenic sfGFP biosensor was observed to have no significant signal when cells were induced with other heavy metals.

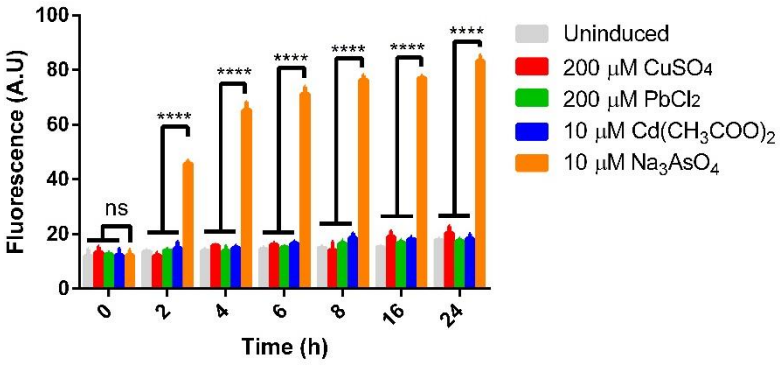

Figure 126. Time-dependent cross-reactivity characterization of the pET22b-ABS-ParsR-ArsR-sfGFP-ProD-HucR sensor with 200 µM $CuSO_4$, 200 µM $PbCl_2$, 10 µM $Cd(CH_3CO_2)_2$, 10 µM Na_3AsO_4 separately. *E. coli PRO* cells were grown in chemically defined MOPS buffered minimal growth media. Experiments were repeated in triplicates, and measurements were taken at 0^{th}, 2^{nd}, 4^{th}, 6^{th}, 8^{th}, 16^{th} and 24^{th} hours after induction. The results were analyzed with two-way analysis of variance (ANOVA) (GraphPad Prism version 9.0.0), the differences between the groups were marked with "*" ($p \leq 0.05$, $p \leq 0.01$, $p \leq 0.001$ and $p \leq 0.0001$ is represented by "*", "**", "***" and "****" respectively). "ns" was used in the groups that did not show significant differences.

1.3.19 Construction of Multi-Input Multi-Output Whole-Cell Copper and Lead Biosensor

To construct multi-input multi-output whole-cell biosensor system for copper and lead biosensors, pET22b-10mer-RBS30-PpbrR-sfGFP-ProD-PbrR-PcopA-RBS30-mScarlet vector was designed (Figure 127). pET22b-10mer-RBS30-PpbrR-sfGFP-ProD-PbrR was linearly amplified with PCR reaction and PcopA-RBS30-mScarlet region was amplified from pET22b-PcopA-RBS30-mScarlet backbone (Figure 128). Then PCR products were extracted from agarose gel and subjected to Gibson Assembly. The new vector was named as pET22b-10mer-RBS30-PpbrR-sfGFP-ProD-PbrR-PcopA-RBS30-mScarlet. Plasmid map for copper RBS30 mScarlet lead -10 mer RBS30 sfGFP biosensor and Sanger sequencing result can be found at Appendix C and D, respectively.

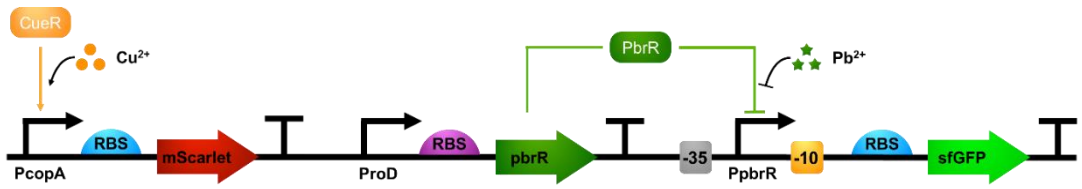

Figure 127. Copper RBS30 mScarlet lead -10 mer RBS30 sfGFP multi-input multi-output biosensor biological parts and working mechanism. CueR transcription factor binds to PcopA promoter in the presence of copper ions within the cell, and activates downstream expression of mScarlet with stronger RBS30. PbrR transcription factor binds to PpbrR promoter in the absence of lead ions within the cell. When lead ions present, upon release of PbrR from PpbrR promoter, downstream expression of sfGFP is activated with stronger RBS30.

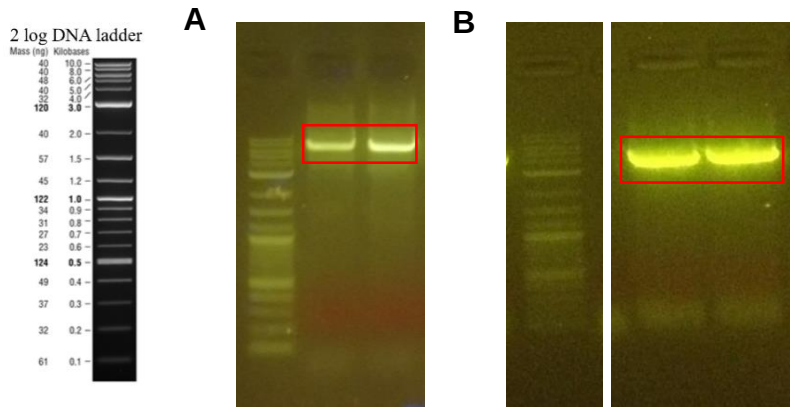

Figure 128. Agarose gel image of the biological part required for the cloning of the pET22b-10mer-RBS30-PpbrR-sfGFP-ProD-PbrR-PcopA-RBS30-mScarlet vector. A. PCR product of the linear pET22b-10mer-RBS30-PpbrR-sfGFP-ProD-PbrR- backbone, 6420 bp. B. PCR product of PcopA-RBS30-mScarlet region, 1144 bp

1.3.20 Characterization of Multi-Input Multi-Output Whole-Cell Copper and Lead Biosensor

Time dependent and dynamic range analysis of the pET22b-10mer-RBS30-PpbrR-sfGFP-ProD-PbrR-PcopA-RBS30-mScarlet sensor was made with copper (II) sulfate ($CuSO_4$) and lead(II) chloride ($PbCl_2$) salt. Uninduced *E. coli* PRO cells carrying the same vector was used as a control. Time dependent measurements were taken at 0^{th}, 2^{nd}, 4^{th}, 6^{th}, 8^{th}, 16^{th} and 24^{th} hours after induction with $CuSO_4$ and $PbCl_2$ (Figure 129). In order to understand the response of the pET22b-10mer-RBS30-PpbrR-sfGFP-ProD-PbrR-PcopA-RBS30-mScarlet sensor to different $CuSO_4$ and $PbCl_2$ concentrations, dynamic range with varying $CuSO_4$ and $PbCl_2$ concentrations was performed at 2^{nd} hour after induction. Multi-input multi-output whole-cell copper and lead biosensor responded even to a concentration as low as 10 µM of each heavy metal (Figure 130).

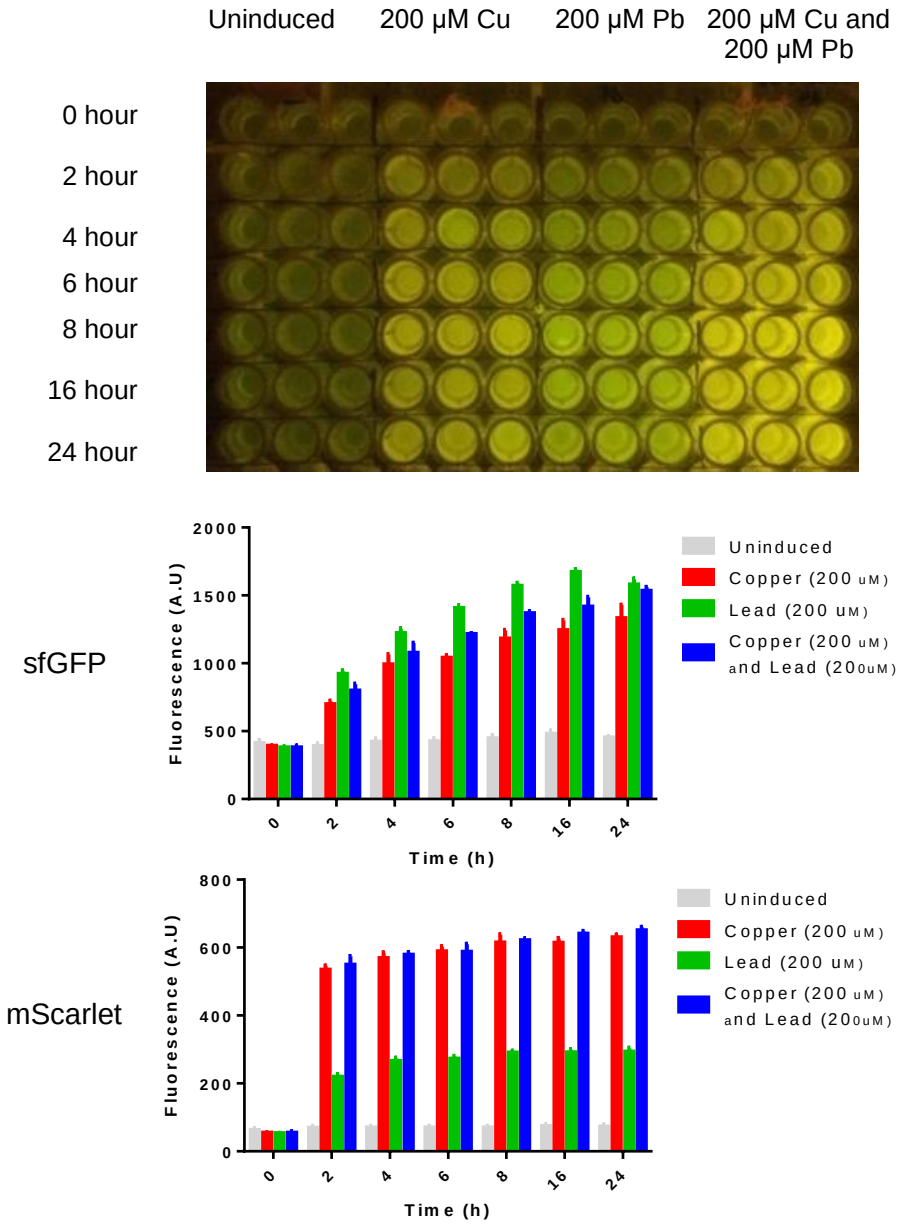

Figure 129. Time dependent characterization of the pET22b-10mer-RBS30-PpbrR-sfGFP-ProD-PbrR-PcopA-RBS30-mScarlet sensor with 200 µM copper (II) sulfate ($CuSO_4$) and 200 µM lead(II) chloride ($PbCl_2$). Experiments were performed in triplicates and measurements were taken at the 0^{th}, 2^{nd}, 4^{th}, 6^{th}, 16^{th} and 24^{th} hours after induction. The results were analyzed with two-way analysis of variance (ANOVA) (GraphPad Prism version 9.0.0), the differences between the groups were marked with "*" ($p \leq 0.05$, $p \leq 0.01$, $p \leq 0.001$ and $p \leq 0.0001$ is represented by "*", "**", "***" and "****" respectively). No marking was made in the groups that did not show significant differences. E. coli cells were grown in chemically defined MOPS buffered minimal growth media.

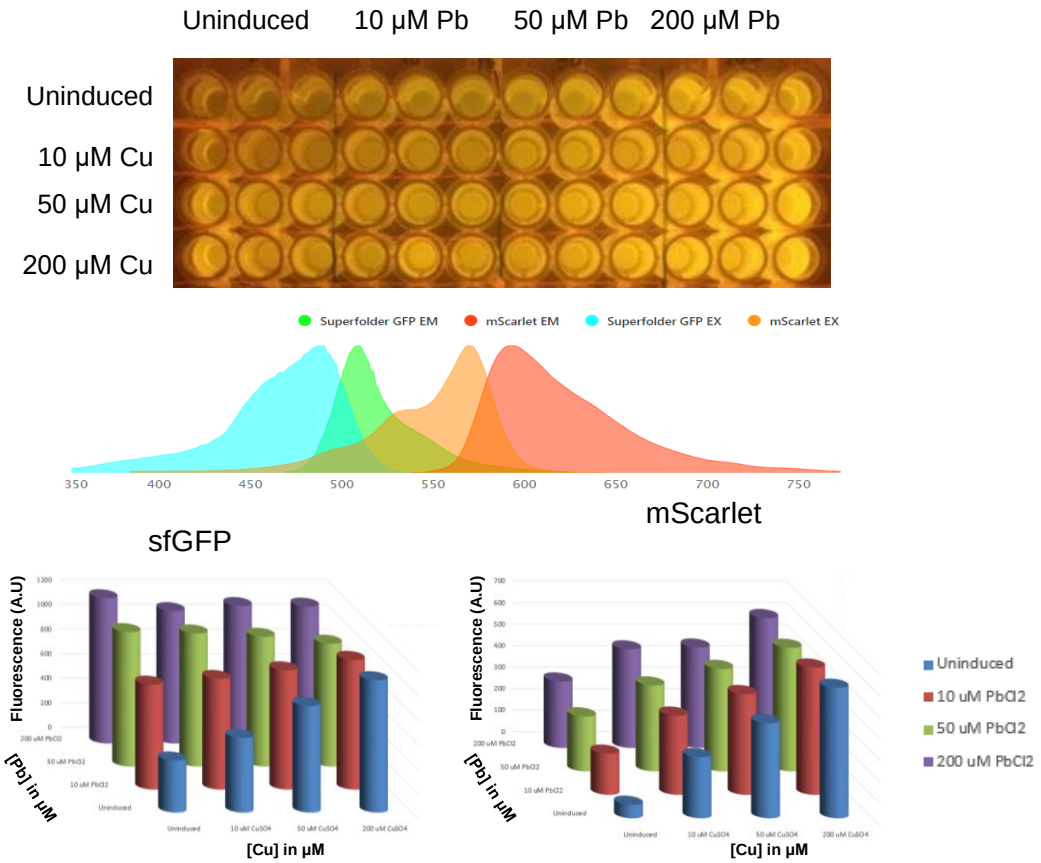

Figure 130. Concentration-dependent characterization of the pET22b-10mer-RBS30-PpbrR-sfGFP-ProD-PbrR-PcopA-RBS30-mScarlet sensor with $CuSO_4$ and $PbCl_2$. Experiments were repeated in triplicates, and measurements were taken at the 2nd hour of induction. E. coli cells were grown in chemically defined MOPS buffered minimal growth media.

1.4. Conclusion and Future Perspectives

In this study, various heavy metal biosensors have been characterized in terms of time and concentration dependency. Then, selected engineered biosensors were further optimized for environmental conditions (pH, temperature and salt concentration) and inducer solutions (water and serum) to see the compatibility of sensing system to different conditions.

Copper biosensor was optimized with *E.coli*'s inner transcription factor CueR and its cognate promoter PcopA. When RBS region is replaced with a stronger RBS region (RBS30) from iGEM's RBS library, signal level elevated and dynamic range increased without changing the sensor's specificity as no significant signal increase was observed for cross reactivity analysis. Copper biosensor was observed to have higher background and no dynamic range when implemented with hrp synthetic amplification circuit. As copper already present within the cells as cofactors in trace amounts, the system is triggered before the induction. Hence, applicability of synthetic amplifier to activator systems are not promising. Different inoculation and growth conditions was experimented to find the best sensor performance. When cells are induced in LB media, background signal level was observed to be higher compared to cases when cells are inoculated and induced in MOPS buffered minimal growth media. These results suggest that, usage of chemically defined minimal media is preferable for characterization assays. Different reporter system for copper biosensor, copper RBS30 mScarlet biosensor was tested for response signal level against copper RBS30 sfGFP. The decrease in signal level and narrowing of dynamic range shows the importance of choosing reporter for

whole-cell biosensor systems. Although signal level is lower for copper RBS30 mScarlet, the reporter is visible to eye, so it is more practical for implementing whole-cell biosensors for point-of-care devices.

Lead biosensor was utilized with PbrR (transcriptional repressor) which released from PpbrR promoter upon lead ion binding. Then, downstream gene's transcription is activated. PbrR and PpbrR sequences were obtained from *Cupriavidus metallidurans CH34* genome as it was previously shown to be responsive to lead ions. -10 region on PpbrR promoter was replaced with -10 mer region which is shown to increase signal level while decreasing the signal level to other heavy metals. Then, RBS region was replaced with stronger RBS30 sequence. Signal level and dynamic range was increased as in the case of copper biosensor. Synthetic amplification circuit implemented to lead -10 mer sfGFP sensor, the signal level increased in great extent although dynamic range was lost as the sensor's behavior changed from analog to digital. However, serum experiments showed that synthetic amplifier enhanced the sensors dynamic range with serum media as signal level was lower in lead -10 mer RBS30 case. These findings are promising as it is revealed that changing the detection media requires another optimization for the biosensor system. Cross reactivity analysis of lead sensors showed no reactivity with copper and arsenic; however, both lead -10 mer RBS30 sfGFP and lead -10 mer hrp sfGFP biosensors showed significant increase in the presence of cadmium ions.

Cadmium biosensor consists of two units: CadR transcriptional repressor and PcadA (promoter) from *Pseudomonas aeruginosa*. Although lead biosensor's transcription factor was constitutively expressed under strong ProD promoter in high copy pET22b (+) backbone, when cadR gene cloned downstream of Prod promoter, several mutations across cadR gene was observed. Another organism's gene can be toxic or cause high-burden to the host organism. Therefore, cadR gene was cloned downstream of highly strict tetR based riboregulator system for controlled expression within *E.coli* cells. CadR (transcriptional repressor) binds to PcadA promoter and represses transcription. Binding of cadmium ion releases CadR from PcadA promoter, then downstream gene is transcribed. Cadmium sensor was optimized with stronger RBS30 and hrp synthetic amplifier. Even though mid dynamic range signal level is digital in PcadA hrp sfGFP biosensor, lower limit of sensor was as low as 10 nM for cadmium inducer. Cross reactivity analysis of cadmium sensors showed no reactivity with copper and arsenic; however, both cadmium RBS30 sfGFP and cadmium hrp sfGFP biosensors showed significant increase in the presence of lead ions.

Arsenic biosensor consists of two units: ArsR transcriptional repressor and ParsR (promoter) from *E.coli*. When arsenic biosensor's transcription factor was constitutively expressed under strong ProD promoter in high copy pET22b(+) backbone, the signal level and dynamic range of arsenic sensor was not at desired level. As the number of repressors are shown to be low in the cells for quick and better response in repressor based systems, arsR gene was removed from the backbone. However, neither signal level nor dynamic

range was as desired. Then, arsR gene was cloned between ParsR promoter and sfGFP gene to create negative feedback loop within the cell. Compared to other sensors, inducible arsR arsenic sensor was best performing although its dynamic range and signal level yet to be optimized.

Copper RBS30 mScarlet and lead -10 mer RBS30 sfGFP biosensors are combined in a single vector for multi-input multi-output multiplexed system to detect analytes simultaneously. The signal level was increased for sfGFP even though there was no lead in the system, this can happen due to either excitation and emission overlap of sfGFP and mScarlet reporters, or combined sensory system is leaky. Cadmium biosensor was constructed with mTagBFP but arsenic sensor is yet to be optimized and transferred to another reported gene for simultaneous detection of copper, lead, cadmium and arsenic.

Overall, multiplexed system implementation for these four biosensors would decrease the number of needed specific tools for individual detection of analytes also the time required for multiple detection. This study shows that for environmental and diagnostic applications, whole-cell biosensors could be used due to their specificity, quick response-time and low-cost.

Chapter 2 – Biofilm Mediated Surface Attachment of Cells

2.1 Introduction

Amyloids are aggregated protein fibrils which are unbranched and elongated. Misfolded proteins are the main source of amyloid formation. In addition, when soluble proteins are incubated in a destabilizing solution, the higher structures (secondary and tertiary) of the proteins are disturbed; this results in insoluble and β-sheet rich structures thus forming amyloids. Amyloid fibrils are rich in β-sheet structures, in amyloid skeleton β-sheets are parallel to each other but perpendicular to the axis of fibril [42]. The core of amyloid fibrils are amyloid fragments consisting of soluble monomeric peptides [43]. Assembly of β-sheet structures follows hierarchical growth starting with β-sheets forming protofilament, filament and fibril in order. The amyloid formation begins with nucleation phase, then oligomers come together for de-polymerization in elongation phase, and plaque formation occurs at last in stationary phase [44–46]. Sawaya et al. showed that within a pair of β-sheets of fibril forming proteins (eg. Islet amyloid polypeptide), the facing side chains of these sheets form a structure called “steric zipper” [43,47]. The β-sheets interact with neighbor sheets through hydrogen bonds and side chains [48].

Amyloids can be disease-associated or functional, according to their course of action and origin. Pathological amyloids are mainly caused my aggregates of

misfolded proteins [49,50]. Well-known example for pathological amyloids is the Aβ amyloid precursor protein, its aggregation results in plaque formation leading to Alzheimer's disease [49]. Another example, aggregation of unfolded α-Synuclein initiates pathogenesis of Parkinson disease [46]. However, in nature functional amyloids serve diverse range of biological purposes, including antibacterial activity, cell adhesion, survival of environmental stress [51–53]. From single cellular microorganisms to mammalians like humans developed functional amyloids to cope with various stress conditions [54]. Pmel17 forms amyloid structure in human mammalian cells during melanin synthesis to seclude diffusion of poisonous precursors [55]. Fungi shields itself with a proteinaceous layer made up of self-assembled hydrophobin proteins which provides structural stability [56]. Silkmoth's self-assembled amyloid protein, namely chorion, contributes to the architectural strength of its eggshell [57]. Bacteria like *Bacillus subtilis, Pseudomonas sp, Staphylococcus aureus* and *Escherichia coli* use their respective proteins TasA, FapC, PSM and Curli for biofilm formation [51,58–60].

Escherichia coli species are well-established experimental model organisms to investigate basic aspects of biology. As *E.coli* is one of the most thoroughly studied bacterial species for distinct research concepts such as gene expression and protein synthesis [61]. The ease of handling, rapid growth rate, variable growth conditions makes *E.coli* especially valuable as experimental model organism to study in the laboratory. Furthermore, the whole-cell biosensors established in this study (see Chapter 1) have been characterized

in *E.coli* host, and Curli operon is an established biofilm pathway whose application will be explored in Chapter 2.

Curli fibers are surface functional amyloids of *E.coli* whose fibrillization process is tightly controlled via numerous proteins [62–64]. Curli specific genes (csg) are regulated by csgBCA and csgDEFG operons. Formation of Curli fibers requires CsgA and CsgB subunits to be secreted to extracellular matrix. CsgA is secreted as a soluble protein and CsgB nucleator-anchor protein initiates CsgA proteins' amyloidization as well as acts as membrane surface anchor with the help of CsgF [62,65]. Unfolded CsgA secreted to periplasm retains its unfolded soluble form via interaction with CsgC protein [66]. The main regulator of curli system is CsgD transcription factor which controls csgBCA and csgDEFG operons as well as other biofilm-state adaptive mechanisms [62]. CsgE guides unfolded soluble CsgA and CsgB monomers to CsgG secretion channel located on the outer membrane [65].

Amyloid biofilms are developing, widely-applied functional biomaterials owing to simplicity of their engineering and physicochemical properties. To date, functional amyloids have been integrated into various application areas such as material synthesis [67,68], immobilization of enzymes [69,70] and removal of toxic compounds from water [71]. Engineered functional amyloids have been used for cell adhesion for various biomedical applications [72,73]. However, functional amyloid biofilm proteins haven not been investigated as cellular adhesives to paper based surfaces. Here, curli mediated

immobilization of cells on filter paper was employed for multiple analyte detection. To do so, controlled overexpression of CsgA, CsgG, CsgE and CsgF proteins have been investigated. Formation of functional curli amyloids have been analyzed with Congo red staining. Both curli formation and cell adhesion to paper surface was investigated with environmental scanning electron microscopy imaging. The aim of this study is to investigate potential usage of curli as cellular adhesives for prolonged storage of whole-cell biosensors for various point-of-care device applications (Figure 131).

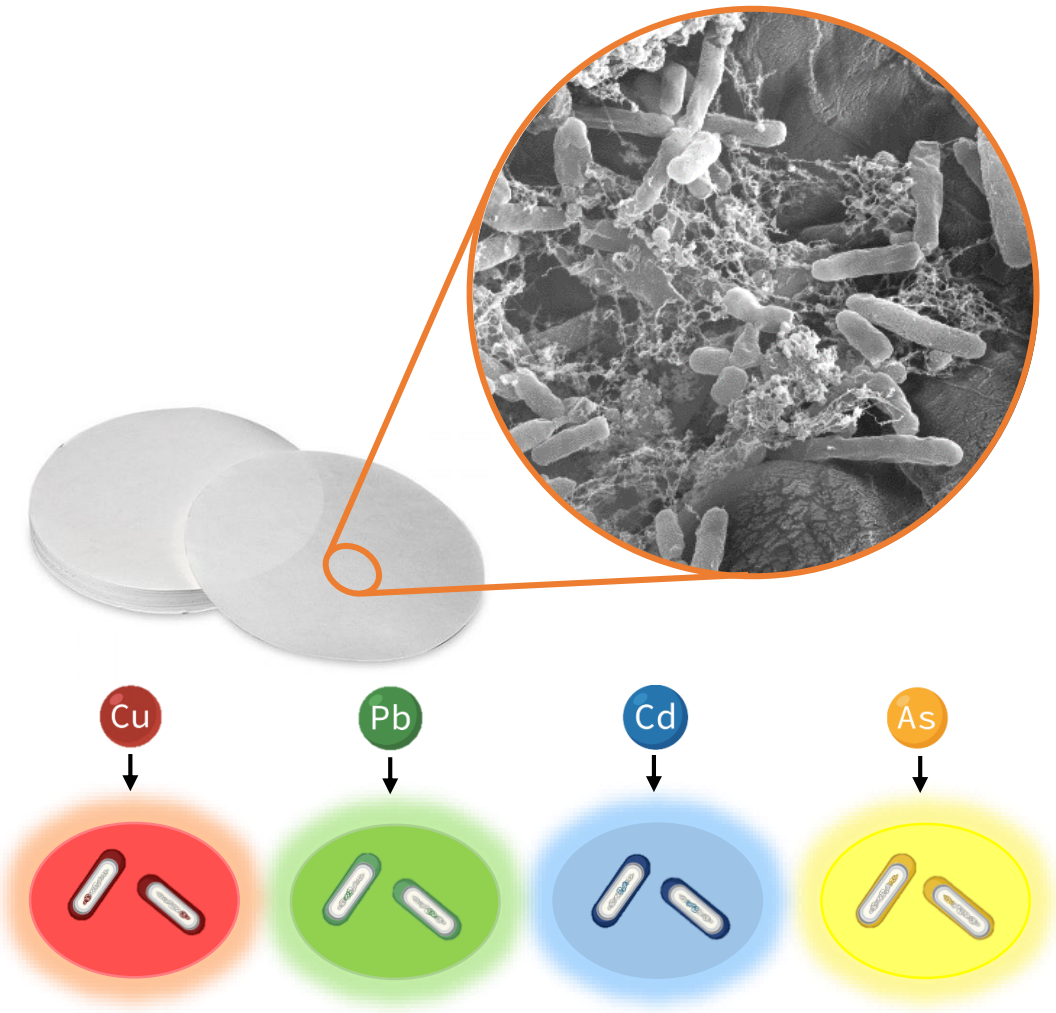

Figure 131. Lyophilized paper-based cellular immobilization for point-of-care device implementation of multi-input multi-output detection system for heavy metals from environmental or biological samples. Illustration is drawn on Biorender.

2.2 Materials and Methods

2.2.1 Cell Strains, Growth, Maintenance and Storage

In this part of the study, *Escherichia coli (E. coli)* DH5α PRO (New England Biolabs, Inc.) strain was used for cloning and characterization, also *E. coli* DH5α ΔcsgA strain was used for characterization assays. Cells were grown in Lysogeny Broth (LB) growth media (recipe can be found in Appendix Table 3) supplied with proper antibiotics (1:1000) at 37˚C with shaking at 200 rpm unless otherwise stated. Glycerol cell stocks were prepared as described in Chapter 1, and stored at -80˚C storage. Overnight cultures were prepared from glycerol cell stocks, and incubated for 12-16 hours in LB media supplied with proper antibiotics.

2.2.2 Chemical Competent Cell Preparation and Transformation

Chemical competent cell stocks and transformation were performed as described in Chapter 1. For multi-plasmid cells, *E. coli* DH5α ΔcsgA cells containing biofilm plasmid were used as the first competent cell preparation. Then, corresponding heavy metal biosensors' plasmids were transformed.

2.2.3 Construction of Plasmids and Cloning Procedure

All the plasmid constructs were designed using Benchling (http://benchling.com). CsgGEF region was amplified with polymerase chain reaction (PCR) from pSC101 ORI - pLac/Ara csgGEF vector (gift from Ebru Şahin Kehribar) and backbone was amplified from pBAD csgA – HisTag vector (gift from Ebru Şahin Kehribar). Forward and reverse primers of

aforementioned parts in this study can be seen in Appendix Table 2. For all PCR amplified parts, Q5 Hot Start High-Fidelity DNA Polymerase (New England Biolabs, Inc.) was used, constituents and conditions of PCRs can be found in Appendix Table 5. The pZa pBAD csgA pLac/Ara csgGEF vector was constructed with Gibson assembly method as described in Chapter 1.

2.2.4 Verification of Constructs and Sequence Alignments

Sequence verification of pZa pBAD csgA pLac/Ara csgGEF vector was performed as described in detail in Chapter 1. Sequences of promoters, transcription factors and regulatory subunits used in this study can be found in Appendix Table 1. Maps of all the vectors constructed in this study and their respective verification results of Sanger sequencing can be found in Appendix C and Appendix D, respectively.

2.2.5 Biofilm Experiment Procedure

Biofilm experiments were started with inoculating (1:100) overnight grown cells into fresh growth media (either LB or M63 minimal growth media) (M63 media recipe can be found in Appendix Table 7) with proper antibiotics. For characterization assays performed with M63 minimal growth media, overnight grown cells were inoculated in fresh LB with proper antibiotics (1:100) and 0.2% glycerol until OD_{600} reaches 0.5 at 37˚C with shaking at 200 rpm. Then cells were centrifuged at 8000 g for 5 minutes. Cell pellets were resuspended in equal volume of fresh M63 minimal growth media supplied with appropriate antibiotics and corresponding inducers. Following induction, cells were

incubated in 30°C incubator without shaking. On the third day, growth media was replaced with fresh M63 minimal growth media supplied with the same amount of inducers for biofilm formation and with specified amount of heavy metals. On the sixth day, the same procedure was repeated with the same initial concentrations. Cells were induced with isopropyl β-d-1-thiogalactopyranoside (IPTG) with final concentration of 1mM and 0.2% arabinose.

2.2.6 Lyophilization of Immobilized Filter Paper Samples

Lyophilization of immobilized *E.coli* cells on filter paper (Whatman) experiments were started with inoculating (1:100) overnight grown cells into fresh M63 minimal growth media with proper antibiotics (1:100), 0.2% glycerol and corresponding inducers. Following induction, cells were incubated in 30°C incubator without shaking for three days. On the third day, trehalose was added to each sample with a final concentration of 100mM. Samples were frozen at -80˚C storage overnight, then subjected to lyophilization also known as freeze-drying conducted with a lyophilizer (FreeZone 4.5, Labconco) for two days. The procedure was performed at -50˚C with 0.1 mBar. Then, samples were stored at -20˚C storage for five days and incubated in fresh M63 media with proper inducers.

2.2.7 Sample Preparation and Fluorescence Measurement

All the fluorescence measurements in this study was conducted with a microplate reader (SpectraMax M5, Molecular Devices), SoftMax Pro

(Molecular Devices) software was used for measurements. Samples were prepared for fluorescence measurements as follows: 200 µL of samples were taken into Corning 96-well plates (clear flat bottom, polystyrene) without disturbing the paper part. Excitation and emisson wavelengths for fluorescence reporters were set as follows: sfGFP (ex: 485 nm, em: 538 nm) and mScarlet (ex: 544 nm, em: 612 nm). OD_{600} measurement was done by setting wavelength to 600 nm at absorbance measurement tool in SoftMax Pro software.

2.2.8 Congo Red Analysis

Overnight grown cells inoculated (1:100) into fresh M63 minimal growth media with proper antibiotics (1:100), 0.2% glycerol and corresponding inducers. Following induction, cells were incubated in 30°C stationary incubator for three days. On the third day, 2 mL of samples were centrifuged at 8000 rpm for 5 minutes. Pellets were resuspended in half volume of 1x PBS solution. Samples were centrifuged at 8000 rpm for 5 minutes. Pellets were resuspended in equal volume of 1x PBS solution. 200 µL resuspension was used for optical density OD_{600} measurement. Remaining samples were centrifuged at 8000 rpm for 5 minutes and resuspended in 1x congo red solution. Samples were incubated for 30 minutes at room temperature. Then, samples were centrifuged at 8000 rpm for 3 minutes. 180 µL of supernatant was used for optical density measurements at 480 nm (OD_{480}). Signal normalization was done as follows: blank OD_{480}measurement was subtracted from each samples' OD_{480}measurement then absolute of the result is divided by blank OD_{600} measurement subtracted from each samples' OD_{600} measurement.

2.2.9 Sample Preparation for Environmental Scanning Electron Microscopy Analysis

Cells were grown overnight in LB media and directly diluted into LB media for overnight experiments or M63 growth media for 3 day experiments. For OD_{600} 0.01 cases, overnight grown cells were directly 1:100 diluted into respective growth media (either LB or M63 minimal media) onto paper discs placed on 24 well plates. For OD_{600} 0.5 cases, overnight grown cells were 1:100 diluted into respective growth media (either LB or M63 minimal media). When OD_{600} reached 0.5, solution was added onto paper discs placed on 24 well plates. All cases were grown at 30˚C without in stationary incubator. Growth media was removed from the plates and filter papers were washed with 1x PBS for 1 hour with 200 rpm shaking at room temperature. Then, cells on filter paper were fixed with 400 µL 2.5% (w/v in 1x PBS) glutaraldehyde at +4˚C for 16 hours or at room temperature for 1 hour. Then, samples were washed with 400 µL 25% ethanol for 5 minutes, 400 µL 50% ethanol for 5 minutes, 400 µL 75% ethanol for 5 minutes, 400 µL 100% ethanol for 10 minutes on shaker at room temperature. Paper samples were dried with a critical point dryer (SUPERCRITICAL Automegasamdri®-915B, Series C). Dried paper samples were placed on top of SE stabs with a conductive tape, and coated with Au/Pd until thickness of coating reaches 0.1 µm, beam energy was set to 5 keV.

2.2.10 Statistical Data Analysis

For all the biofilm immobilized biosensor assays' data analysis in this study signal normalization was done as follows: blank fluorescence measurement was subtracted from each samples' fluorescence measurement, and blank

OD_{600} measurement was subtracted from each samples' OD_{600} measurement. Then calculated fluorescence value was divided by calculated OD_{600} value for each sample. All measurements were done as duplicates, unless otherwise stated. Data was displayed as mean ± standard deviation. Plotting of graphs and statistical analysis were done on GraphPad Prism version 9.0.0 for Windows, GraphPad Software (www.graphpad.com). Depending on the experimental data sets, one-way or two-way analysis of variance (ANOVA) followed by Dunnett's multiple comparisons tests were performed.

2.3. Results and Discussion

2.3.1 Construction of Biofilm Proteins' Expression Vector

Biofilm protein expression vector was designed to be inducible for easily controlling the system. Backbone containing csgA gene under control of PBAD promoter was PCR amplified from pZa pBAD csgA - HisTag plasmid and csgGEF simultaneous expression construct was PCR amplified from pSC101 ORI - pLac/Ara csgGEF vector (Figure 132), both template backbones are gift from Ebru Şahin Kehribar. Primers can be found at Appendix B. After PCR products were run on 1% agarose gel, they were isolated from the gel with Macherey-Nagel's PCR Clean-up kit according to the manufacturer's instructions and assembled with the Gibson Assembly method. Samples selected from the single colonies were first verified by colony PCR (Figure 134), and then the samples selected from the colony PCR verification were sent for Sanger sequencing analysis. Plasmid map for biofilm proteins' expression vector and Sanger sequencing result can be found at Appendix C and D, respectively.

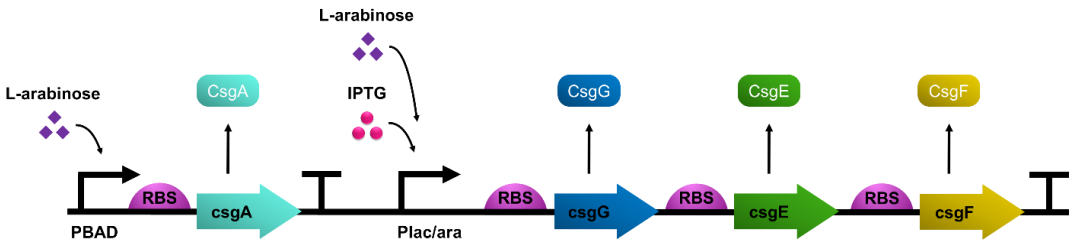

Figure 132. Biofilm proteins' biological parts and working mechanism.

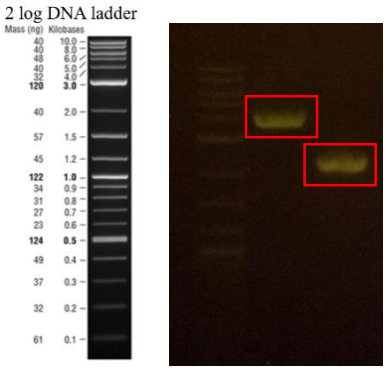

Figure 133. Agarose gel image of the biological parts required for the cloning of the pZa pBAD csgA pLac/Ara csgGEF vector. PCR product of the linear pZa pBAD csgA backbone (left), 3672 bp, PCR product of PcopA promoter region, 2173 bp (right).

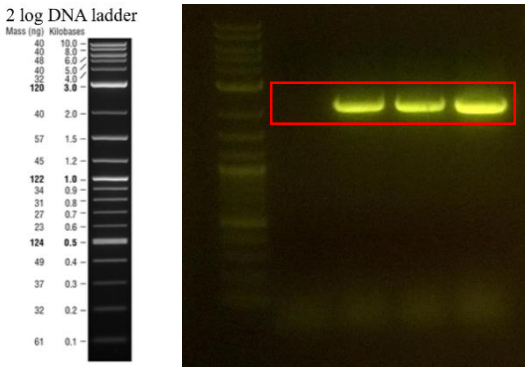

Figure 134. Confirmation of the pZa pBAD csgA pLac/Ara csgGEF vector with colony PCR, expected band size 2173 bp.

2.3.2 Visual Characterization of Biofilm Mediated Immobilization of Cells

Surface immobilization of bacteria cells via biofilm proteins was examined by growing cells in either LB media or M63 minimal growth media in stationary incubator at 30°C. Filter papers are placed in 24 well plates and incubated under UV light for 30 minutes. Then, either LB or minimal media was added on top of papers, and the cells are added into the liquid part. Cells were grown overnight for LB growth media condition and grown for 3 days if cells are grown in M63 minimal growth media. Environmental scanning electron microscopy

(ESEM) samples were prepared as described in Chapter 2 Materials and Methods part. The effected of initial number of cells for biofilm adhesion on filter paper, two set of experiments were conducted. For OD_{600} 0.01 condition, overnight grown cells were diluted into media with 1:100 dilution ratio. For OD_{600} 0.5 condition, overnight grown cells were diluted into either LB media or M63 minimal growth media until OD_{600} reaches 0.5. Compared to OD_{600} 0.5 case, cell adhesion and count was considerably high in OD_{600} 0.01 condition. These results suggest that lower initial number of cells are promising for further experiments.

First, *E.coli PRO* cells without any plasmid (Figure 135), with pZa pBAD csgA vector (Figure 136), with pSC101 Plac/ara csgGEF vector (Figure 137) and both of the pZa PBAD csgA and pSC101 Plac/ara csgGEF vectors (Figure 138) have been investigated for biofilm mediated cell adhesion on filter paper. Overnight grown cells were directly diluted (1:100) onto filter paper with media. Uninduced cells were used as control and 0.2% arabinose and 1mM IPTG induced cells are marked as induced. However, when both plasmids present at the same time and induced, the number of immobilized cells and biofilm formation was observed to be insufficient (Figure 138) compared to when only csgA protein is induced (Figure 136).

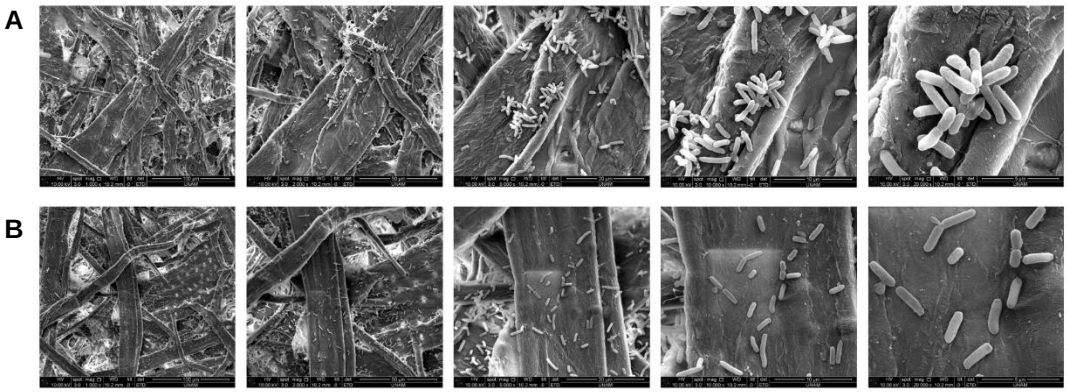

Figure 135. Biofilm mediated immobilization of cells on filter paper assay with Environmental scanning electron microscopy (ESEM). A. Uninduced E.coli PRO cells grown in LB overnight with OD_{600} 0.01. A. 0.2% arabinose and 1mM IPTG induced E.coli PRO cells grown in LB overnight with OD_{600} 0.01 Images are taken with x1000, x2000, x5000, x10000, x20000 magnification from left to right in order.

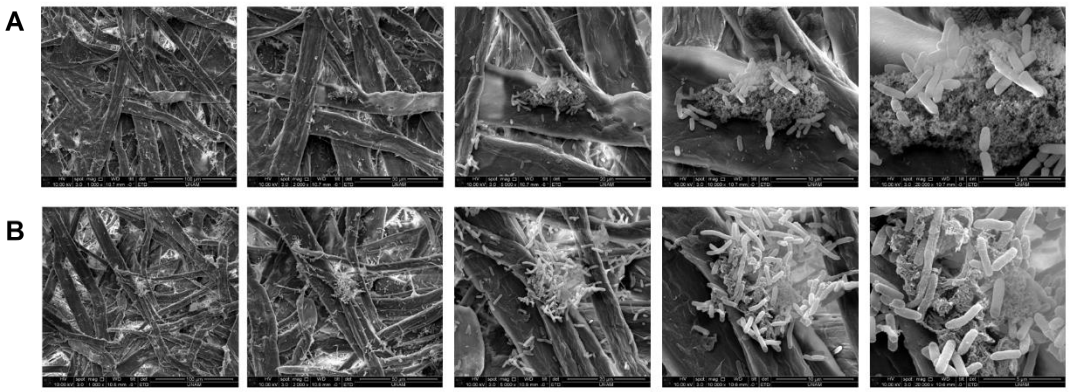

Figure 136. Biofilm mediated immobilization of cells on filter paper assay with Environmental scanning electron microscopy (ESEM). A. Uninduced E.coli PRO cells containing pZa pBAD csgA vector grown in LB overnight with OD_{600} 0.01. A. 0.2% arabinose and 1mM IPTG induced E.coli PRO cells containing pZa pBAD csgA vector grown in LB overnight with OD_{600} 0.01 Images are taken with x1000, x2000, x5000, x10000, x20000 magnification from left to right in order.

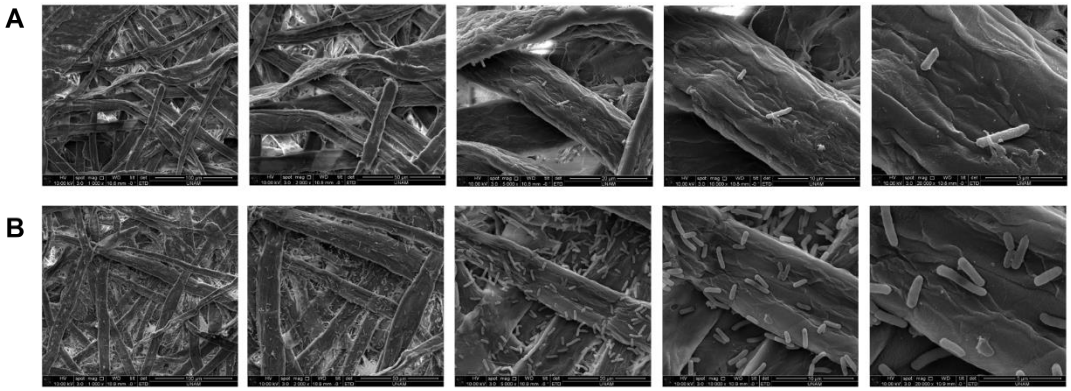

Figure 137. Biofilm mediated immobilization of cells on filter paper assay with Environmental scanning electron microscopy (ESEM). A. Uninduced E.coli PRO cells containing pSC101 Plac/ara csgGEF vector grown in LB overnight with OD_{600} 0.01. A. 0.2% arabinose and 1mM IPTG induced E.coli PRO cells containing pSC101 Plac/ara csgGEF vector grown in LB overnight with OD_{600} 0.01 Images are taken with x1000, x2000, x5000, x10000, x20000 magnification from left to right in order.

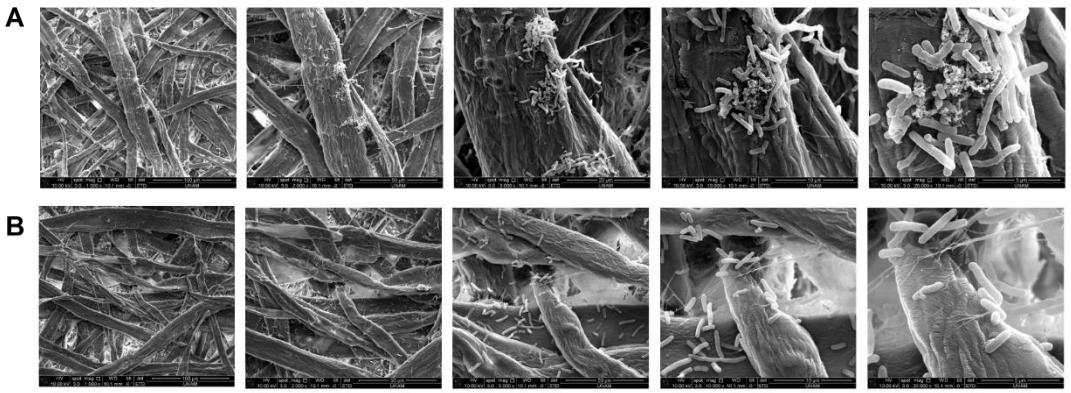

Figure 138. Biofilm mediated immobilization of cells on filter paper assay with Environmental scanning electron microscopy (ESEM). A. Uninduced E.coli PRO cells containing both pZa PBAD csgA and pSC101 Plac/ara csgGEF vectors grown in LB overnight with OD_{600} 0.01. A. 0.2% arabinose and 1mM IPTG induced E.coli PRO cells containing both pZa PBAD csgA and pSC101 Plac/ara csgGEF vectors grown in LB overnight with OD_{600} 0.01 Images are taken with x1000, x2000, x5000, x10000, x20000 magnification from left to right in order.

Second, *E.coli PRO* cells without any plasmid (Figure 139), with pZa pBAD csgA vector (Figure 140), with pSC101 Plac/ara csgGEF vector (Figure 141) and both of the pZa PBAD csgA and pSC101 Plac/ara csgGEF vectors (Figure 142) have been investigated for biofilm mediated cell adhesion on filter paper. Overnight grown cells were directly diluted (1:100) into fresh LB media with

proper antibiotics and grown until OD_{600} reaches 0.5, then cells are added onto filter paper. Uninduced cells were used as control and 0.2% arabinose and 1mM IPTG induced cells are marked as induced. Even though, initial number of cells were higher and both plasmids were induced (Figure 142), cell adhesion and biofilm formation was not at the desired level.

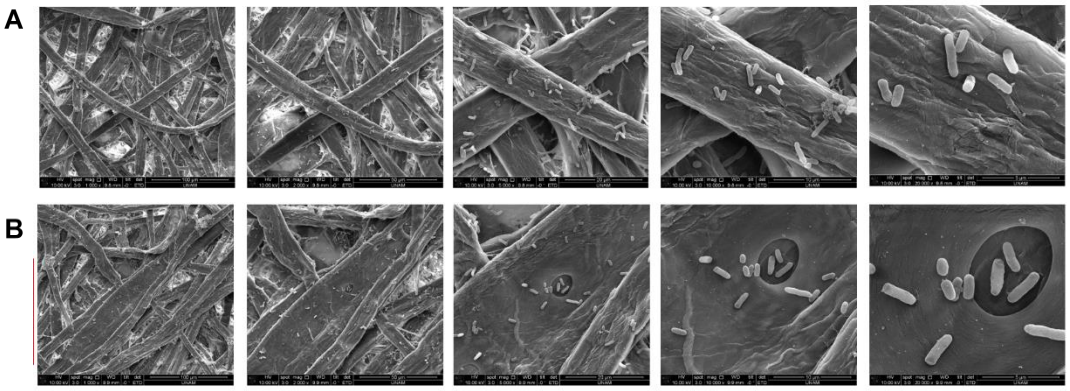

Figure 139. Biofilm mediated immobilization of cells on filter paper assay with Environmental scanning electron microscopy (ESEM). A. Uninduced E.coli PRO cells grown in LB overnight and diluted into fresh LB until OD_{600} 0.5. A. 0.2% arabinose and 1mM IPTG induced E.coli PRO cells grown in LB overnight and diluted into fresh LB until OD_{600} 0.5. Images are taken with x1000, x2000, x5000, x10000, x20000 magnification from left to right in order..

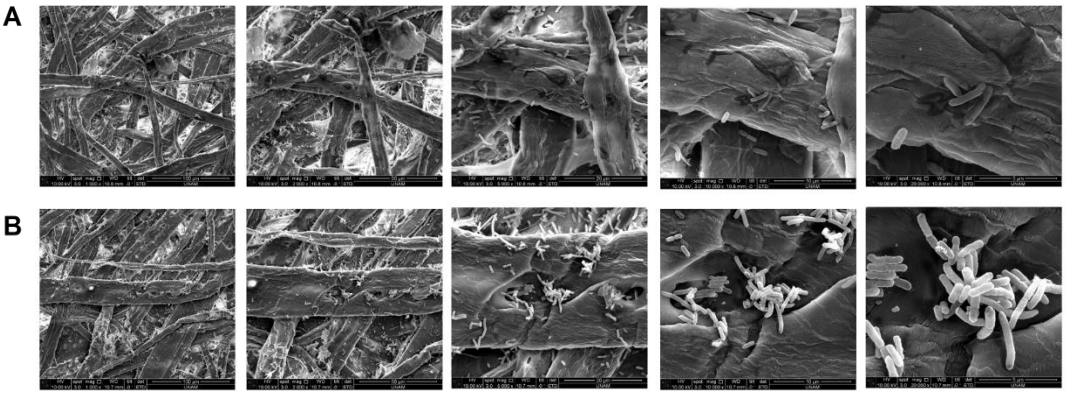

Figure 140. Biofilm mediated immobilization of cells on filter paper assay with Environmental scanning electron microscopy (ESEM). A. Uninduced E.coli PRO cells containing pZa pBAD csgA vector grown in LB overnight and diluted into fresh LB until OD_{600} 0.5. A. 0.2% arabinose and 1mM IPTG induced E.coli PRO cells containing pZa pBAD csgA vector grown in LB overnight and diluted into fresh LB until OD_{600} 0.5. Images are taken with x1000, x2000, x5000, x10000, x20000 magnification from left to right in order.

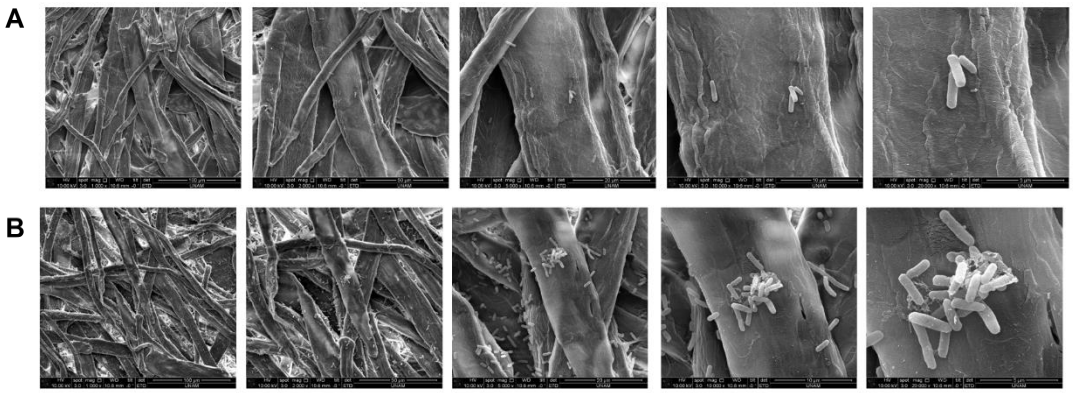

Figure 141. Biofilm mediated immobilization of cells on filter paper assay with Environmental scanning electron microscopy (ESEM). A. Uninduced E.coli PRO cells containing pSC101 Plac/ara csgGEF vector grown in LB overnight and diluted into fresh LB until OD_{600} 0.5. A. 0.2% arabinose and 1mM IPTG induced E.coli PRO cells containing pSC101 Plac/ara csgGEF vector grown in LB overnight and diluted into fresh LB until OD_{600} 0.5. Images are taken with x1000, x2000, x5000, x10000, x20000 magnification from left to right in order.

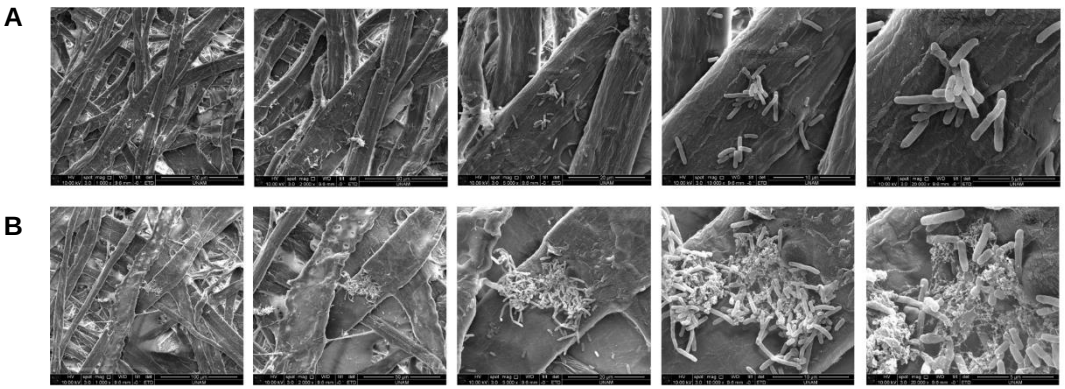

Figure 142. Biofilm mediated immobilization of cells on filter paper assay with Environmental scanning electron microscopy (ESEM). A. Uninduced E.coli PRO cells containing both pZa PBAD csgA and pSC101 Plac/ara csgGEF vectors grown in LB overnight and diluted into fresh LB until OD_{600} 0.5. A. 0.2% arabinose and 1mM IPTG induced E.coli PRO cells containing both pZa PBAD csgA and pSC101 Plac/ara csgGEF vectors grown in LB overnight and diluted into fresh LB until OD_{600} 0.5. Images are taken with x1000, x2000, x5000, x10000, x20000 magnification from left to right in order.

Third, *E.coli PRO* cells without any plasmid (Figure 143) and both of the pZa PBAD csgA and pSC101 Plac/ara csgGEF vectors (Figure 144) have been investigated for biofilm mediated cell adhesion on filter paper. Overnight grown cells were directly diluted (1:100) into fresh M63 minimal growth media with proper antibiotics and grown until OD_{600} reaches 0.5, then cells are added onto

filter paper. Uninduced cells were used as control and 0.2% arabinose and 1mM IPTG induced cells are marked as induced. The initial number of cells were higher and both plasmids were induced (Figure 144), cell adhesion and biofilm formation was almost at the desired level, cells even produced biofilm when they are not induced. Suggesting that the biofilm protein expression system is leaky.

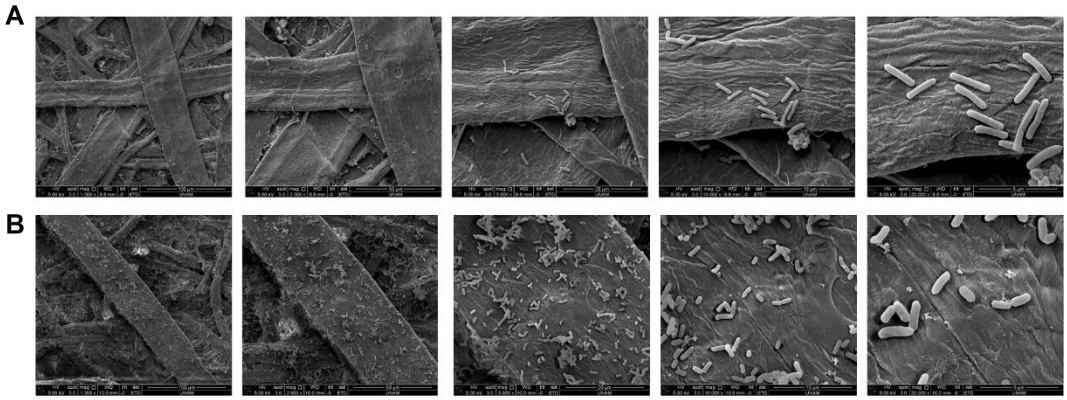

Figure 143. Biofilm mediated immobilization of cells on filter paper assay with Environmental scanning electron microscopy (ESEM). A. Uninduced E.coli PRO cells grown in LB overnight and diluted into fresh M63 minimal growth media until OD_{600} 0.5. A. 0.2% arabinose and 1mM IPTG induced E.coli PRO cells grown in LB overnight and diluted into fresh M63 minimal growth media until OD_{600} 0.5. Images are taken with x1000, x2000, x5000, x10000, x20000 magnification from left to right in order.

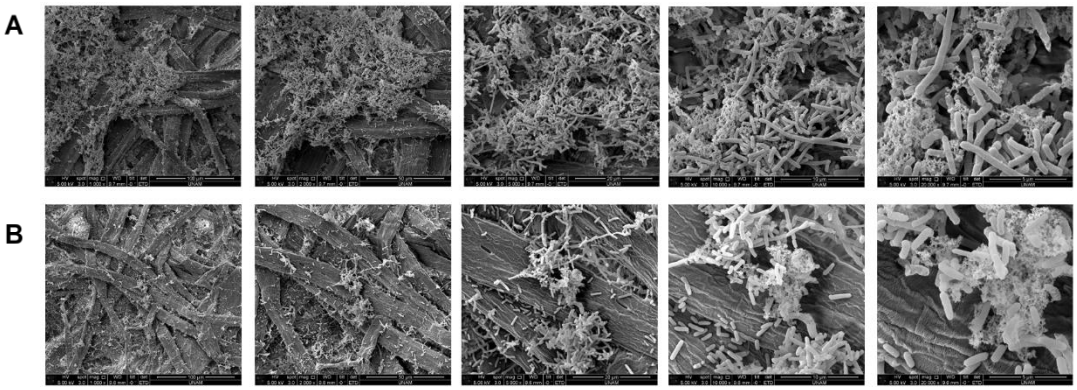

Figure 144. Biofilm mediated immobilization of cells on filter paper assay with Environmental scanning electron microscopy (ESEM). A. Uninduced E.coli PRO cells containing both pZa PBAD csgA and pSC101 Plac/ara csgGEF vectors grown in LB overnight and diluted into fresh M63 minimal growth media until OD_{600} 0.5. A. 0.2% arabinose and 1mM IPTG induced E.coli PRO cells containing both pZa PBAD csgA and pSC101 Plac/ara csgGEF vectors grown in LB overnight and diluted into fresh M63 minimal growth media until OD_{600} 0.5. Images are taken with x1000, x2000, x5000, x10000, x20000 magnification from left to right in order.

2.3.3 Analysis of Biofilm Formation with Congo Red Assay

Formation of Csg based curli nanofibers were quantified with amyloid dye named Congo red which binds to structures rich in β-sheet. As Csg biofilm is β-sheet rich, red remains bound to the biofilm complex, hence lower in liquid form when incubated with biofilm forming cells. As seen in Figure 145 biofilm formation in *ΔcsgA E.coli PRO* cells were lower compared to case when pZa PBAD csgA Plac/ara csgGEF vector is present within the cell and induced with their cognate inducers. When the initial number of cells are lower (OD_{600} 0.01) biofilm formation was observed to be higher in a considerable extent. These results suggest that biofilm formation and biofilm complex's interaction with the filter paper surface increases the number of cells immobilized on the surface even though samples prepared for ESEM were subjected to number of washing cycles.

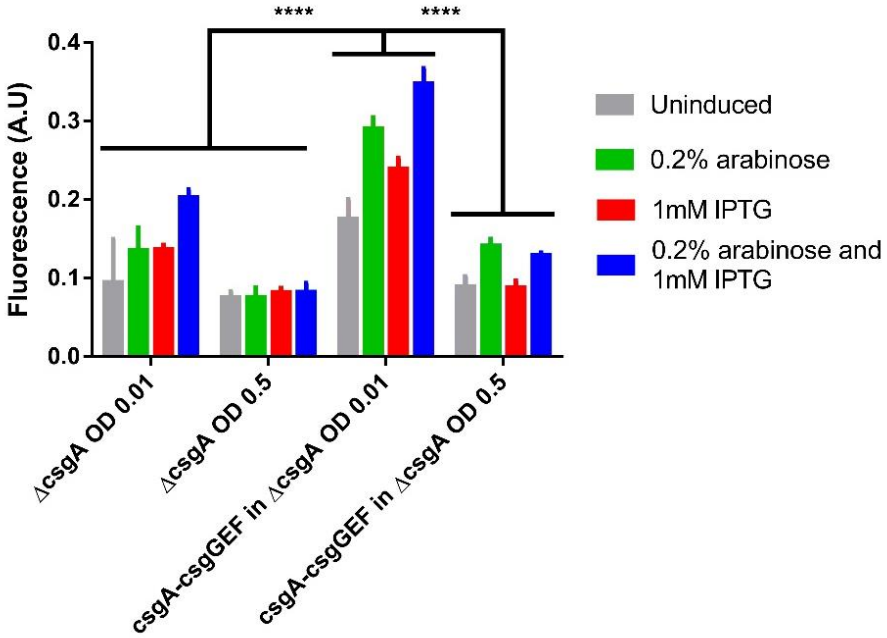

Figure 145. Congo red assay for biofilm formation of *ΔcsgA E.coli PRO* cells without any plasmid or pZa PBAD csgA Plac/ara csgGEF vector. Experiments were repeated in triplicates. The results were analyzed with two-way analysis of variance (ANOVA) (GraphPad Prism version 9.0.0), the differences between the groups were marked with "*" ($p \leq 0.05$, $p \leq 0.01$, $p \leq 0.001$ and $p \leq 0.0001$ is represented by "*", "**", "***" and "****" respectively).

2.3.4 Characterization of Biofilm Immobilized Engineered Cells on Paper in Liquid

Immobilization of cells on filter paper has been shown with ESEM visualization and biofilm formation was shown with both ESEM and congo red staining. To show the inducibility of biosensors in immobilized cells, *ΔcsgA E.coli PRO* without any plasmid (Figure 146), cells containing pZa PBAD csgA Plac/ara csgGEF vector (Figure 147) was cotransformed with either copper RBS30 mScarlet sensor (pET22b-PcopA-RBS30-mScarlet) (Figure 148) or lead -10 mer RBS30 sfGFP sensor (pET22b-10mer-RBS30-PpbrR-sfGFP-ProD-PbrR) (Figure 149) vectors. Overnight grown cells were directly diluted (1:100) into fresh M63 minimal growth media with proper antibiotics onto filter paper discs and grown for 3 days in stationary incubator at 30˚C. Uninduced cells were used as control and 0.2% arabinose and 1mM IPTG induced cells are marked as induced. On the third day, old media was replaced with fresh media with proper supplements and antibiotics. Then, cells were induced with 10 µM and 200 µM $CuSO_4$, 10 µM and 200 µM $PbCl_2$, 100 µM $Cd(CH_3CO_2)_2$, 10 µM Na_3AsO_4 separately. Induction of copper RBS30 mScarlet with copper and lead -10 mer RBS30 sfGFP biosensor with cadmium was observable after 24 hours of induction with blue light illuminator with orange filter. As mScarlet seen as pink, it was visible to eye without an illuminator.

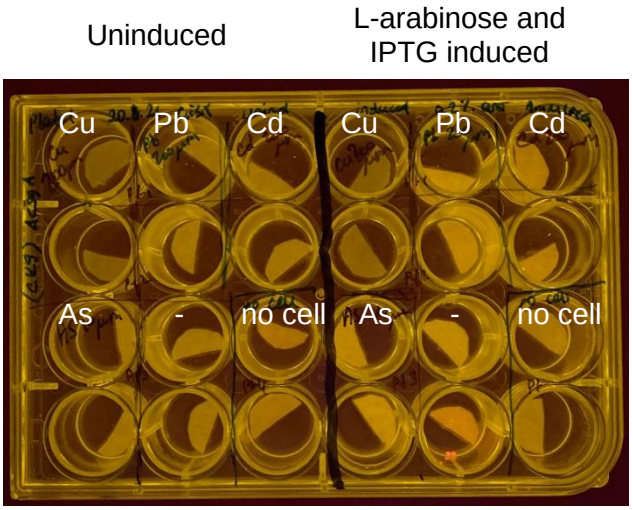

Figure 146. Pictures of induction of biofilm mediated immobilized *ΔcsgA E.coli PRO* cells on filter paper. Cells were induced with 200 μM $CuSO_4$, 200 μM $PbCl_2$, 100 μM $Cd(CH_3CO_2)_2$, 10 μM Na_3AsO_4 separately, – indicates no induction and no cell means no cell was added onto sample. Image was taken on the third day of induction with blue light illuminator with orange filter.

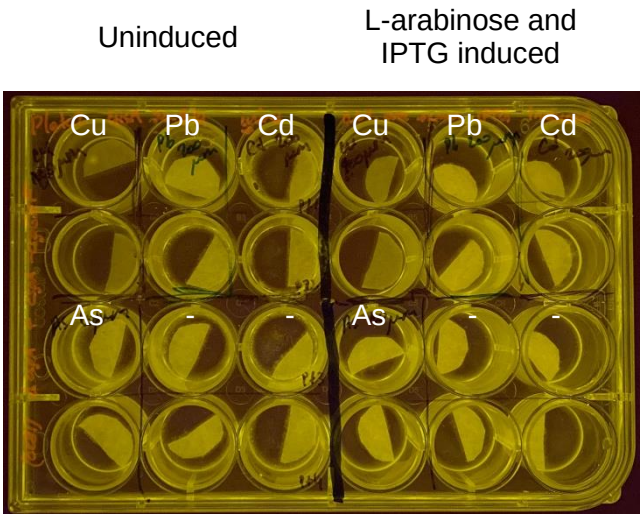

Figure 147. Pictures of induction of biofilm mediated immobilized engineered *ΔcsgA E.coli PRO* cells with pZa PBAD csgA Plac/ara csgGEF vector on filter paper. Cells were induced with 200 μM $CuSO_4$, 200 μM $PbCl_2$, 100 μM $Cd(CH_3CO_2)_2$, 10 μM Na_3AsO_4 separately, – indicates no induction and no cell means no cell was added onto sample. Image was taken on the third day of induction with blue light illuminator with orange filter.

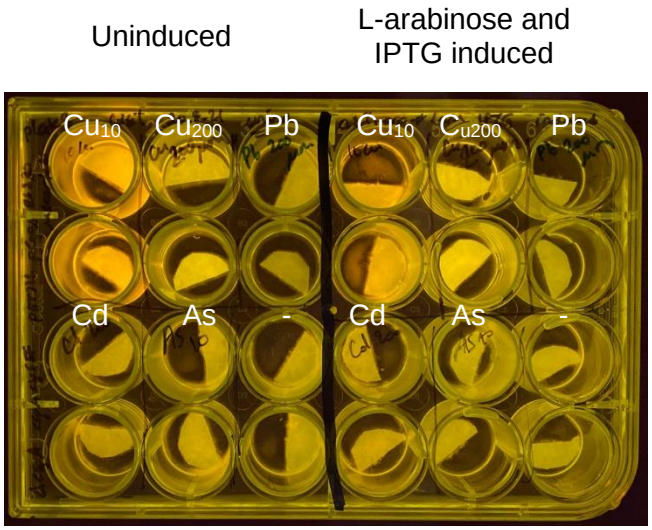

Figure 148. Pictures of induction of biofilm mediated immobilized engineered *ΔcsgA E.coli PRO* cells with pZa PBAD csgA Plac/ara csgGEF vector and copper RBS30 mScarlet sensor (pET22b-PcopA-RBS30-mScarlet) on filter paper. Cells were induced with 10 μM and 200 μM $CuSO_4$ (indicated as Cu_{10} and Cu_{200}, respectively), 200 μM $PbCl_2$, 100 μM $Cd(CH_3CO_2)_2$, 10 μM Na_3AsO_4 separately, – indicates no induction and no cell means no cell was added onto sample. Image was taken on the third day of induction with blue light illuminator with orange filter.

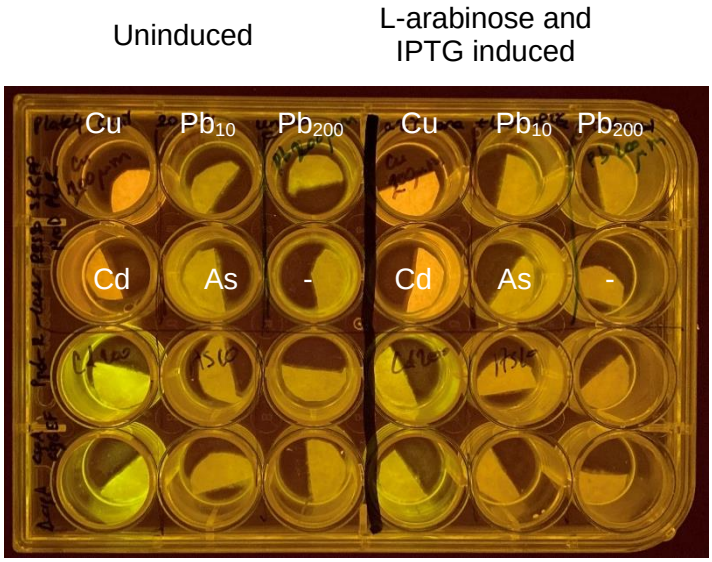

Figure 149. Pictures of induction of biofilm mediated immobilized engineered *ΔcsgA E.coli PRO* cells with pZa PBAD csgA Plac/ara csgGEF vector and lead -10 mer RBS30 sfGFP sensor (pET22b-10mer-RBS30-PpbrR-sfGFP-ProD-PbrR) vector on filter paper. Cells were induced with 200 μM $CuSO_4$, 10 μM and 200 μM $PbCl_2$(indicated as Pb_{10} and Pb_{200}, respectively), 100 μM $Cd(CH_3CO_2)_2$, 10 μM Na_3AsO_4 separately, – indicates no induction and no cell means no cell was added onto sample. Image was taken on the third day of induction with blue light illuminator with orange filter.

2.3.5 Characterization of Lyophilized Biofilm Immobilized Cells on Paper

Immobilization of cells on filter paper has been shown with ESEM visualization and biofilm formation was shown with both ESEM and congo red staining. To store paper discs with immobilized engineered cells, lyophilization step was investigated as a possible solution. Here, *ΔcsgA E.coli PRO* cells without any plasmid (Figure 151) or with pZa PBAD csgA Plac/ara csgGEF vector (Figure 152) was used the controls and *ΔcsgA E.coli PRO* cells containing pZa PBAD csgA Plac/ara csgGEF vector with either copper mScarlet sensor (pET22b-PcopA-RBS30-mScarlet) (Figure 153) or lead sfGFP biosensor (pET22b-10mer-RBS30-PpbrR-sfGFP-ProD-PbrR) (Figure 154) was used as potential candidates for point-of-care device application.

ΔcsgA E.coli PRO cells without any plasmid, with pZa PBAD csgA Plac/ara csgGEF vector, with pZa PBAD csgA Plac/ara csgGEF and pET22b-PcopA-RBS30-mScarlet vectors, with pZa PBAD csgA Plac/ara csgGEF and pET22b-10mer-RBS30-PpbrR-sfGFP-ProD-PbrR were investigated for lyophilized biofilm immobilized engineered cells for paper based heavy metal detection system. Overnight grown cells were directly diluted (1:100) into fresh M63 minimal growth media with proper antibiotics onto filter paper discs and grown for 3 days in stationary incubator at 30˚C. Uninduced cells were used as control and 0.2% arabinose and 1mM IPTG induced cells are marked as induced. Paper discs and their growth media was transferred to 15 mL falcons, trehalose solution was added with a final concentration of 100mM into the falcons. Samples are frozen at -80˚C overnight, then caps are removed and the lids are covered with tissue and stabilized with rubber bands. Falcons were

placed vertically to glass holders of lyophilizer, and incubated 2 days for complete removal of water molecules in paper samples. The pictures of lyophilization process was shown in Figure 150.

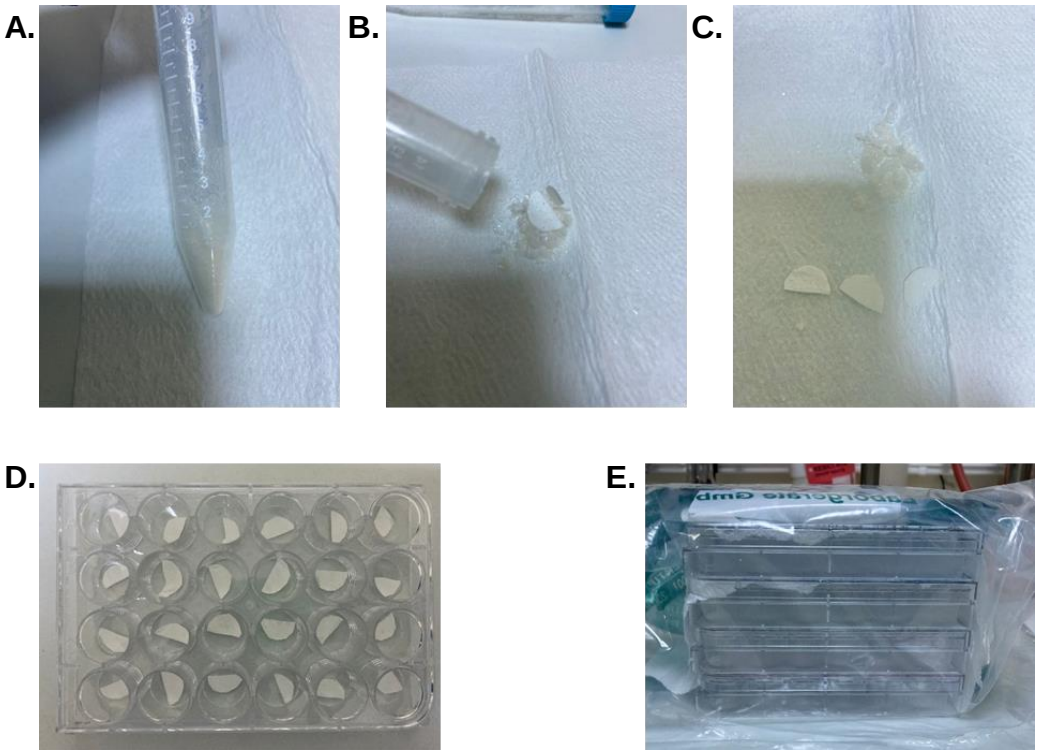

Figure 150. Pictures of lyophilization process of biofilm mediated immobilization of engineered cells on filter paper. A. Falcon with remaining salts and paper discs after lyophilization. B. and C. Removal of paper discs from falcon and then salt, respectively. D. Placement of paper discs to their 24 well holders. E. Storage of lyophilized paper discs at -20˚C.

Immobilization of cells on filter paper has been shown with ESEM visualization and biofilm formation was shown with both ESEM and congo red staining. To show the inducibility of biosensors in immobilized cells, *ΔcsgA E.coli PRO* cells containing pZa PBAD csgA Plac/ara csgGEF vector was cotransformed with either copper RBS30 mScarlet sensor (pET22b-PcopA-RBS30-mScarlet) or lead -10 mer RBS30 sfGFP sensor (pET22b-10mer-RBS30-PpbrR-sfGFP-ProD-PbrR) vectors. Overnight grown cells were directly diluted (1:100) into

fresh M63 minimal growth media with proper antibiotics onto filter paper discs and grown for 3 days in stationary incubator at 30˚C. Uninduced cells were used as control and 0.2% arabinose and 1mM IPTG induced cells are marked as induced. On the third day, paper discs were placed into 15mL falcons. Then, trehalose solution was added onto M63 media with paper discs with a final concentration of 100 mM. Samples were frozen at -80˚C, next samples were freeze dried for two nights. Lyophilized paper discs were stored at -20˚C for five days. Lyophilized paper discs were incubated in M63 minimal growth media for 20 minutes, then heavy metal inducers 10 µM and 200 µM $CuSO_4$, 10 µM and 200 µM $PbCl_2$, 100 µM $Cd(CH_3CO_2)_2$, 10 µM Na_3AsO_4 were added separately. Induction of copper RBS30 mScarlet with copper with copper was observable after 28 hours of induction with blue light illuminator with orange filter. As mScarlet seen as pink, it was visible to eye without an illuminator. No significant signal was observed for any induction case of lead -10 mer RBS30 sfGFP biosensor.

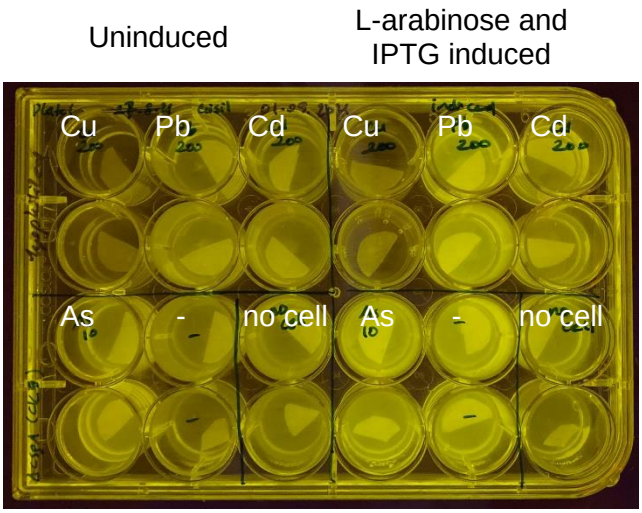

Figure 151. Pictures of induction of biofilm mediated immobilized *ΔcsgA E.coli PRO* cells on filter paper. Cells were induced with 200 µM $CuSO_4$, 200 µM $PbCl_2$, 100 µM $Cd(CH_3CO_2)_2$, 10 µM Na_3AsO_4 separately, – indicates no induction and no cell means no cell was added onto sample. Image was taken on the third day of induction with blue light illuminator with orange filter.

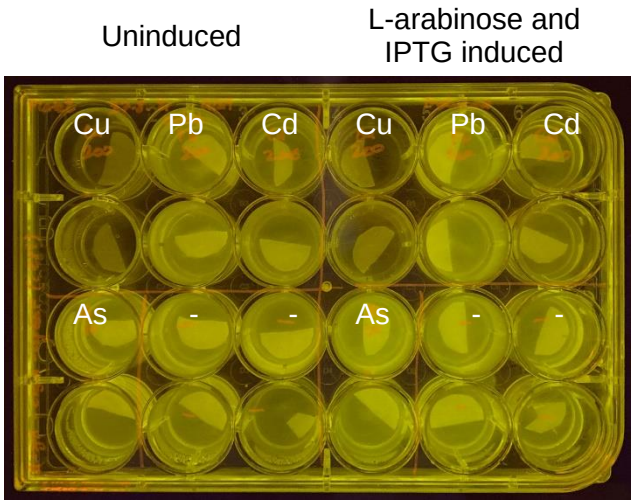

Figure 152. Pictures of induction of biofilm mediated immobilized engineered *ΔcsgA E.coli PRO* cells with pZa PBAD csgA Plac/ara csgGEF vector on filter paper. Cells were induced with 200 μM $CuSO_4$, 200 μM $PbCl_2$, 100 μM $Cd(CH_3CO_2)_2$, 10 μM Na_3AsO_4 separately, – indicates no induction and no cell means no cell was added onto sample. Image was taken on the third day of induction with blue light illuminator with orange filter.

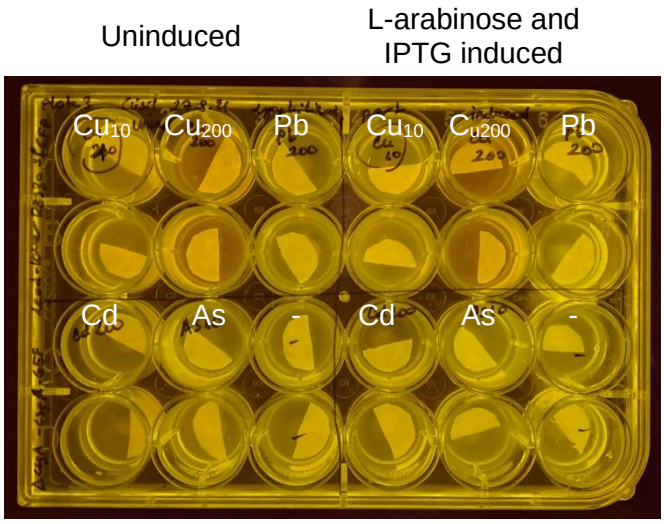

Figure 153. Pictures of induction of biofilm mediated immobilized engineered *ΔcsgA E.coli PRO* cells with pZa PBAD csgA Plac/ara csgGEF vector and copper RBS30 mScarlet sensor (pET22b-PcopA-RBS30-mScarlet) on filter paper. Cells were induced with 10 μM and 200 μM $CuSO_4$ (indicated as Cu_{10} and Cu_{200}, respectively), 200 μM $PbCl_2$, 100 μM $Cd(CH_3CO_2)_2$, 10 μM Na_3AsO_4 separately, – indicates no induction and no cell means no cell was added onto sample. Image was taken on the third day of induction with blue light illuminator with orange filter.

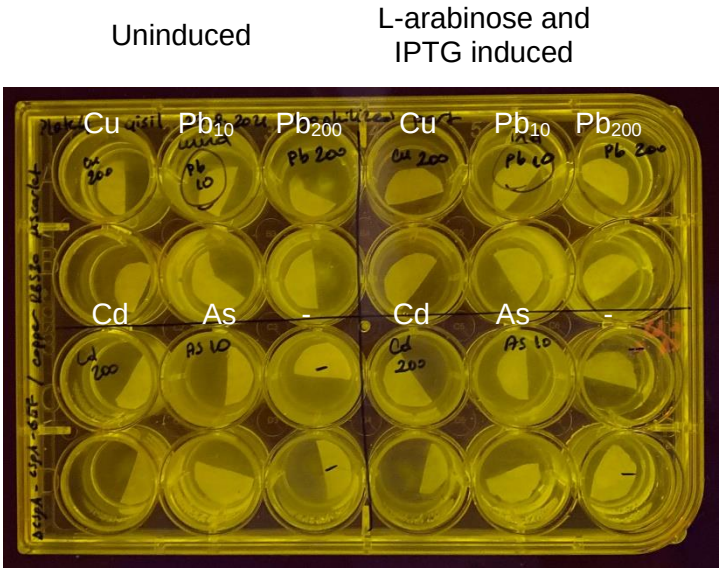

Figure 154. Pictures of induction of biofilm mediated immobilized engineered *ΔcsgA E.coli PRO* cells with pZa PBAD csgA Plac/ara csgGEF vector and lead -10 mer RBS30 sfGFP sensor (pET22b-10mer-RBS30-PpbrR-sfGFP-ProD-PbrR) vector on filter paper. Cells were induced with 200 µM $CuSO_4$, 10 µM and 200 µM $PbCl_2$(indicated as Pb_{10} and Pb_{200}, respectively), 100 µM $Cd(CH_3CO_2)_2$, 10 µM Na_3AsO_4 separately, – indicates no induction and no cell means no cell was added onto sample. Image was taken on the third day of induction with blue light illuminator with orange filter.

2.4. Conclusion and Future Perspectives

Biofilms are functional amyloids widely used as adhesives for organisms and materials to surfaces. Physicochemical and mechanical properties of biofilms protect the inner content from outer stress conditions. Here, various biofilm formation conditions have been investigated for cell attachment to paper-based surface for analyte detection with whole-cell biosensors.

The effect of overexpression of curli specific genes (CsgA, CsgG, CsgE and CsgF) on cell adhesion have been characterized in terms of amyloid formation and cell count via visualization. Even though cells were grown in rich media (LB media), biofilm formation was observed for overnight grown *E.coli* cells when CsgA, CsgG, CsgE and CsgF proteins are overexpressed. However, LB media interferes with sfGFP measurements and visualization with blue light. Hence, M63 minimal growth media was selected for growth media for characterization analysis as it has been shown in previous studies that minimal media triggers biofilm formation. When cells lack csgA gene (*E. coli* DH5α ΔcsgA strain), biofilm formation is impaired even when CsgG, CsgE and CsgF proteins are overexpressed.

To investigate the effect of initial cell count on biofilm formation different dilutions were investigated. The experimental data suggest that, minimal initial cell number was crucial for more biofilm formation as verified with Congo red staining. Then, selected conditions were further optimized for biosensors integrated applications in liquid and lyophilized form. For simultaneous and

sensitive detection of analytes, copper RBS30 mScarlet and lead -10mer RBS30 sfGFP sensors was selected to further characterize. *E. coli* DH5α ΔcsgA cells are cotransformed with both CsgA, CsgG, CsgE and CsgF proteins' expression vector and either copper or lead biosensor vectors. Overnight grown cells were diluted into M63 minimal growth media directly and incubated for 3 days with or without inducers of curli protein expression. Then, half of each paper discs were collected for freeze-drying (lyophilization) assay. Lyophilized samples were stored for 5 days at -20°C to see the effect of both lyophilization and storage condition for prolonged usage of paper based sensory system. The other half of paper discs were incubated in fresh M63 minimal growth media with heavy metal inducers. Paper immobilized sensory cells remained in liquid media have shown higher fluorescence for lower concentrations of copper and lead. However, no significant visible change was observed for higher concentrations. In lyophilized paper samples, higher copper concentration yielded higher signals but less change was observed for lower concentrations of copper biosensor. For lead biosensor, in liquid media although sfGFP was seen in cadmium cross reactant no signal was observed for neither high nor low concentrations of lead inducer. The lower signal level in uninduced cells for biofilm formation indicates that due to hydrophobic biofilm structure, diffusion of heavy metal ions to cells might be sequestered.

The results of mScarlet reported based whole-cell biosensor is promising as the change can be seen in sun light. Other reporters (eg. YFP, mTagBFP, lacZ) should be investigated for paper-based systems for detection of best performing reporters. As the sensing platform contains only cells adhered to

paper based surface, the disposal alternatives includes burning without any toxic waste. Moreover, the cost of end-product of point-of-care device would be cheaper than conventional detection systems. The sensory system requires only paper-based cell immobilized discs, M63 minimal media for testing. However, the need for M63 minimal growth media at the time of detection can be eliminated with further optimizations. Similarly, storage conditions can be optimized as long as humidity does not interfere with lyophilized sample, using vacuumed bags can be an alternative to -20°C freezers.

To sum up, newly developed lyophilized paper-based cellular immobilization for multi-input multi-output detection system for heavy metals holds great potential for environmentally-friendly, low-cost, easy-to-handle and waste-free disposable point-of-care device applications from environmental or biological samples. The possible usage areas of using proposed system includes routine environmental screening and possible poisoned patients as it is cheap, practical, highly durable although response time requires further optimization.

Chapter 3 – SARS-CoV-2 Detection with De Novo Designed Synthetic Riboregulators

This work is partially described in the following publication [74]

İlkay Çisil Köksaldı [1,2, #], Sıla Köse [1,2, #], Recep Erdem Ahan [1,2, #], Nedim Hacıosmanoğlu [1,2, #], Ebru Şahin Kehribar [1,2, #], Murat Alp Güngen [1,2,] Aliye Baştuğ [3], Bedia Dinç [3], Hürrem Bodur [3], Aykut Özkul[4,5], Urartu Özgür Şafak Şeker[1,2]

1 UNAM−National Nanotechnology Research Center, Bilkent University, 06800 Ankara, Turkey

2 Institute of Materials Science and Nanotechnology, Bilkent University, 06800 Ankara, Turkey

3 Department of Infectious Diseases and Clinical Microbiology, Health Science University Turkey, Ankara City Hospital, 06800 Ankara, Turkey

4 Faculty of Veterinary Medicine, Department of Virology, Ankara University 06110 Ankara, Turkey

5 Biotechnology Institute, Ankara University 06135 Ankara, Turkey

Corresponding Author:

Dr. Urartu Özgür Şafak Şeker

urartu@bilkent.edu.tr

#These authors contributed equally

Adapted with permission from Köksaldı, İlkay Çisil, et al. “Sars-Cov-2 Detection with De Novo-Designed Synthetic Riboregulators.” *Analytical Chemistry*, vol. 93, no. 28, 30 June 2021, pp. 9719–9727., doi:10.1021/acs.analchem.1c00886.

3.1 Introduction

Coronavirus disease 2019 (COVID-19) is a global pandemic caused by a novel coronavirus, severe acute respiratory syndrome coronavirus 2 (SARS-CoV-2), that infects angiotensin-converting enzyme 2 (ACE2) positive cells found in the human body. Several tissues and organ systems, including the upper respiratory tract, small intestine, liver, and nervous system, are susceptible to SARS-CoV-2 infection [75,76]. As diverse clinical manifestations of COVID-19 are vaguely defined, the shared symptoms with other common infectious disease states such as the seasonal flu may cause misdiagnosis[77,78]. Person-to-person transmission and, most importantly, lack of rapid and adequate testing resulted in the loss of opportunity to prevent the spread of the virus in numerous countries at the beginning of the pandemic. Furthermore, the presence of asymptomatic and pre-symptomatic SARS-CoV-2 infected people accounting for the silent transmission in super-spreading events aggravates pandemic worldwide by posing risk to elderly people and chronically ill patients [79].

Test-track-isolate is a fundamental strategy to mitigate the risk of overwhelming the healthcare system until a viable therapeutic solution can be produced [80]. Therefore, widespread testing for COVID-19 is vital to block the viral transmission chain. Molecular diagnosis of COVID-19 heavily relied on quantitative real-time polymerase chain reaction (qRT-PCR) that detects the presence of SARS-CoV-2 RNA in the nasopharynx, trachea or bronchus. However, testing capacity failed to meet increasing demand due to the global shortage in qRT-PCR reagents (i.e., reaction mix, polymerase, reverse

transcriptase, etc.) [81,82]. Additionally, qRT-PCR tests generally require a testing facility and trained staff. To compensate for the gap between test numbers and the pace of infection, many agencies declared an emergency use of in vitro diagnostic products for SARS-CoV-2. Consequently, numerous methods, excluding qRT-PCR, were developed for virus detection by targeting its proteins or nucleic acid components [83–86]. Notably, CRISPR Dx tools, SHERLOCK [87] and DETECTR [84], were rapidly developed to sense SARS-CoV-2 presence with improvements in their sensing pipeline such as SHERLOCK with unextracted samples and amplification free Cas13a sensing. Even though the limit of detection (LoD) of newly proposed tests is not as high as qRT-PCR, it is speculated that the point-of-care (PoC) device implementation will be useful to detect particularly people with high virus titer who are the main cause of super-spreading events [87].

Synthetic biology broadens the scope of diagnostic tool alternatives, among which programmable riboregulator toehold switches are straightforward and inexpensive to develop [6,88]. The versatility of toehold switches enabled researchers to develop biosensors for pathogenic viruses such as Zika[23], Ebola [88], an antibiotic resistance gene [88], and microorganisms found in the human gut [24]. Combined with the cell-free transcription/translation (TXTL) technology, toehold switches can be used to detect the presence of specific nucleic acid sequences in a PoC device in which the output signal can be a fluorescent protein or the colorimetric degradation product of an enzyme [23]. Besides, the LoD of toehold-based sensors can be increased with a simple isothermal amplification reaction such as nucleic acid sequence–based

amplification (NASBA) or recombinase polymerase amplification (RPA) prior to the TXTL reaction [89]. Owing to their fast prototyping capability and easy-to-use format, the utilization of toehold switch sensor mechanism together with the TXTL reaction is an excellent candidate to develop an assay with. Such an assay can be implemented in a PoC device for surveillance of SARS-CoV-2 in substantial portions of populations, which do not have access to a centralized facility to perform sophisticated diagnosis assays such as qRT-PCR or next-generation sequencing (NGS). Alongside mass testing: the need for such testing systems in less developed countries, where the necessary infrastructure and trained personnel are not always available, is paramount in preventing diseases from spreading. In order to help these countries, the World Health Organization (WHO) has developed the ASSURED (Affordable, Sensitive, Specific, User-friendly, Rapid and robust, Equipment-free and Deliverable to end-users) criteria [90]. Creating POC devices that complies with these criteria increases the likelihood of better containing pandemics by using them in developing countries as well as by compensating for the growing need for testing in developed countries.

Here, we designed toehold switches to detect the presence of the SARS-CoV-2 virus. Specifically, regions in the SARS-CoV-2 genome, ORF1ab, M, ORF678, and S coding sequences, those compatible with the NASBA reaction were selected as potential triggers. Switch sequences specific to their cognate triggers that control the expression of superfolder green fluorescent protein (sfGFP) were constructed and tested. Two out of four trigger sequences (the regions found in ORF1ab and S proteins) were detected with designed switch

sequences both in vivo on a genetic circuit and in vitro through TXTL reactions. Then, selected trigger/switch sensor couples are characterized for optimum conditions in NASBA and TXTL reactions to be used with real samples, as shown in Figure 156. Last of all, patient samples are tested with the designed system and efficiency is compared with qRT-PCR analysis. In the light of the results obtained, the promisingness of the toehold-based biosensors implemented in a PoC device to help monitor and control the transmission of the disease, especially in rural and less developed regions has been demonstrated thanks to the fact that it is cheap, accessible and does not require expertise (Figure 155).

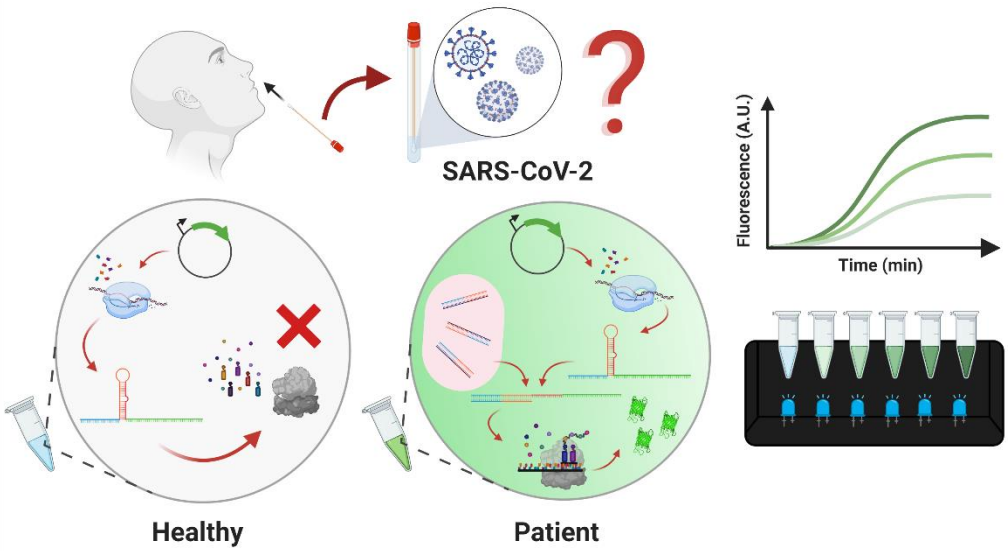

Figure 155. Point-of-care device implementation of synthetic riboregulator based cell free detection of SARS-CoV-2 virus from human samples. Illustration is drawn on Biorender.

3.2 Materials and Methods

3.2.1 In Silico Design

In order to develop an integrated workflow for designing NASBA primers and toehold switches together, a combination of web tools was used throughout the design procedure. For the generation of trigger sequence candidates with primer sites, Primer-BLAST was used (https://www.ncbi.nlm.nih.gov/tools/primer-blast/) by setting temperature parameters to 60ºC and PCR product size between 120-160 bp. Using the input gene sequences derived from reference SARS-CoV-2 genome (GenBank: MN908947.3), we generated a set of trigger candidates with NASBA compatible primer sets for the whole SARS-CoV-2 reference genome. Next, we used a web-based analysis tool of NUPACK software (http://www.nupack.org/) to investigate free energies of trigger candidates and applied a -25 kJ/mol constraint for selecting designs for the next step. Then, by using NCBI-BLAST web tool (https://blast.ncbi.nlm.nih.gov/Blast.cgi), we aligned candidate sequences with six human coronaviruses (229E, NL63, OC43, HKU1, SARS and MERS) to maximize specificity. Candidate triggers that passed energy and BLAST tests were transferred to the design phase by using the design tool of NUPACK software again to generate switch candidates. 10 candidate switches for each trigger candidate were designed. After completion of the designs, defects, similar sequences and stop codon carrying constructs were eliminated by using a defect function threshold of 25%. Overall, 503 trigger candidates designed with Primer-BLAST, 123 candidates have passed the minimum energy and BLAST requirements, and 5 trigger candidates resulted in up to 4 different switch constructs. Toehold

domains for each trigger targeting different regions in SARS-CoV-2 genome contains b*, a*, conserved domain, a and linker regions as previously reported [6]. Recognition domain consist of b* and a* regions; a*, conserved domain and a region creates the stem and loop domains. The length of domains are as follows b*: 24 bp, a*: 12 bp, conserved domain: 28 bp (containing 8 bp RBS and ATG sequences as well), a: 12 bp and linker region: 21 bp. De novo designed riboregulators specific to SARS-CoV2 are given in Table 15.

3.2.2 Assembling Sensor Constructs

For the generation of switch and trigger plasmids, a pET22B backbone (high copy number, AmpR resistance) for triggers; and a pZA backbone (mid copy number, CmR resistance) for switches were used as vectors. In our design, pET22B backbone carries a T7 promoter and a T7 terminator, which can be induced by IPTG addition. On the other side, pZA backbone carries a T7 promoter with sfGFP, superfolder Green Fluorescent Protein gene from the pJT119b plasmid [91] (deposited to the Addgene by Jeffrey Tabor, Addgene #50551) and rrnB_T1 terminator from Registry of Standard Biological Parts at the downstream of sfGFP. Inserts selected during in silico design phase were ordered from Genewiz Inc. with Gibson Assembly overlaps. Sequence verification of cloned constructs was done with Sanger sequencing (Genewiz) after the cloning. DH5α strain of *Escherichia coli* was used for all cloning stages.

3.2.3 Whole-Cell Sensor Test

As the first stage of characterizations, switch constructs with a matching trigger sequence were transformed into *E. coli* BL21(DE3) cells with chemical transformation. Meanwhile, standalone switch constructs were transformed as control groups. A single colony from each plate was selected and grown overnight in LB medium at 37ºC in a 200 rpm orbital shaker with appropriate antibiotics. Next, cells were diluted in fresh LB medium with antibiotics and induced with 1 mM IPTG at an OD_{600} value between 0.2-0.3. Total fluorescence emission of the trigger plasmid carrying cells and control groups were measured by M5 SpectraMax (Molecular Devices) at 2, 4, 8 and 16 hours.

3.2.4 Flow Cytometry Analysis

Flow Cytometry measurements were performed by using BD Accuri C6 device (BD Biosciences). Cells were grown and induced as described in the whole-cell sensor test section. For each sample, 300 µL of cells were taken then washed with 1X PBS and diluted as 1/100 before the measurement. Forward scatter (FSC) and side scatter (SSC) thresholds of 10,000 was used to eliminate any background. 100,000 events were recorded for each measurement and the resulting data analysed with BD Accuri C6 Plus software (BD Biosciences).

3.2.5 Isolating SARS-CoV-2 RNA from Viral and Patient Samples

Nasopharyngeal swab samples were obtained from the laboratory-confirmed COVID-19 patients and considered as inpatients at Ankara City Hospital, Department of Infectious Diseases and Clinical Microbiology while following proper ethical and clinical regulations. All the samples collected and stored in viral transfer media following the sample collection guidelines provided by WHO. After heat inactivation at 60°C for 90 minutes, viral RNA isolation is performed by using Quick-RNA Viral RNA extraction kit (Zymogen) with the standard protocol provided by the supplier. Prior to experiments, all the patient samples and their isolated RNA were tested with Voliron™ (Synbiotik LLC) SARS-CoV-2 qRT-PCR test kit to identify viral RNA. Viral samples used as a positive control template during the experiments were provided by Prof. Dr. Aykut Özkul, and viral RNA isolated with the same protocol that is used for the patient samples.

3.2.6 NASBA Reactions

Overall strategy for the NASBA reactions is adopted from Pardee et al. [23]. As a summary, each reaction constituted with first 1.675 µL 3x NASBA Reaction Buffer (Life Sciences, NECB-1-24), 0.8375 µL 6x Nucleotide Mix (Life Sciences, NECN-1-24), 0.025 µL Protector RNase Inhibitor (Roche) and 0.1 µL of 12.5 µM Primer mix according to the targeted genomic region. After that, 1.125 µL of isolated viral RNA added to the reaction. After incubation at 65°C for 2 min and 41°C for 10 min, 1.2375 µL of NASBA Enzyme Cocktail (Life Sciences, NEC-1-24) added to each reaction. Trigger RNA fragments produced by HiScribe™ T7 High Yield RNA Synthesis Kit (NEB) and cleaned

up with Monarch® RNA Cleanup Kit (NEB) used as positive control during the tests. As the template, T7 controlled trigger plasmid from sensor validation step used for each toehold switch construct. Same trigger pairs with 750 ng plasmid DNA are also used for NASBA efficiency tests. Plasmid DNA used during the tests isolated by Nucleobond Xtra Midi kit (MN). Note that all the stages of the reaction assembled at 4°C and the final NASBA reaction kept at 41°C for 2 hours.

3.2.7 Testing Designs and Samples with Cell-Free Expression Systems

Cell-free testing of designed systems was performed by using a commercial cell-free expression kit (NEB, PURExpress) and following the protocol provided by the supplier. For each test sample, isolated switches construct plasmid (31.5 nM) and linear trigger DNA (0.34 mM) are used for testing initial designs. For the measurements with isolated viral RNA, changing amounts of completed NASBA reactions (1 µL or 2 µL per reaction) and different concentrations of switch plasmid (500-750 and 1000 ng per reaction) are used with the previous protocol. Unless otherwise stated, a total volume of 10 µL cell-free reactions are used for each test and the volumes adjusted with nuclease-free ddH2O for changing conditions. Reactions were measured with M5 SpectraMax (Molecular Devices) for 3 or 5 hours at 37°C to monitor sfGFP expression by tracking fluorescence emission at 538 nm.

3.2.8 Cross Reactivity Analysis of Best Performing Switch Sensors

Isolation of viral RNA from HKU1 viral sample also carried out with Zymogen Quick RNA kit. In order to verify isolated HKU1 RNA, a primer set from the literature [92] used with SuperScript III Reverse Transcriptase/Taq Enzyme mix and SYBR/ROX Reaction mixture by using standard protocol provided by the supplier. Toehold assay for HKU1 cross reactivity is also performed using SARS-CoV-2 protocol previously mentioned in detail.

3.2.9 Statistical Analysis and Illustrations

Statistical analysis and graphing of data generated in this article were done with Graphpad Prism 8 software. All the illustrations in this manuscript are created with BioRender.com and Adobe Illustrator by the authors.

3.2.10 Building a Hand-size Transilluminator

The circuit of the blue light hand illuminator, based on a modified version of Jung et al. [20], consists of eight 470nm light emitting diodes (LEDs) connected in series to two resistors: one normal and one variable. The normal resistor is used to limit the current that flows into the LEDs, and the variable resistor is used to adjust their brightness. The case of the illuminator was drawn using Solidworks 2019 then produced with a Makerbot Replicator+ 3D printer using a PLA filament. The case was coated in multiple layers of black spray paint prior to assembly. An orange-transparent cellophane sheet, located in front of sample tubes, is used as the filter. The illuminator powered with three regular 1.5V alkaline batteries was used to inspect the result of TXTL reactions.

3.2.11 Data Availability

All data generated and analysed in this study are available within the article and Supplementary Information is available from the corresponding author upon request.

3.3. Results and Discussion

We designed synthetic programmable toehold switch sensors to detect SARS-CoV-2 specific genomic regions. Toehold switches are synthetic programmable riboregulators that consist of two main components: a trigger RNA and a switch RNA. The switch RNA structure prevents downstream gene translation through concealment of ribosome binding site (RBS) and start codon through cis-acting RNA interactions. Following the binding of a trans-acting trigger RNA to the switch, RBS and start codon are relieved, resulting in the activation of downstream gene(s) (Figure 156a) [6]. LoD of the toehold switch sensor alone might not be clinically sufficient, hence, primer-based RNA magnification step of trigger region is a requisite to be included before toehold switch sensor detection. Therefore, to screen amplification compatible candidate trigger regions from the whole SARS-CoV-2 genome (NC_045512.2), NCBI's Primer-BLAST tool was utilized. Free energy of secondary structures of candidate triggers were analyzed with Nucleic Acid Package (NUPACK) [93]. Candidates that have free energy over -25.00 (kcal/mol) were selected for further analysis. Selected sequences are aligned using BLAST against the genomes of human and close relatives of SARS-

CoV-2 to exclusively select SARS-CoV-2 specific triggers. These specific toehold sensors for top five successor triggers are generated using an *in silico* algorithm, based on multi-tube design of NUPACK [94] with parameters specified previously [6]. For each trigger candidate, top-ranked switch designs were checked to prevent in frame stop codons. After all of the described filtering processes, overall, 18 SARS-CoV-2 specific toehold switch sensors were designed with four trigger sequences (Figure 156b).

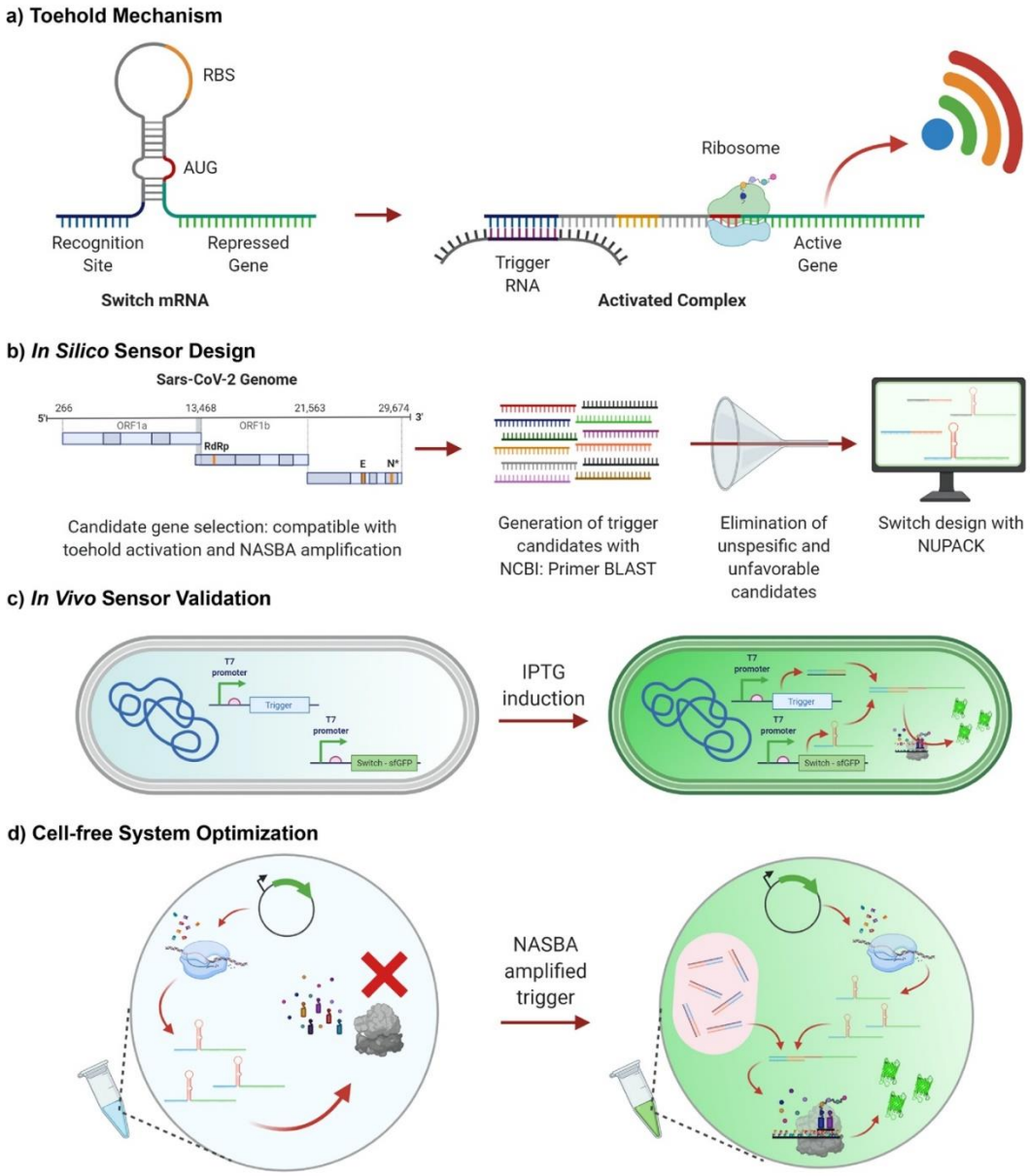

Figure 156 a) Schematics of the operating principle of toehold biosensors. b) in silico design of triggers and switches specific to SARS-CoV-2 genome. Toehold triggers are generated using NCBI Primer BLAST. The trigger candidates that have non-optimal free energy predictions and candidates that are not compatible with species specific amplification were eliminated. Eligible candidates were then used in the design of their respective toehold switches in silico using NUPACK software. c) in vivo validation of designed toehold switches. Triggers were cloned downstream of T7-LacO promoter. Switches were cloned downstream of T7-LacO promoter and upstream of sfGFP reporter gene. Both constructs were transformed into Escherichia coli (E. coli) BL21 (DE3) cells. Cells that only have the switch plasmid and the cells that have both switch and trigger plasmids were induced with Isopropyl-β-D-thiogalactoside (IPTG). d) Optimization of NASBA and cell-free systems.

To test sensors in vivo, fragments for switch and trigger regions were assembled into T7 driven expression p15A and ColE1 origin vectors, respectively. *E. coli* BL21 (DE3) cells were transformed with both plasmids and induced with IPTG (Figure 156c). Cells were analyzed with a flow cytometer 90 minutes after induction (Figure 157, Figure 158, Figure 159, Figure 160 and Figure 161). Additionally, total fluorescence from cells was measured at 2, 4, 8, and 16 hours following the IPTG addition to check background signal accumulation (Figure 157, Figure 158, Figure 159, Figure 160 and Figure 161). These in vivo experiments indicated that triggers selected from ORF1ab and S coding regions can be utilized to activate switch repressed translation with high signal-to-background ratio (Figure 157a and Figure 157b).

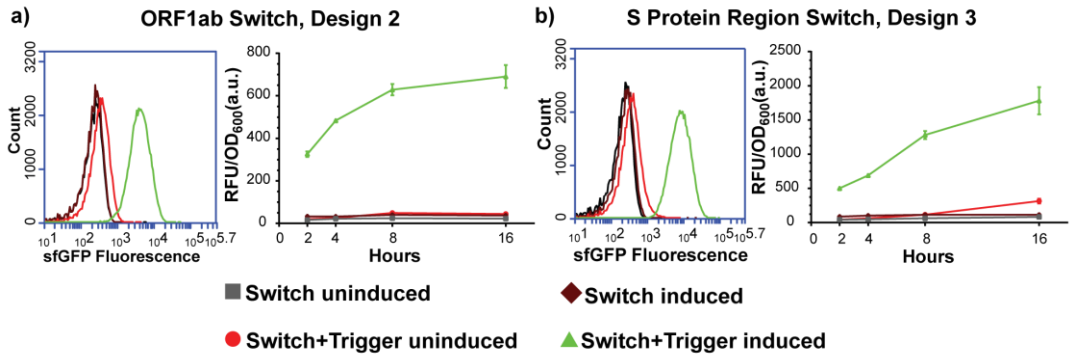

Figure 157. Characterization of best performing two trigger sequences found in ORF1ab and S protein regions in vivo. Flow cytometry results were taken after 90 minutes. Meanwhile, cells were monitored for 16 hours via total cell fluorescence measurements using a microplate reader. Cytometer results and total cell fluorescence measurements of designed switch for trigger sequence found in a) ORF1ab and b) S protein regions. For all microplate measurements, the average and standard errors (SE) of three replicates are shown.

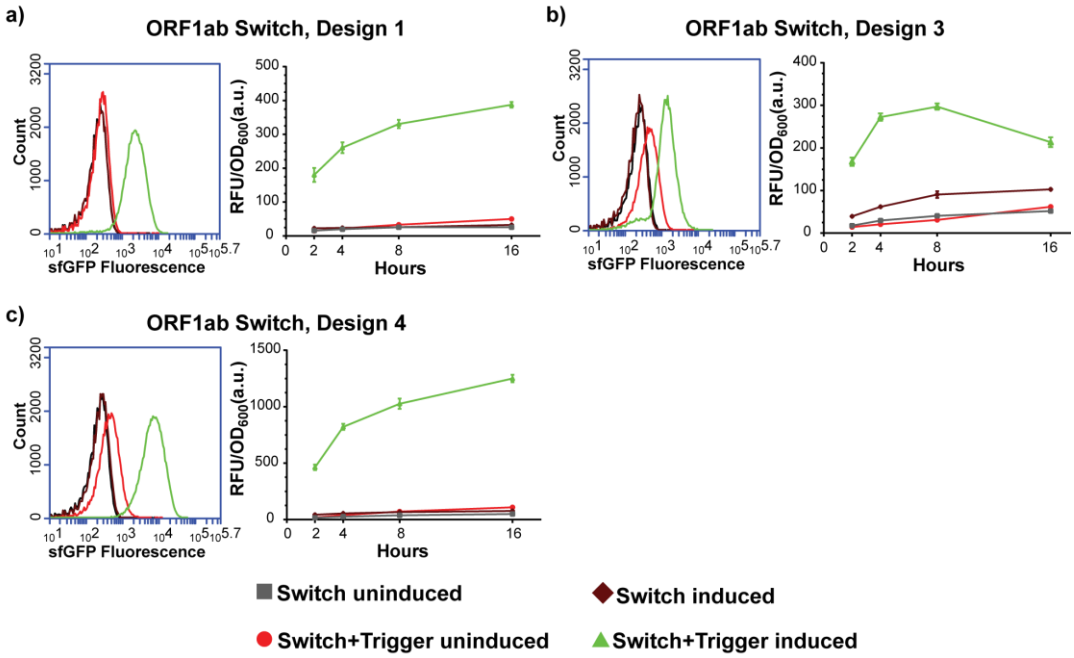

Figure 158. Performance of designed sensing switches to trigger sequence found in ORF1ab region in E. coli BL21 (DE3). Flow cytometry results were taken after 90 minutes. Meanwhile, cells were monitored for 16 hours via total cell fluorescence measurements using a microplate reader. For all microplate measurements, the average and standard errors (SE) of three replicates are shown.

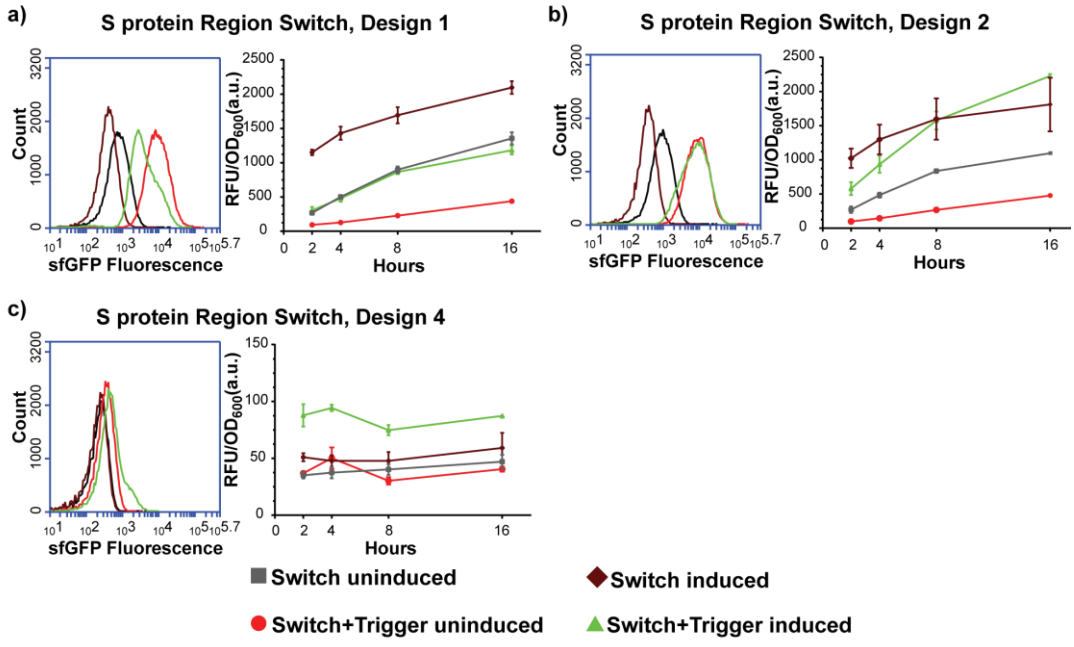

Figure 159. Performance of designed sensing switches to trigger sequence found in S protein region in E. coli BL21 (DE3). Flow cytometry results were taken after 90 minutes. Meanwhile, cells were monitored for 16 hours via total cell fluorescence measurements using a microplate reader. For all microplate measurements, the average and standard errors (SE) of three replicates are shown.

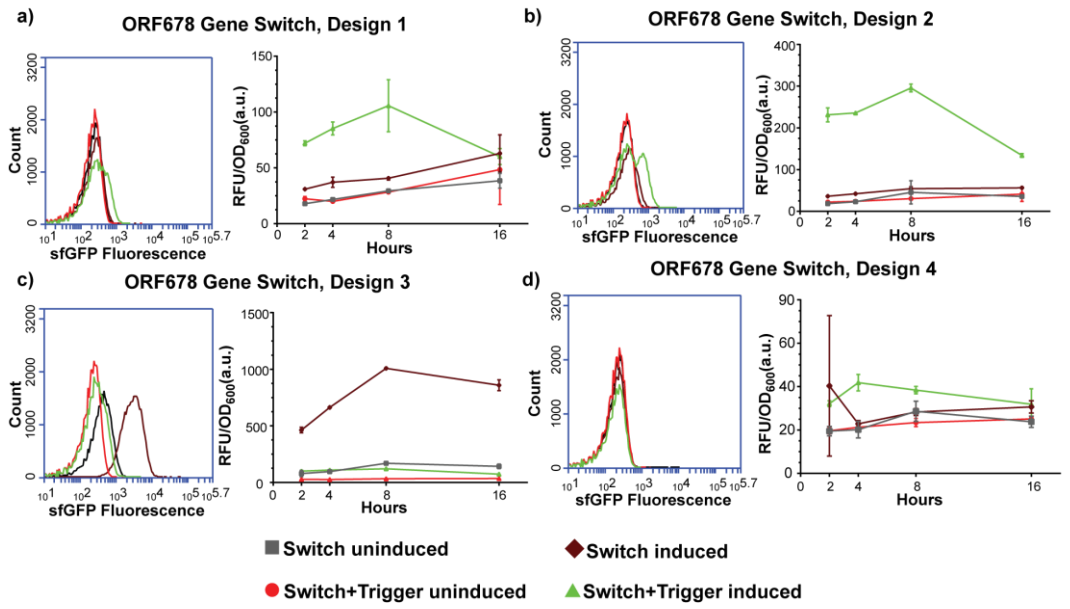

Figure 160. Performance of designed sensing switches to trigger sequence found in ORF678 region in E. coli BL21 (DE3). Flow cytometry results were taken after 90 minutes. Meanwhile, cells were monitored for 16 hours via total cell fluorescence measurements using a microplate reader. For all microplate measurements, the average and standard errors (SE) of three replicates are shown.

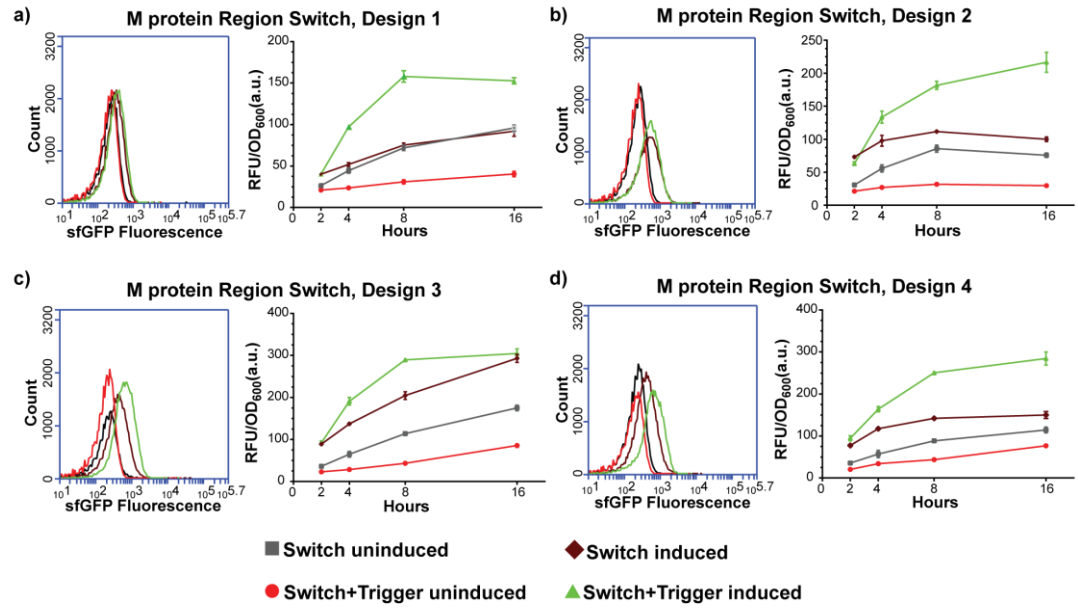

Figure 161. Performance of designed sensing switches to trigger sequence found in M protein region in E. coli BL21 (DE3). Flow cytometry results were taken after 90 minutes. Meanwhile, cells were monitored for 16 hours via total cell fluorescence measurements using a microplate reader. For all microplate measurements, the average and standard errors (SE) of three replicates are shown.

Based on in vivo assessment of all sensors, the top two best performing trigger/switch couples (trigger in ORF1ab region/design 2 and trigger in S region/design 3) were characterized in cell-free reaction (Figure 162). In reaction set-up, PCR amplified triggers with T7 promoter region and switch plasmids that bear T7 promoter, corresponding switch sequence and sfGFP coding sequence were used. After addition of DNA molecules, reactions were transferred into a 384-well plate and fluorescence measurement was performed for 6 hours with 10 minute intervals. Both ORF1ab and S trigger/switch pairs showed similar kinetics in the TXTL reaction in terms of total fluorescence which were saturated after 180 minutes. Expectedly, no significant increase in fluorescence signal for 'switch alone' circuits was observed. Trigger activated switch can be distinguished under blue light from mock controls after 40 minutes incubation (Figure 162c and Figure 162d).

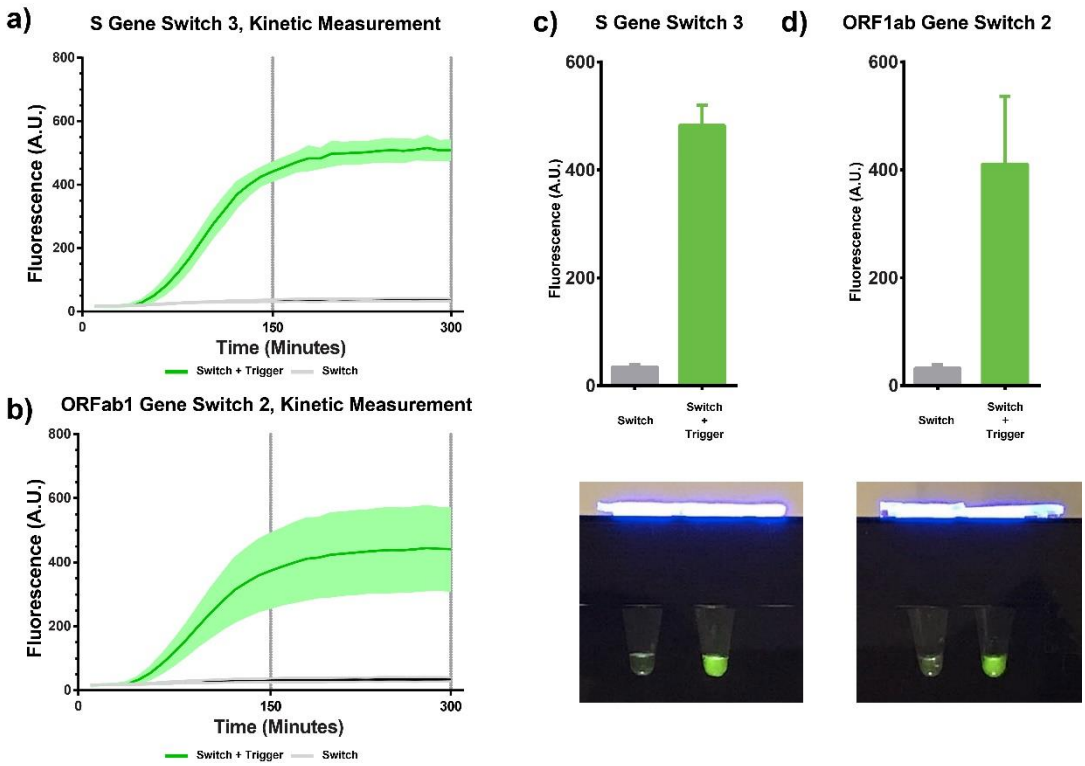

Figure 162. Characterization of S trigger/switch and ORF1ab trigger/switch couples in TXTL reaction. TXTL reactions were set-up in triplicates with addition of PCR amplified triggers and switch vectors. Reactions were monitored for 300 minutes with 10 minute intervals. Fluorescence measurements of **a)** S trigger/switch couple and **b)** ORF1ab trigger/switch couple. *End point analysis of **c**) S and **d)** ORF1ab sensors and their corresponding reaction mixtures are monitored using the DIY hand illuminator.*

Improving SARS-CoV-2 Sensor Sensitivity

The viral loads of clinical specimens were beyond the limit of detection of toeholds sensors since the swab samples taken from the upper respiratory tract have been documented to have 6.76×10^5 copies per sample on average. Furthermore, these values can drop to 3.44×10^5 copies per sample if they are taken 5 days after onset of symptoms which lowers the detection rate to 39.93% with qRT-PCR [95]. Therefore, incorporation of an isothermal RNA amplification step was necessary to transform our SARS-CoV-2 sensors to a field-ready detection platform. To do so, an isothermal RNA amplification technique, nucleic acid sequence-based amplification (NASBA), was utilized prior to TXTL assay.

Briefly, NASBA amplification begins with a reverse transcription step with a sequence specific primer bearing a T7 promoter which results in a formation of RNA/DNA duplex. Then the enzyme RNase H recognizes the RNA/DNA duplex and degrades the RNA template which allows the second primer to bind and initiate the elongation of the complementary strand. The synthesized double stranded DNA serves a template for T7-mediated transcription by T7 RNA polymerase (RNAP). Since the end product of NASBA is also a single stranded RNA, it is the starting material for the next amplification cycle as demonstrated in Figure 163a. After the first denaturation step at 65°C, NASBA

is carried at 41°C without a need for thermal cycling. The elimination of the denaturation step at 65°C was shown to cause loss of the signal level, hence all NASBA reactions are carried out with denaturation (unpublished data).

To perform NASBA, we have designed primer sets that would specifically amplify and add a T7 promoter to the amplified triggers of ORF1ab and S sensors from the SARS-CoV-2 genome (Figure 163a). NASBA reactions were run for two hours and 1:10 of the completed reactions were added to cell-free reactions. We first demonstrated the value of a prior isothermal amplification step into our detection platform in terms of improving sensitivity. To do so, we compared the overall fluorescent signal levels of TXTL reactions that were ran with the same initial in vitro transcribed trigger RNA concentration; however, in one set same amount of trigger RNA was subjected to NASBA amplification before adding it to TXTL reaction (Figure 163b and Figure 163c).

After that, to optimize the signal levels of sensors when tested with clinical specimens, the patient samples that have been all tested positive previously but had varying Cq values have been pooled. The NASBA reactions were performed with the isolated RNA obtained from the pooled patient samples. To determine the best performing trigger to switch ratio in TXTL reactions, a combinatorial experiment was set up. Here, addition of 1:10 and 1:5 of NASBA reactions were tested against 500, 750, 1000 ng of switch plasmid in cell-free reactions for both ORF1ab and S sensors respectively (Figure 163d, Figure 163e and Figure 164). An increase in the signal levels was observed for all

cases where the NASBA volume was increased in the cell free reactions. Since there was not a linear response to increasing switch concentration, it was thought that the concentrations of triggers and switches in the TXTL reactions may not be the only contributing factor of the reaction efficiency. Transcription efficiency in the cell free reactions may have also been affected by the availability of free T7 RNAP. Therefore, the best performing switch to NASBA ratio was determined to be moderate levels of switch (750 ng) to high volume of NASBA reactions (2 µL) for further experiments.

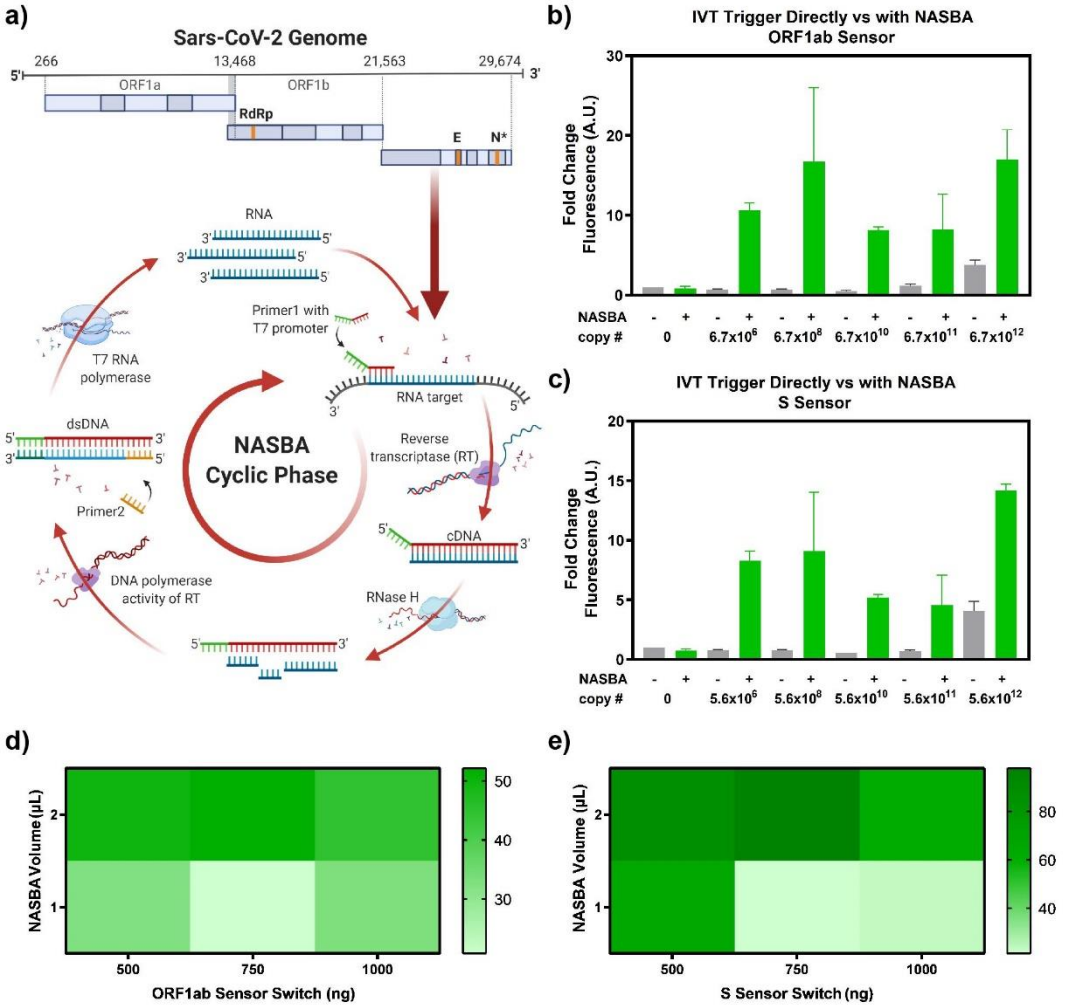

Figure 163. Characterization and optimization of ORF1ab trigger/switch and S trigger/switch couples in TXTL reactions. a) Representation of working principle of NASBA reaction. In vitro transcribed triggers are either added to TXTL reactions directly or after NASBA reactions, measurements at 60th minute are given for b) ORF1ab and c) S trigger/switch couple. The average and SE of duplicate experiments are shown. NASBA volume and switch vector amounts are optimized in TXTL reactions. Reactions were monitored for 120 minutes with 10 minute intervals and endpoint fluorescence measurements of d) ORF1ab and e) S trigger/switch couple are given. Representative average and SE of triplicate experiments are shown.

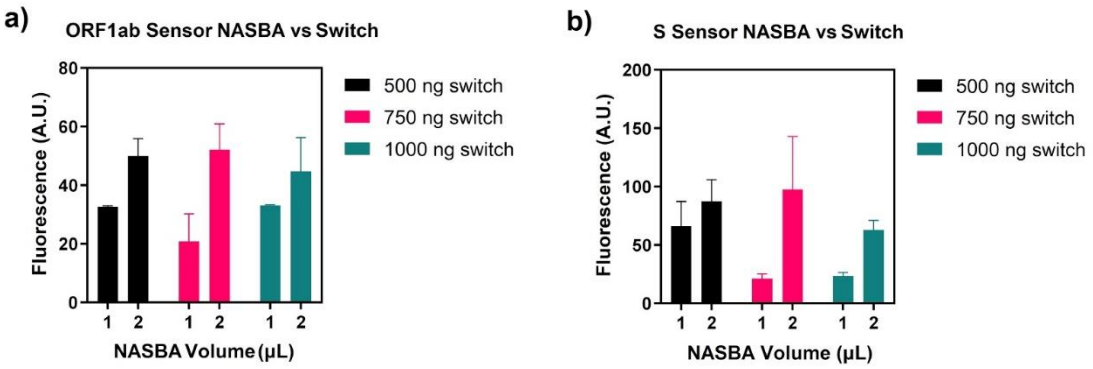

Figure 164. Characterization of NASBA volume and switch plasmid amount in TXTL reactions for **a)** ORF1ab trigger/switch and **b)** S trigger/switch couples. Representative results of triplicate experiments are shown.

Monitoring Human Samples with Portable, Low-Cost PoC Device

Collected clinical swab samples are stored in viral lysis and transfer media and then inactivated. Afterwards, viral RNA is isolated to be added to the NASBA reaction to amplify trigger regions specific to SARS-CoV-2 genome. Amplified trigger regions are added to TXTL reactions containing switch plasmid with the optimum ratios as determined previously (750 ng switch with 2µL of NASBA in 10 µL reactions). TXTL reactions are incubated for 2 hours at 37°C, reactions are then visualized with the in-house built blue-light illuminator (Figure 166a).

Pooled patient RNA samples used for NASBA volume to switch amount optimization have demonstrated that the system is applicable to clinical samples. Moreover, both S and ORF1ab switch sensors are shown not to give significant results to HKU viral RNA under the same experimental conditions (Figure 165). First, to minimize the duration of reaction time to get a detectable signal change, RNA samples isolated from patients are tested with NASBA-TXTL assay in kinetic time measurement in a microplate reader (Figure 166b).

With an instrument as sensitive as a microplate reader the signal change is detectable at 60th minute but with naked eye through the in-house built illuminator at 90th to 120th minutes. Second, to detect LoD minima, toehold sensor responses of cell-free reactions at 120th minute are compared with quantification cycle (Cq) values obtained from qRT-PCR tests (Table 16). Toehold switch sensor response is inversely correlated with Cq value, parallel to our expectations (Figure 166b). Then, patient samples are monitored using the hand illuminator for the visibility of their toehold sensor responses as seen in Figure 166c. Consequently, COVID-19 positive individuals' samples can be visualized with our proposed detection platform. Altogether, these findings suggest the applicability of our designed diagnostic platform can be used as a quick responsive and portable tool as it does not require expensive instruments, special laboratory environment or experts.

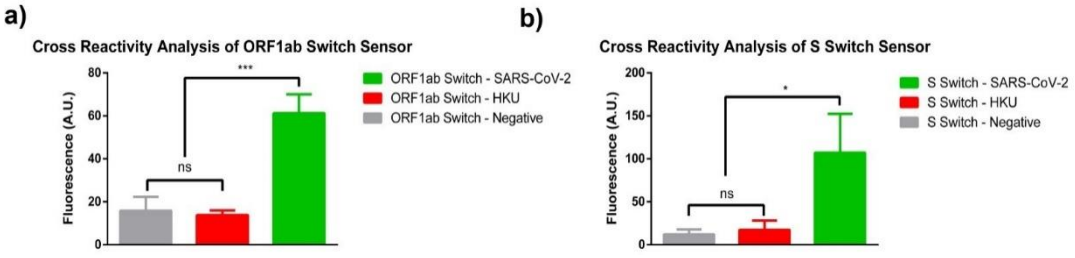

Figure 165. Cross reactivity analysis of a) ORF1ab trigger/switch and b) S trigger/switch couples with HKU1 viral RNA. Representative results of triplicate experiments are shown.

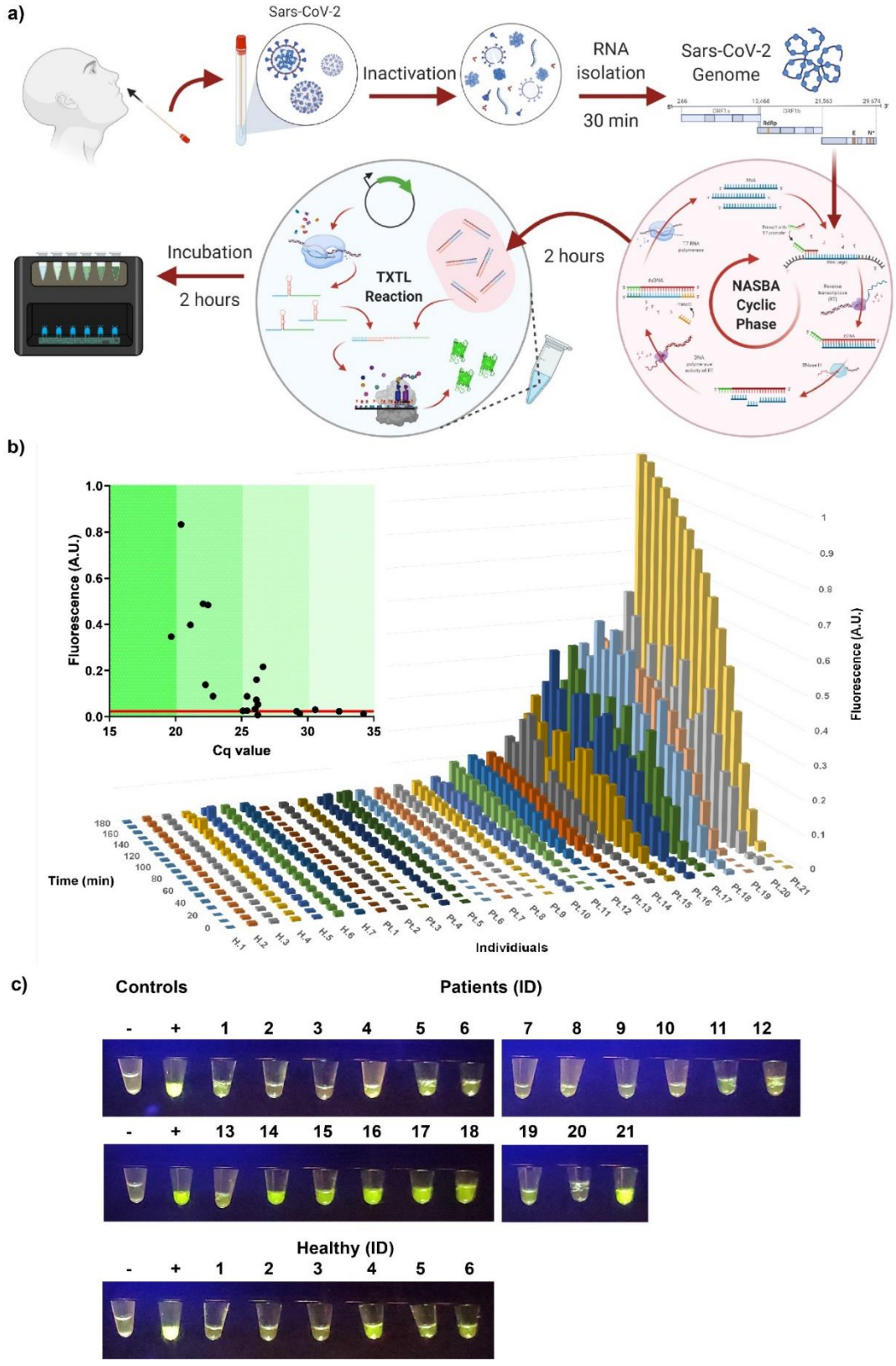

Figure 166. a) Workflow of the patient sample testing with ORF1ab trigger/switch couple. Viral RNA is isolated from patients' swab samples, and incubated in NASBA reactions for 2 hours. Once incubation is completed, 2 µL of NASBA reaction is added to TXTL cell free mixture containing 750 ng switch. Reactions were monitored with the blue light hand illuminator after 120 minutes. b) Fluorescence measurements of patient samples with ORF1ab trigger/switch couple at different time points, which were

monitored for 120 minutes with 10 minute intervals in a microplate reader. The abbreviations of H and Pt are healthy and patients, respectively. Comparison of patient samples' Cq values and corresponding toehold switch sensor responses of cell-free reactions at 120th minute, red line shows the sum of average of healthy samples with three times standard deviation. c) Toehold sensor responses of patient samples are monitored using the in-house built hand illuminator.

3.4. Conclusion and Future Perspectives

We have successfully developed a de novo designed riboregulator system to detect the presence of the SARS-CoV-2 specific genomic regions. To develop the diagnostic system, an in vitro synthetic biology tool has been employed. More than four hundred riboregulator designs have been screened in silico in terms of their stability, energy, applicability to NASBA reactions and specificity to SARS-CoV-2. After selecting top five promising candidates, trigger/switch couples are tested in vivo, then candidates with low background and high fold changes are analyzed using in vitro TXTL assay. As a result, the most promising candidates, a region from the spike protein (S) and ORF1ab region of the SARS-CoV-2 viral genome, have been selected for further optimization to be used in the diagnostic device. First, S and ORF1ab sensors' response to different copy numbers with and without amplification step prior to TXTL assay was investigated. The sensor targeting ORF1ab region showed higher fold change at low copy numbers compared to S sensor with prior NASBA reaction. Whereas S sensor's response was higher when TXTL reaction components (NASBA volume and switch plasmid amount) are optimized. Considering the detection of low copy numbers is pivotal in the diagnosis of infected individuals, the studies were continued with the ORF1ab sensor. Healthy and patient samples (qRT- PCR negative and positive respectively) obtained from Ankara City Hospital have been tested with our proposed diagnostic platform. Kinetic measurement of the cell-free systems showed that this system can detect the

viral genome parts in 60 minutes via highly sensitive detectors of microplate reader though eye-visibility with blue light illumination with a transparent orange filter is achieved in 2 hours. Even though the sensors have been shown to be sensitive to low copy numbers by IVT assay, the results are not reflected in human samples. The minimal copy number distinguished with our proposed system is determined to be as low as 1800 copies. By changing the primer pairs to shift the trigger region while covering the recognition site on its corresponding switch is an alternative [24]. These findings suggest that further optimization of the NASBA primers would increase the sensitivity when applied to human samples.

Considering the requirements of the steps in the diagnostic system, it is a promising platform due to its easy application without the need for a laboratory environment, an expert in the field or special and highly expensive equipment. Duration of RNA isolation step can be decreased to several minutes with the use of functionalized magnetic beads. The NASBA reaction can be reduced to 90 to 60 minutes, with the possibility of lower signal levels with shortened response time. Similarly, the incubation time of TXTL reaction can be shortened; whereas the eye-visibility of the results might not be applicable, and the integration of highly sensitive sensors into the PoC device will increase the cost to a great extent.

Another crucial aspect when developing a PoC device is the cost of the end product. As in our calculations, isothermal nucleic acid amplification and cell-free reaction used in the test cost 0.89 cent per sample based on the current price on NEB website, yet it can be further decreased with mass production.

In addition, the monitoring device can be manufactured for as low as 30$ according to prototyping companies that we contacted in Turkey.

To sum up, although vaccination has been started for many countries, achieving herd immunity requires a substantial time based on the vaccination rate. Moreover, many underdeveloped countries will not have access to vaccines in the near future, making mass testing the only option to suppress the spread. Compared with other commercially available tests such as qRT-PCR or serological assays, the de novo designed riboregulator based sensing platforms have more advantages for detection of SARS-CoV-2 genome. First, considering the ease of engineering our proposed system can be re-designed/engineered to sense new strains of SARS-CoV-2 in the midst of continuing pandemic and other pathogens in the future. Second, designing and testing of sensor candidates can be completed within a week. Third, the steps in the diagnostic system are isothermal, hence there are no needs for specific equipment, laboratory environment or experts, so the system can be used as a portable diagnostic tool. Fourth, the cost of each test is lower than a dollar also the hand illuminator device can be used multiple times. Taken together, albeit the LoD of our proposed test is not as high as qRT-PCR, the implementation into a quick-responsive, portable and low-cost PoC device is promising.

BIBLIOGRAPHY

[1] P. Siuti, J. Yazbek, T.K. Lu, Nat Biotechnol 31 (2013) 448–452.
[2] F. Farzadfard, T.K. Lu, Science 346 (2014) 1256272.
[3] S.D. Perli, C.H. Cui, T.K. Lu, Science 353 (2016) aag0511–aag0511.
[4] M.B. Elowitz, S. Leibler, Nature 403 (2000) 335–338.
[5] R. Daniel, J.R. Rubens, R. Sarpeshkar, T.K. Lu, Nature 497 (2013) 619–623.
[6] A.A. Green, P.A. Silver, J.J. Collins, P. Yin, Cell 159 (2014) 925–939.
[7] S. Toda, L.R. Blauch, S.K.Y. Tang, L. Morsut, W.A. Lim, Science (2018) eaat0271.
[8] J. Sheng, X. Feng, Front Microbiol 6 (2015) 554.
[9] E. Bach, V. Sant'Anna, D.J. Daroit, A.P.F. Corrêa, J. Segalin, A. Brandelli, Process Biochemistry 47 (2012) 2455–2462.
[10] D. Singh, S. Rawat, M. Waseem, S. Gupta, A. Lynn, M. Nitin, N. Ramchiary, K.K. Sharma, Biochem Biophys Res Commun 469 (2016) 306–312.
[11] X. Luo, M.A. Reiter, L. d'Espaux, J. Wong, C.M. Denby, A. Lechner, Y. Zhang, A.T. Grzybowski, S. Harth, W. Lin, H. Lee, C. Yu, J. Shin, K. Deng, V.T. Benites, G. Wang, E.E.K. Baidoo, Y. Chen, I. Dev, C.J. Petzold, J.D. Keasling, Nature 567 (2019) 123–126.
[12] A.R. Awan, B.A. Blount, D.J. Bell, W.M. Shaw, J.C.H. Ho, R.M. McKiernan, T. Ellis, Nat Commun 8 (2017) 15202.
[13] B. Saltepe, E.U. Bozkurt, N. Hacıosmanoğlu, U.Ö.Ş. Şeker, ACS Synth. Biol. 8 (2019) 2404–2417.
[14] J. Cayron, E. Prudent, C. Escoffier, E. Gueguen, M.-A. Mandrand-Berthelot, D. Pignol, D. Garcia, A. Rodrigue, Environ Sci Pollut Res 24 (2017) 4–14.
[15] D.M. Watstein, M.P. Styczynski, ACS Synth Biol 7 (2018) 267–275.
[16] T. Sato, Y. Kobayashi, J Bacteriol 180 (1998) 1655–1661.
[17] H. Chong, C.B. Ching, ACS Synth. Biol. 5 (2016) 1290–1298.
[18] A. Kumari, P. Pasini, S. Daunert, Anal Bioanal Chem 391 (2008) 1619–1627.
[19] P. Banerjee, A.K. Bhunia, Biosens Bioelectron 26 (2010) 99–106.
[20] J.K. Jung, K.K. Alam, M.S. Verosloff, D.A. Capdevila, M. Desmau, P.R. Clauer, J.W. Lee, P.Q. Nguyen, P.A. Pastén, S.J. Matiasek, J.-F. Gaillard, D.P. Giedroc, J.J. Collins, J.B. Lucks, Nat Biotechnol 38 (2020) 1451–1459.
[21] X. Wang, K. Zhu, D. Chen, J. Wang, X. Wang, A. Xu, L. Wu, L. Li, S. Chen, Ecotoxicology and Environmental Safety 207 (2021) 111273.
[22] J.S. Gootenberg, O.O. Abudayyeh, M.J. Kellner, J. Joung, J.J. Collins, F. Zhang, Science 360 (2018) 439–444.
[23] K. Pardee, A.A. Green, M.K. Takahashi, D. Braff, G. Lambert, J.W. Lee, T. Ferrante, D. Ma, N. Donghia, M. Fan, N.M. Daringer, I. Bosch, D.M. Dudley, D.H. O'Connor, L. Gehrke, J.J. Collins, Cell 165 (2016) 1255–1266.
[24] M.K. Takahashi, X. Tan, A.J. Dy, D. Braff, R.T. Akana, Y. Furuta, N. Donghia, A. Ananthakrishnan, J.J. Collins, Nature Communications 9 (2018) 3347.
[25] C.J. Vörösmarty, P.B. McIntyre, M.O. Gessner, D. Dudgeon, A. Prusevich, P. Green, S. Glidden, S.E. Bunn, C.A. Sullivan, C.R. Liermann, P.M. Davies, Nature 467 (2010) 555–561.
[26] Z.L. He, X.E. Yang, P.J. Stoffella, J Trace Elem Med Biol 19 (2005) 125–140.
[27] P.B. Tchounwou, C.G. Yedjou, A.K. Patlolla, D.J. Sutton, Exp Suppl 101 (2012) 133–164.
[28] TOXICOLOGY OF METALS, VOLUME I., CRC Press, Place of publication not identified, 2019.

[29] B.R. Stern, J Toxicol Environ Health A 73 (2010) 114–127.
[30] L.J. Harvey, H.J. McArdle, Br J Nutr 99 Suppl 3 (2008) S10-13.
[31] P.B. Tchounwou, C. Newsome, J. Williams, K. Glass, Met Ions Biol Med 10 (2008) 285–290.
[32] U. Najeeb, W. Ahmad, M.H. Zia, M. Zaffar, W. Zhou, Arabian Journal of Chemistry 10 (2017) S3310–S3317.
[33] M. Jaishankar, T. Tseten, N. Anbalagan, B.B. Mathew, K.N. Beeregowda, Interdisciplinary Toxicology 7 (2014) 60–72.
[34] H. Horiguchi, E. Oguma, F. Kayama, Arch Toxicol 80 (2006) 680–686.
[35] A. Rani, A. Kumar, A. Lal, M. Pant, Int J Environ Health Res 24 (2014) 378–399.
[36] A. Cuypers, M. Plusquin, T. Remans, M. Jozefczak, E. Keunen, H. Gielen, K. Opdenakker, A.R. Nair, E. Munters, T.J. Artois, T. Nawrot, J. Vangronsveld, K. Smeets, Biometals 23 (2010) 927–940.
[37] C. Giaginis, E. Gatzidou, S. Theocharis, Toxicol Appl Pharmacol 213 (2006) 282–290.
[38] R.N. Ratnaike, Postgrad Med J 79 (2003) 391–396.
[39] W. Kharroubi, S. Haj Ahmed, T. Nury, P. Andreoletti, R. Sakly, M. Hammami, G. Lizard, J Environ Sci (China) 51 (2017) 44–51.
[40] B. Wang, M. Barahona, M. Buck, Nucleic Acids Res 42 (2014) 9484–9492.
[41] M.S. Cyert, C.C. Philpott, Genetics 193 (2013) 677–713.
[42] A.W.P. Fitzpatrick, G.T. Debelouchina, M.J. Bayro, D.K. Clare, M.A. Caporini, V.S. Bajaj, C.P. Jaroniec, L. Wang, V. Ladizhansky, S.A. Muller, C.E. MacPhee, C.A. Waudby, H.R. Mott, A. De Simone, T.P.J. Knowles, H.R. Saibil, M. Vendruscolo, E.V. Orlova, R.G. Griffin, C.M. Dobson, Proceedings of the National Academy of Sciences 110 (2013) 5468–5473.
[43] M.R. Sawaya, S. Sambashivan, R. Nelson, M.I. Ivanova, S.A. Sievers, M.I. Apostol, M.J. Thompson, M. Balbirnie, J.J.W. Wiltzius, H.T. McFarlane, A.Ø. Madsen, C. Riekel, D. Eisenberg, Nature 447 (2007) 453–457.
[44] W.-F. Xue, S.W. Homans, S.E. Radford, Proc Natl Acad Sci U S A 105 (2008) 8926–8931.
[45] S.I.A. Cohen, S. Linse, L.M. Luheshi, E. Hellstrand, D.A. White, L. Rajah, D.E. Otzen, M. Vendruscolo, C.M. Dobson, T.P.J. Knowles, Proc Natl Acad Sci U S A 110 (2013) 9758–9763.
[46] M.G. Iadanza, M.P. Jackson, E.W. Hewitt, N.A. Ranson, S.E. Radford, Nat Rev Mol Cell Biol 19 (2018) 755–773.
[47] R. Nelson, M.R. Sawaya, M. Balbirnie, A.Ø. Madsen, C. Riekel, R. Grothe, D. Eisenberg, Nature 435 (2005) 773–778.
[48] K. Tsemekhman, L. Goldschmidt, D. Eisenberg, D. Baker, Protein Science 16 (2007) 761–764.
[49] R.N. Rambaran, L.C. Serpell, Prion 2 (2008) 112–117.
[50] F. Shewmaker, R.P. McGlinchey, R.B. Wickner, Journal of Biological Chemistry 286 (2011) 16533–16540.
[51] S.G. Biesecker, L.K. Nicastro, R.P. Wilson, Ç. Tükel, Biomolecules 8 (2018) E5.
[52] C.B. Ramsook, C. Tan, M.C. Garcia, R. Fung, G. Soybelman, R. Henry, A. Litewka, S. O'Meally, H.N. Otoo, R.A. Khalaf, A.M. Dranginis, N.K. Gaur, S.A. Klotz, J.M. Rauceo, C.K. Jue, P.N. Lipke, Eukaryot Cell 9 (2010) 393–404.
[53] C.L.L. Pham, A.H. Kwan, M. Sunde, Essays in Biochemistry 56 (2014) 207–219.

[54] D. Romero, R. Kolter, International Microbiology (2014) 65–73.
[55] D.M. Fowler, A.V. Koulov, C. Alory-Jost, M.S. Marks, W.E. Balch, J.W. Kelly, PLoS Biol 4 (2005) e6.
[56] J. Bayry, V. Aimanianda, J.I. Guijarro, M. Sunde, J.-P. Latgé, PLoS Pathog 8 (2012) e1002700.
[57] V.A. Iconomidou, G. Vriend, S.J. Hamodrakas, FEBS Letters 479 (2000) 141–145.
[58] A. Diehl, Y. Roske, L. Ball, A. Chowdhury, M. Hiller, N. Molière, R. Kramer, D. Stöppler, C.L. Worth, B. Schlegel, M. Leidert, N. Cremer, N. Erdmann, D. Lopez, H. Stephanowitz, E. Krause, B.-J. van Rossum, P. Schmieder, U. Heinemann, K. Turgay, Ü. Akbey, H. Oschkinat, Proc Natl Acad Sci USA 115 (2018) 3237–3242.
[59] A. Bleem, G. Christiansen, D.J. Madsen, H. Maric, K. Strømgaard, J.D. Bryers, V. Daggett, R.L. Meyer, D.E. Otzen, Journal of Molecular Biology 430 (2018) 3751–3763.
[60] R. Wang, B.A. Khan, G.Y.C. Cheung, T.-H.L. Bach, M. Jameson-Lee, K.-F. Kong, S.Y. Queck, M. Otto, J Clin Invest 121 (2011) 238–248.
[61] G.M. Cooper, The Cell: A Molecular Approach, 2. ed, ASM Press [u.a.], Washington, DC, 2000.
[62] Z. Bian, S. Normark, EMBO J 16 (1997) 5827–5836.
[63] H. Loferer, M. Hammar, S. Normark, Mol Microbiol 26 (1997) 11–23.
[64] M.R. Chapman, Science 295 (2002) 851–855.
[65] P.C. Ke, R. Zhou, L.C. Serpell, R. Riek, T.P.J. Knowles, H.A. Lashuel, E. Gazit, I.W. Hamley, T.P. Davis, M. Fändrich, D.E. Otzen, M.R. Chapman, C.M. Dobson, D.S. Eisenberg, R. Mezzenga, Chem. Soc. Rev. 49 (2020) 5473–5509.
[66] L. Matilla-Cuenca, A. Toledo-Arana, J. Valle, Antibiotics 10 (2021) 795.
[67] P.Q. Nguyen, Z. Botyanszki, P.K.R. Tay, N.S. Joshi, Nat Commun 5 (2014) 4945.
[68] T.T. Olmez, E. Sahin Kehribar, M.E. Isilak, T.K. Lu, U.O.S. Seker, ACS Synth. Biol. 8 (2019) 2152–2162.
[69] S.M. Pilkington, S.J. Roberts, S.J. Meade, J.A. Gerrard, Biotechnol Prog 26 (2010) 93–100.
[70] E. Sahin Kehribar, M.E. Isilak, E.U. Bozkurt, J. Adamcik, R. Mezzenga, U.O.S. Seker, Biomater. Sci. 9 (2021) 3650–3661.
[71] S. Bolisetty, N.M. Coray, A. Palika, G.A. Prenosil, R. Mezzenga, Environ. Sci.: Water Res. Technol. 6 (2020) 3249–3254.
[72] S.L. Gras, A.K. Tickler, A.M. Squires, G.L. Devlin, M.A. Horton, C.M. Dobson, C.E. MacPhee, Biomaterials 29 (2008) 1553–1562.
[73] N.P. Reynolds, K.E. Styan, C.D. Easton, Y. Li, L. Waddington, C. Lara, J.S. Forsythe, R. Mezzenga, P.G. Hartley, B.W. Muir, Biomacromolecules 14 (2013) 2305–2316.
[74] İ.Ç. Köksaldı, S. Köse, R.E. Ahan, N. Hacıosmanoğlu, E. Şahin Kehribar, M.A. Güngen, A. Baştuğ, B. Dinç, H. Bodur, A. Özkul, U.Ö.Ş. Şeker, Anal. Chem. 93 (2021) 9719–9727.
[75] S.-R. Li, Z.-J. Tang, Z.-H. Li, X. Liu, Eur J Clin Microbiol Infect Dis 39 (2020) 1021–1026.
[76] M. Hoffmann, H. Kleine-Weber, S. Schroeder, N. Krüger, T. Herrler, S. Erichsen, T.S. Schiergens, G. Herrler, N.-H. Wu, A. Nitsche, M.A. Müller, C. Drosten, S. Pöhlmann, Cell 181 (2020) 271-280.e8.

[77] J. Baj, H. Karakuła-Juchnowicz, G. Teresiński, G. Buszewicz, M. Ciesielka, E. Sitarz, A. Forma, K. Karakuła, W. Flieger, P. Portincasa, R. Maciejewski, J Clin Med 9 (2020) E1753.
[78] W.-H. Hsih, M.-Y. Cheng, M.-W. Ho, C.-H. Chou, P.-C. Lin, C.-Y. Chi, W.-C. Liao, C.-Y. Chen, L.-Y. Leong, N. Tien, H.-C. Lai, Y.-C. Lai, M.-C. Lu, J Microbiol Immunol Infect 53 (2020) 459–466.
[79] E.A. Meyerowitz, A. Richterman, I.I. Bogoch, N. Low, M. Cevik, The Lancet Infectious Diseases 21 (2021) e163–e169.
[80] E. Morales-Narváez, C. Dincer, Biosens Bioelectron 163 (2020) 112274.
[81] M.J. Loeffelholz, Y.-W. Tang, Emerg Microbes Infect 9 (2020) 747–756.
[82] M.N. Esbin, O.N. Whitney, S. Chong, A. Maurer, X. Darzacq, R. Tjian, RNA 26 (2020) 771–783.
[83] In Vitro Diagnostics EUAs - Molecular Diagnostic Tests for SARS-CoV-2, n.d.
[84] J.P. Broughton, X. Deng, G. Yu, C.L. Fasching, V. Servellita, J. Singh, X. Miao, J.A. Streithorst, A. Granados, A. Sotomayor-Gonzalez, K. Zorn, A. Gopez, E. Hsu, W. Gu, S. Miller, C.-Y. Pan, H. Guevara, D.A. Wadford, J.S. Chen, C.Y. Chiu, Nat Biotechnol 38 (2020) 870–874.
[85] G.-S. Park, K. Ku, S.-H. Baek, S.-J. Kim, S.I. Kim, B.-T. Kim, J.-S. Maeng, J Mol Diagn 22 (2020) 729–735.
[86] R. Lu, X. Wu, Z. Wan, Y. Li, X. Jin, C. Zhang, IJMS 21 (2020) 2826.
[87] P. Fozouni, S. Son, M. Díaz de León Derby, G.J. Knott, C.N. Gray, M.V. D'Ambrosio, C. Zhao, N.A. Switz, G.R. Kumar, S.I. Stephens, D. Boehm, C.-L. Tsou, J. Shu, A. Bhuiya, M. Armstrong, A.R. Harris, P.-Y. Chen, J.M. Osterloh, A. Meyer-Franke, B. Joehnk, K. Walcott, A. Sil, C. Langelier, K.S. Pollard, E.D. Crawford, A.S. Puschnik, M. Phelps, A. Kistler, J.L. DeRisi, J.A. Doudna, D.A. Fletcher, M. Ott, Cell 184 (2021) 323-333.e9.
[88] K. Pardee, A.A. Green, T. Ferrante, D.E. Cameron, A. DaleyKeyser, P. Yin, J.J. Collins, Cell 159 (2014) 940–954.
[89] H. de Puig, I. Bosch, J.J. Collins, L. Gehrke, Annu. Rev. Biomed. Eng. 22 (2020) 371–386.
[90] K.J. Land, D.I. Boeras, X.-S. Chen, A.R. Ramsay, R.W. Peeling, Nat Microbiol 4 (2019) 46–54.
[91] E.J. Olson, L.A. Hartsough, B.P. Landry, R. Shroff, J.J. Tabor, Nat Methods 11 (2014) 449–455.
[92] A.K. Cordes, W.M. Rehrauer, M.A. Accola, B. Wölk, B. Hilfrich, A. Heim, J Med Virol 93 (2021) 4438–4445.
[93] J.N. Zadeh, C.D. Steenberg, J.S. Bois, B.R. Wolfe, M.B. Pierce, A.R. Khan, R.M. Dirks, N.A. Pierce, J Comput Chem 32 (2011) 170–173.
[94] B.R. Wolfe, N.J. Porubsky, J.N. Zadeh, R.M. Dirks, N.A. Pierce, J. Am. Chem. Soc. 139 (2017) 3134–3144.
[95] R. Wölfel, V.M. Corman, W. Guggemos, M. Seilmaier, S. Zange, M.A. Müller, D. Niemeyer, T.C. Jones, P. Vollmar, C. Rothe, M. Hoelscher, T. Bleicker, S. Brünink, J. Schneider, R. Ehmann, K. Zwirglmaier, C. Drosten, C. Wendtner, Nature 581 (2020) 465–469.

Appendix

Appendix A

DNA sequences of constructs used in Chapter 1

	Part	Function	Sequence (5’ to 3’)
Copper	PcopA	Promoter	CTTTTGTTAACTCCTTTTTATAG ATGCGGGAGGTAATTCCTCACC CCGGTGCCGATTTTCAGGCATC CTGATTTAACTTAGCACCCGCA ACTTAACTACAGGAAAACAAAG AGATAAATGTCTAATCCTGATGC AAATCGAGCCGATTTTTTAATCT TTACGGACTTTTACCCGCCTGG TTTATTAATTTCTTGACCTTCCC CTTGCTGGAAGGTTTAACCTTTA TCACAGCCAGTCAAAA
Lead	PpbrR	Promoter	TTGACTCTATAGTAACTAGAGG GTGTTAAATCGGCAACGCGAGA TG
	PpbrR -10 mer	Engineered promoter	TTGACTCTATAGTAACTAGAGG GTGTaAggTCGGCAACGCGAGA TG
	PbrR	Transcription factor	ATGAATATCCAGATCGGCGAGC TTGCCAAGCGCACCGCATGCCC GGTGGTGACCATTCGCTTCTAC GAACAAGAAGGGCTGTTGCCGC CGCCGGGCCGCAGCCGGGGGA ATTTTCGCCTGTATGGCGAGGA GCACGTGGAGCGCTTGCAGTTC ATTCGTCACTGCCGGTCTCTGG ATATGCCGTTGAGCGACGTACG GACCTTATTGAGTTACCGGAAG CGGCCCGACCAGGATTGCGGT GAAGTCAATATGCTCTTGGATG AGCACATCCGTCAGGTCGAATC TCGGATCGGAGCTTTGCTCGAA CTGAAGCACCATTTGGTGGAAC TGCGCGAAGCCTGTTCTGGTGC CAGGCCCGCCCAATCGTGCGG GATTCTGCAGGGACTGTCGGAC TGCGTGTGTGATACGCGGGGG

			ACCACCGCCCATCCAAGCGACTAG
Cadmium	PcadA	Promoter	GGCTTGACCCTATAGTGGCTACAGGGTGTTCACTTGGCAACAGGC
	CadR	Transcription factor	ATGAAGATCGGAGAACTGGCCAAAGCCACCGACTGCGCCGTGGAAACCATCCGCTACTACGAGCGTGAACAGCTGCTGCCGGAGCCGGCACGCAGCGACGGCAACTACCGGCTGTACACCCAGGCCCACGTCGAGCGGCTTACCTTCATCCGCAACTGCCGCACCCTGGACATGACCCTGGATGAAATCCGCAGCCTGCTACGCCTGCGCGACAGCCCCGATGATTCGTGCGGCAGCGTCAATGCGCTGATCGACGAGCATATCGAGCATGTGCAGGCACGGATCGATGGTCTGGTGGCGTTGCAGGAACAGCTGGTGGAGCTGCGGCGGCGCTGCAATGCACAAGGGGCGGAGTGTGCGATCTTGCAGCAACTGGAGACGAACGGGGCGGTATCGGTGCCGGAAACCGAGCATTCGCATGTAGGGCGAAGCCACGGGCATTAA
Arsenic	ParsR	Promoter	CATTCGTTAAGTCATATATGTTTTTGACTTATCCGCTTCGAAGAGAGACACTACCTGCAAC
	ArsR	Transcription factor	ATGTCATTTCTGTTACCCATCCAATTGTTCAAAATTCTTGCTGATGAAACCCGTCTGGGCATCGTTTTACTGCTCAGCGAACTGGGAGAGTTATGCGTCTGCGATCTCTGCACTGCTCTCGACCAGTCGCAGCCCAAGATCTCCCGCCACCTGGCATTGCTGCGTGAAAGCGGGCTATTGCTGGACCGCAAGCAAGGTAAGTGGGTTCATTACCGCTTATCACCGCATATTCCAGCATGGGCGGCGAAAATTATTGATGAGGCCTGGCGATGTGAACAGGAAAAGGTTCAGGCGATTGTCCGCAACCTGGCTCGACAAAACTGTTCCGGGGACAGTAAGAACATTTGCAGTTAA
Riboregulator	PltetO-taRNA rrnBT1	Riboregulator	GACGTCAAAGGGCCCTCCCTATCAGTGATAGAGATTGACATCCCTATCAGTGATAGAGATACTGAG

	terminator PltetO-crRNA-RBS		CACAGTCGACACCCAAATCCAG GAGGTGATTGGTAGTGGTGGTT AATGAAAATTAACTTACTACTAC CATATATCTCTAGATGCCTGGC GGCAGTAGCGCGGTGGTCCCA CCTGACCCCATGCCGAACTCAG AAGTGAAACGCCGTAGCGCCGA TGGTAGTGTGGGGTCTCCCCAT GCGAGAGTAGGGAACTGCCAG GCATCAAATAAAACGAAAGGCT CAGTCGAAAGACTGGGCCTTCT CGAGTCCCTATCAGTGATAGAG ATTGACATCCCTATCAGTGATAG AGATACTGAGCACATCAGCAGG ACGCACTGACCGAATTCTACCA TTCACCTCTTGGATTTGGGTATT AAAGAGGAGAAAGGTACC
Reporter	sfGFP	Protein	ATGCGTAAAGGCGAAGAGCTGT TCACTGGTGTCGTCCCTATTCT GGTGGAACTGGATGGTGATGTC AACGGTCATAAGTTTTCCGTGC GTGGCGAGGGTGAAGGTGACG CAACTAATGGTAAACTGACGCT GAAGTTCATCTGTACTACTGGTA AACTGCCGGTACCTTGGCCGAC TCTGGTAACGACGCTGACTTAT GGTGTTCAGTGCTTTGCTCGTT ATCCGGACCATATGAAGCAGCA TGACTTCTTCAAGTCCGCCATG CCGGAAGGCTATGTGCAGGAAC GCACGATTTCCTTTAAGGATGA CGGCACGTACAAAACGCGTGC GGAAGTGAAATTTGAAGGCGAT ACCCTGGTAAACCGCATTGAGC TGAAAGGCATTGACTTTAAAGAA GACGGCAATATCCTGGGCCATA AGCTGGAATACAATTTTAACAGC CACAATGTTTACATCACCGCCG ATAAACAAAAAAATGGCATTAAA GCGAATTTTAAAATTCGCCACAA CGTGGAGGATGGCAGCGTGCA GCTGGCTGATCACTACCAGCAA AACACTCCAATCGGTGATGGTC CTGTTCTGCTGCCAGACAATCA CTATCTGAGCACGCAAAGCGTT CTGTCTAAAGATCCGAACGAGA AACGCGATCATATGGTTCTGCT GGAGTTCGTAACCGCAGCGGG CATCACGCATGGTATGGATGAA CTGTACAAA

	mScarlet-I	Protein	ATGAGTAAAGGAGAAGCTGTGA TTAAAGAGTTCATGCGCTTCAAA GTTCACATGGAGGGTTCTATGA ACGGTCACGAGTTCGAGATCGA AGGCGAAGGCGAGGGCCGTCC GTATGAAGGCACCCAGACCGCC AAACTGAAAGTGACTAAAGGCG GCCCGCTGCCTTTTTCCTGGGA CATCCTGAGCCCGCAATTTATG TACGGTTCTAGGGCGTTCATCA AACACCCAGCGGATATCCCGGA CTATTATAAGCAGTCTTTTCCGG AAGGTTTCAAGTGGGAACGCGT AATGAATTTTGAAGATGGTGGT GCCGTGACCGTCACTCAGGACA CCTCCCTGGAGGATGGCACCCT GATCTATAAAGTTAAACTGCGTG GTACTAATTTTCCACCTGATGGC CCGGTGATGCAGAAAAAGACGA TGGGTTGGGAGGCGTCTACCG AACGCTTGTATCCGGAAGATGG TGTGCTGAAAGGCGACATTAAA ATGGCCCTGCGCCTGAAAGATG GCGGCCGCTATCTGGCTGACTT CAAAACCACGTACAAAGCCAAG AAACCTGTGCAGATGCCTGGCG CGTACAATGTGGACCGCAAACT GGACATCACCTCTCATAATGAA GATTATACGGTGGTAGAGCAAT ATGAGCGCTCCGAGGGTCGTCA TTCTACCGGTGGCATGGATGAA CTATACAAATAA
	mTagBFP	Protein	ATGAGCGAACTGATCAAAGAGA ACATGCACATGAAGCTGTACAT GGAAGGCACCGTTGACAACCAC CACTTTAAGTGCACGTCTGAGG GTGAGGGTAAGCCGTACGAAG GCACCCAAACCATGCGTATCAA AGTTGTGGAGGGCGGTCCACT GCCGTTCGCTTTTGACATTCTG GCGACCAGCTTCCTGTACGGTT CCAAAACGTTCATTAACCATACT CAGGGCATTCCGGATTTCTTCA AACAGAGCTTTCCGGAAGGTTT CACCTGGGAGCGTGTCACCAC GTATGAAGATGGTGGTGTGTTG ACCGCCACCCAAGATACCTCCC TGCAAGATGGCTGTCTGATCTA TAACGTGAAAATTCGTGGCGTC AACTTTACGAGCAATGGTCCGG

			TGATGCAGAAGAAAACCCTGGG TTGGGAGGCGTTTACGGAAACC CTGTATCCGGCCGATGGTGGCC TGGAGGGCCGTAACGACATGG CACTGAAGCTGGTTGGTGGCAG CCATTTGATCGCAAATATCAAGA CGACGTACCGCAGCAAGAAACC GGCGAAAAATCTGAAGATGCCG GGTGTTTACTATGTCGACTACC GTCTGGAACGCATTAAAGAAGC GAATAATGAGACTTACGTGGAG CAGCACGAGGTTGCAGTCGCG CGCTATTGCGACTTGCCTAGCA AGCTGGGTCATAAACTGAAT
Amplification circuit elements	hrpR	Protein	ATGAGTACAGGCATCGATAAGG ACGTCCGAGAGTGTTGGGGCG TAACTGCATTATCAGCGGGTCA TCAAATTGCAATGAATAGCGCG TTTCTGGATATGGACTTGCTGTT GTGCGGGGAAACCGGCACCGG CAAGGACACACTGGCCAACCGC ATTCACGAGTTGTCCAGCAGGT CGGGACCCTTTGTGGGCATGAA CTGCGCCGCCATTCCCGAGTCG CTGGCAGAGAGCCAGTTATTCG GTGTGGTCAACGGTGCATTCAC CGGCGTATGCCGGGCTCGCGA GGGCTACATAGAGGCCTCCAGT GGTGGCACCTTGTACCTGGATG AAATCGACAGCATGCCGTTGAG CCTGCAAGCCAAACTGCTGCGT GTGTTGGAGAGTCGAGGTATCG AGCGTCTGGGCTCGACCGAATT TATCCCGGTGGATCTGCGGATC ATTGCCTCGGCCCAGCGGCCA CTGGATGAACTGGTGGAACAAG GACTTTTCCGTCGCGACCTGTT TTTTCGGCTCAACGTGCTGACG CTTCACTTGCCAGCCTTGCGCA AACGTCGTGAACAGATCCTGCC ATTGTTCGACCAGTTCACCCAG GGTATCGCTGCCGAGTTCGGAC GTCCCGCTCCTGCGCTGGACA GCGGGCGTGTGCAGCTGCTGC TCAGCCACGACTGGCCGGGCA ACATCCGCGAATTGAAGTCTGC GGCCAAGCGCTTCGTACTCGGC TTCCCCTTGCTGGGCGCCGACC CTGTGGAAGCGCTTGACCCTGC CACGGGGCTGCGCACGCAAAT

			GCGCATCATCGAGAAAATGCTC ATCCAGGATGCCTTGAAGCGGC ACAGGCACAATTTCGACGCGGT GCTTCAGGAGTTGGAGTTGCCA AGACGCACCCTGTATCACCGCA TGAAGGAACTGGGAGTTGCAGC GCCGATCGCTGCGACGGCCGG GGTCTAATAA
	hrpS	Protein	ATGAGTCTTGATGAAAGGTTTG AGGATGATCTGGACGAGGAGC GGGTTCCGAATCTGGGGATAGT TGCCGAAAGTATTTCGCAACTG GGTATCGACGTGCTGCTATCGG GTGAGACCGGCACGGGCAAAG ACACGATTGCCCGACGGATTCA TGAGATGTCAGGCCGCAAAGG GCGCCTGGTGGCGATGAATTGC GCGGCCATTCCGGAGTCCCTC GCCGAGAGCGAGTTATTCGGC GTGGTCAGCGGTGCCTACACC GGCGCTGATCGCTCCAGAGTC GGTTATGTCGAAGCGGCGCAG GGCGGCACGCTGTACCTGGAT GAGATCGATAGCATGCCGCTGA GCCTGCAAGCCAAATTGCTGAG GGTGCTGGAAACCCGAGCGCTT GAACGGCTGGGTTCGACGTCG ACGATCAAGCTGGATATCTGCG TGATCGCCTCCGCCCAATGCTC GCTGGACGACGCCGTCGAGCG GGGGCAGTTTCGTCGCGATCTG TATTTTCGCCTGAACGTCCTGA CACTCAAGCTTCCTCCGCTACG TAACCAGTCTGATCGCATAGTT CCCCTGTTCACACGTTTTACGG CCGCCGCCGCGAGGGAGCTCG GTGTTCCCGTTCCCGATGTTTG CCCACTGCTGCACAAAGTGCTG CTGGGCCACGACTGGCCCGGC AATATCCGTGAGCTCAAGGCGG CAGCCAAACGCCATGTGCTGGG TTTCCCCTTGCTGGGCGCCGAG CCGCAGGGCGAAGAGCACTTG GCCTGTGGGCTCAAATCGCAAT TGCGAGTGATCGAAAAAGCCCT GATTCAGGAGTCGCTCAAGCGC CACGACAATTGTGTGGATTCGG TAAGCCTGGAACTGGACGTGCC ACGCCGTACGCTCTATCGACGC

			ATCAAAGAATTGCAGATCTAATAA
	PhrpL	Promoter	GCCGGATTATGTCCGCTGAGTGGGTCACGGTCCCGGATCAGTTCCCTTGCGAAGCTGACCGATGTTTTTGTGCCAAAAGCTGTTGTGGCAAAAAACGGTTTGCGCAAAGTTTTGTATTACAAAGAATTTCACATTTTAAAATATCTTTATAAATCAATCAGTTATTTCTATTTTTAAGCTGGCATGGTTATCGCTATAGGGCTTGTAC
RBS			AAGGAG
RBS30			CTAGAGATTAAAGAGGAGAAATACTAGATG
epsilon			TTAACTTTA

Table 1. Sequences of sensory units of copper, lead, cadmium and arsenic.

DNA sequences of constructs used in Chapter 2

	Part	Function	Sequence (5' to 3')
Biofilm protein	csgA	Protein	ATGAAACTTTTAAAAGTAGCAGCAAT TGCAGCAATCGTATTCTCCGGTAGC GCTCTGGCAGGTGTTGTTCCTCAGT ACGGCGGCGGCGGTGGCAACCAC GGTGGTGGCGGTAATAACAGCGGT CCGAATTCAGAGCTGAATATTTACC AGTACGGTGGCGGTAACTCTGCTCT TGCTCTGCAAGCTGACGCCCGTAAC TCTGATCTGACCATTACCCAGCACG GCGGCGGTAATGGCGCAGATGTGG GCCAAGGTTCTGATGACAGCTCAAT CGATCTGACTCAGCGTGGTTTCGGC AACAGCGCTACTCTTGATCAGTGGA ATGGTAAAGATTCTACTATGACTGTT AAACAGTTCGGTGGCGGTAACGGT GCTGCTGTTGACCAGACTGCATCTA ACTCCAGCGTTAACGTCACTCAGGT TGGCTTTGGTAACAACGCGACCGCT CATCAGTACTAA
	csgG	Protein	ATGCAGCGCTTATTTCTTTTGGTTG CCGTCATGTTACTGAGCGGATGCTT AACCGCCCCGCCTAAAGAAGCCGC CAGACCGACATTAATGCCTCGTGCT CAGAGCTACAAAGATTTGACCCATC TGCCAGCGCCGACGGGTAAAATCTT TGTTTCGGTATACAACATTCAGGAC GAAACCGGGCAATTTAAACCCTACC CGGCAAGTAACTTCTCCACTGCTGT TCCGCAAAGCGCCACGGCAATGCT GGTCACGGCACTGAAAGATTCTCGC TGGTTTATACCGCTGGAGCGCCAG GGCTTACAAAACCTGCTTAACGAGC GCAAGATTATTCGTGCGGCACAAGA AAACGGCACGGTTGCCATTAATAAC CGAATCCCGCTGCAATCTTTAACGG CGGCAAATATCATGGTTGAAGGTTC GATTATCGGTTATGAAAGCAACGTC AAATCTGGCGGGGTTGGGGCAAGA TATTTTGGCATCGGTGCCGACACGC AATACCAGCTCGATCAGATTGCCGT GAACCTGCGCGTCGTCAATGTGAGT ACCGGCGAGATCCTTTCTTCGGTGA ACACCAGTAAGACGATACTTTCCTA

			TGAAGTTCAGGCCGGGGTTTTCCG CTTTATTGACTACCAGCGCTTGCTT GAAGGGGAAGTGGGTTACACCTCG AACGAACCTGTTATGCTGTGCCTGA TGTCGGCTATCGAAACAGGGGTCAT TTTCCTGATTAATGATGGTATCGAC CGTGGTCTGTGGGATTTGCAAAATA AAGCAGAACGGCAGAATGACATTCT GGTGAAATACCGCCATATGTCGGTT CCACCGGAATCCTGA
	csgE	Protein	ATGAAACGTTATTTACGCTGGATTG TGGCGGCAGAATTTCTGTTCGCCGC AGGGAATCTTCACGCCGTTGAGGTA GAAGTCCCGGGATTGCTAACTGACC ATACTGTTTCATCTATTGGCCATGAT TTTTACCGAGCCTTTAGTGATAAATG GGAAAGTGACTATACGGGTAACTTA ACGATTAATGAAAGGCCCAGTGCAC GATGGGGAAGCTGGATCACTATAAC GGTCAATCAGGACGTTATTTTCCAG ACTTTTTTATTTCCGTTGAAAAGAGA CTTCGAGAAAACTGTCGTCTTTGCA CTGATTCAAACTGAAGAAGCACTAA ATCGTCGCCAGATAAATCAGGCGTT ATTAAGTACGGGCGATTTGGCGCAT GATGAATTCTAA
	csgF	Protein	ATGCGTGTCAAACATGCAGTAGTTC TACTCATGCTTATTTCGCCATTAAGT TGGGCTGGAACCATGACTTTCCAGT TCCGTAATCCAAACTTTGGTGGTAA CCCAAATAATGGCGCTTTTTTATTAA ATAGCGCTCAGGCCCAAAACTCTTA TAAAGATCCGAGCTATAACGATGAC TTTGGTATTGAAACACCCTCAGCGT TAGATAACTTTACTCAGGCCATCCA GTCACAAATTTTAGGTGGGCTACTG TCGAATATTAATACCGGTAAACCGG GCCGCATGGTGACCAACGATTATAT TGTCGATATTGCCAACCGCGATGGT CAATTGCAGTTGAACGTGACAGATC GTAAAACCGGACAAACCTCGACCAT CCAGGTTTCGGGTTTACAAAATAAC TCAACCGATTTTTAA
Regulator	**araC**	Protein	ATGGCTGAAGCGCAAAATGATCCCC TGCTGCCGGGATACTCGTTTAATGC CCATCTGGTGGCGGGTTTAACGCC GATTGAGGCCAACGGTTATCTCGAT TTTTTTATCGACCGACCGCTGGGAA TGAAAGGTTATATTCTCAATCTCACC ATTCGCGGTCAGGGGGTGGTGAAA

			AATCAGGGACGAGAATTTGTTTGCC GACCGGGTGATATTTTGCTGTTCCC GCCAGGAGAGATTCATCACTACGGT CGTCATCCGGAGGCTCGCGAATGG TATCACCAGTGGGTTTACTTTCGTC CGCGCGCCTACTGGCATGAATGGC TTAACTGGCCGTCAATATTTGCCAA TACGGGGTTCTTTCGCCCGGATGAA GCGCACCAGCCGCATTTCAGCGAC CTGTTTGGGCAAATCATTAACGCCG GGCAAGGGGAAGGGCGCTATTCGG AGCTGCTGGCGATAAATCTGCTTGA GCAATTGTTACTGCGGCGCATGGAA GCGATTAACGAGTCGCTCCATCCAC CGATGGATAATCGGGTACGCGAGG CTTGTCAGTACATCAGCGATCACCT GGCAGACAGCAATTTTGATATCGCC AGCGTCGCACAGCATGTTTGCTTGT CGCCGTCGCGTCTGTCACATCTTTT CCGCCAGCAGTTAGGGATTAGCGT CTTAAGCTGGCGCGAGGACCAACG TATCAGCCAGGCGAAGCTGCTTTTG AGCACCACCCGGATGCCTATCGCC ACCGTCGGTCGCAATGTTGGTTTTG ACGATCAACTCTATTTCTCGCGGGT ATTTAAAAAATGCACCGGGGCCAGC CCGAGCGAGTTCCGTGCCGGTTGT GAAGAAAAAGTGAATGATGTAGCCG TCAAGTTGTCATAA
Promoter	**Plac/ara**	Promoter	TAAGAAACCATTAGCTAGTCCTGTT CTAGCTAGCTAGACATGCAACCACC GGTCGCTTGGACTCCTGTTGATATC CCCCCGGGGGGAACATAGCATTTTT ATCCATAAGATTAGCGGATCTAACC TTTACAATTGTGAGCGCTCACAATTA TGATAGATTCAATTGTGAGCGGATA ACAATTTCACACA
	PBAD	Promoter	CTGACGCTTTTTATCGCAACTCTCTA CTG

Table 2. Sequences of biofilm proteins' genes.

DNA sequences of constructs used in Chapter 3

Trigger #	Target region	Switch #	Recognition Domain		series B conserved sequence - domain S bold: RBS region red: ATG	RBS	a	linker (Green et al) - domain l
			b*	a*				
1	**ORF1ab**	1	ATTCATTATGGTATTCGGCAAGAC	TATGCTCAGGTC	GGACTTTAGAAC**AGAGGAGA**TAAAG**ATG**	**AGAGGAGA**	GACCTGAGCATA	AACCTGGCGGCAGCGCAAAAG
		2	CAGATTCATTATGGTATTCGGCAA	ACTATGCTCAG			CTGAGCATAGTA	
2	**S protein**	1	AAAGAAAGGTAAGAACAAGTCCTG	GTTGAATGTAA			TTACATTCAACG	
		2	AAGAAAGGTAAGAACAAGTCCTGA	GTTGAATGTAAA			TTTACATTCAAC	
		3	AGGGTAATAAACACCACGTGTGAA	GAATTAGTGTA			TACACTAATTCG	
		4	TCTGGTTGTAAGATTAACACACTG	CTAGAGACTAG			CTAGTCTCTAGG	
3	**M protein**	1	CACGAAGGATCACAGCTCCGATTA	GAGTTCACTTT			AAAGTGAACTCA	
		2	ACGAAGGATCACAGCTCCGATTAC	AGTTCACTTTC			GAAAGTGAACTA	
		3	CGAAGGATCACAGCTCCGATTACG	AGTTCACTTTC			AGAAAGcGAACA	
		4	AAGGATCACAGCTCCGATTACGAG	AGTTCACTTTC			CTAGAAAGTGAT	
4	**ORF678**	1	CATGTTCGTTTAATCAATCTCCAT	CATTGGTTGCTC			GAAGAGCAACCT	

		2	TCATGTTCGTTTAATCAATCTCCA	CATTGGTTGCTC			AAGAGCAACCAC	
		3	TTTCATGTTCGTTTAATCAATCTC	CATTGGTTGCTC			GAGCAACCAATG	
		4	TCGTTTAATCAATCTCCATTGGTT	CTCTTCATCTA			TAGATGAAGAGA	
5	**ORF1ab**	1	CAGTTTCTTCTCTGGATTTAACAC	CTTTCTGTACA			TGTACAGAAAGC	
		2	AGTTTCTTCTCTGGATTTAACACA	CTTTCTGTACAA			TTGTACAGAAAG	
		3	TAGGCCAGTTTCTTCTCTGGATTT	ACACACTTTCT			AGAAAGTGTGTA	
		4	TGAGTGCGTGACAAATGTTTCACC	AAATTCAAGGC			GCCTTGAATTTC	

Table 3. Sequences of synthetic riboregulator switch sensors of SARS-CoV-2.

Trigger #	Target region	Trigger Sequence	Forward Primer bold: T7 promoter	Reverse Primer	Length (bp)
1	**ORF1ab**	GCCACTACTTGTGGTTACT TAccccaaaatgctgttgttaaaatttat tgtccagcatgtcacaattcagaagtag gacctgagcatagtcttgccgaatAC CATAATGAATCTGGCTTG	-	-	120
2	**S protein**	CTAGTCTCTAGTCAGTGTG TTaatcttacaaccagaactcaattac cccctgcatacactaattctttcacacgt ggtgtttattaccctgacaaagttttcaga tcctcagttttacattcaactcaggacttg ttcttacctttcttTTCCAATGTTAC TTGGTTCC	aattc**TAATACG ACTCACTATA GGG**CTAGTCT CTAGTCAGTG TGTT	GGAACCAAGTAACAT TGGAA	169
3	**M protein**	CTAGAAAGTGAACTCGTAA TCGgagctgtgatccttcgtggacatc ttcgtattgctggacaccatctaggacg ctgtgacatcaaggacctgcctaaaga AATCACTGTTGCTACATCA C	-	-	121
4	**ORF678**	TAGATGAAGAGCAACCAAT Ggagattgattaaacgaacatgaaaa ttattcttttcttggcactgataacactcgc tacttgtgagctttatcactaccaagagt GTGTTAGAGGTACAACAGT AC	aattc**TAATACG ACTCACTATA GGG**TAGATGA AGAGCAACCA ATG	GTACTGTTGTACCTC TAACAC	126
5	**ORF1ab**	GCCTTGAATTTAGGTGAAA Catttgtcacgcactcaaagggattgta cagaaagtgtgttaaatccagagaag aaactggcctactcatgcctctaaaagc cccaaaagaaattatcttCTTAGAG GGAGAAACACTTC	**TAATACGACT CACTATAGGG** GCCTTGAATTT AGGTGAAAC	GAAGTGTTTCTCCCT CTAAG	139

Table 4. Sequences of trigger sensors of SARS-CoV-2 with NASBA suitable primers.

Appendix B

Primers Used in Chapter 1

Primer ID	Amplified region	Sequence (5' to 3')
ICK3	PcopA Promoter	CGCATGGTACCATCTCCTTCTTAAAGTTAATTTTGACTGGCTGTGATAAAG
ICK4		GGATAGTTAATGATCAGCCCACTGACGCGTCTTTTGTTAACTCCTTTTTATAGATGC
ICK2	pET22b backbone with sfGFP	TTAACTTTAAGAAGGAGATGGTACCATGCG
ICK1		ACGCGTCAGTGGGCTGATCATTAA
ICK11	pET22b PcopA RSB30 sfGFP backbone	CATCTAGTATTTCTCCTCTTTAATCTCTAGCTTAAAGTTAATTTTGACTGGCTGT
ICK12		CTACTAGAGATTAAAGAGGAGAAATACTAGATGCGTAAAGGCGAAGAGCT
ICK12	pET22b PcopA hrp sfGFP backbone	CTACTAGAGATTAAAGAGGAGAAATACTAGATGCGTAAAGGCGAAGAGCT
ICK26		GGTACCATCTCCTTCTTAAAGTTAATTTTGACTGG
ICK22	Hrp amplification circuit	ATTTCTCCTCTTTAATCTCTAGTAGTACAAGCCCTATAGCGATA
ICK25		CAGTCAAAATTAACTTTAAGAAGGAGATGGTACCATGAGTACAGGCATCGATAAGGACG
ICK11	pET22b PcopA RSB30 mScarlet-I backbone	CATCTAGTATTTCTCCTCTTTAATCTCTAGCTTAAAGTTAATTTTGACTGGCTGT
ICK42		CTCGAGCACCACCACCACCAC
ICK8	PpbrR Promoter insertion to Pet22B backbone	AACTAGAGGGTGTTAAATCGGCAACGCGAGATGTCTAGAATTAACTTTAAGAAGGAGATGGTACCATGCG
ICK7		CTCGCGTTGCCGATTTAACACCCTCTAGTTACTATAGAGTCAAACGCGTCAGTGGGCTGATCATTAACTATC
ICK9	PpbrR -10 mer Engineered promoter	GGTGTAAGGTCGGCAACGCGAGATGTCTAGAA

ICK10		GCGTTGCCGACCTTACACCCTCTAGTTACTAT
ICK5	PbrR Transcription factor integration to pET22b backbone	TTCCCTCTACAAATAATTTTGTTTAACTTTAAGGAGGGATCCAATGAATATCCAGATCGGCGAG
ICK6		TTTGATGCCACGCGTTCACTAGTCGCTTGGATGGGC
ICK27	PcadA Promoter	GTGAACACCCTGTAGCCACTATAGGGTCAAGCCGACACGCGTCAGTGGGCTGATC
ICK28		TAGTGGCTACAGGGTGTTCACTTGGCAACAGGCTCTAGAATTAACTTTAAGAAGGAGATGGTACCATGCG
ICK29	CadR Transcription factor	TAATTTTGTTTAACTTTAAGGAGGGATCCAATGAAGATCGGAGAACTGGCC
ICK30		CGTTTTATTTGATGCCACGCGTTCACTAGTTTAATGCCCGTGGCTTCG
ICK12	PcadA RBS30 backbone	CTACTAGAGATTAAAGAGGAGAAATACTAGATGCGTAAAGGCGAAGAGCT
ICK19		TCTAGTATTTCTCCTCTTTAATCTCTAGCTTAAAGTTAATTCTAGAGCCTGTTGCCAA
ICK54	PltetO-taRNA rrnB T1 terminator PltetO-crRNA-RBS Riboregulator insert	CTGAGGCCTGCAGGGATCCAAGCTTTTAATGCCCGTGGCTTCG
ICK55		TTACCAGAGGGCGCCCCAGCTGGCAATTCCGACGTCAAAGGGCCCTC
pREA97	pZs kanR backbone for riboregulator	GACGTCGGAATTGCCAGCTG
pREA98		CTGCAGGGATCCAAGCTT

SK30	ArsR Transcription factor insert	TTCCCTCTACAAATAATTTTGTTTAACTTTAAGGAGGGATCCATGTCATTTCTGTTACCCATC
SK29		AGTAAGAACATTTGCAGTTAATGAACGCGTGGCATCAAATAAAACGAAAGG
SK20	pET22b backbone for arsenic sensor	CCCTCTACAAATAATTTTGTTTAACTTT
pREA29		TGAACGCGTGGCATCAAATAAAAC
ICK59	pET22b lead -10 mer RBS30 sfGFP backbone for multiplexed sensor	GTCTTGACTCTATAGTAACTAGAGGGTGTAAGGT
ICK1		ACGCGTCAGTGGGCTGATCATTAA
ICK58	PcopA RBS30 mScarlet insert for multiplexed sensor	ACCTTACACCCTCTAGTTACTATAGAGTCAAGACGACGTCATATAGTTCCTCCTTTCAGCAAAA
ICK57		TAGTTAATGATCAGCCCACTGACGCGTAAGCTTCTTTTGTTAACTCCTTTTTATAGATGC
ICK40	mScarlet-I insert	TTAAAGAGGAGAAATACTAGATGAGTAAAGGAGAAGCTGTG
ICK41		TCAGTGGTGGTGGTGGTGGTGCTCGAGTTATTTGTATAGTTCATCCATGCC

ICK11	Pet22B PcopA RBS30 backbone	CATCTAGTATTTCTCCTCTTTAATCTCTAG CTTAAAGTTAATTTTGACTGGCTGT
ICK42		CTCGAGCACCACCACCACCAC
ICK78	mTagBFP insert into pET22b PcadA RBS30 backbone	CTAGAGATTAAAGAGGAGAAATACTAGAT GATGAGCGAACTGATCAAAGA
ICK79		ATCTCAGTGGTGGTGGTGGTGGTGCTCG AGTCAATTCAGTTTATGACCCAGCTT
ICK90	pET22b PcadA RBS30 backbone	GGTACCATCTCCTTCTTAAAGTTAATTCTA GAGCCTGTTGCC
CK42		CTCGAGCACCACCACCACCAC
CK22	hrpR, hrpS Proteins and PhrpL Promoter	ATTTCTCCTCTTTAATCTCTAGTAGTACAA GCCCTATAGCGATA
ICK23		GTCTAGAATTAACTTTAAGAAGGAGATGG TACCATGAGTACAGGCATCGATAAGGAC G

Table 5. Primers used for cloning sensory units of copper, lead, cadmium and arsenic.

Primers Used in Chapter 2

Primer ID	Amplified region	Sequence (5’ to 3’)
ICK91	pZa csgA backbone	GCATTTTTATCCATAAGATTAGCGG
ICK92		TATGGCATAGCAAAGTGTGAC
ICK94	Plac/ara csgG csgE csgF insert	TAGGATCCGCTAATCTTATGGATAAAAAT GCCAGATCCTTGGCGGCAAGAAAG
ICK93		TTGCACGGCGTCACACTTTGCTATGCCAT AATTGCTCAGCGGTGGCAG

Table 6. Primers used for cloning biofilm protein expression vector.

Appendix C

Plasmid Maps Used in This Study

Copper biosensors' plasmid maps

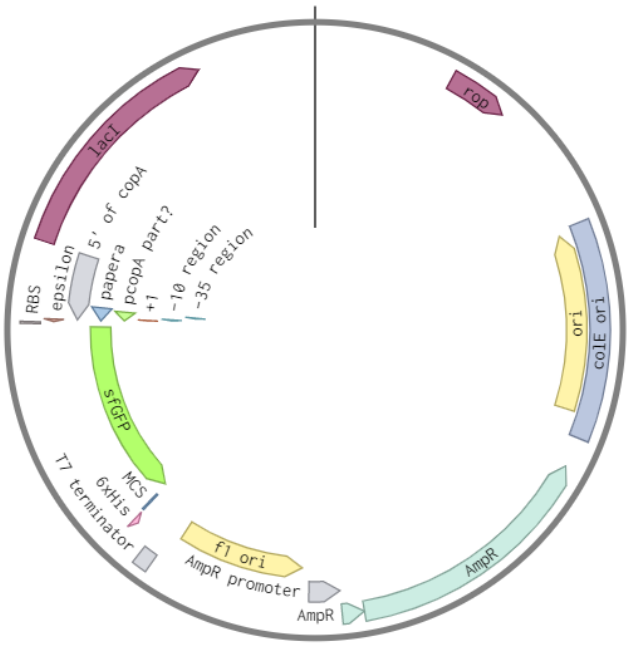

Figure 167. Schematic representation of pET22b-PcopA-sfGFP vector.

Figure 168.Schematic representation of pET22b-PcopA-RBS30-sfGFP vector.

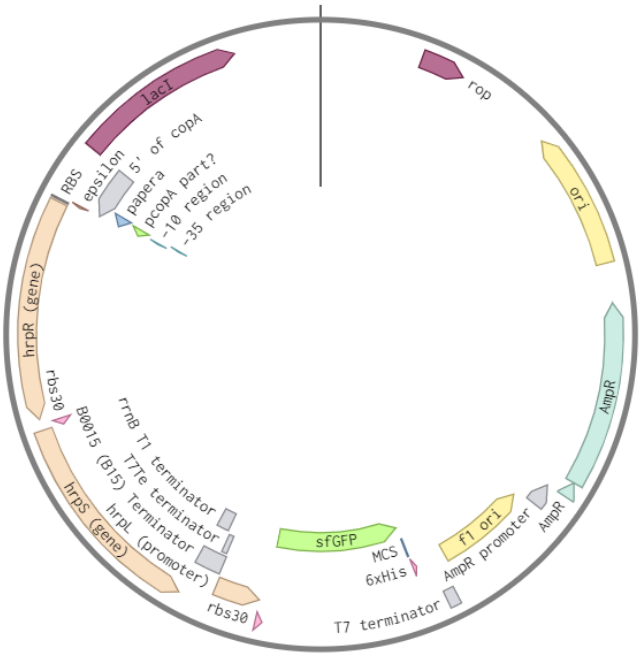

Figure 169.Schematic representation of pET22b-PcopA-hrp-sfGFP vector.

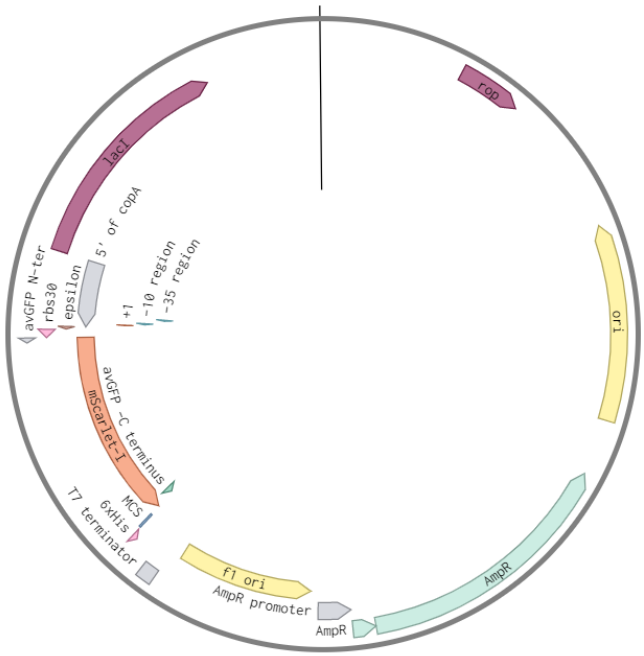

Figure 170.Schematic representation of pET22b-PcopA-RBS30-mScarlet vector.

Lead biosensors' plasmid maps

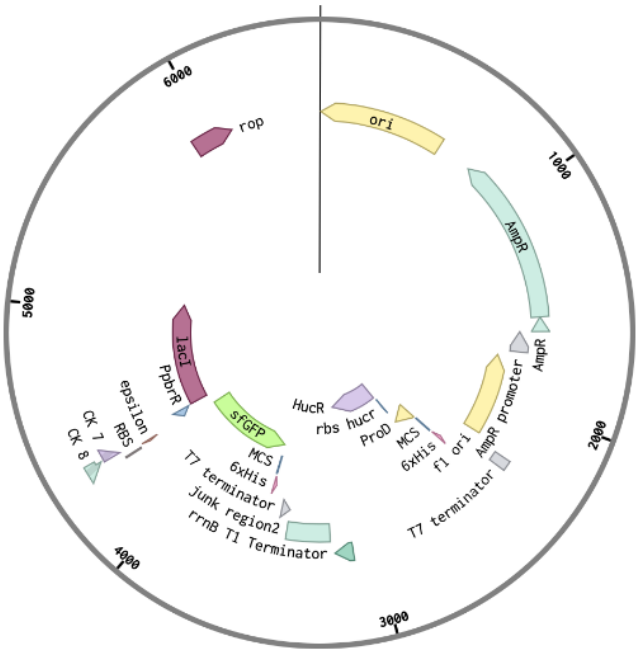

Figure 171.Schematic representation of pET22b-PpbrR-sfGFP-ProD-HucR vector.

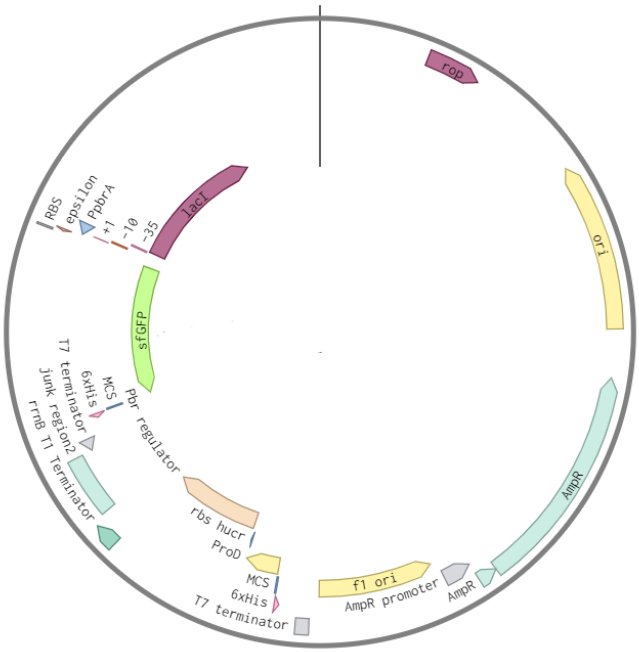

Figure 172. Schematic representation of pET22b-PpbrR-sfGFP-ProD-PbrR vector.

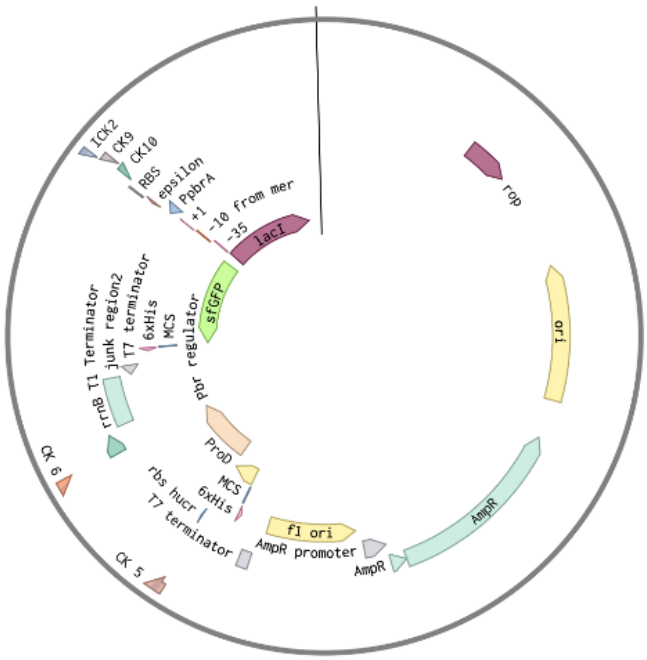

Figure 173. Schematic representation of pET22b-10mer-PpbrR-sfGFP-ProD-PbrR vector.

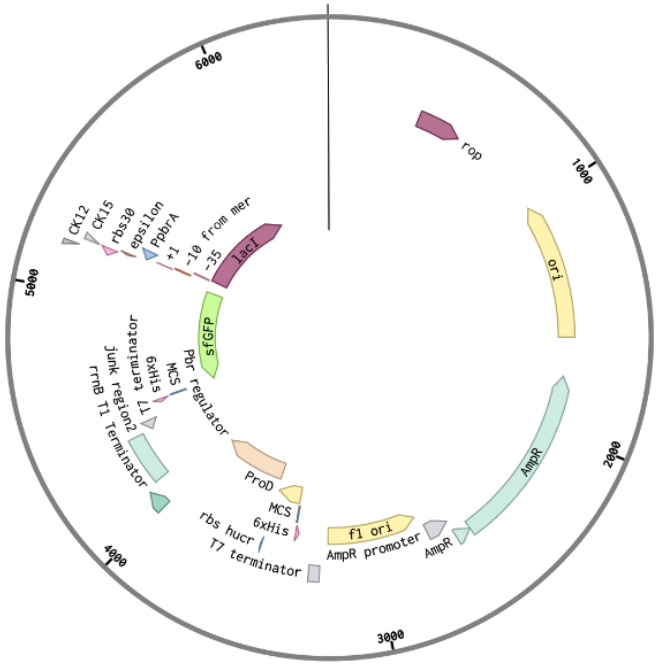

Figure 174. Schematic representation of pET22b-10mer-RBS30-PpbrR-sfGFP-ProD-PbrR vector.

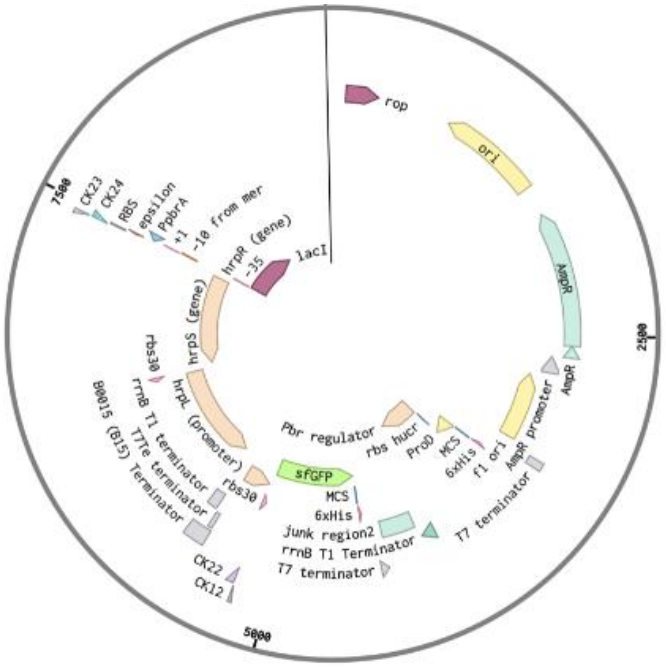

Figure 175. Schematic representation of pET22b-10mer-PpbrR-hrp-sfGFP-ProD-PbrR vector.

Cadmium biosensors' plasmid maps

Figure 176. Schematic representation of pET22b-PcadA-sfGFP-ProD-PbrR vector.

Figure 177. Schematic representation of pET22b-PcadA-sfGFP-ProD-CadR vector.

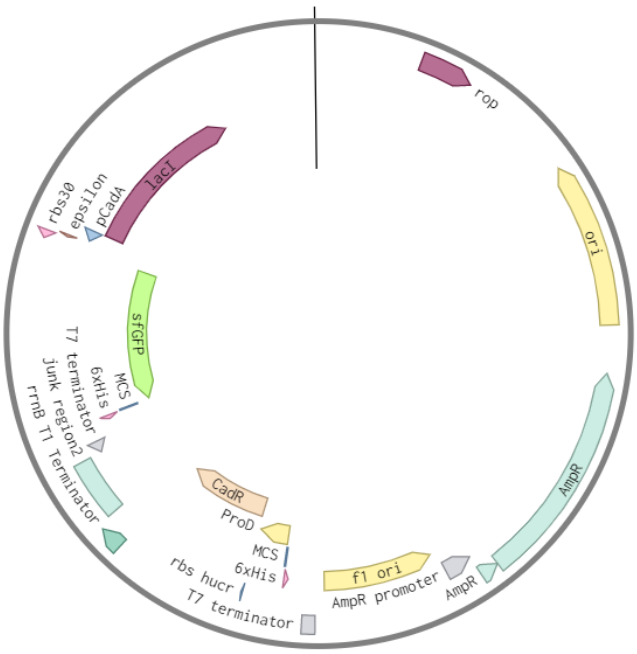

Figure 178. Schematic representation of pET22b-PcadA-RBS30-sfGFP-ProD-CadR vector.

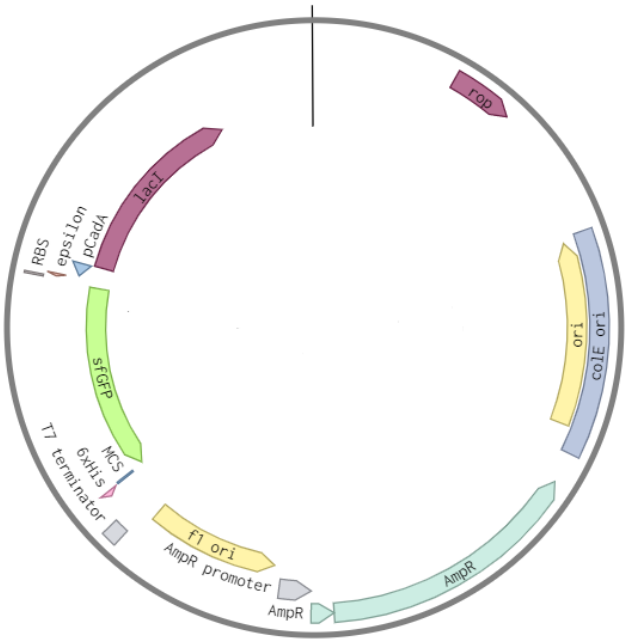

Figure 179. Schematic representation of pET22b-PcadA-sfGFP vector.

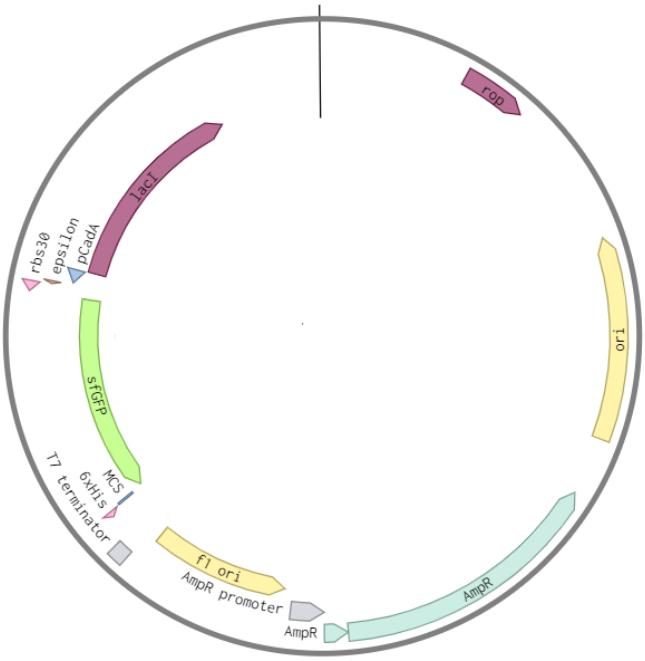

Figure 180. Schematic representation of pET22b-PcadA-RBS30-sfGFP vector.

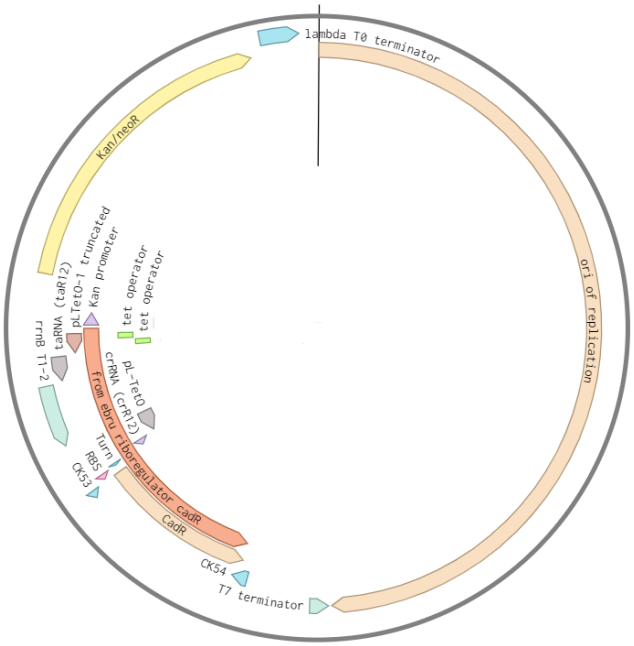

Figure 181. Schematic representation of pZs-PlTetO-riboregulator-CadR-KanR vector.

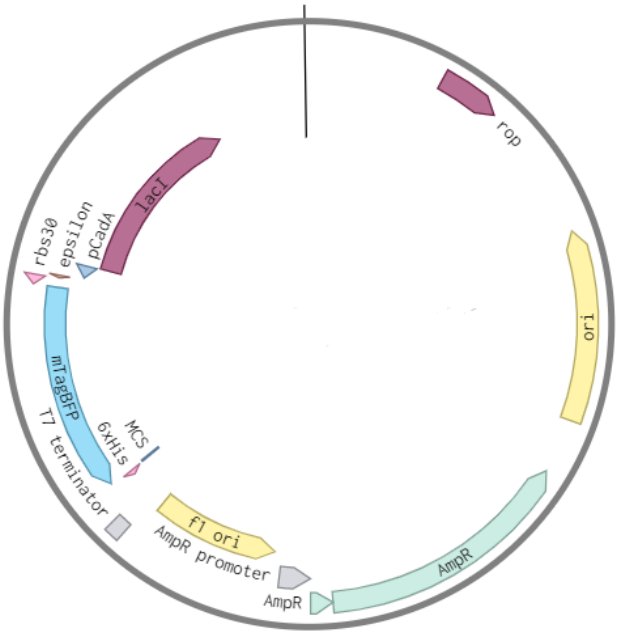

Figure 182. Schematic representation of pET22b-PcadA-RBS30-mTagBFP vector.

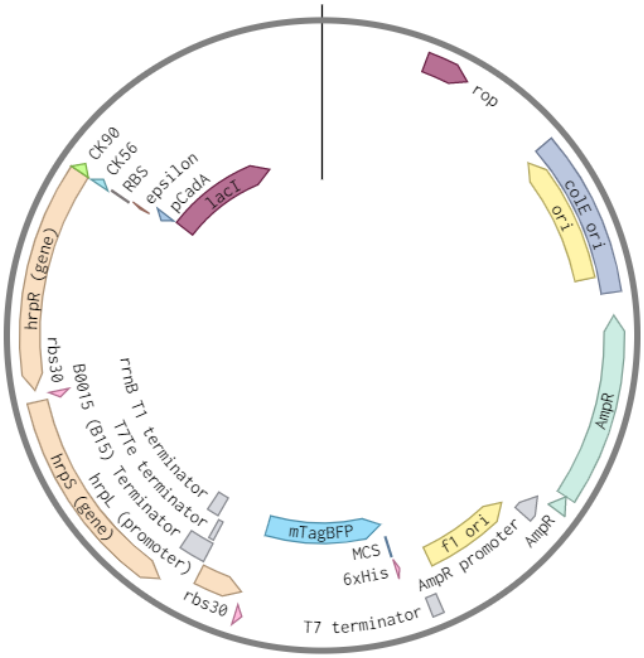

Figure 183. Schematic representation of pET22b-PcadA-hrp-mTagBFP vector.

Arsenic biosensors' plasmid maps

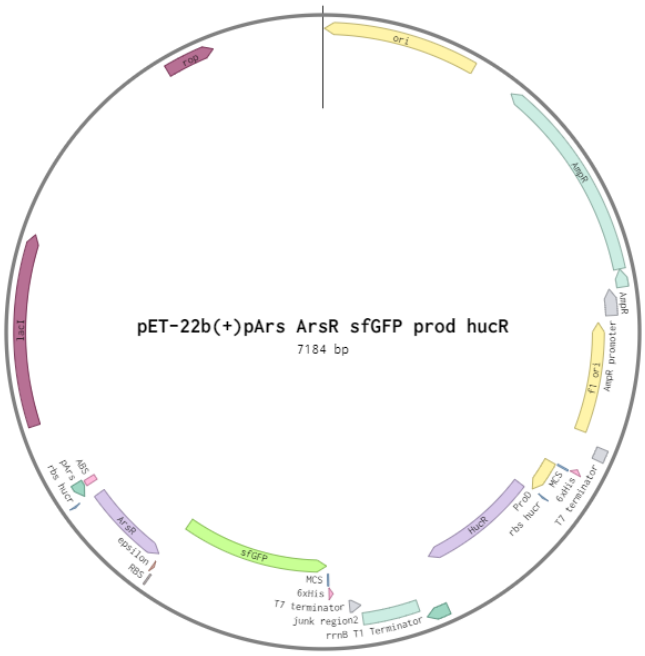

Figure 184. Schematic representation of pET22b -ParsR-sfGFP-ProD-HucR vector.

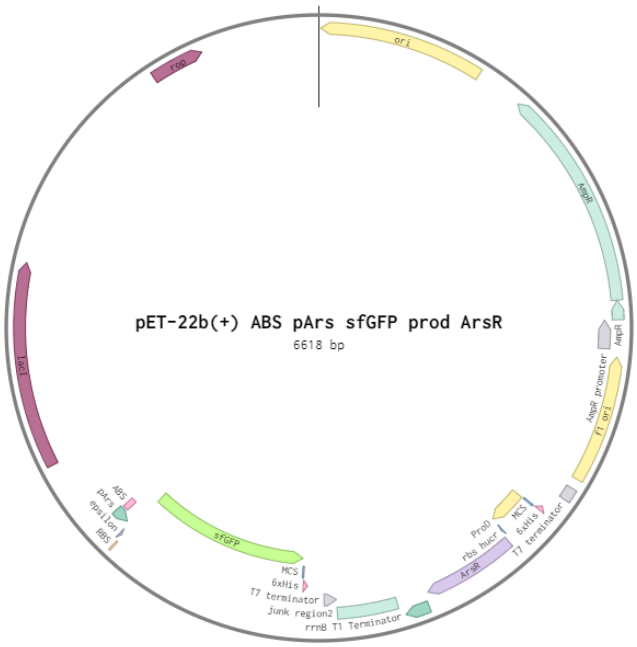

Figure 185. Schematic representation of pET22b-ABS-ParsR-sfGFP-ProD-ArsR vector.

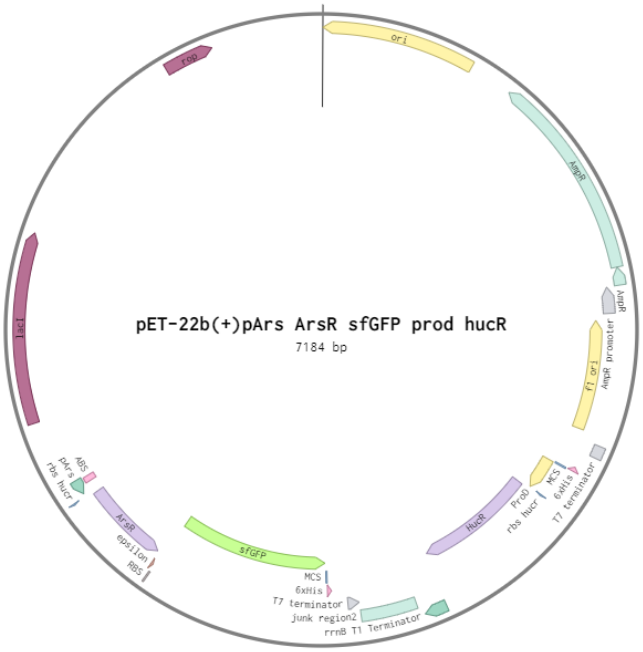

Figure 186. Schematic representation of pET22b-ABS-ParsR-ArsR-sfGFP-ProD-HucR vector.

Copper and lead multi-input multi-output biosensors' plasmid map

Figure 187. Schematic representation of pET22b-10mer-RBS30-PpbrR-sfGFP-ProD-PbrR-PcopA-RBS30-mScarlet vector.

Biofilm part plasmid maps

Figure 188. Schematic representation of pZa PBAD csgA - HisTag vector.

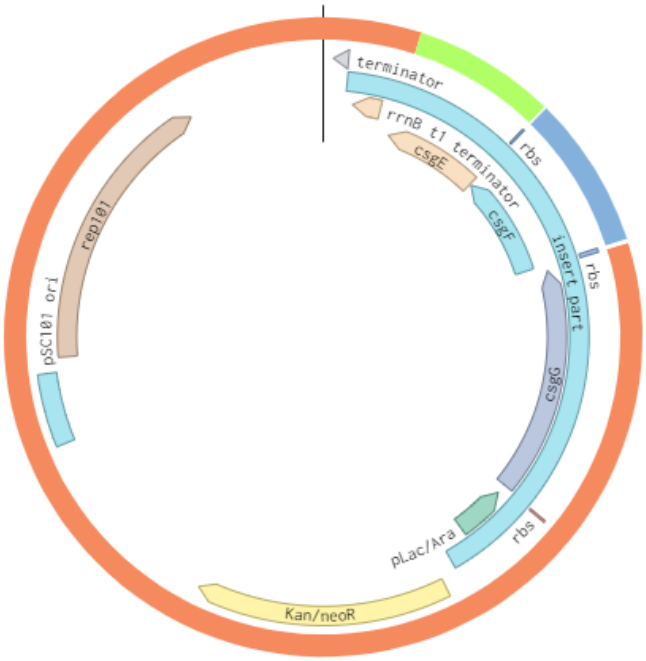

Figure 189. Schematic representation of pSC101 ORI - pLac/Ara csgGEF vector.

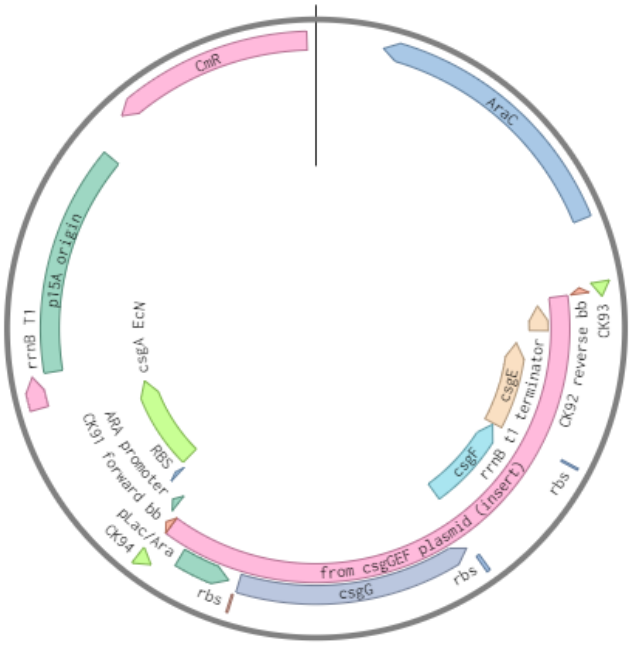

Figure 190. Schematic representation of pZa PBAD csgA pLac/Ara csgGEF vector.

Synthetic Riboreguator Plasmid Maps

SARS-CoV-2 ORFab1 trigger 1 sensor

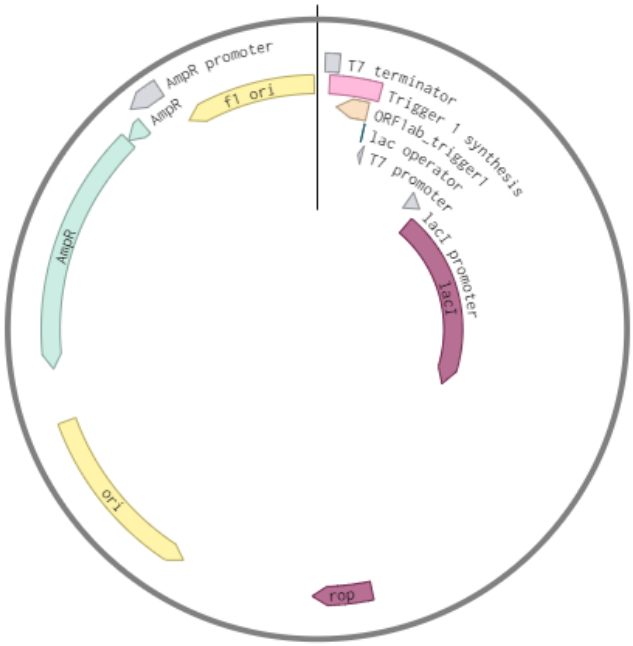

Figure 191. Schematic representation of pET-22b(+) ORFab1_trigger1 vector.

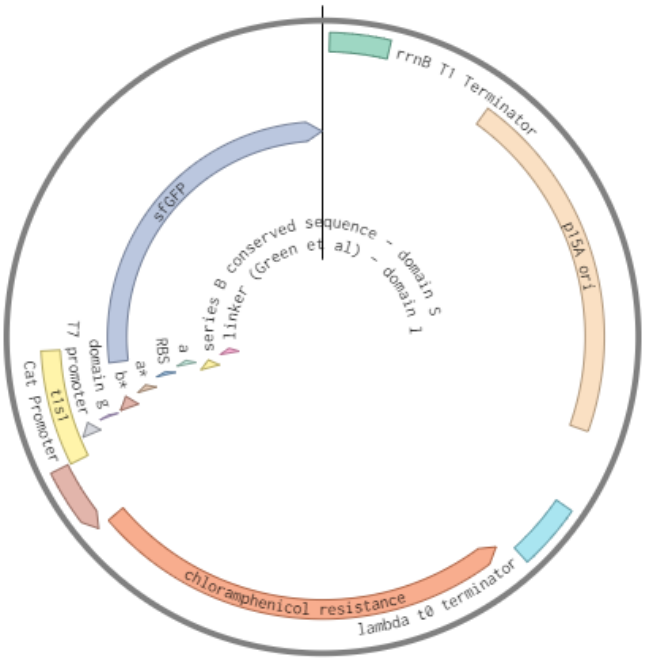

Figure 192. Schematic representation of pZa sfGFP T7 ORF1ab switch1 vector.

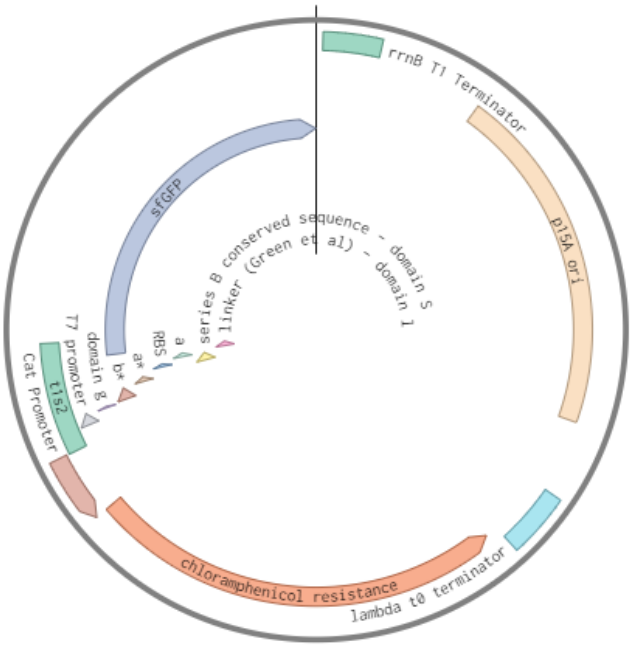

Figure 193. Schematic representation of pZa sfGFP T7 ORF1ab switch2 vector.

SARS-CoV-2 S Protein trigger 2 sensor

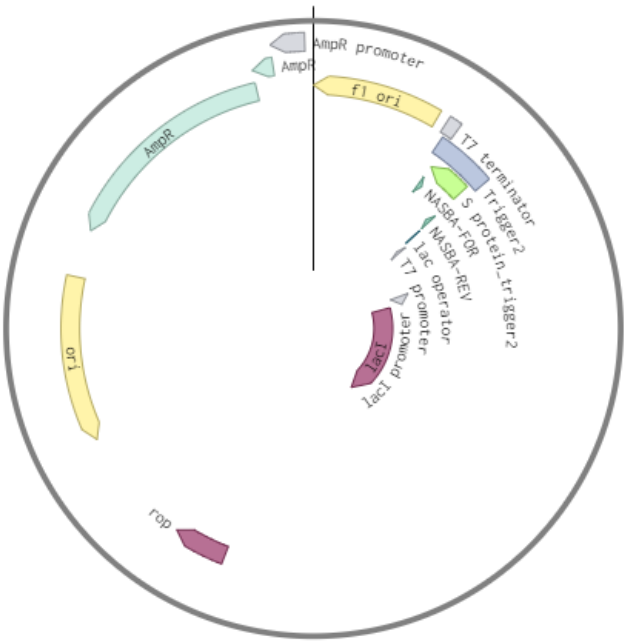

Figure 194. Schematic representation of pET-22b(+) S Protein_trigger2 vector.

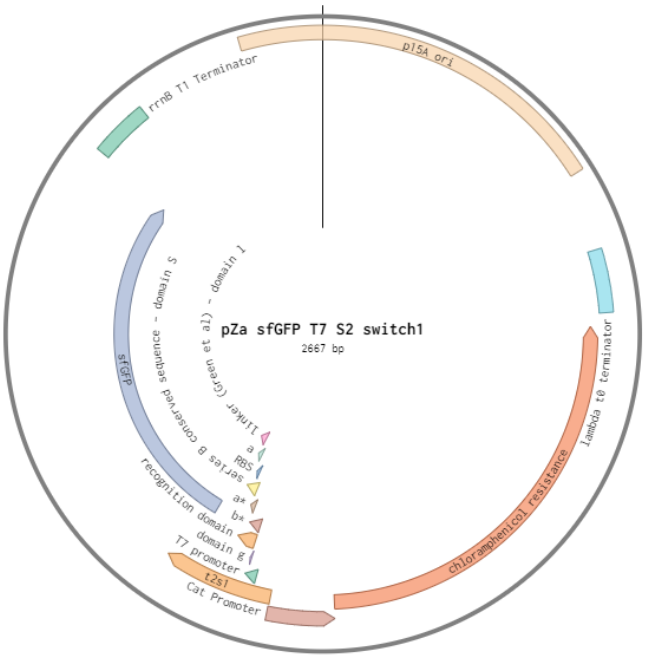

Figure 195. Schematic representation of pZa sfGFP T7 S2 switch1 vector.

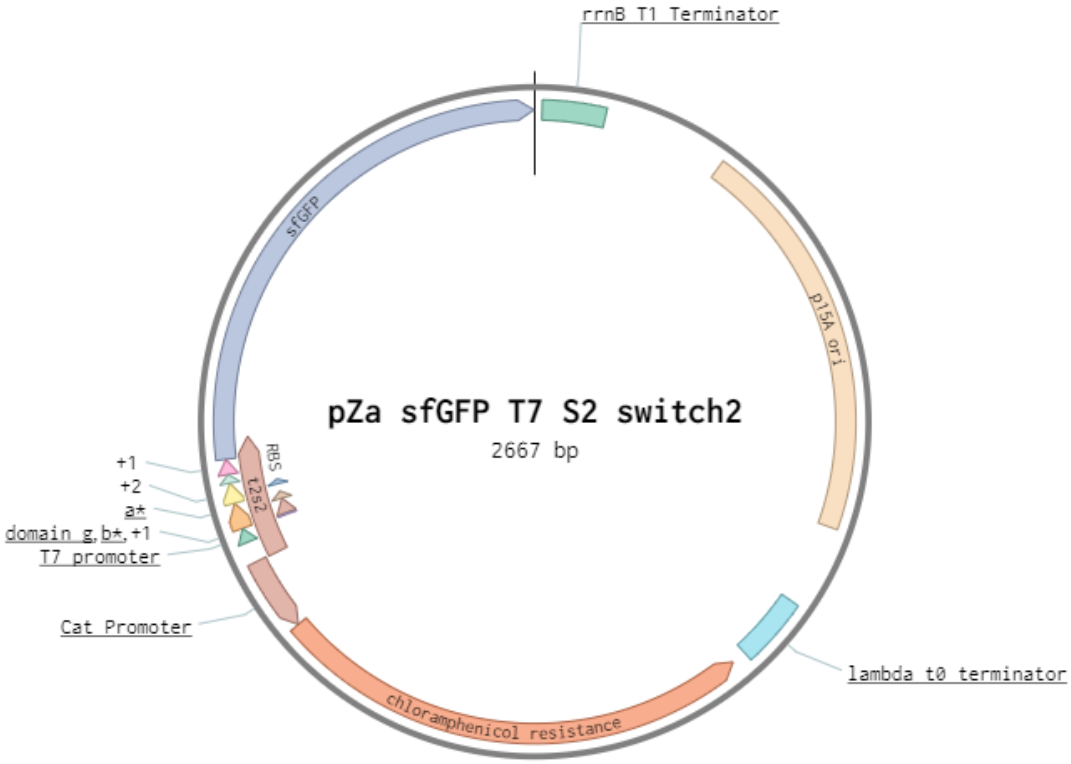

Figure 196. Schematic representation of pZa sfGFP T7 S2 switch2 vector.

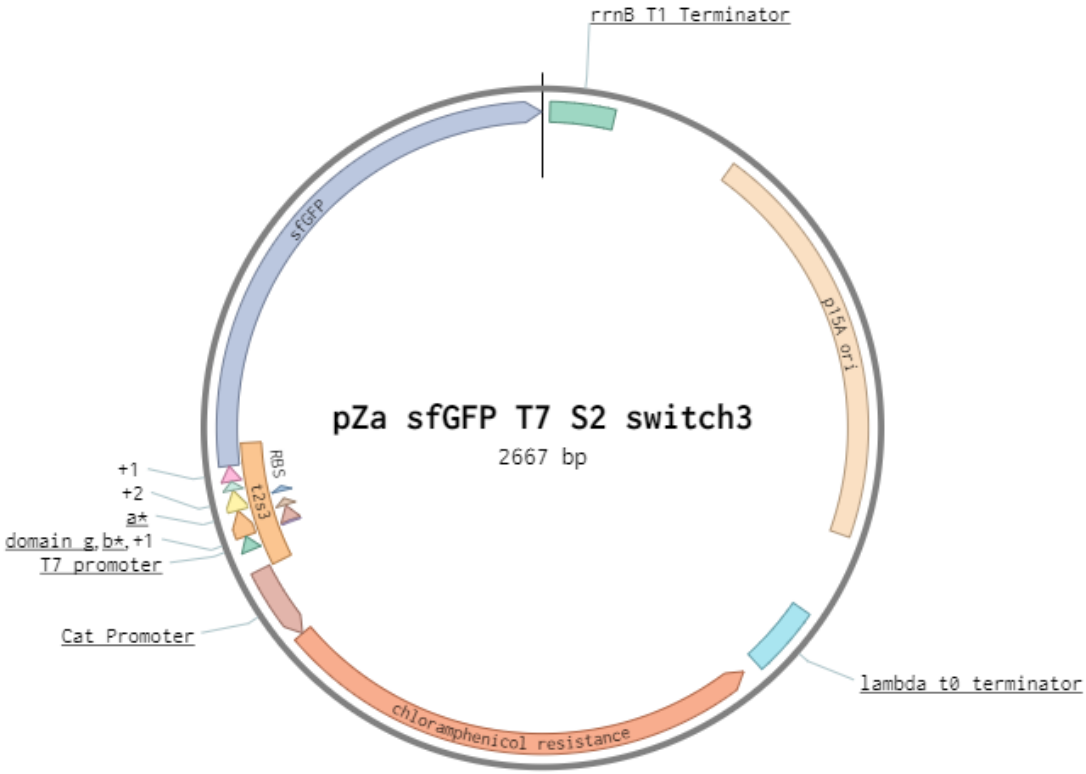

Figure 197. Schematic representation of pZa sfGFP T7 S2 switch3 vector.

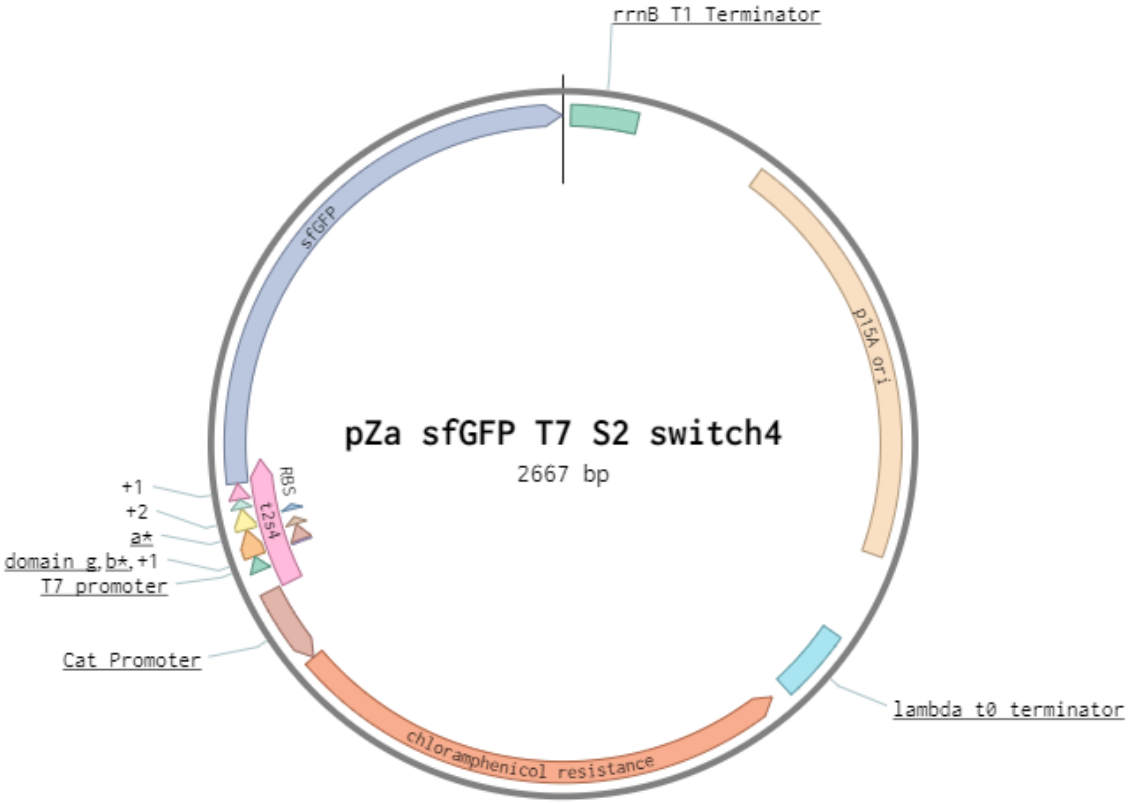

Figure 198. Schematic representation of pZa sfGFP T7 S2 switch4 vector.

SARS-CoV-2 M Protein trigger 3 sensor

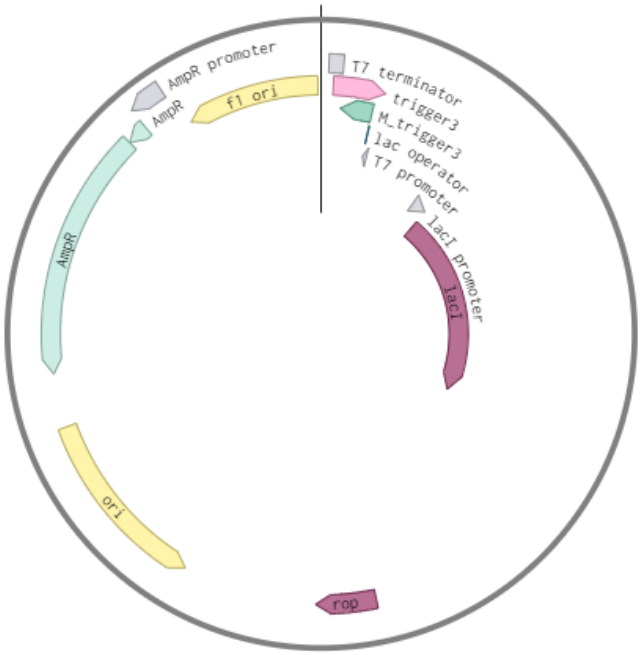

Figure 199. Schematic representation of pET-22b(+) M Protein_trigger3 vector.

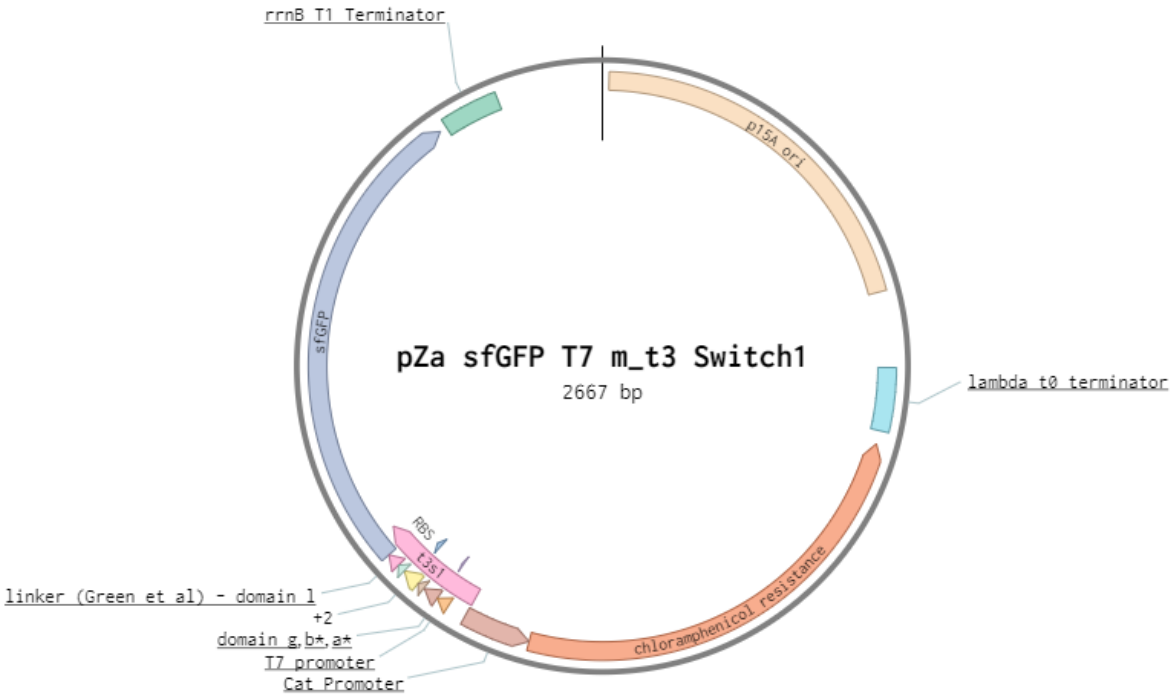

Figure 200. Schematic representation of pZa sfGFP T7 m_t3 Switch1 vector.

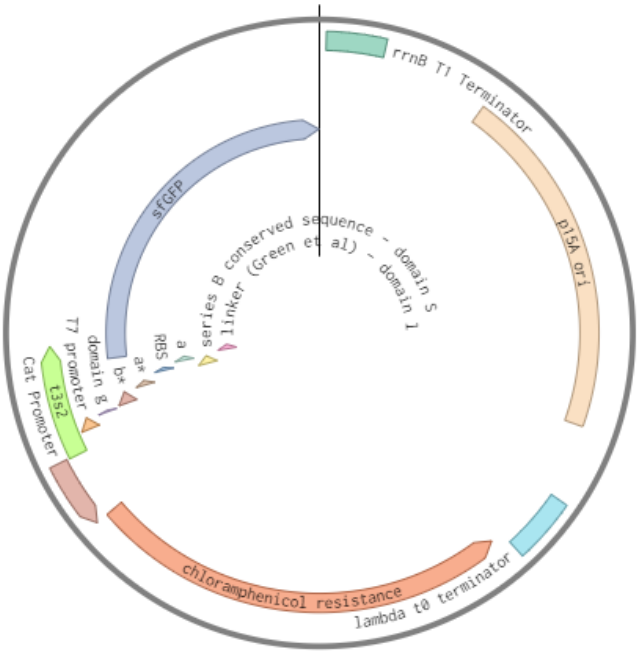

Figure 201. Schematic representation of pZa sfGFP T7 m_t3 Switch2 vector.

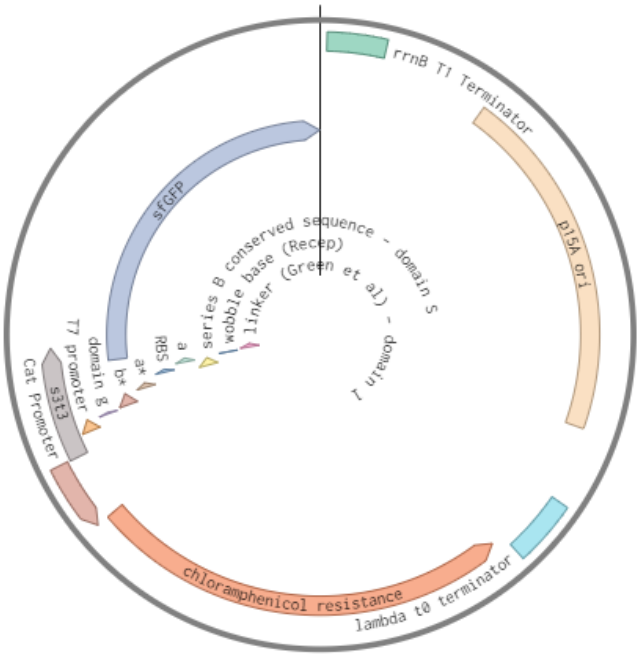

Figure 202. Schematic representation of pZa sfGFP T7 m_t3 Switch3 vector.

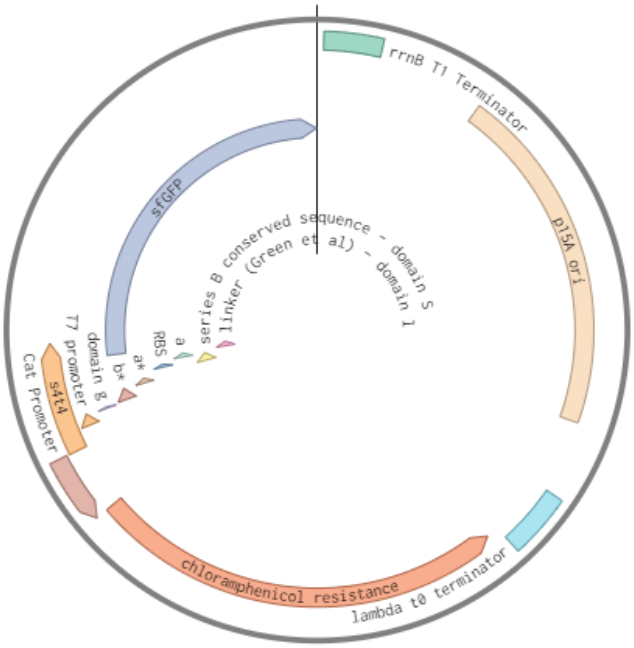

Figure 203. Schematic representation of pZa sfGFP T7 m_t3 Switch4 vector.

SARS-CoV-2 ORF678 trigger 4 sensor

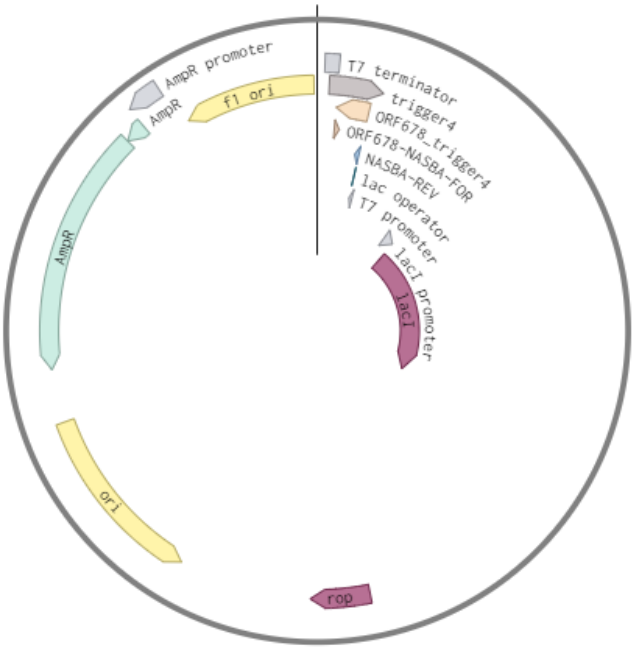

Figure 204. Schematic representation of pET-22b(+) ORF678_trigger4 vector.

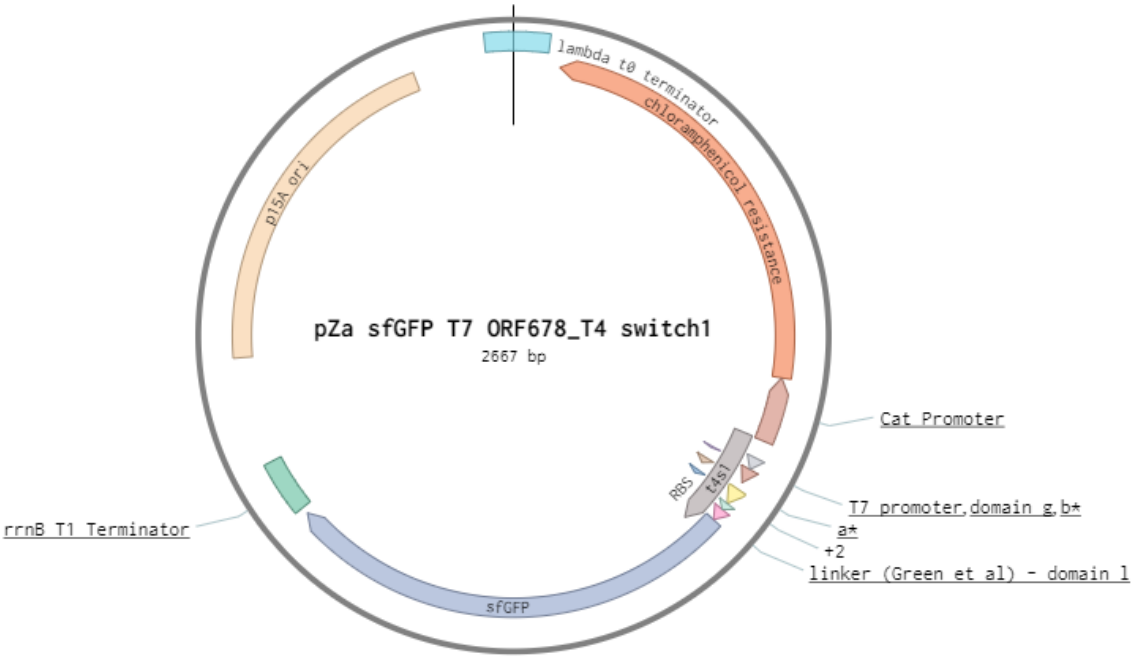

Figure 205. Schematic representation of pZa sfGFP T7 ORF678_T4 switch1 vector.

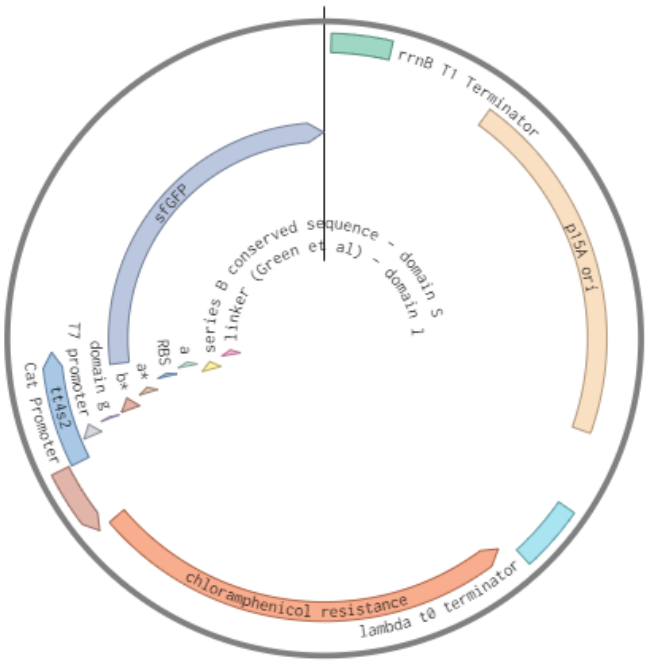

Figure 206. Schematic representation of pZa sfGFP T7 ORF678_T4 switch2 vector.

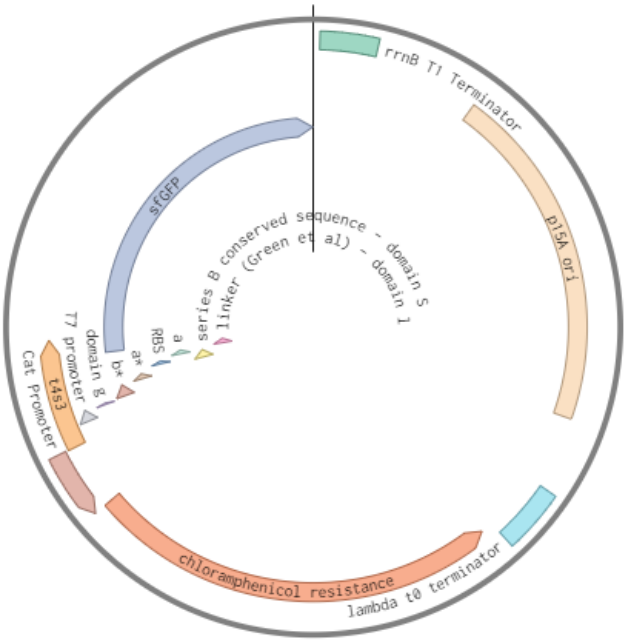

Figure 207. Schematic representation of pZa sfGFP T7 ORF678_T4 switch3 vector.

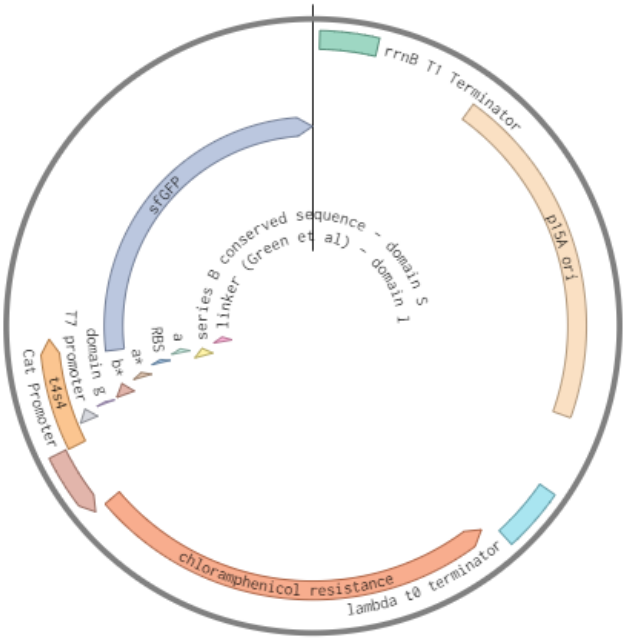

Figure 208. Schematic representation of pZa sfGFP T7 ORF678_T4 switch4 vector.

SARS-CoV-2 ORFab1Protein trigger 5 sensor

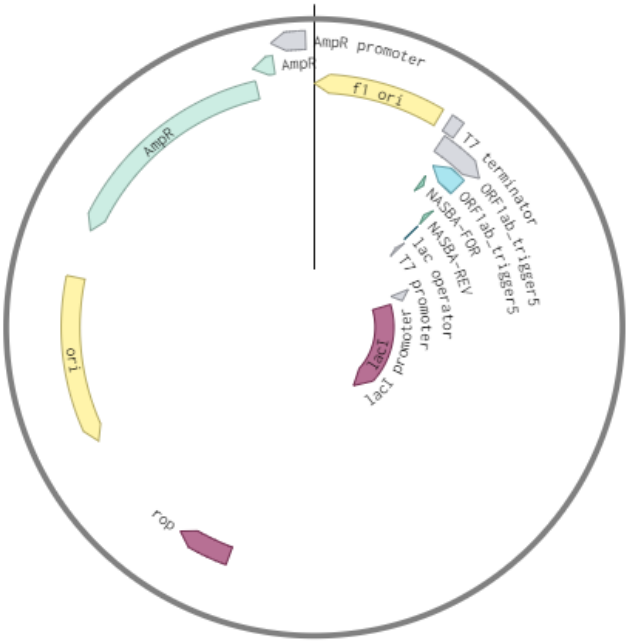

Figure 209. Schematic representation of pET-22b(+) ORFab1_trigger5 vector.

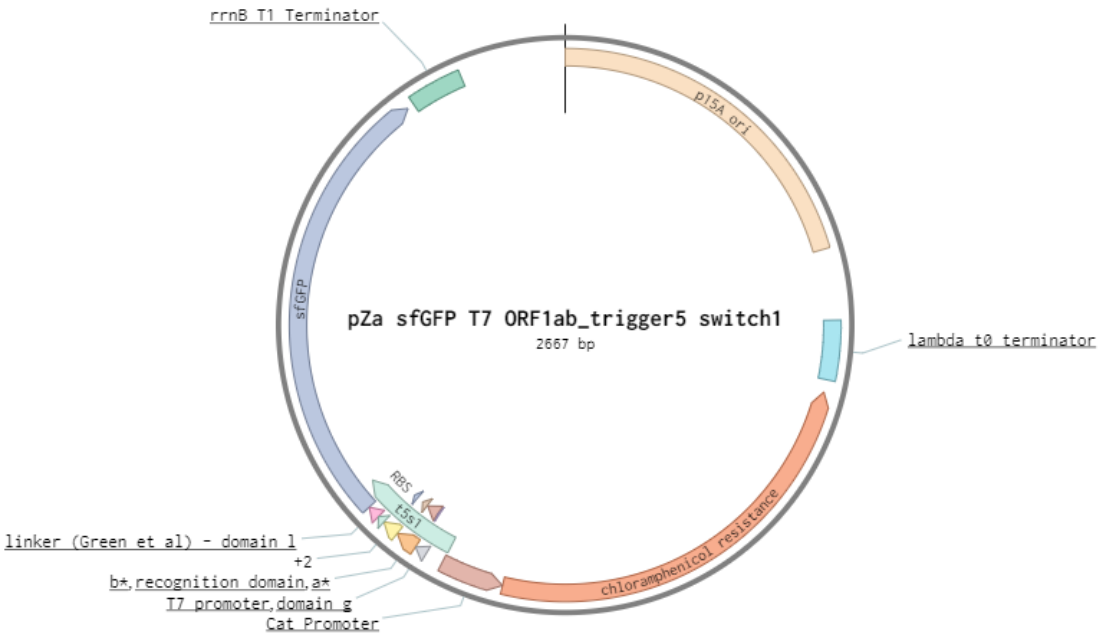

Figure 210. Schematic representation of pZa sfGFP T7 ORF1ab_trigger5 switch1 vector.

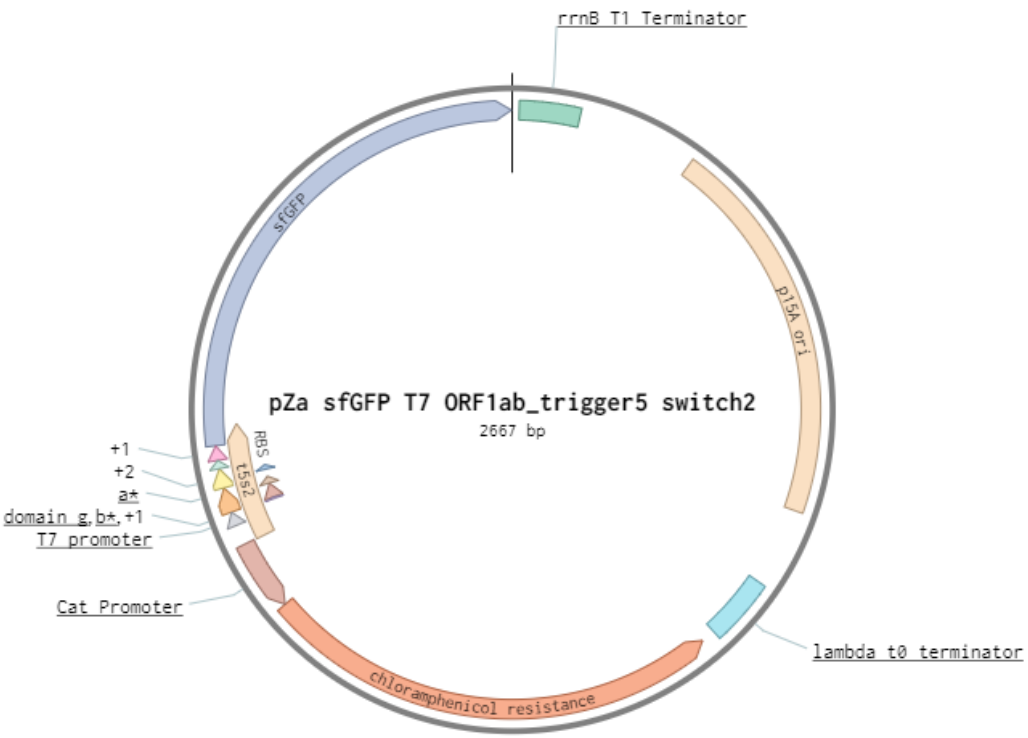

Figure 211. Schematic representation of pZa sfGFP T7 ORF1ab_trigger5 switch2 vector.

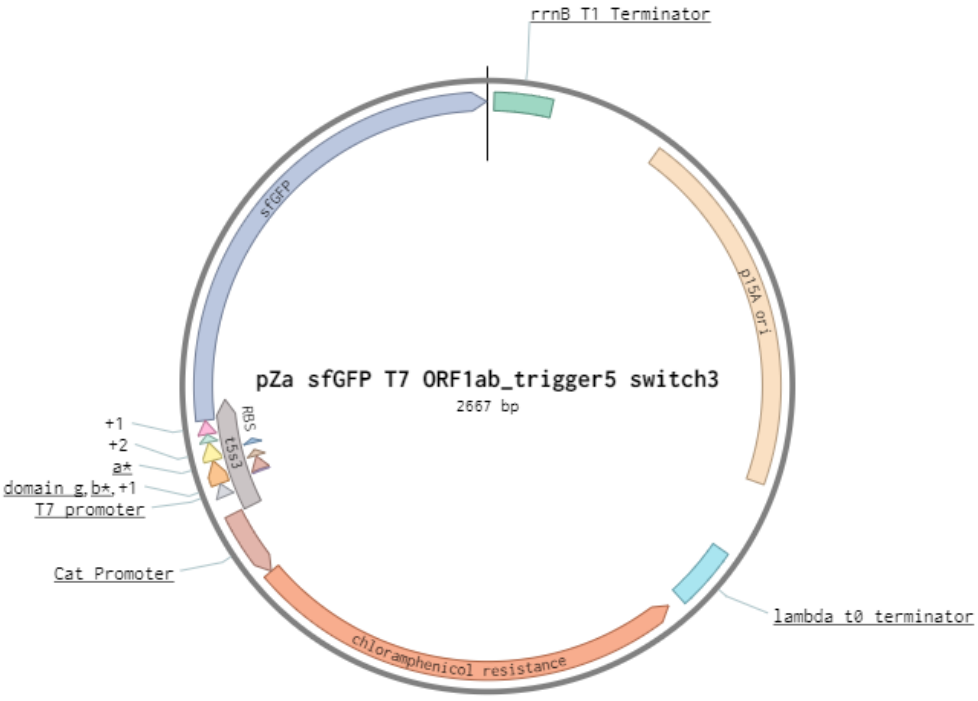

Figure 212. Schematic representation of pZa sfGFP T7 ORF1ab_trigger5 switch3 vector.

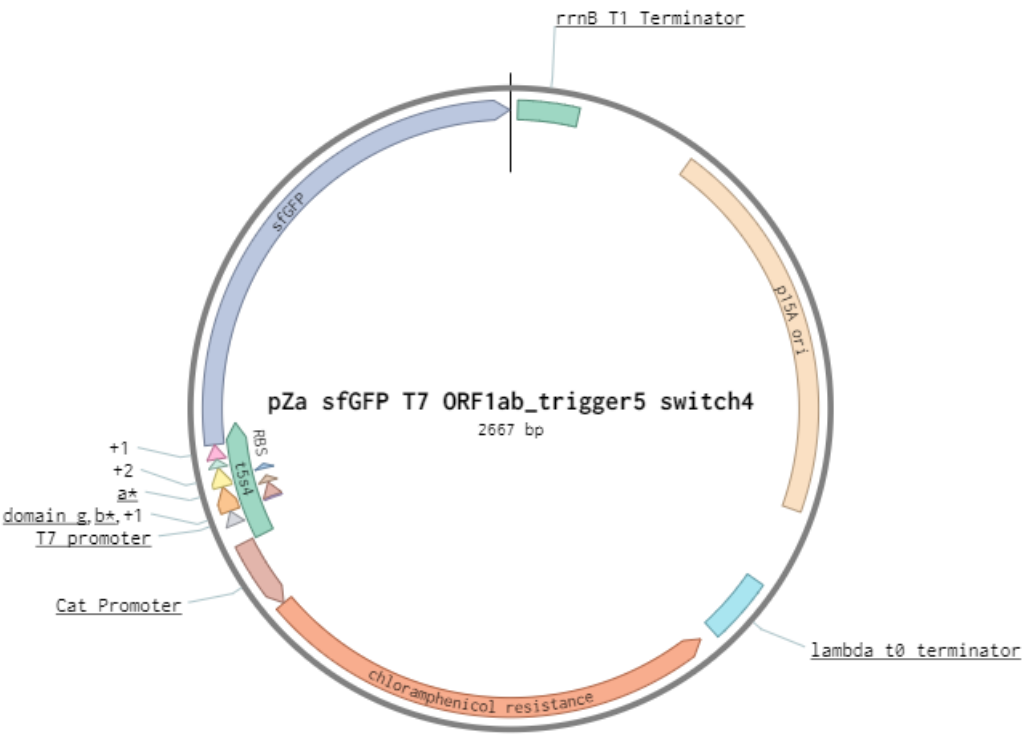

Figure 213. Schematic representation of pZa sfGFP T7 ORF1ab_trigger5 switch4 vector.

Appendix D

Next Generation and Sanger Sequencing Verification Results of the Plasmids in This Thesis

Sequencing results of vectors used in Chapter 1:

Copper biosensors' sequencing results

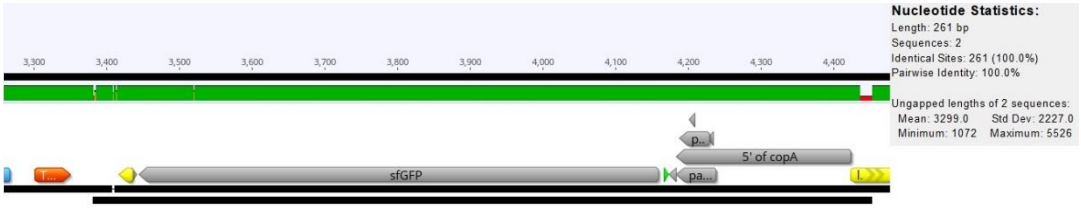

Figure 214. Sanger sequencing results of pET22b-PcopA-sfGFP vector.

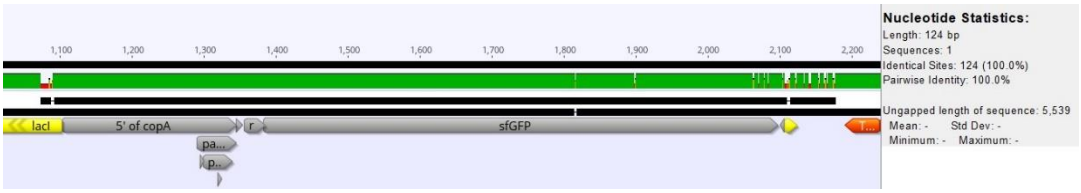

Figure 215. Sanger sequencing results of pET22b-PcopA-RBS30-sfGFP vector.

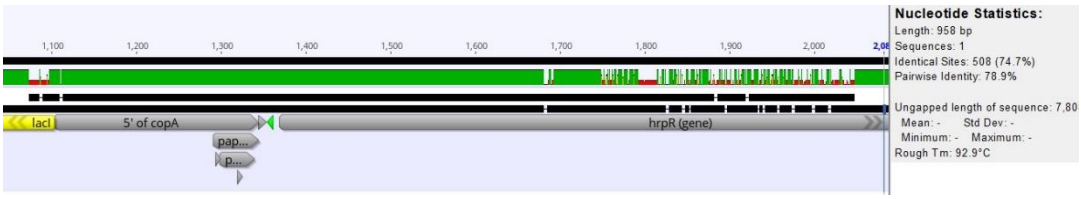

Figure 216. Sanger sequencing results of pET22b-PcopA-hrp-sfGFP vector.

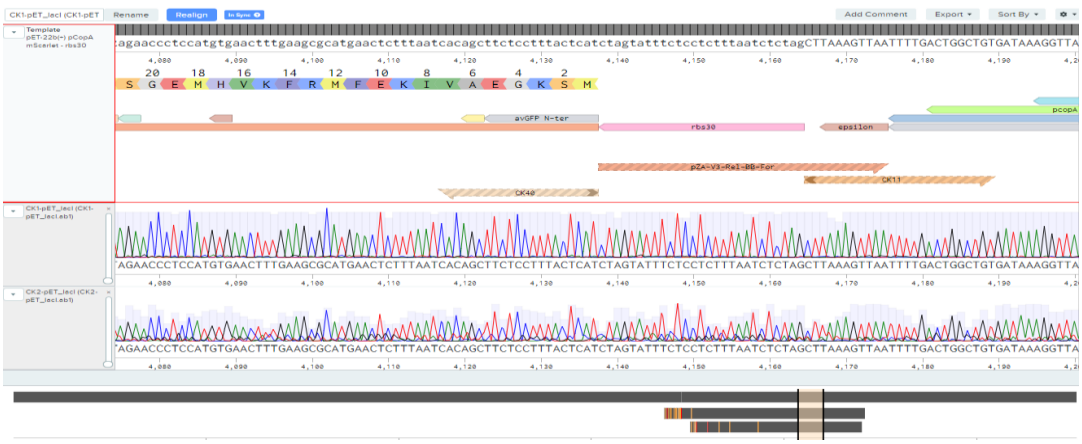

Figure 217. Sanger sequencing results of pET22b-PcopA-RBS30-mScarlet vector.

Lead biosensors' sequencing results

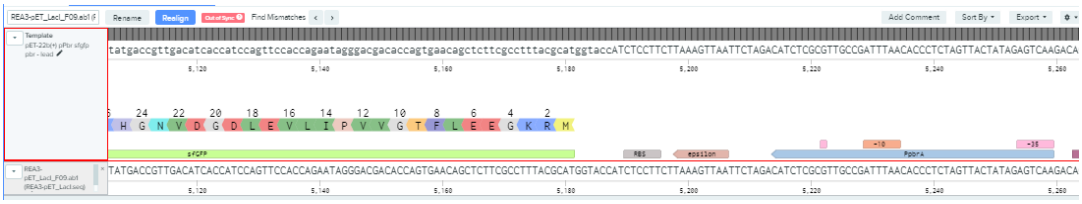

Figure 218. Sanger sequencing results of pET22b-PpbrR-sfGFP-ProD-HucR vector.

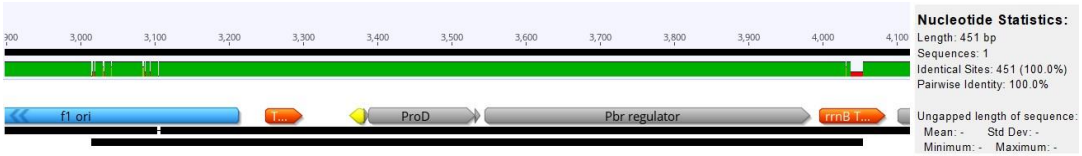

Figure 219. Sanger sequencing results of pET22b-PpbrR-sfGFP-ProD-PbrR vector.

Figure 220. Sanger sequencing results of pET22b-10mer-PpbrR-sfGFP-ProD-PbrR vector.

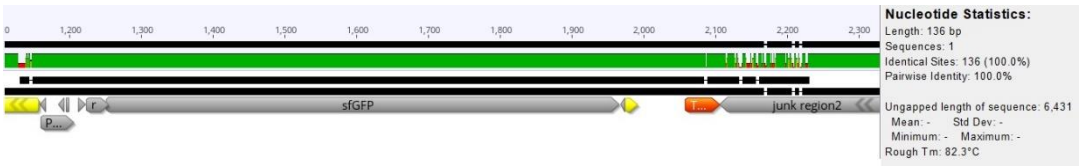

Figure 221. Sanger sequencing results of pET22b-10mer-RBS30-PpbrR-sfGFP-ProD-PbrR vector.

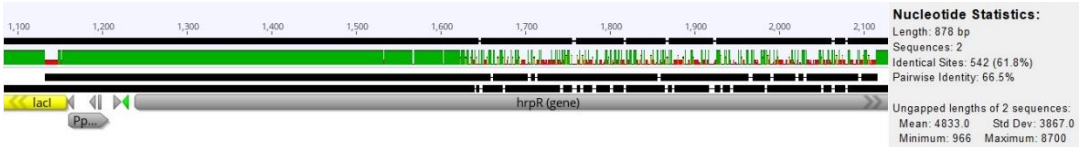

Figure 222. Sanger sequencing results of pET22b-10mer-PpbrR-hrp-sfGFP-ProD-PbrR vector.

Cadmium biosensors' sequencing results

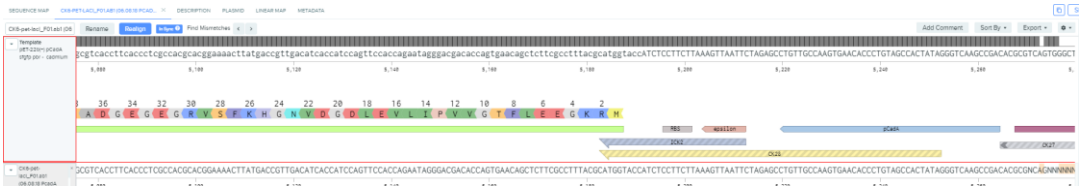

Figure 223. Sanger sequencing results of pET22b-PcadA-sfGFP-ProD-PbrR vector.

Figure 224. Sanger sequencing results of pET22b-PcadA-sfGFP-ProD-CadR vector, red rectangle shows mutated basepairs.

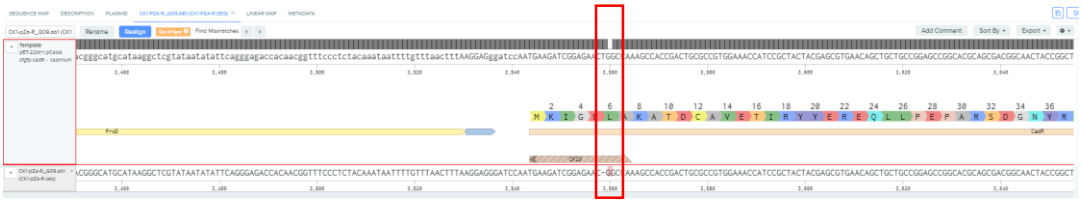

Figure 225. Sanger sequencing results of pET22b-PcadA-RBS30-sfGFP-ProD-CadR vector, red rectangle shows mutated basepairs.

Figure 226. Sanger sequencing results of pET22b-PcadA-sfGFP vector. Both promoter region PcadA (bottom) and the absence of ProD-CadR region (top) was verified.

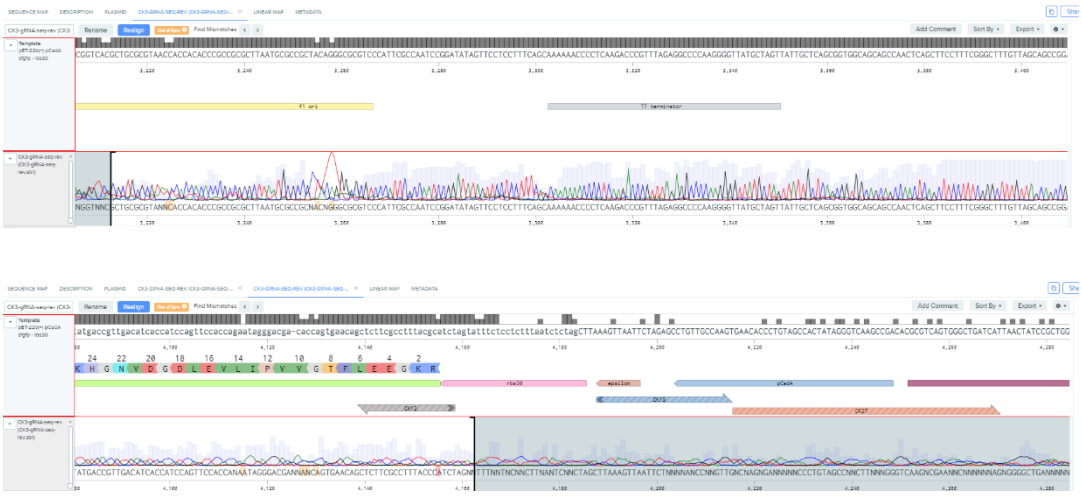

Figure 227. Sanger sequencing results of pET22b-PcadA-RBS30-sfGFP vector. Both promoter region PcadA-RBS30 (bottom) and the absence of ProD-CadR region (top) was verified.

Figure 228. Sanger sequencing results of pZs-PlTetO-riboregulator-CadR-KanR vector.

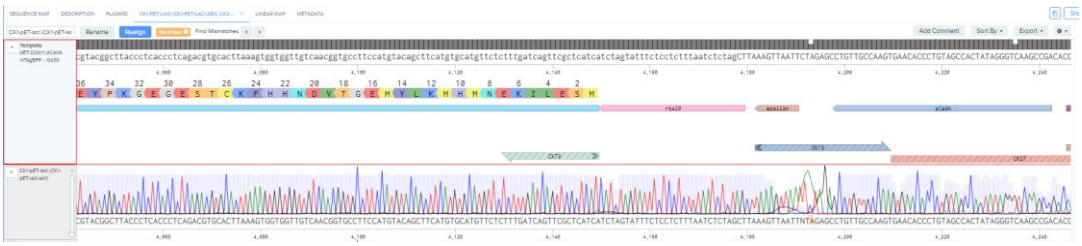

Figure 229. Sanger sequencing results of pET22b-PcadA-RBS30-mTagBFP vector.

Figure 230. NGS sequencing results of pET22b-PcadA-hrp-mTagBFP vector, twp basepair mutation in RBS region before mTagBFP gene observed.

Arsenic biosensors' sequencing results

Figure 231. Sanger sequencing result of pET22b -ParsR-sfGFP-ProD-HucR vector.

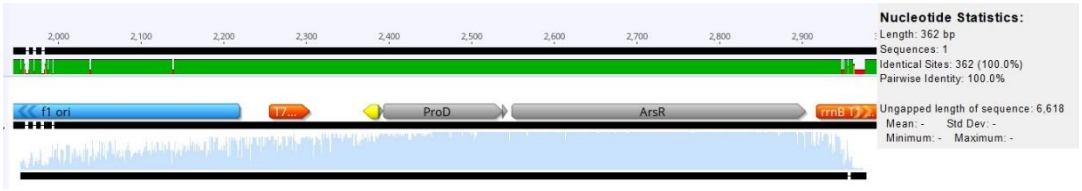

Figure 232. Sanger sequencing result of pET22b-ABS-ParsR-sfGFP-ProD-ArsR vector.

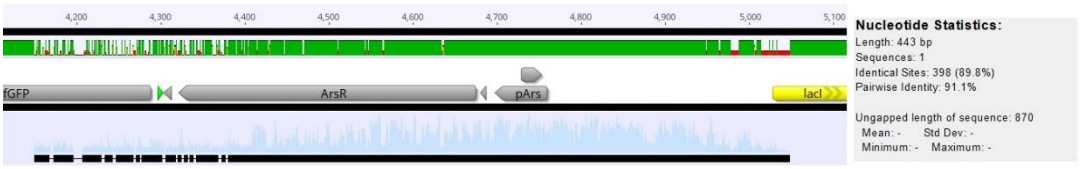

Figure 233. Sanger sequencing result of pET22b-ABS-ParsR-ArsR-sfGFP-ProD-HucR vector.

Copper and lead multi-input multi-output biosensor’s sequencing results

Figure 234. Sanger sequencing results of pET22b-10mer-RBS30-PpbrR-sfGFP-ProD-PbrR-PcopA-RBS30-mScarlet vector. PpbrR-10mer-RBS30 promoter region (top), T7 terminator mScarlet 3’ region (middle), PcopA promoter region (bottom).

Sequencing results of vectors used in Chapter 2:

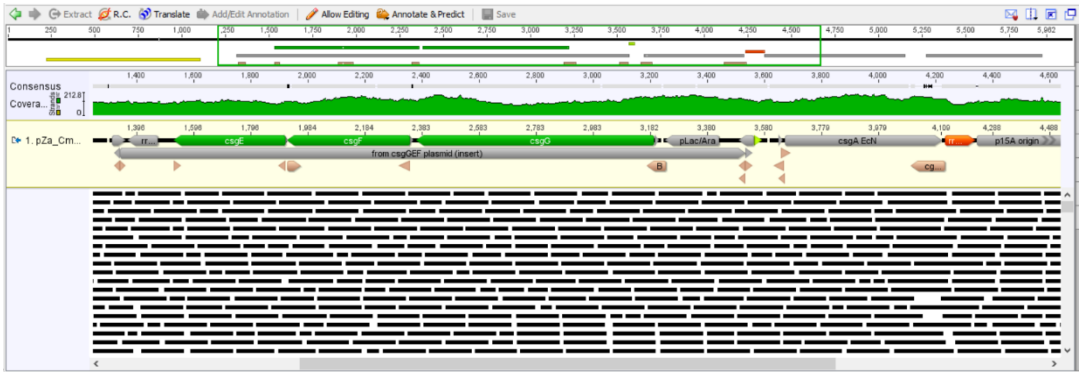

Figure 235. NGS sequencing results of pZa PBAD csgA pLac/Ara csgGEF vector.

Sequencing results of vectors used in Chapter 3:

SARS-CoV-2 ORFab1 trigger 1 sensor

Figure 236. Sanger sequencing results of pET-22b(+) ORFab1_trigger1 vector.

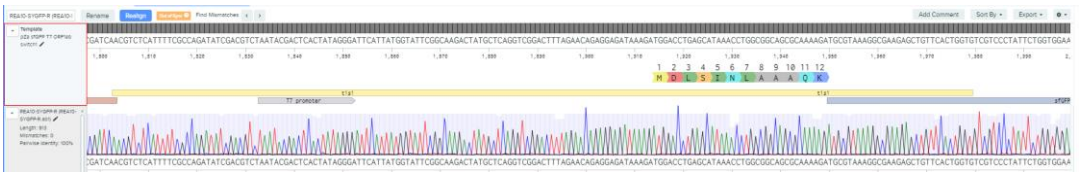

Figure 237. Sanger sequencing results of pZa sfGFP T7 ORF1ab switch1 vector.

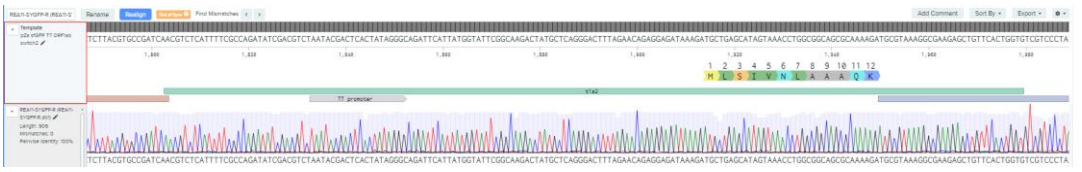

Figure 238. Sanger sequencing results of pZa sfGFP T7 ORF1ab switch2 vector.

SARS-CoV-2 S Protein trigger 2 sensor

Figure 239. Sanger sequencing results of pET-22b(+) S Protein_trigger2 vector.

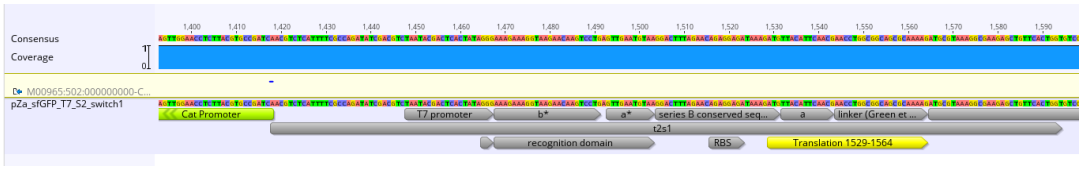

Figure 240. Sanger sequencing results of pZa sfGFP T7 S2 switch1 vector.

Figure 241. Sanger sequencing results of pZa sfGFP T7 S2 switch2 vector.

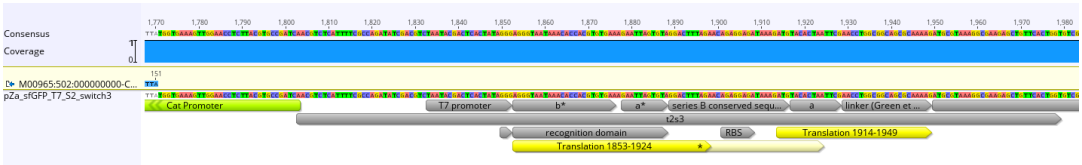

Figure 242. Sanger sequencing results of pZa sfGFP T7 S2 switch3 vector.

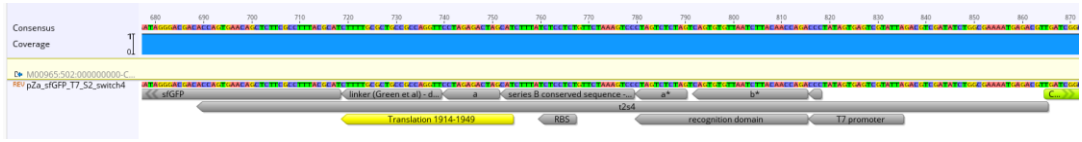

Figure 243. Sanger sequencing results of pZa sfGFP T7 S2 switch4 vector.

SARS-CoV-2 M Protein trigger 3 sensor

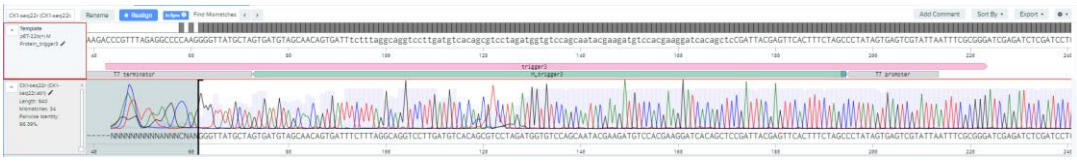

Figure 244. Sanger sequencing results of pET-22b(+) M Protein_trigger3 vector.

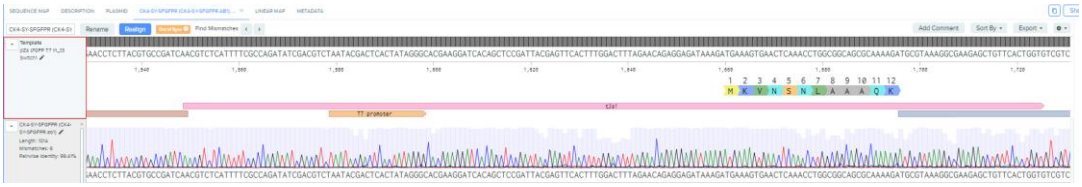

Figure 245. Sanger sequencing results of pZa sfGFP T7 m_t3 Switch1 vector.

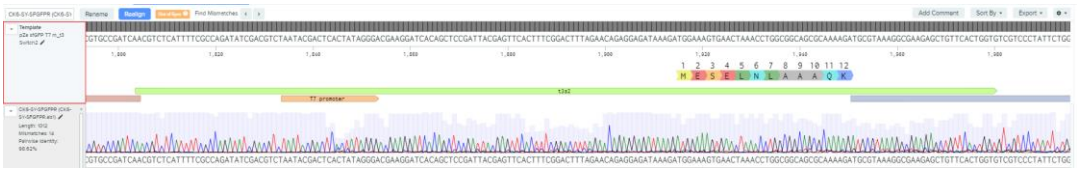

Figure 246. Sanger sequencing results of pZa sfGFP T7 m_t3 Switch2 vector.

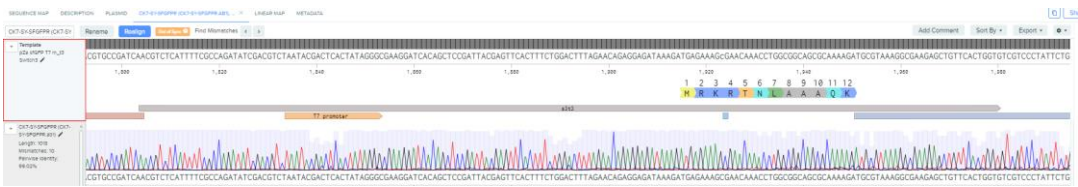

Figure 247. Sanger sequencing results of pZa sfGFP T7 m_t3 Switch3 vector.

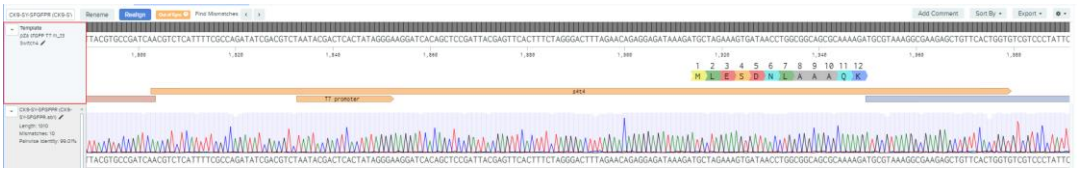

Figure 248. Sanger sequencing results of pZa sfGFP T7 m_t3 Switch4 vector.

SARS-CoV-2 ORF678 trigger 4 sensor

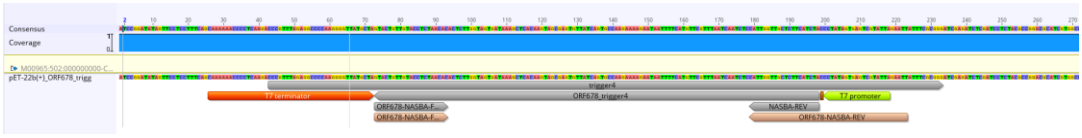

Figure 249. Sanger sequencing results of pET-22b(+) ORF678_trigger4 vector.

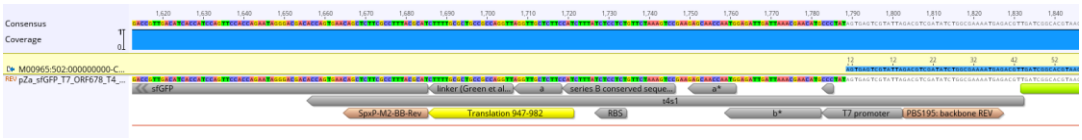

Figure 250. Sanger sequencing results of pZa sfGFP T7 ORF678_T4 switch1 vector.

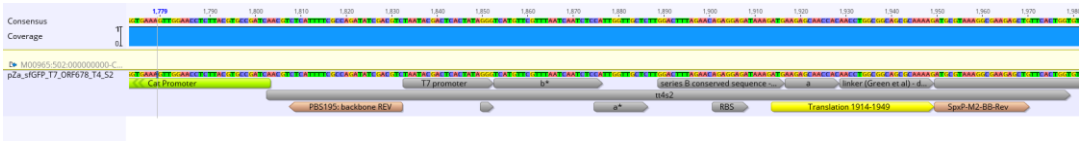

Figure 251. Sanger sequencing results of pZa sfGFP T7 ORF678_T4 switch2 vector.

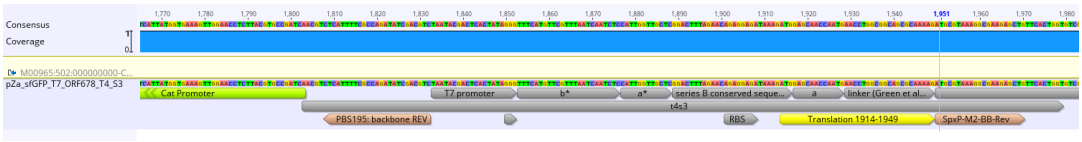

Figure 252. Sanger sequencing results of pZa sfGFP T7 ORF678_T4 switch3 vector.

Figure 253. Sanger sequencing results of pZa sfGFP T7 ORF678_T4 switch4 vector.

SARS-CoV-2 ORFab1 Protein trigger 5 sensor

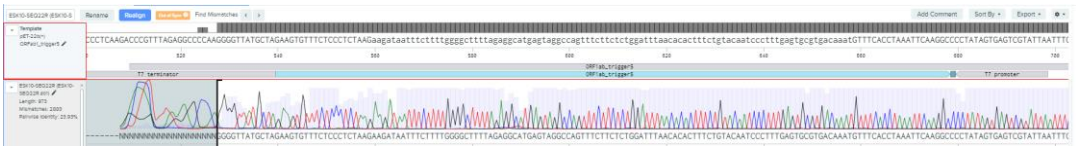

Figure 254. Sanger sequencing results of pET-22b(+) ORFab1_trigger5 vector.

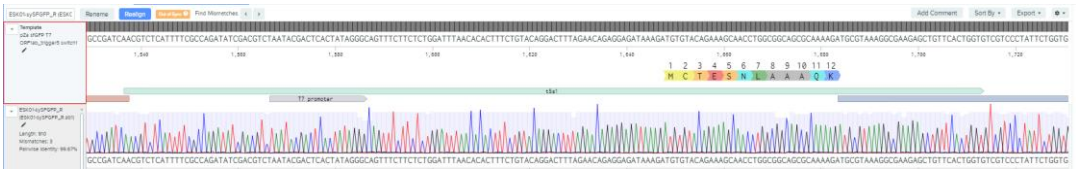

Figure 255. Sanger sequencing results of pZa sfGFP T7 ORF1ab_trigger5 switch1 vector.

Figure 256. Sanger sequencing results of pZa sfGFP T7 ORF1ab_trigger5 switch2 vector.

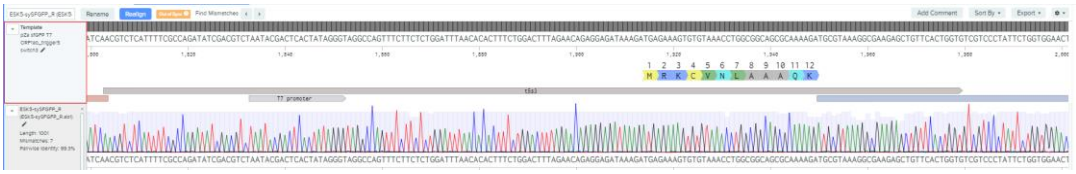

Figure 257. Sanger sequencing results of pZa sfGFP T7 ORF1ab_trigger5 switch3 vector.

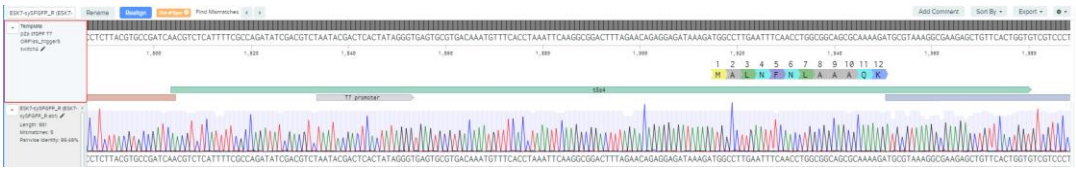

Figure 258. Sanger sequencing results of pZa sfGFP T7 ORF1ab_trigger5 switch4 vector.

Appendix E

Detailed Reaction Recipes and Methods

Luria-Bertani cell growth media

Tryptone	1% (w/v)
Yeast extract	0.5% (w/v)
NaCl	0.5% (w/v)
Proper antibiotics	1:1000

Table 7. Luria-Bertani (LB) growth media

Transformation and storage solution

PEG-8000	10% (w/v)
DMSO	5% (w/v)
$MgCl_2$	50 mM
	pH is adjusted to 6.5 in LB

Table 8. Transformation and Storage Solution (TSS)

Polymerase chain reaction (PCR) constituents and reaction conditions

Constituent	Final Concentration
5X Q5 Reaction Buffer	1 X
10 mM dNTPs	200 µM
10 µM Forward Primer	0.5 µM
10 µM Reverse Primer	0.5 µM
Template DNA	~100 ng
Q5 DNA Polymerase	0.02 U/ µl
5 X Q5 GC Enhancer	1 X
ddH_2O	To reaction volume

Table 9. Q5 Hot Start High-Fidelity DNA Polymerase chain reaction constituents

	Temperature (°C)	Time
Initial Denaturation	98	
Denaturation	98	5-10 s
Annealing	50-72	10-30 s
Extension (25-35 cycles)	72	20-30 s/kb
Final Extension	72	5 min
Hold	+4	until samples are taken

Table 10. Q5 Hot Start High-Fidelity DNA Polymerase reaction conditions

NEB Restriction enzyme digestion reaction

Constituent	Final Volume for 10 µl Reaction
10 X Buffer	1 µl
DNA	1000-2000 ng
Restriction Enzyme 1	0.2 µl
Restriction Enzyme 2	0.2 µl
ddH_2O	To reaction volume

Table 11. NEB Restriction enzyme digestion reaction constituents

MOPS buffered minimal growth media

Constituent	Volume for 500 mL
ddH_2O	15 mL
MOPS	4.186 g
Tricine	0.3585 g
10 mM $FeSO_4$ (freshly prepared)	250 µL
1.9 M NH_4Cl	2.5 mL
0.276 M K_2SO_4	500 µL
0.02 M $CaCl_2.2H_2O$	12.5 µL
2.5 M $MgCl_2$	105 µL
5 M NaCl	5 mL
Micronutrient Stock	10 µL

ddH_2O	19.35 mL
0.132 M K_2HPO_4	5 mL
1 mg/mL Thiamine	50 µL
ddH_2O	Add up to 500 uL

Table 12. MOPS buffered minimal growth media

M63 minimal growth media

Constituent	Volume for 500 mL
NH_4SO_4	5 g
K_2HPO_4	34 g
$FeSO_4$	1.75 mg
100 mM $MgSO_4$	5 mL
1 mg/mL Thiamine	50 µL
ddH_2O	Add up to 500 uL

Table 13. M63 minimal growth media

Phosphate buffered saline solution (PBS)

Constituent	Final Concentration
NaCl	137 mM
KCl	2.7 mM
Na_2HPO_4	4.3 mM
KH_2PO_4	1.47 mM
	pH is adjusted to 7.4

Table 14. 1x Phosphate Buffered Saline Solution (PBS)

Appendix F

Additional Results

Target domains and the lengths of de novo designed riboregulators specific to SARS-CoV-2 used in Chapter 3.

Trigger #	Target region	Length (bp)
1	ORF1ab	120
2	S protein	169
3	M protein	121
4	ORF678	126

Table 15. Target domains and the lengths of de novo designed riboregulators specific to SARS-CoV-2 used in this study.

qRT-PCR measurements of patient samples with Voliron™ qPCR kit, corresponding Cq values for Texas RED channel used in Chapter 3.

Patient Order	Cq Value	Copy Number
Pt.1	26.23	2412.08998
Pt.2	34.23	9.76197
Pt.3	29.41	270.61485
Pt.4	30.57	121.89044
Pt.5	25.41	4249.97676
Pt.6	32.37	35.22851
Pt.7	29.15	323.72619
Pt.8	25.10	5266.59854
Pt.9	26.01	2819.79225
Pt.10	26.24	2393.93934

Pt.11	26.11	2626.98122
Pt.12	22.83	25183.87417
Pt.13	25.41	4241.87096
Pt.14	22.26	37372.00588
Pt.15	26.12	2599.78718
Pt.16	26.62	1846.24185
Pt.17	19.67	222474.37587
Pt.18	22.45	32686.89947
Pt.19	21.12	81592.93637
Pt.20	22.08	42282.42395
Pt.21	20.41	133014.77655

Table 16. qRT-PCR measurements of patient samples with Voliron™ qPCR kit, corresponding Cq values for Texas RED channel are given. Copy number is calculated with dsDNA standards using CFX Maestro Software analysis tool.